INFORMATION TO USERS

This manuscript has been reproduced from the microfilm master. UMI films the text directly from the original or copy submitted. Thus, some thesis and dissertation copies are in typewriter face, while others may be from any type of computer printer.

The quality of this reproduction is dependent upon the quality of the copy submitted. Broken or indistinct print, colored or poor quality illustrations and photographs, print bleedthrough, substandard margins, and improper alignment can adversely affect reproduction.

In the unlikely event that the author did not send UMI a complete manuscript and there are missing pages, these will be noted. Also, if unauthorized copyright material had to be removed, a note will indicate the deletion.

Oversize materials (e.g., maps, drawings, charts) are reproduced by sectioning the original, beginning at the upper left-hand corner and continuing from left to right in equal sections with small overlaps. Each original is also photographed in one exposure and is included in reduced form at the back of the book.

Photographs included in the original manuscript have been reproduced xerographically in this copy. Higher quality 6" x 9" black and white photographic prints are available for any photographs or illustrations appearing in this copy for an additional charge. Contact UMI directly to order.

UMI

A Bell & Howell Information Company
300 North Zeeb Road, Ann Arbor MI 48106-1346 USA
313/761-4700 800/521-0600

Université d'Ottawa • University of Ottawa

Speckle Reduction for the Reconstruction of Synthetic Aperture Radar Imagery

by

Ko Bong Fung

A thesis submitted to the
School of Graduate Studies and Research
in partial fulfillment of the requirements for the degree of

Doctor of Philosophy

Ottawa-Carleton Institute for Electrical Engineering
Department of Electrical and Computer Engineering
Faculty of Engineering
University of Ottawa
March 1997

National Library of Canada

Acquisitions and Bibliographic Services

395 Wellington Street
Ottawa ON K1A 0N4
Canada

Bibliothèque nationale du Canada

Acquisitions et services bibliographiques

395, rue Wellington
Ottawa ON K1A 0N4
Canada

Your file Votre référence

Our file Notre référence

0-612-21029-4

Canada

ABSTRACT

This thesis is aimed towards a deep analysis and synthesis of Kalman filters for reducing the speckle noise in Synthetic Aperture Radar (SAR) images. The motivation stems from an increased number of applications of radar imagery in civilian related projects. For example, in 1996, SAR images acquired from the Canadian RADARSAT satellite were used for environmental monitoring, oil spill detection off the Japanese coast, and floods in northwest United States. Many other useful applications can be mentioned in agriculture, hydrology, geology, forestry, oceanography, etc. Despite its wide usage in the above domains the radar imagery encounters a major drawback due to the quantity of a large speckle component. The purpose of the filters developed in this thesis is the reduction of this component using a Kalman filter in combination with model identification techniques. A justification for using Kalman filters is given. This justification is based, besides a theoretical analysis of the speckle reduction problem, on a set of experiments and tests which are applied to almost all the known filters used in this problem. Special Kalman filters are developed theoretically and applied on practical test and real life images. Special attention is given to the noise component. In the Kalman filtering technique it is well known that small variations in the values of the noise covariances affect the performance. A special chapter is dedicated to the development of an optimal technique for determining the appropriate covariance matrices. Many results and illustrations shown in chapter 7 demonstrate practically the validity of the approach.

ACKNOWLEDGEMENT

I wish to express my sincere gratitude to my supervisor, Dr. Dan Ionescu, for his constant guidance, encouragement, and support throughout my research. Not only once, but time after time, whenever I ran into obstacles or became discouraged, he was always there, giving me the necessary encouragement. He not only provided me with the insight to handle problems on hand, but he did so with a sense of humour and the words: "It CAN be done". I am sure that without him, I would not have been able to complete my research.

I thank the Department of Natural Resources of Canada for providing financial support; and the management of Canada Centre for Remote Sensing for allowing me to pursue my graduate studies. In addition, I thank Dr. David Goodenough, who was my section head. He not only encouraged me to further my studies, but actually prepared a recommendation document to CCRS management for my education leave. It was Dr. Robert O'Neil, Dr. Leo Sayn-Wittgenstein and Mr. Hugh O'Donnel who approved my education leave. Futhermore, the staff at the Canada Centre for Remote Sensing was very helpful in many useful technical discussions and in gathering the necessary data for my research, particularly: Dr. Zhanghao Shi, Dr. Karl Staenz, Mr. Michael Robson, Mr. Julius Princz and Mr. Gunar Fedosejevs.

I thank the faculty and staff of the Department of Electrical and Computer Engineering, University of Ottawa, for their kindness and support.

Above all I would like to thank my friends, my mother Mrs. Bo-Wah Fung, my family for their constant support and especially my wife, Winnie, for her love and care, and my children, Gerry, Irene and Jeannie, who would have enjoyed more time together with their father.

Contents

Abstract ii

Acknowledgement iii

Table of Contents v

List of Tables xi

List of Figures xiii

Notation xix

1 Introduction **1**

1.1 Introduction 1

1.2 Rationale 2

1.3 Known Filters for Speckle Removal in SAR Images 4

1.4 Kalman Filters 5

1.5 New Developments in the Speckle Reduction Problem 7

1.6 Thesis Content 8

2 Introduction to SAR Image Formation and Speckle Noise 10

2.1 Introduction 10

2.2 A Brief Review of Synthetic Aperture Radar 11

2.2.1 Resolution of SAR imagery 11

2.2.2 Focused and Unfocused Arrays 17

2.3 Synthetic Aperture Radar imagery 18

2.4 Speckle as a stochastic process 23

2.5 Suppression of Speckle 28

2.6 Speckle Suppression By Processing Multiple Looks 28

2.7 Conclusions 31

3 Review of Speckle Noise Filters 32

3.1 Introduction 32

3.2 Existing Filters for SAR Images 33

3.2.1 Simple Filters for Speckle Noise Reduction 34

3.2.2 Homomorphic Filters 35

3.2.3 Sigma Filter 36

3.2.4 Local Statistic Filter by Lee 38

3.2.5 Kuan and Map Filters 43

3.2.6 Maximum *A Posteriori* (MAP) Filter 46

3.2.7 Frost and Edge directed Frost Filters 49

3.2.8 Variations of Local Statistical Filters 52

3.2.9 Other Filters 55

3.3 Kalman Filtering of SAR Images 56

3.4 Fullplane Kalman filters 61

3.4.1 A General 2-D Linear Model for Kalman Filtering 61

3.4.2 A Full Plane Semicausal Model for SAR Speckle Reduction . . 62

3.5 Conclusion 64

4 Two Full Plane Kalman Filters for Speckle Noise Reduction in SAR Images 65

4.1 Introduction 65

4.2 The Full Plane Kalman Filter 66

4.2.1 Building a Full Plane Image Model 66
4.2.2 Kalman Filter Equations for a Full Plane Region of Support . 74
4.3 Parameter Estimation 76
4.4 Online Parameter Estimation Equations 79
4.5 Adaptive Kalman Filters 84
4.6 A Kalman Filter with State Multiplicative Noise Parameters 87
4.7 Online Parameter Estimation Equations for the State Multiplicative Noise Case 95
4.8 Conclusions 96

5 Kalman Filters with Non-Gaussian Noise for Speckle Reduction 97

5.1 Introduction 97
5.2 A Kalman Filter for Speckle Noise Reduction in SAR Images Using Markov Noise in the Observation 99
5.3 Online Parameter Estimation Equations 104
5.4 A Kalman Filter for SAR Speckle Reduction with Markov State Noise 105
5.5 Modifications for the Online Parameter Estimation Equations 110
5.6 Conclusions 111

6 An Optimized Full Plane Modified Kalman Filter 113

6.1 Introduction 113

6.2 An Optimal Technique for Determining the Noise Parameters of the Kalman Filter 114

6.2.1 The Image Model 114

6.2.2 Transforming the Filtering Problem into a Control Problem . 115

6.2.3 Defining a Cost Index 117

6.2.4 A Riccati Equation and its Solution 119

6.3 The Gradient of the Cost Index 120

6.4 An Optimization Algorithm for Determining the Noise Parameters of the Kalman Filter for SAR Speckle Reduction 126

6.5 Conclusions 132

7 Results and Performance Evaluation 134

7.1 Principles of Evaluations 134

7.1.1 Homogeneous Areas 136

7.2 Test Results on Filters for Speckle Noise Reduction 140

7.2.1 Edges 152

7.2.2 Point Target 162

7.2.3 Linear Structures 170

7.2.4 Angular Structure 182

7.3 Results on Applying Various Filters on a Real SAR Image 190

7.4 Conclusions 201

8 Conclusions **202**

8.1 Summary of Contributions 205

8.2 Further Work 206

A Gâteaux Derivative and Gradient **208**

A.1 Definition of Gâteaux Derivative 208

A.2 Definition of Gradient 209

List of Tables

7.1 Statistics of the areas on the test image 136

7.2 Statistics of the smoothed areas by box filter 141

7.3 Statistics of the smoothed areas by Lee filter 142

7.4 Statistics of the smoothed areas by Kuan filter 143

7.5 Statistics of the smoothed areas by Enhanced Lee filter with K = 0.1 144

7.6 Statistics of the smoothed areas by Enhanced Lee filter with K = 1.0 145

7.7 Statistics of the smoothed areas by Enhanced Lee filter with K = 10 . 146

7.8 Statistics of the smoothed areas by Frost filter with K = 0.1 147

7.9 Statistics of the smoothed areas by Frost filter with K = 1 148

7.10 Statistics of the smoothed areas by Frost filter with K = 10 149

7.11 Statistics of the smoothed areas by Enhanced Frost filter with K = 0.1 150

7.12 Statistics of the smoothed areas by the Enhanced Frost filter with K = 1 151

7.13 Statistics of the smoothed areas by Enhanced Frost filter with K = 10 152

7.14 Speckle Reduction Performance of Kalman Filters; Full Plane (FABKF), State Multiplicative Noise Kalman Filter (SMABKF), and Markov State Multiplicative Noise Kalman Filter (MMABKF) 153

7.15 Responses of the test filters to a step function in terms of mid-point and slope. 161

7.16 Responses of the Kalman filters to a step function in terms of mid-point and slope 163

List of Figures

2.1 Geometry of a simple SAR configuration 12

2.2 The profile of a simple SAR configuration 13

2.3 The geometry of a target at Xo within the radar pulse generated at X. 14

2.4 A configuration in the slant plane showing the change in range distance as it is being observed during the duration the target is within the coverage of the radar pulses 17

2.5 Single-Look Intensity Image of Victoria, B.C. from ERS-1. 22

2.6 Map of Victoria, B.C. Showing Area of SAR Image. 22

3.1 Homomorphic Filtering Process 36

3.2 Results of Lee Statistical Filter(5x5) Applied to SAR Image 43

3.3 Full Plane region of support for 2-D AR image model. 62

4.1 Example Mapping of 2-D blocks to Block Vector. 68

4.2 Example Mapping Full Plane Parameters to Each Region of Support. 69

4.3 Block Diagram of Modified Fullplane Block Kalman Filter. 88

6.1 Program flowchart for the full plane Kalman filter under the condition of unknown noise values. 127

6.2 Links between the needed programs for the full plane Kalman filter under the condition of unknown noise values. 128

7.1 Test image created by putting together two homogeneous areas . . . 137

7.2 The normalized histogram of the homogeneous test area no. 1 (with mean = 972.31). 138

7.3 The theoretical exponential distribution with mean at 972.31. 138

7.4 The normalized histogram of the homogeneous test area no. 2 (with mean at 2395.22) 139

7.5 The theoretical exponential distribution with mean at 2395.22. 139

7.6 The input image profile of the step edge generated from the homogeneous test image. It is used to test the step response of the speckle reduction filters 155

7.7 Diagram showing how the slope is computed. Superimposed on it is a filtered profile by using a Box filter with a scanning window of 11 x 11. 155

7.8 The filtered response to a step edge by the Box Filter with a 5x5 scanning window 156

7.9 The filtered response to a step edge by the Lee Filter with a 5x5 scanning window 156

7.10 The filtered response to a step edge by the Kuan Filter with a 5x5 scanning window 157

7.11 The filtered response to a step edge by the Enhanced Lee Filter (K=0.1) with a 5x5 scanning window 157

7.12 The filtered response to a step edge by the Frost Filter (K=0.1) with a 5x5 scanning window 158

7.13 The filtered response to a step edge by the Frost Filter (K=1) with a 5x5 scanning window 158

7.14 The filtered response to a step edge by the Enhanced Frost Filter (K=0.1) with a 5x5 scanning window 159

7.15 The filtered response to a step edge by the Enhanced Frost Filter (K=1) with a 5x5 scanning window 159

7.16 The filtered response to a step edge by the Gamma Filter with a 5x5 scanning window 160

7.17 The filtered response to a step edge by the Kalman Filter. 162

7.18 The simulated point target before multiplicative speckle noise is injected. 164

7.19 The simulated point target after speckle noise is injected. The speckle noise is modeled after the RADARSAT fine mode beam pattern and its corresponding signal processor 165

7.20 The result of filtering the noisy speckled point target by the Box Filter with a 11 x 11 scanning window 165

7.21 The result of filtering the noisy speckled point target by the Lee Filter with a 11 x 11 scanning window 166

7.22 The result of filtering the noisy speckled point target by the Kuan Filter with a 11 x 11 scanning window 166

7.23 The result of filtering the noisy speckled point target by the Enhanced Lee Filter (K=1) with a 11 x 11 scanning window 167

7.24 The result of filtering the noisy speckled point target by the Frost Filter (K=1) with a 11 x 11 scanning window 167

7.25 The result of filtering the noisy speckled point target by the Enhanced Frost Filter (K=1) with a 11 x 11 scanning window 168

7.26 The result of filtering the noisy speckled point target by the Gamma Filter with a 11 x 11 scanning window 168

7.27 Results of Kalman Filters on Noisy Point Target. 169

7.28 Comparison of Results of Kalman filters Filter with Varying Cr_{max} on Noisy Point Target. 169

7.29 The linear line-pair pattern before speckle noise is injected. 171

7.30 The appearance of the linear line-pairs after speckle noise is injected. 173

7.31 The appearance of the linear line-pairs after a box filter with a scanning window of 11 x 11 is applied. 174

7.32 The appearance of the linear line-pairs after a Lee filter with a scanning window of 11 x 11 is applied. 175

7.33 The appearance of the linear line-pairs after a Kuan filter with a scanning window of 11 x 11 is applied. 176

7.34 The appearance of the linear line-pairs after a Enhanced Lee filter (K=1) with a scanning window of 11 x 11 is applied. 177

7.35 The appearance of the linear line-pairs after a Frost filter (K=1) with a scanning window of 11 x 11 is applied. 178

7.36 The appearance of the linear line-pairs after a Enhanced Frost filter (K=1) with a scanning window of 11 x 11 is applied. 179

7.37 The appearance of the linear line-pairs after a Gamma filter with a scanning window of 11 x 11 is applied. 180

7.38 The appearance of the linear line-pairs after a Markov full plane Kalman filter with a $\sigma_u^2 = 3.e06$ is applied. 181

7.39 The appearance of the linear line-pairs after a full plane Kalman filter with a multiplicative noise and $\sigma_u^2 = 3.e07$ is applied. 183

7.40 The appearance of the linear line-pairs after an optimal full plane Kalman filter with a $\sigma_u^2 = 3.e06$ is applied. 184

7.41 The pattern of the angular structure on the test image 185

7.42 The result of the angular pattern after filtering by Gamma Map filter with a scanning window of 11 x 11 185

7.43 The result of the angular pattern after filtering by Box Filter with a scanning window of 11 x 11 186

7.44 The result of the angular pattern after filtering by Lee Filter with a scanning window of 11 x 11 186

7.45 The result of the angular pattern after filtering by Kuan Filter with a scanning window of 11 x 11 187

7.46 The result of the angular pattern after filtering by Enhanced Lee Filter (K=1) with a scanning window of 11 x 11 187

7.47 The result of the angular pattern after filtering by Frost Filter (K=1) with a scanning window of 11 x 11 188

7.48 The result of the angular pattern after filtering by Enhanced Frost Filter (K=1) with a scanning window of 11 x 11 188

7.49 The result of the angular pattern after filtering by a full plane Kalman filter with $\sigma^2 = 3.0e5$ 189

7.50 Single-Look Intensity Image of Victoria, B.C. from ERS-1. 192

7.51 Single-Look Intensity Image of Victoria, B.C. from ERS-1 filtered by a Lee 5x5 window filter. 192

7.52 Single-Look Intensity Image of Victoria, B.C. from ERS-1 filtered by a Lee 7x7 window filter. 193

7.53 Single-Look Intensity Image of Victoria, B.C. from ERS-1 filtered by a Frost 5x5 window filter. 193

7.54 Single-Look Intensity Image of Victoria, B.C. from ERS-1 filtered by a modified Frost 5x5 window filter. 194

7.55 Single-Look Intensity Image of Victoria, B.C. from ERS-1 filtered by a Kuan 5x5 window filter. 194

7.56 Results of Kalman Filters Applied to SAR Image 197

7.57 Comparison of FABKF with varying State Transition Variance on a SAR image 199

7.58 Effect of Changing Threshold Coefficient of Variation on a SAR image, $Cr_{max} = 2.0$, using FABKF. 200

7.59 The norm of the Kalman filter gain matrix for the first 10 rows of the SAR image of Victoria. 200

Notation

Various symbols, superscripts, subscripts, and abbreviations used frequently in this thesis are summarized below. All notation is fully defined where it first arises in the text.

Symbols used in description of synthetic aperture radar

ΔT	Round trip delay of a radar echo.
R	Distance in range from radar to target.
c	Speed of the radar echo.
τ	Time between two radar pulses.
ΔR	Difference in range distance between two resolvable points.
ΔR_g	Ground range resolution.
ψ	Depression angle of the line of sight to the target with respect to local horizon
$p()$	Magnitude of radar pulse.
ω_0	Modulated frequency.
α	Amplitude coefficient.
θ	Phase shift associated with the reflection process.
σ	Radar cross-section.
f_d	Doppler frequency.

u	Velocity of the radar platform.
λ	Wavelength.
ΔR_y	Minimum resolvable distance in y-direction.
T	Acquisition time; it is also used as inter-pulse time between two radar echos.
L	Length of footprint in y-direction.
l	Physical antenna length in y-direction.
β	Antenna beam width.
s_t	Transmitted sinusoid.
s_r	Received sinusoid.
$\lvert\cdots\rvert$	Absolute value.
ν	Monochromatic frequency.
$A(x,y)$	Amplitude of a complex phasor.
$I(x,y)$	Observed irradiance.
$< A_x >$	Ensemble average of the x component of phasor A.
$\langle\rangle$	Inner product operator.
$f(\cdots)$	Probability density function.
$\overline{A_e}$	The envelope mean of A.
P_i	Irradiance from the ith image.
$\Gamma(.)$	Gamma function.

$E(\cdots)$	Statistical expectation.
$\hat{x}$	Estimate of the image pixel.
δ	Kronecker delta.
$z(i,j)$	Observed image intensity at Cartesian coordinate (i,j).
$n(i,j)$	Noise at Cartesian coordinate (i,j).
H	H is the blurring matrix in the formulation of Kuan and MAP filters.
C_{xz}	Cross variance of x and z.
Cov_{zz}	Covariance of z.
$h(x,y)$	System impulse response.
$S_r(f)$	Power spectral density of reflectivity.
ϵ	Mean square error.
$var_x(i,j)$	Local variance of x measured from a window centred at Cartesian coordinate (i,j).

Symbols

$\mathcal{I}_{16}$	Integers quantized to 16 bits.
$\mathcal{E}(\ )$	The mathematical expectation.
$x(i,j)$	The state values of the image.
$\mathbf{X}$	Block state space value of image.

$y(i,j)$	The observed values of the image.
$\mathbf{Y}$	Block state space value of observed image.
$\mathbf{I}$	Identity matrix
$\zeta^o(\mathbf{R})$	Mean backscatter received from transmitted radar.
$P(\ )$	Probability distribution.
$Z(t)$	Innovation/Estimation error.
K	Kalman gain.
$\mathcal{L}$	Parameter estimation gain.
$P()$	Error Covariance of Kalman Filter.
$\mathcal{R}$	Approximation of Hessian of quadratic norm.
R_z	Covariance of innovation process.
C_o	Coefficient of variation.
C_r	Contrast Ratio.

Greek Letters

γ/Γ	Multiplicative observation noise
ψ/Ψ	Multiplicative dynamic process noise
μ_x	The mean of the value x
σ_x^2	Statistical variance of x

Σ_a	Estimation derivative
$\mathbf{\Phi}$	Parameter vector
Δ	Gradient
∇	Gâteux Derivative or directional derivative
κ	Derivative of Kalman Gain
λ	Forgetting Factor

Special Symbols

$\bar{x}$	The mean of the value x
$\hat{x}$	The estimate of the value x
z^{-1}	Spatial shift operator

Acronyms and Definitions

2-D	Two Dimensional
AR	Auto-regressive
ABKF	Adaptive Block Kalman Filter
FABKF	Full Plane Adaptive Block Kalman Filter
MFABKF	Modified Full Plane Adaptive Block Kalman Filter
MMABKF	Markov Modified Full Plane Adaptive Block Kalman Filter

SMABKF	State Multiplicative Full Plane Adaptive Block Kalman Filter
ENL	Equivalent Number of Looks
SAR	Synthetic Aperture Radar.
RUPK	Reduced Update Kalman filter
NSHP	Non-Symmetric Half Plane
LSI	Linear Space Invariant
RPE	Recursive Parameter Estimation
EKF	Extended Kalman Filter
MAP	Maximum A Posteriori
MMSE	Minimum Mean Square Error
LLMMSE	Localy Linear Minimum Mean Square Error
SNR	Signal to Noise Ratio

Chapter 1

Introduction

1.1 Introduction

Synthetic Aperture Radar (SAR) images are used more and more for various remote sensing projects such as ice reconnaissance, ocean current measurement, oil slick detection, natural resource monitoring, geological structure identification, and topological mapping etc. However, the quality of SAR images is affected by noise and especially by a component of it which is called speckle noise. The speckle noise was classified by various researchers of the field [28, 21, 40, 49] as multiplicative noise present in the observation (image). The removal of this component has been the subject of research. Different kinds of filters were designed and applied on various SAR images. The degree of successfully removing this noise component is variable and disputable. So far, there are no precise scientific and well-recognized measurement methods for assessing the performance of a speckle filter. In this thesis a few Kalman filtering techniques will be developed and explored. As well as a series of qualitative and quantitative measurements for evaluating the performance of speckle noise filters in SAR images will be devised.

1.2 Rationale

Airborne and space borne synthetic aperture radars have important economic values, particularly in monitoring natural resources and land applications [71]. Its ability to "see through" clouds is significant for civilian applications. St-Pierre [73] pointed out that *between 1986 and 1988 Canada received and archived 245,559 SPOT images of which only 8.9% were completely cloud free images and 15.3% were called usable images (containing a limited amount of clouds). After three years of operation, there were still areas of Canada for which Canada had not yet been able to obtain at least a usable image.*

Speckle obscures information on radar images. Consequently, applications of radar images are affected. For example, speckle reduces the accuracy of measurement of terrain heights [62], it causes classification errors in crop identifications [29], and target identifications. Speckle also makes image registration difficult [23]. However, the high spatial resolution of the images and the capability to image the surface of earth through cloud and in darkness make SAR a unique sensor complementary to optical sensors.

To reduce or remove the speckle effects on images generated from echo returns of synthetic aperture radar (SAR) has been a big problem for target recognition and image interpretation. Despite decades of research and different suggested ways to reduce speckle effect, the problem remains. Some experimenters suggest trading off the speckle effect by reducing spatial resolution. This approach has a certain degree of success, but it cannot satisfy the need for more advanced applications. Numerous attempts have been made to reduce speckle effects on SAR images. The more successful approach is to use digital filters with local statistics [44][41][21][36][45] [46][55]. These filters work well with multiple-look SAR images which are of better signal to noise (SNR) ratio. Multiple look technique lowers image spatial resolution according to $\sqrt{M}$, where M is the number of looks, and it also reduces speckle noise by the same factor.

Recently, more advanced applications of SAR images require that the phase information of an image be well preserved. Raney [65] describes that in the late 1980's, conventional SAR image processors have proved to be inadequate for advanced application (such as terrain heights estimation), special SAR processors based on Differential Range Deramp (DRD) [83] or Chirp Scaling algorithm, are built. The main feature of the new generation SAR processors is their capability to perform accurate Range Cell Migration Correction (RCMC) without using any interpolation procedure. Consequently, these processors preserve the phase of a point target on a single look image. Raney [64] also points out that by using interference pattern derived from two different pairs of SAR images of the same area, it is possible to derive terrain heights which can be accurate to a fraction of its wavelength. However, only single look image can provide meaningful phase information. Phase information is generally destroyed in the process of generating multiple look image.

Because of the above fact, we emphasize our speckle reduction efforts on single look SAR images.

In order to reduce speckle effectively, we suggest establishing a system model, and characterizing the speckle noise accordingly. In fact, we introduce a noise factor to account for the changes in the system state equation; and another factor in the observation model. The ensemble statistics of speckle is then used in deriving the covariance matrices. A reduced update approach is used in the implementation. However, the speckle noise is modeled as a wide sense stationary Markov process in the filter support.

In this thesis, we approach the speckle method from the basics. We concentrate on the speckle problem in the single look situation which is the worst case as far as noise is concerned. Our research begins with modeling the image as a Markov random field and treats the speckle problem as a bandlimited colour noise. By following the statistical distribution of the speckle noise in power and intensity images, we construct an auto-regressive image model based on Markov random field. The multiplicative effect of the speckle noise is modeled both in the state representation and the observation equation. The thermal noise is included in the observation equation. To improve the transitions of the filter around edges a multiplicative noise effect will be introduced in the state equation.

1.3 Known Filters for Speckle Removal in SAR Images

Different forms of digital filters for speckle reduction in SAR images have been suggested [49]. The simplest form includes the mean and median filters. Digital image restoration and enhancement methods are also used [41] to design speckle reduction filters. However, the more popular filters are derived using estimation theory and simplification with the use of local statistics from a scanning window. Speckle noise is assumed to be fully developed. Under such a condition, speckle noise is modeled as a noise term multiplied by the input signal. This kind of digital filter includes the MAP filter [41], the different versions of Lee filters [49], Sigma filter [45] and Frost filter. Lopes et al [55] found that the local statistics filters should include the effects of texture within the local scanning window. They proposed an enhanced version of the popular SAR filters by introducing the speckle index to differentiate the homogeneity of the regions.

There are also other filters that are not used as widely as the local statistics filter [49]. They include the homomorphic filter [36, 4, 5], the Crimmins geometric filter [16] etc. There have been many variations of the basic digital filters. Some of them are modified to locate specific features, such as edges [58, 49]. However, the main concern of this thesis is in the research and development of basic SAR speckle reduction filters.

1.4 Kalman Filters

Kalman filter is known as the best estimator for stochastic signals produced by linear systems. Extensions of Kalman filter to image processing are also known [85, 87]. Due to its complexity and difficulty in tuning its paramaters, only a few researchers apply Kalman filter to speckle reduction to SAR images. One of the last implementations is the work done by Geling [24] where a half plane and full plane model [9, 6] were explored. Here we will work only on the full plane model which seems to produce better results when applied to one-look speckled SAR images.

The Kalman filter is applied to state space model of the image in the form of :

$$
\begin{aligned}
X_k &= \mathbf{A}X_{k-1} + \mathbf{B}U_k \quad \textit{state transition} && (1.1) \\
Y_k &= \mathbf{C}\Gamma_k X_k + V_k \quad \textit{observation} && (1.2)
\end{aligned}
$$

where $\mathbf{A}, \mathbf{B}$ and $\mathbf{C}$ the following matrices:

$$\mathbf{A} = \begin{bmatrix} \mathbf{0} & \mathbf{I} & \mathbf{0} & \mathbf{0} & \mathbf{0} & \mathbf{0} & \mathbf{0} & \mathbf{0} & \mathbf{0} \\ \mathbf{0} & \mathbf{0} & \mathbf{0} & \mathbf{0} & \mathbf{0} & \mathbf{I} & \mathbf{0} & \mathbf{0} & \mathbf{0} \\ \mathbf{0} & \mathbf{0} & \mathbf{0} & \mathbf{I} & \mathbf{0} & \mathbf{0} & \mathbf{0} & \mathbf{0} & \mathbf{0} \\ \mathbf{0} & \mathbf{0} & \mathbf{0} & \mathbf{0} & \mathbf{0} & \mathbf{0} & \mathbf{0} & \mathbf{I} & \mathbf{0} \\ \mathbf{0} & \mathbf{0} & \mathbf{0} & \mathbf{0} & \mathbf{0} & \mathbf{0} & \mathbf{I} & \mathbf{0} & \mathbf{0} \\ \mathbf{0} & \mathbf{0} & \mathbf{0} & \mathbf{0} & A_{54} & A_{55} & A_{56} & A_{57} & \mathbf{0} \\ \mathbf{0} & \mathbf{0} & \mathbf{0} & \mathbf{0} & \mathbf{0} & \mathbf{0} & A_{66} & \mathbf{0} & \mathbf{0} \\ \mathbf{0} & \mathbf{0} & \mathbf{0} & \mathbf{0} & A_{74} & A_{75} & A_{76} & A_{77} & \mathbf{0} \\ A_{80} & A_{81} & A_{82} & A_{83} & A_{84} & A_{85} & A_{86} & A_{87} & A_{88} \end{bmatrix} \tag{1.3}$$

$$\mathbf{B} = \begin{bmatrix} 0 & 0 & 0 & 0 & 0 & 0 & 0 & 0 & 0 \\ 0 & 0 & 0 & 0 & 0 & 0 & 0 & 0 & 0 \\ 0 & 0 & 0 & 0 & 0 & 0 & 0 & 0 & 0 \\ 0 & 0 & 0 & 0 & 0 & 0 & 0 & 0 & 0 \\ 0 & 0 & 0 & 0 & 0 & 0 & 0 & 0 & 0 \\ 0 & 0 & 0 & 0 & 0 & B_{55} & 0 & 0 & 0 \\ 0 & 0 & 0 & 0 & 0 & 0 & B_{66} & 0 & 0 \\ 0 & 0 & 0 & 0 & 0 & 0 & 0 & B_{77} & 0 \\ 0 & 0 & 0 & 0 & 0 & 0 & 0 & 0 & B_{88} \end{bmatrix} \tag{1.4}$$

$$\mathbf{C} = \begin{bmatrix} 0 & 0I & 0 & 0 & 0 & \mathbf{I}0 & 0 & 0 & 0 \\ 0 & 0 & 0 & 0 & 0 & 0 & \mathbf{I} & 0 & 0 \\ 0 & 0 & 0 & 0 & 0 & 0 & 0 & \mathbf{I} & 0 \\ 0 & 0 & 0 & 0 & 0 & 0 & 0 & \mathbf{I} & 0 \\ 0 & 0 & 0 & 0 & 0 & 0 & 0 & 0 & \mathbf{I} \end{bmatrix} \tag{1.5}$$

A filtered image is obtained in terms of the *a posteriori* estimate given by the following equation:

$$X_k^{(+)} = X_k^{(-)} + K_k Z_k \tag{1.6}$$

where K_k is the Kalman filter gain given as in Chapter 4 by:

$$K_k = \mu_\gamma P_k^{(-)} \mathrm{C}^T R_{z\ k}^{-1} \tag{1.7}$$

where the details of the derivation of the previous equation are given, and Z_k is the innovation process defined also in Chapter 4 by the following equation:

$$Z_k = Y_k - C\mu_\gamma X_k^{(-)} \tag{1.8}$$

The a posteriori estimate is used to rebuild the image using the observation equation given above. The new image obtained will have the additive and multiplicative noise greatly removed by the Kalman filter. Distortions of the original image might appear in the result depending on the various combinations of the values of the Kalman filter parameters. The excessive sensitivity of the Kalman filter on the above parameters is a very known fact.

1.5 New Developments in the Speckle Reduction Problem

In this thesis we have concentrated on the following developments:

- The development of a full plane based Kalman filter for SAR speckle noise reduction with state multiplicative noise;
- The development of a full plane based Kalman filter for SAR speckle noise reduction with additive output noise being Markov;
- The development of a full plane based Kalman filter for SAR speckle noise reduction with Markovian state multiplicative noise;
- The development of a full plane based Kalman filter for SAR speckle noise reduction under unknown noise conditions;
- A series of test methods for filters for SAR speckle noise removal.

1.6 Thesis Content

This thesis is organized as follows. Chapter 2 reviews briefly the synthetic aperture radar: its image formation process, the theoretical image resolution in the azimuth and range directions. It then continues to describes the radiometric and geometric characteristics of images formed from radar echoes. Finally, it continues to show the statistical characteristics of speckle noise in terms of different image formation processes. Chapter 3 provides a review of the existing popular speckle filters. It begins with the simple digital speckle reduction filters and finishes with the Kalman filtering techniques. Chapter 4 is dedicated to the development of a full plane Kalman filter and its extension to the state multiplicative noise case. Chapter 5 examines the extension of the Kalman filter when the output and the state multiplicative noises are Markovian. Chapter 6 is dedicated to the development of the Kalman filter equations under unknown noise conditions. In chapter 7, a series of tests and results from applying the above tests to the new Kalman filters and previously developed filters (Lee, Kuan etc.) are introduced. Finally conclusions are given in chapter 8.

Chapter 2

Introduction to SAR Image Formation and Speckle Noise

2.1 Introduction

Radar had a major impact during the Second World War [39]. After that, the development of synthetic radars marked one of the major innovations in imaging. There are two types of imaging radars: real aperture and synthetic aperture radars (SAR). SAR is also referred to as array imaging radar [33]. Both the real and synthetic aperture radars obtain their y-direction (along track) resolution by antenna beam width. Since the antenna beam width in each direction is inversely proportional to its length, the y-direction resolution of real array imaging radars is obtained through the use of long antenna typically mounted at the bottom of the platform. Synthetic aperture radar uses synthetic array to increase its antenna length (which uses the incremental Doppler shift of the adjacent points on the ground) to increase its resolution in the y-direction. Both types of radars use transmitted pulse length for the x-direction (cross-track) resolution.

Since the successful demonstration of the C-band radar by the SEASAT satellite, attention has been focused on using synthetic aperture radar for civil applications. This chapter first describes what is a synthetic aperture radar (SAR), then it follows up with a description on the SAR imagery, and concludes with a statistical characterization of different types of SAR images.

2.2 A Brief Review of Synthetic Aperture Radar

The concept of synthetic aperture radar was first introduced by Carl Wiley of the Goodyear Aircraft Corp. in the 1950s [12][39]. It was observed that a one-to-one correspondence exists between the along-track coordinate of a reflecting object and the instantaneous Doppler shift of the signal reflected to the radar by that object. The famous "Doppler Sharpening Concept" was born. It suggested *a frequency analysis of the reflected signals could enable finer along-track resolution than that permitted by the along-track width of the physical beam itself.*

2.2.1 Resolution of SAR imagery

Synthetic Aperture Radar is a side looking radar. Its basic imaging geometry for imaging terrain is shown in Figure 2.1. The radar on a moving platform (airborne or space borne) emits the microwave pulse of a designed beam pattern which is usually narrow in the along-track (azimuth) direction. The terrain is illuminated strip by strip as the platform moves in the azimuth direction Figure 2.1.

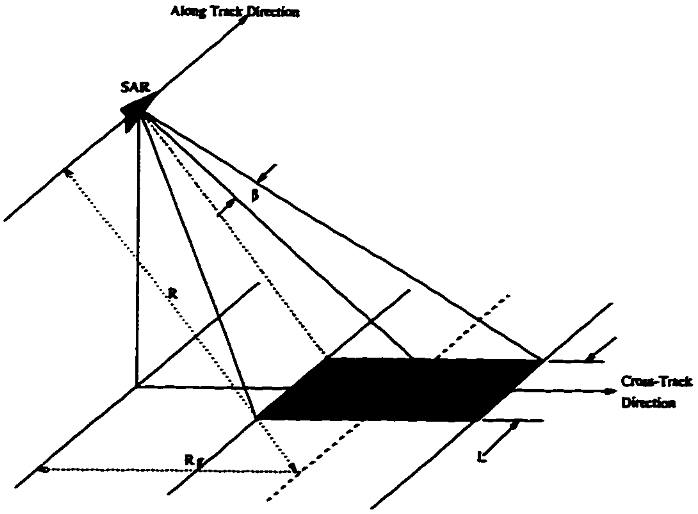

Figure 2.1: Geometry of a simple SAR configuration

The slant range resolution is achieved by the use of pulsing and time-delay 2.1. For an object on the surface of the earth, the round trip delay of a radar echo depends on its slant distance from the radar. Therefore, the round trip time for a radar echo ΔT is given by

$$\Delta T = \frac{2R}{c} \tag{2.1}$$

where c is the speed of the radar echo. The delays of an echo return from two adjacent points on the surface in the slant range are different. If this delay is smaller than the pulse width, these two points will not be resolvable in the image. Therefore, the pulse width of the radar governs the resolution in the range direction. By reasoning this way, the range resolution, ΔR can be determined as:

$$\Delta R \geq \frac{c\tau}{2} \tag{2.2}$$

By reasoning in a similar way, the maximum measurable range R_{max} is a function of inter-pulse period T, and is given by [33]:

$$R_{max} = \frac{cT}{2} \tag{2.3}$$

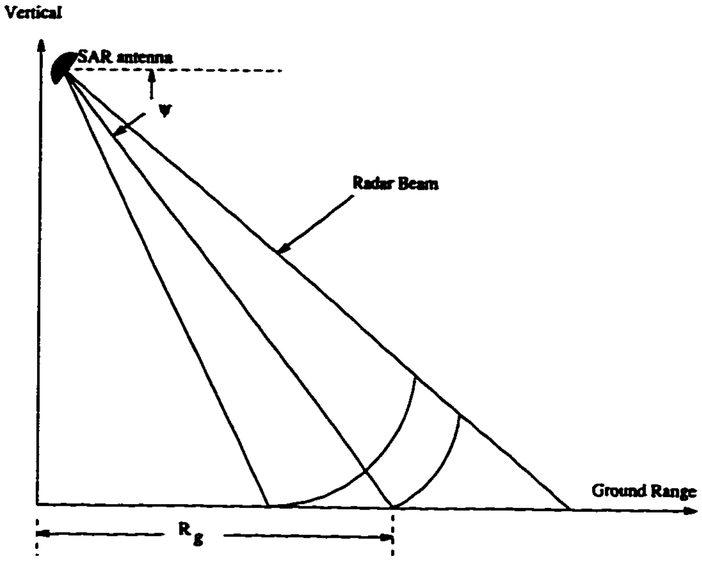

Figure 2.2: The profile of a simple SAR configuration

The corresponding ground range resolution is

$$\Delta R_g = \frac{c\tau}{2} \sec \psi \tag{2.4}$$

where ψ is the depression angle of the line of sight to the target with respect to local horizon (see figure 2.2).

The correspondence between the along-track coordinate of a reflecting object and the instantaneous Doppler shift is explained by Chastant [14]. Referring to figure 2.3, assume a simple case that the radar emits an amplitude-modulated sinusoid

$$s_t(t) = p(t) \cos(\omega_0 t) \tag{2.5}$$

which illuminates a target at slant range R_0 and along-track position X_0. The reflected echo has the form

$$s_r(t) = \alpha p(t - \frac{2R}{c}) \cos[\omega_0 (t - \frac{2R}{c}) + \theta] \tag{2.6}$$

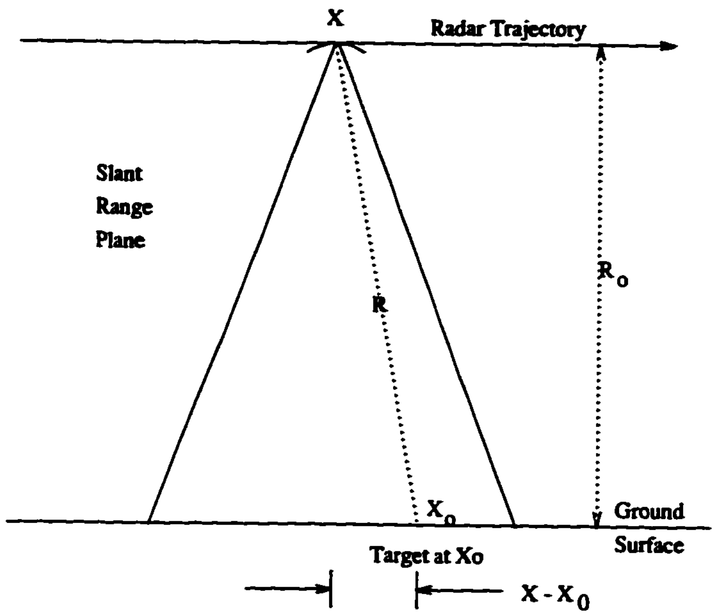

Figure 2.3: The geometry of a target at Xo within the radar pulse generated at X.

where

α = amplitude coefficient such that α^2 is proportional to the radar cross section (σ) of the target

θ = phase shift associated with the reflection process.

For a first order approximation, each single pulse $p(t)$ provides range resolution, while the modulated sinusoid $\cos[\omega_0(t-\frac{2R}{c})+\theta]$ contains the information to obtaining fine along track resolution.

From figure 2.3, it is obvious that

$$R_0^2 \gg |x - x_0|^2 \tag{2.7}$$

Using binomial expansion, equation 2.7 can be expressed as

$$R \approx R_0 + \frac{(x - x_0)^2}{2R_0} \tag{2.8}$$

and the reflected sinusoid can be expressed in the expanded form of

$$cos[\omega_0 t - \frac{2\omega_0 R_0}{c} - \frac{\omega_0}{R_0 c}(x - x_0)^2 + \theta] \tag{2.9}$$

This signal, equation 2.9, is received and then coherently detected. The output of the synchronous demodulator has the form:

$$\cos[(\theta - \frac{2\omega_0 R_0}{c}) - \frac{\omega_0}{R_0 c}(x - x_0)^2] \tag{2.10}$$

where the first term is a time-invariant phase; the second term, a quadratic in $(x - x_0)$, varies with time as the radar proceeds along its trajectory.

After demodulation, this sinusoid has an instantaneous frequency of

$$f_d = \frac{1}{2\pi}\frac{d}{dt}[-\frac{\omega_0}{R_0 c}(x - x_0)^2] \tag{2.11}$$

This is the *Doppler frequency* of the echo return from the target. Since the radar moves with a velocity u along its trajectory, therefore using $x = ut$, we can express f_d as

$$f_d = \frac{1}{2\pi}\frac{d}{dt}[-\frac{\omega_0}{R_0 c}(ut - x_0)^2] \tag{2.12}$$

therefore,

$$f_d = \frac{-\omega_0 u}{\pi R_0 c}(x - x_0) \tag{2.13}$$

which reduces to

$$f_d = \frac{-2u}{\lambda R_0}(x - x_0) \tag{2.14}$$

From equation 2.14, it is obvious that the Doppler shift is linear in $(x - x_0)$ with a slope in terms of $u, \lambda, and R_0$. However, this relationship only holds for $|x - x_0| \ll R_0$.

With equation 2.14, Hovanessian [33] derives the theoretical maximum resolution in azimuth direction. The derivation assumes a simple case, such that $(x - x_0)$

is the minimum resolvable distance represented by ΔR_y, by neglecting the direction sign, equation 2.14 can be written as

$$\Delta R_y = \frac{\lambda R f_d}{2u} \tag{2.15}$$

In a matched transmit/receive system, the duration of target illumination T is designed to be $\frac{1}{f_d}$. That means, during the acquisition time T of a target, the radar moves a distance of uT, where u is the velocity. Thus

$$L = uT = \frac{u}{f_d} \tag{2.16}$$

By substituting in equation 2.14 and ignoring the sign, we have

$$L = \frac{\lambda R_0}{2\Delta R_y} \tag{2.17}$$

or

$$\Delta R_y = \frac{\lambda R_0}{2L} \tag{2.18}$$

Maximum resolution in the along track (azimuth) direction can be obtained by considering the fact that the antenna coverage on the ground should be greater than the equivalent antenna array length. This insures the return of target energy from a point on the ground during the filter charge up time $T = 1/f_d$. Thus referring to figure 2.1, the length of the footprint L in azimuth direction is proportional to $R\beta$, but according to antenna theory, β is proportional to $\frac{\lambda}{l}$ where λ is the half power bandwidth of the beam, and l is the physical antenna length. That is:

$$L < \frac{\lambda}{l} \tag{2.19}$$

Substituting equation 2.17 into equation 2.19, we have

$$\Delta R_y \geq \frac{l}{2} \tag{2.20}$$

That is, the best azimuth direction resolution obtainable is equal to one half of the physical antenna length l.

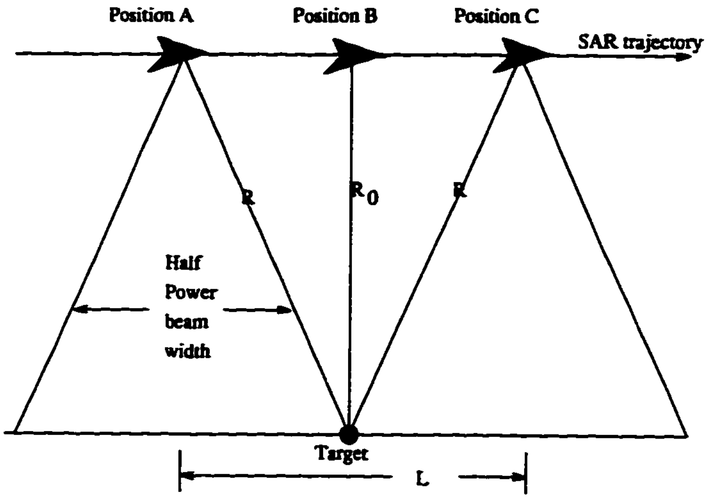

Figure 2.4: A configuration in the slant plane showing the change in range distance as it is being observed during the duration the target is within the coverage of the radar pulses

2.2.2 Focused and Unfocused Arrays

As the synthetic aperture radar moves from position A to position B (Figure 2.4), or as the target on the ground enters and leaves the coverage of the radar pulses, the range distance of the target to the radar changes from R to R_0 and then back up R again. Since the radar wavelength λ is much smaller than the range distance R, this change represents changes in phase angles at the receiver by the reflected signal.

In order to have the azimuth resolution close to the theoretical limit, the echo returns at the receiver during the period that the radar travels from position A to position B, must be phase corrected. In synthetic array radars, this phase correction and adjustment is called *focusing*, and arrays using it are called *focused arrays* [33].

Without phase correction, the resolution is much lower. In fact, it can be deduced as follows. Assuming that the processor can tolerate as much as 90 degrees of phase shift of the received radar echo returns, let L be the distance that the radar travels corresponding to this 90 degrees phase shift. Since 90 degrees corresponds to $\frac{\lambda}{8}$ for a one way phase shift, therefore, using the triangle properties, we have

$$\begin{aligned} R_0^2 + (\frac{L}{2})^2 &= (R_0 + \frac{\lambda}{8})^2 \qquad (2.21) \\ R_0^2 + \frac{L^2}{4} &= R_0^2 + \frac{\lambda R_0}{4} + \frac{\lambda^2}{64} \qquad (2.22) \end{aligned}$$

Simplifying and dropping the small term $\frac{\lambda^2}{64}$,

$$L = \sqrt{\lambda R_0} \qquad (2.23)$$

Substituting equation 2.23 into equation 2.17, we have

$$\Delta R_y = \frac{\sqrt{\lambda R_0}}{2} \qquad (2.24)$$

Thus, the unfocused resolution in the azimuth direction is only $\frac{\sqrt{\lambda R_0}}{2}$.

2.3 Synthetic Aperture Radar imagery

Synthetic aperture radar (SAR) imagery finds an increasing number of applications nowadays due to its capacity for displaying the objects on the scene. Its usage is multiple, ranging from military to civil applications. Imagery from space borne and airborne synthetic aperture radars has been used in several remote sensing disciplines such as geologic feature mapping, oceanic phenomena studies, land use and urban morphology studies, flood and disasters mappings and environmental monitoring [50]. SAR images are generated by coherently summing the radar echoes generated and received by a moving antenna (which simulates a very long aperture antenna). High cross-track (range) resolution in a SAR image is accomplished by transmitting short, coded pulses (such as *chirps*). High along- track (azimuth) resolution is obtained by synthesizing a large antenna aperture and moving the platform with coherent return received over many radar echoes. The maximum achievable resolution along azimuth is independent of height, but is approximately half the physical antenna length the radar [33]. Furthermore, the width of the impulse response in either the range or the azimuth dimension is inversely proportional to the bandwidth of the processed signal in that dimension. Thus, in order to obtain high resolution imagery, large bandwidths are required (i.e. a narrow impulse response) [66][67][50]. Because the image formation process depends on the time traveled by the radar echoes from target to the receiver, radar images differ in many ways from optical images. Geometrically, curved features, such as mountain ranges, may appear folded together; tall objects are displaced towards the radar antenna, and there are also radar shadows which are devoid of measurements. However, the most noticeable radiometric effect is the speckle (also referred to as a *fading* or a *scintillation* effect [50]). Other parameters influencing SAR images include the presence of moisture, the presence of waves on water surfaces, the wind in areas covered by vegetation, etc.

It is very well known that from urban areas it is difficult to identify and extract (both manually and by digital computer) the linear features due to some of a series of geometrical distortions already mentioned above, such as relief layover, object folding, radar shadow, corner reflection effects, directional pattern effects, and the density of buildings, etc. [32][42].

In general, one can say that the noise content in a SAR image is quite high such that the signal to noise ratio is low. The dominant factor affecting the interpretation of SAR images is the speckle or the granular noise. The speckle noise is caused by the coherent summation of the wavelets emanating from the microscopic scatterers on the surface. In general terms, the speckle is caused by the roughness of the surface when compared to the wavelength of the radar signal. [28].

This kind of granular patterns have been observed also when objects are illuminated by light from a highly coherent continuous wave (cw) laser. It appears to be chaotic and unordered, extremely complex, and bears no resemblance to the macroscopic properties of the illuminated object. When compared to the wavelengths of the electro-magnetic radiation in the visible and microwave region, both natural and artificial objects appear to be rough. A small illuminated area consists of numerous microscopic surfaces acting as scatterers. When an monochromatic light falls on such a surface, the reflected light composes of wavelets generated from these scatterers. At a distant observation point, these wavelets add or subtract each other according to their differences in phases due to delays and geometry in propagation. Bright spots are formed at a point where the interference is highly constructive, while dark spots are formed where the interference is highly destructive. Thus, on a distant observation plane, the speckle pattern has many bright and dark spots as the irradiance at each point on the plane varies according to the contribution by each scatterer. As the observation plane moves, the propagation paths of each scatterer change, thus the speckle pattern changes as well.

Goodman [28] gives a description of speckle formation process as follows: *The image formed at a given point in the observation plane consists of a superposition of a multitude of complex amplitude spread functions, each arising from a different scattering point on the surface of the object. As a consequence of the roughness of this surface, the various amplitude spread functions add with different phases, resulting again in a complex pattern of interference, or a speckle pattern superimposed on the image of interest.*

The appearance of speckle is not limited to imagery formed from reflected light. The same phenomenon appears equally well to images formed by passing monochromatic light through a diffuser such as photographic transparency, as long as the wave front transmitted by the transparency satisfies the same basic assumptions of discrete scatterers.

It is known that for single look[1] images the signal to noise ratio gets as low as 1:1. The effect of the large noise contents, as described above, is a considerable reduction in the image resolution and in its utility. Due to the large noise content, image processing techniques usually experience great difficulty when applied to SAR imagery [48]. Examples which sustain our statement can be found in a set of domain literature papers such as : [19], [34],[57]. Ulaby et al [81] reported that the per pixel classifiers that were successfully used to classify optical images from LANDSAT yielded poor results when applied to radar images. Attempts to improve the classification results by averaging have met with limited success. It is also well known that edge detection is a real problem when dealing with SAR images. Many specialized edge detection methods have been developed solely for application to SAR imagery [25],[78],[70],[13] and many prefiltering techniques developed are specifically modified to preserve edges in SAR imagery [75],[43]. These arguments can be illustrated by various SAR images. We include here a set of such images and will comment on the specificity of each of these cases. All the images presented here are images taken by ERS-1 in August 1993 and are single look images . The images are all 256x256 pixels, but they are displayed with non-square pixels due to the higher along-track sampling rate of the single-look image. These images illustrate how the speckle noise severely reduces the interpretability of the image. The large variations in the image make it difficult to clearly identify region boundaries, and this problem is greatly exacerbated when computer algorithms are used. The images

---

[1] images obtained by coherently summing the radar echo returns from the scene.

were chosen on purpose from non-homogeneous areas. Many processing algorithms assume homogeneous regions and have difficulty handling images that have such different regions.

In what follows, however, we will refer and use the same test image, as it was used in [24] in order to compare our results to those obtained by Geling [24].

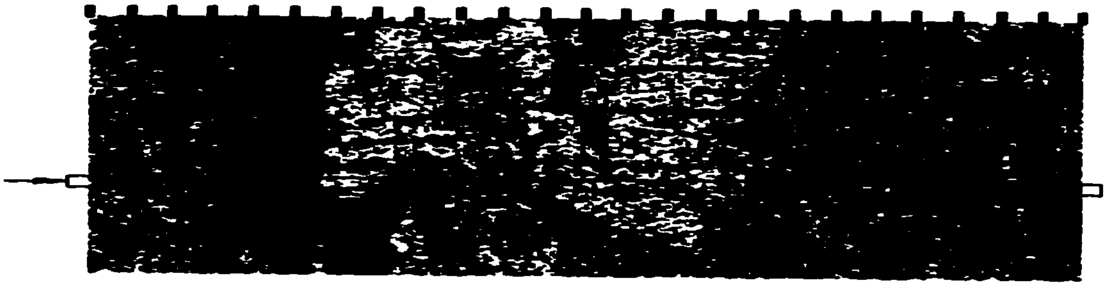

Figure 2.5: Single-Look Intensity Image of Victoria, B.C. from ERS-1.

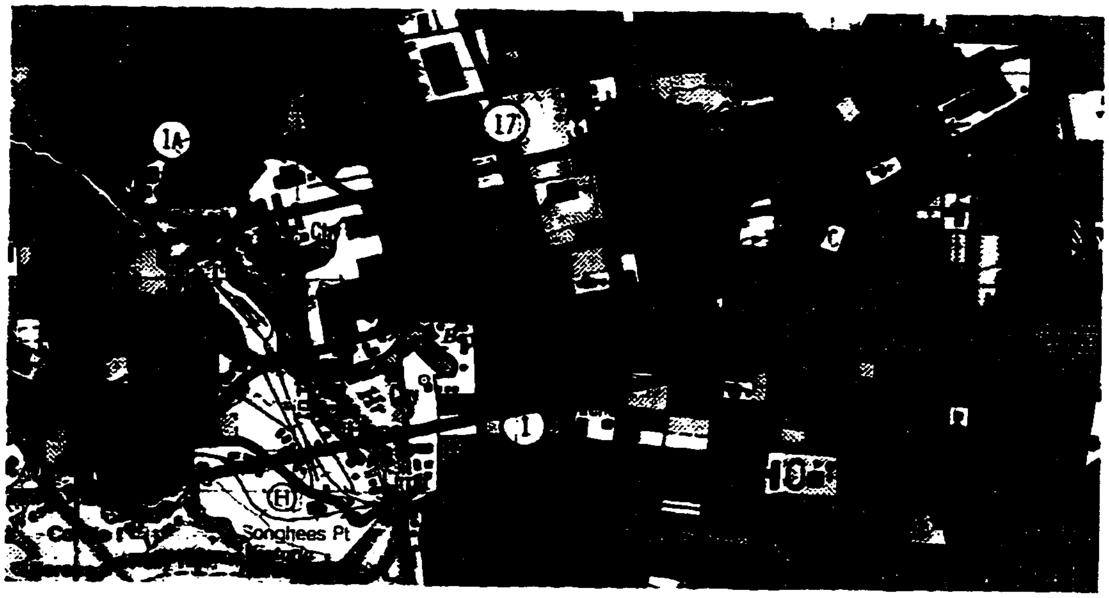

Figure 2.6: Map of Victoria, B.C. Showing Area of SAR Image.

Speckle is of concern in all the domains using coherent imagery, including radar astronomy, synthetic aperture radar, and acoustic imagery. In what follows, the speckle noise will be described in terms of stochastic processes. After introducing the functions which describe the density function for various cases of SAR images, a conclusion referring to the type of filter needed to best suppress the speckle noise will be drawn.

2.4 Speckle as a stochastic process

In what follows we will assume that, in a fully monochromatic polarized imaging situation, each of the complex valued analytical signals arriving from the field of incidence at a point (x, y) from a scatterer has a voltage of $u(x, y)$ such that

$$u(x,y) = A(x,y)exp(i2\pi\nu t) \tag{2.25}$$

where ν is the monochromatic frequency and $A(x, y)$ is a complex phasor amplitude

$$A(x,y) = |A(x,y)|exp[i\theta(x,y)]. \tag{2.26}$$

Therefore, the observed irradiance I at (x, y) can be represented as:

$$I(x,y) = \lim_{T\to\infty} \frac{1}{T} \int_{-\frac{T}{2}}^{\frac{T}{2}} |u(x,y;t)|^2 dt = |A(x,y)|^2. \tag{2.27}$$

The complex amplitude of the field at (x, y) is the sum of the contributions from many scatterers on the rough surface. Therefore, the phasor amplitude of the field can be found by

$$A(x,y) = \sum_{k=1}^{N} |a_k| exp(i\phi_k), \tag{2.28}$$

where $|a_k|$ and ϕ_k represent the amplitude and phase of the contribution from the kth scatterer. This may be expressed in terms of the envelope amplitude A_e and a phase angle ϕ as follows:

$$A = A_e e^{j\phi} \tag{2.29}$$

By decomposing the phasor A into its x, y components, we have

$$\begin{aligned} A_x &= A_e cos\phi = \sum_{i=1}^{N} A_i cos\phi_i \\ A_y &= A_e sin\phi = \sum_{i=1}^{N} A_i sin\phi_i \end{aligned} \tag{2.30}$$

As $N \to \infty$, and using the central limit theorem, and also assuming A_x and A_y are normally distributed with mean

$$\begin{aligned} < A_x > &= \sum_{i=1}^{N} < A_i cos\phi_i >, \\ < A_y > &= \sum_{i=1}^{N} < A_i sin\phi_i > . \end{aligned} \tag{2.31}$$

By taking the following assumptions:

- The scatterers are statistically uncorrelated and statistically independent. The amplitude and the phase of the $k$the scatterer are independent of each other, and of the amplitudes and phases of all other elementary phasors.
- The surface is rough compared with the wavelength. The phases ϕ_k is uniformly distributed, i.e. equally likely to lie anywhere in the interval $(-\pi, \pi)$.

Under these conditions, the speckle is known as fully developed, and the above two equations becomes:

$$< A_x >= \sum_{i=1}^{N} [< A_i > \frac{1}{2\pi} \int_0^{2\pi} cos\phi_i d\phi_i] = 0 \tag{2.32}$$

and similarly,

$$< A_y >= 0. \tag{2.33}$$

Furthermore,

$$< A_x A_y >= 0. \tag{2.34}$$

Thus, A_x and A_y are uncorrelated and independent with a joint normal probability density function as:

$$f(A_x, A_y) = \frac{1}{2\pi\sigma^2} e^{-\frac{A_x^2 + A_y^2}{2\sigma^2}}. \tag{2.35}$$

where σ^2 is the variance of the phasor.

By representing equation 2.35 in polar coordinates, and changing variables such that $f(A_x, A_y)dA_x dA_y = f(A_e, \phi)dA_e d\phi$, and because

$$\begin{aligned} A_e^2 &= A_x^2 + A_y^2, \\ A_e dA_e d\phi &= dA_x dA_y. \end{aligned} \tag{2.36}$$

The joint probability density of A_e and ϕ is Rayleigh distributed such that:

$$f(A_e, \phi) = \frac{A_e}{2\pi\sigma^2} e^{\frac{-A_e^2}{2\sigma^2}} \text{ for } 0 \leq A_e \leq \infty, \text{ and } 0 \leq \phi \leq 2\pi \tag{2.37}$$

The probability density function can be shown as:

$$f(A_e) = \int_0^{2\pi} f(A_e, \phi) d\phi = \begin{cases} \frac{A_e}{\sigma^2} e^{-\frac{A_e^2}{2\sigma^2}} & \text{for } A_e \geq 0 \\ 0 & \text{otherwise} \end{cases} \tag{2.38}$$

$$f(\phi) = \int_0^{\infty} f(A_e, \phi) dA_e = \frac{1}{2\pi} \tag{2.39}$$

The Rayleigh distribution has non-zero mean, the envelope mean, $\overline{A_e}$, is

$$\overline{A_e} = \sqrt{\frac{\pi}{2}}\sigma. \tag{2.40}$$

The second moment is given by

$$\overline{A_e^2} = 2\sigma^2. \tag{2.41}$$

The variance of the ac component, that is the variance of mean squared ac component A_{ac} is given by

$$\overline{A_{ac}^2} = \overline{A_e^2} - \overline{A_e}^2 = (2 - \frac{\pi}{2})\sigma^2 = 0.429\sigma^2. \tag{2.42}$$

The ratio of the mean of the envelope is given by

$$S = \frac{\overline{A_e^2}}{\overline{A_{ac}^2}} = 3.66, \text{ or } 5.6dB. \tag{2.43}$$

The irradiance, or the power in the envelope, $P = A_e^2$. Assuming that the power has developed across a 1-ohm resistor, the differential power to the differential voltage is $dP = 2A_e dA_e$. The Rayleigh distribution can now be converted to a density distribution for power as follows:

$$f(P)dP = f(A_e)dA_e = \frac{1}{2\sigma^2}e^{-\frac{P}{2\sigma^2}}dP. \tag{2.44}$$

That is, P is exponentially distributed with probability density function:

$$f(P) = \frac{1}{2\sigma^2}e^{-\frac{P}{2\sigma^2}}. \tag{2.45}$$

and its mean value is

$$\overline{P} = \overline{A_e^2} = 2\sigma^2. \tag{2.46}$$

By substituting back to the previous equation, we have the density distribution function of P as:

$$f(P) = \begin{cases} \frac{1}{\overline{P}}e^{-\frac{P}{\overline{P}}} & \text{for } P \geq 0 \\ 0 & \text{otherwise} \end{cases} \tag{2.47}$$

The envelope power $\overline{P^2}$ can be shown as:

$$\overline{P^2} = \int_0^\infty \frac{P^2}{\overline{P}}e^{-\frac{P}{\overline{P}}}dP = 2\overline{P}^2, \tag{2.48}$$

thus

$$\sigma_{P_{ac}}^2 = \overline{P^2} - \overline{P}^2 = \overline{P}^2, \tag{2.49}$$

or

$$\sigma_{P_{ac}} = \overline{P}. \tag{2.50}$$

Using the power representation, the Rayleigh distribution of A_e can be written as:

$$f(A_e) = \begin{cases} \frac{2A_e}{P} e^{-\frac{A_e^2}{P}}, & \text{for } A_e \geq 0 \\ 0, & \text{otherwise.} \end{cases} \tag{2.51}$$

2.5 Suppression of Speckle

Speckle reduces the ability to resolve the fine details such as edges and small objects on an image, and it poses problems to image analysis. The presence of speckle in the signal detected by an optical radar system can reduce the probability of target detection and/or cause the radar system to lose track. In practice, suppression of speckle is performed before photo-interpretation and/or image analysis.

2.6 Speckle Suppression By Processing Multiple Looks

From probability theory, the sum of M identically distributed, real valued, uncorrelated random variables has a mean value which is M times the mean of any one component. This has indeed lowered the effect of the speckles, but the resolution of the final image is also lowered by a factor of $\sqrt{M}$.

The radar Doppler frequency spectrum is divided into M segments (known as looks), and then each segment is used to independently form an image. The final image is obtained by summing the images from processed different Doppler frequency segments.

However, addition of speckle pattern on a complex amplitude basis provides no results in another random walk process [28].

According to Lee [47], the speckle of a M-look intensity SAR image has χ^2 distribution with $2M$ degrees of freedom.

The distribution of the M-look images can be derived by assuming the output being the sum of the irradiance, P, from each independent *look* image, such that

$$I = P_1 + P_2 + \cdots + P_m \tag{2.52}$$

where P_i is the irradiance from the ith image with an exponential distribution of

$$f(P) = \begin{cases} \frac{1}{\bar{P}} e^{-\frac{P}{\bar{P}}} & \text{for } P \geq 0 \\ 0 & \text{otherwise} \end{cases} \tag{2.53}$$

Since each image is considered to be independent, the mass density in dV is constant and is equal to $f_{P_1 P_2 \cdots P_m}(P_1, P_2, \cdots, P_m)$, which is

$$f_{P_1 P_2 \cdots P_m}(P_1, P_2, \cdots, P_m) = \frac{1}{\bar{P}^m} e^{-\frac{P_1+P_2+\cdots+P_m}{\bar{P}}} \tag{2.54}$$

or

$$f_I(I) = \frac{1}{\bar{P}^m} e^{-\frac{I}{\bar{P}}}. \tag{2.55}$$

By considering a minute volume $dV = CI^{m-1}dI$, where C is an arbitrary constant. Now,

$$f_I(I)dI = \frac{CI^{m-1}}{\bar{P}^m} e^{-\frac{I}{\bar{P}}} dI. \tag{2.56}$$

That is,

$$f_I(I) = \frac{CI^{m-1}}{\bar{P}^m} e^{-\frac{I}{\bar{P}}}. \tag{2.57}$$

reduction of contrast because the addition of two complex random walk processes

To determine the value of C, one can use the fact that $\int_0^\infty f_I(I)dI = 1$, that is

$$\int_0^\infty \frac{C I^{m-1}}{\overline{P}^m} e^{-\frac{I}{P}} dI = 1. \tag{2.58}$$

This gives $C = \frac{1}{(M-1)!}$. Thus the probability density function of the irradiance of an M-look image is

$$f_I(I) = \frac{I^{m-1}}{(M-1)!\overline{P}^m} e^{-\frac{I}{P}}. \tag{2.59}$$

The mean is $E(I) = m\overline{P}$, and $E(I^2) = m(m+1)\overline{P}^2$, and its variance is

$$\sigma_I^2 = E(I^2) - (E(I))^2 = m\overline{P}^2. \tag{2.60}$$

Similarly, if the M-look image goes through a square root detector, the probability density function can be found by letting $R = \sqrt{P_1 + P_2 + \cdots + P_m}$, and thus

$$R^2 = P_1 + P_2 + \cdots + P_m. \tag{2.61}$$

Therefore,

$$f_R = 2Rf_I(R^2), \tag{2.62}$$

and

$$f_R(R) = \frac{2R^{2m-1}}{(m-1)!\overline{P}^m} e^{-\frac{R^2}{P}}. \tag{2.63}$$

The mean is $\frac{\Gamma(m+\frac{1}{2})}{\Gamma(m)}\sqrt{\overline{P}}$, and the $E(R^2) = m\overline{P}$, and the variance is

$$\sigma_R^2 = E(R^2) - (E(R))^2 = (m - \frac{\Gamma(m+\frac{1}{2})}{\Gamma(m)})\overline{P}, \tag{2.64}$$

where $\Gamma(.)$ denotes Gamma function.

Similarly, the probability density function of a M-look images formed by averaging M intensity images as $z = \frac{P_1+P_2+\cdots+P_m}{m}$,

$$f_z = \frac{m^m z^{m-1}}{(m)!\overline{P}^2} e^{-\frac{mz}{P}} \tag{2.65}$$

and the mean $E(z) = \overline{P}$, $E(z^2) = \frac{m+1}{m}\overline{P}^2$, and the variance is

$$\sigma_z^2 = \frac{\overline{P}^2}{m}. \tag{2.66}$$

Lee et al [49] has tabulated the following ratios of the standard deviation to the mean of multi-look synthetic aperture radar images:

Number of looks	N-look Intensity	N-look Amplitude	N-look Amplitude
		(amp. averaging)	(intensity aver.)
1	1.0000	0.5227	0.5227
2	0.707	0.3696	0.3630
3	0.577	0.3017	0.2941
4	0.500	0.2614	0.2536
6	0.408	0.2134	0.2061
8	0.352	0.1848	0.1781

2.7 Conclusions

The theory of synthetic aperture radar is relatively recent in the field of imaging radars. This chapter introduces first the concept of synthetic aperture radar with respect to the factors affecting its image quality, and the principle of focused arrays. It continues to describe the characteristics of radar images in terms of image formation and the salient speckle phenomenon. The general statistical properties of speckle due to different coherent summings and image formations are also given. Finally, the chapter concludes with a visit to the concept of speckle suppression and the popular methods of speckle suppression by means of multiple looks.

Chapter 3

Review of Speckle Noise Filters

3.1 Introduction

The popular local statistics speckle noise filters [41] [44] [21] use a simple multiplicative model with the assumption that the adjacent pixels are slightly correlated. Raney et al [67] emphasize that the *pixel* concept in SAR is not the same concept as *resolution*. They insist that *Resolution is fundamental, and established by the SAR bandwidth and processing strategy, whereas pixels are chosen to satisfy scale and sampling requirements.* They also point out that there are approximately two pixels per resolution cell in both the range and the azimuth image coordinates. Isolated (point) isotropic scatterers do not suffer from speckle noise when imaged.

Conventional linear system can be fully described by either an impulse response or a frequency response. But in SAR system, which is an energy conservative partially coherent system, both an impulse response and a frequency response are required in order to characterize the system [66][67]. This is due to the fact most of the SAR processors take advantage of the partial coherence to reduce the speckle effects by generating multiple looks in the process of image formation. Consequently, both coherence and resolution are *coloured.* Raney also pointed out that *the SAR system is linear in (complex) amplitude domain before detection, and that the system is linear (in units of power) following detection (the system processor is assumed to use a magnitude square detection approach).*

In general, the radar signal fading statistics are estimated by assuming that the return echoes are generated from the independent scatterers of uniform electromagnetic properties. Ulaby [80] points out that when the echo returns are dominated by a few strong scatterers, the fading process is characterized by the Nakagami-Rice distributions. Ulaby [80] states that *Some experimental observations support the Rayleigh behaviour, while others, particularly in those measured for complex terrain categories, are in closer agreement with the log-normal or the Weibull pdf's, or other more complicated distributions.*

3.2 Existing Filters for SAR Images

There are several methods of speckle reduction, many of which will be summarized here in order of increasing complexity. It is assumed in many SAR speckle reduction procedures that the speckle noise in adjacent pixels is independent. Kuan et al. [41] points out that some authors who apply digital restoration and enhancement techniques for speckle noise reduction assume that speckle noise is multiplicative and uncorrelated. Furthermore, [41] speckle is signal dependent and is spatially correlated, and its correlation function is of importance for speckle reduction. Raney [67] emphasizes that speckle measured in adjacent pixels must be considered correlated.

3.2.1 Simple Filters for Speckle Noise Reduction

The simplest form of noise reduction filters are the mean and median filters. They do not have a noise and signal model. These two filters assume that the pixels under a scanning window are highly correlated and the variance of the intensity values is due to the noise.

The mean filter uses a scanning window of 3 x 3 or 5 x 5 such that the centre pixel is replaced by the mean of the intensity values of pixels in the window.

$$\hat{x} = \frac{\sum_{i=1}^{n} \sum_{j=1}^{n} x_{ij}}{n^2} \tag{3.1}$$

Similarly, the median filter replaces the centre pixel of a scanning window with the median of the pixels in the window. Noticeably, both these techniques perform well in homogeneous areas, but they smooth out too much the high frequency contents such as edges and textures in an image.

One method of speckle reduction is multi-look processing. The image is sampled as several independent, lower resolution images or looks, which are then averaged together. Sampling is achieved by dividing the Doppler frequency spectrum into M segments and processing each segment independently. This method leads to a reduction in the speckle noise of intensity images by a factor of $1/\sqrt{M}$, where M represents the number of independent looks [28]. The averaged result has a gamma distribution [49].

$$f(I_M) = \begin{cases} \frac{M^M I^{M-1}}{(M-1)!\sigma_I^{2M}} \exp^{\frac{-MI}{\sigma_I^2}}, & I \geq 0 \\ 0, & \text{otherwise} \end{cases} \tag{3.2}$$

where

$$I_M = \text{the intensity image after } M \text{ look processing} \tag{3.3}$$

$$\bar{I}_M = \sigma_I^2 \tag{3.4}$$

$$\sigma_{I_M}^2 = \sigma_I^2/M \tag{3.5}$$

Multi-look processing is a speckle reduction technique commonly used by the image formation processor. In the frequency domain processing, because the processor deals with segments of the Doppler spectrum reduced by a factor of M, it may consequently reduce the processing complexity of each segment by a factor as much as M in one of the directions (i.e. azimuth and range directions). However, such a processing gain is at the expense of the image resolution, which it reduces as a consequence by $1/M$. According to Curlander [17], the subsequent additive noise accumulated during the process of summation may bias the image and reduce the gain in signal to noise ratio by a value less than $\sqrt{M}$.

3.2.2 Homomorphic Filters

Since speckle noise is considered multiplicative in nature for fully developed speckle, Homomorphic filtering has been used as suggested in Jain [36] and Arsenault et al [5]. Andrews [4] defines Homomorphic filtering as *a technique in which a signal is mapped from its original representation space into another space where desired processing operations are more easily undertaken.* This method involves a non-linear transform to a domain where the multiplicative noise may be treated as additive noise and removed. The corrected image is then retrieved using a corresponding inverse transform. The process is illustrated in Figure 3.1. The most common Homomorphic transform for multiplicative noise is the log operation. Multiplicative terms in the normal domain become additive in the logarithmic domain. Then, the additive noise component in the new domain is removed using some traditional filtering technique. The processed image is subsequently recovered by taking the inverse transform. Durand et al. [19] analyzed several filters including Homomorphic versions of the box filter, and the homogeneous block filter. They found that the non-Homomorphic filters performed better on real SAR imagery despite the more appropriate multiplicative noise model used.

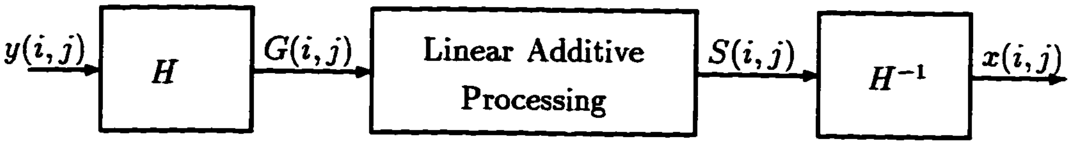

Figure 3.1: Homomorphic Filtering Process

3.2.3 Sigma Filter

Lee [45] proposed a sigma filter to reduce additive noise in images. The principle assumption is that the distribution of the noise in an image is Gaussian. The additive noise is further assumed to have zero mean and a standard deviation $/sigma$. Moreover, the probability that the intensity of an object lies within the range of two standard deviations is 0.955. Therefore, he proposes the following procedure to filter the additive noise by using a local scanning window.

1. Given the centre pixel of the local window is $x(i,j)$, establish the intensity range as $[x(i,j)+\Delta, x(i,j)-\Delta]$, where $\Delta = 2\sigma$.
2. Identify and sum all the pixels in the local window which have intensity values within the range established above.
3. Compute the average of the intensity values found in the above step.

4. Replace the intensity value of $x(i,j)$ with the average found above.

Mathematically, for a window with dimension $(2n+1) by (2m+1)$, the estimate $\hat{x}(i,j)$ is given by:

$$\delta_{k,l} = \begin{cases} 1, & \text{if } [x(i,j)-\Delta] \le x(k,l) \le [x(i,j)+\Delta] \\ 0, & \text{otherwise} \end{cases} \tag{3.6}$$

$$\hat{x}_{i,j} = \frac{\sum_{k=i-n}^{i+n} \sum_{l=j-m}^{j+m} \delta_{k,l} x(k,l)}{\sum_{k=i-n}^{i+n} \sum_{l=j-m}^{j+m} \delta_{k,l}} \tag{3.7}$$

where:

$\hat{x}$	is the estimate of the original image,
$x(k,l)$	is the observed image pixel at location (k,l), and
σ	is the standard deviation of the noise.

In order not to smooth out objects, the filter is designed not to replace the centre pixel of the window when the number of pixels within the prescribed range is less than the K. In this case, the centre pixel will be replaced by the average of its immediate neighbours.

That is, if the number of pixels lies within the two sigma range is M, then the decision rule is defined as:

$$\hat{x} = \begin{cases} \text{two sigma average}, & \text{if } M > K \\ \text{neighbourhood average}, & \text{if } M \le K \end{cases} \tag{3.8}$$

Lee [46] extends this filter to speckle filtering. To adapt to the multiplicative noise, the two sigma range is modified such that:

$$\delta_{k,l} = \begin{cases} 1, & \text{if } (1-2\sigma_n)x(k,l) \le x(i,j) \le (1+2\sigma_n) \\ 0, & \text{otherwise} \end{cases} \tag{3.9}$$

where:

σ_n is the standard deviation of the noise.

The modified sigma filter can be applied repeatedly until the result is satisfactory. No doubt, the filter is computationally efficient when a selective local average of the pixels can be obtained. It appears to retain sharp edges and fine details while smoothing locally uniform regions. However, this hypothesis of the multiplicative noise to be Gaussian distributed is found to be inaccurate in most SAR imagery [58][55]. It is strongly assumed that the pixel at the centre of scanning window is in fact the mean of a Gaussian distribution [56]. Then, the two sigma range is established based on the observed intensity of the image pixel. This can be problematic as the pixel may have an intensity which has been reduced significantly by the speckle noise. In such a case, the two sigma range will be biased towards the low end of the distribution of the intensity of the object. Consequently, the estimate will be lower than what the actual value should be.

3.2.4 Local Statistic Filter by Lee

Lee developed another speckle reduction filter using local statistics [44], [47]. He started with a multiplicative image model as:

$$z(i,j) = x(i,j)n(i,j) \tag{3.10}$$

where $z(i,j)$ is the observed image intensity at Cartesian coordinate (i,j), $x(i,j)$ is the actual intensity before contamination by noise, and $n(i,j)$ is the noise. Let $\overline{n}(i,j)$ denotes the expectation $E[n(i,j)]$, and assume that

$$E[(n(i,j) - \overline{n(i,j)})(n(k,l) - \overline{n(k,l)})] = \sigma_n^2 \delta_{i,k} \delta_{j,l}. \tag{3.11}$$

The image model is then approximated by a linear model given by equation 3.10 as:

$$z(i,j) = Ax(i,j) + Bn(i,j) + C \tag{3.12}$$

where A, B, C are constants (i.e. non-random variables).

By taking the expectations of equation 3.10 and equation 3.12, and equating the two expectations bases on $E[z(i,j)]$, we have

$$\overline{x(i,j)n(i,j)} = A\overline{x(i,j)} + B\overline{n(i,j)} + C \tag{3.13}$$

Rearranging C, it becomes

$$C = \overline{x(i,j)n(i,j)} - A\overline{x(i,j)} - B\overline{n(i,j)} \tag{3.14}$$

By substituting equation 3.14 into equation 3.12, the mean square error is formed as shown in equation 3.15, and it is minimized for variables A and B.

$$J = E[A(x(i,j) - \overline{x(i,j)}) + B(n(i,j) - \overline{n(i,j)}) - (x(i,j)n(i,j) - \overline{x(i,j)n(i,j)})]^2. \tag{3.15}$$

By taking the partial derivatives of J with respect to A and then to B, setting the results to 0, and assuming that x and n are independent, the constants A, B and C can be found as follows:

$$\begin{aligned} A &= \overline{n(i,j)} & (3.16) \\ B &= \overline{x(i,j)} & (3.17) \\ C &= -\overline{n(i,j)x(i,j)} & (3.18) \end{aligned}$$

As a result, the linear image model of equation 3.12 has the relation:

$$z(i,j) = \overline{n(i,j)}x(i,j) + \overline{x(i,j)}[n(i,j)) - \overline{n(i,j)}] \tag{3.19}$$

Since the optimal linear model of x [3] is given by

$$\hat{x}(x,y) = \overline{x(x,y)} + k(i,j)(z(i,j) - \overline{z(i,j)}) \tag{3.20}$$

$k(i,j)$ can be found by using the orthogonality principle [59] such that the error $x - \bar{x}$, and z is orthogonal, that is:

$$E[(x(i,j) - \overline{x(i,j)})z] = 0. \tag{3.21}$$

Substituting $\bar{x}(i,j)$ by equation 3.20, we have

$$E[(x(i,j) - \overline{x(i,j)}) - k(i,j)(z(i,j) - \overline{z(i,j)})] = 0. \tag{3.22}$$

Thus, $k(i,j)$ can be found as:

$$k(i,j) = \frac{E[(x(i,j) - \overline{x(i,j)})z]}{E[(z(i,j) - \overline{z(i,j)})z]} \tag{3.23}$$

By substituting z with the equation 3.19, both numerator and denominator of equation 3.23 can be found as:

$$E[(x(i,j) - \overline{x(i,j)})z] = \overline{n(i,j)}\sigma^2_{x(i,j)} \tag{3.24}$$

$$E[(z(i,j) - \overline{z(i,j)})z] = \overline{n(i,j)}^2\sigma^2_{x(i,j)} + \overline{x(i,j)}^2\sigma^2_n) \tag{3.25}$$

Thus, by equations 3.24 and 3.25, $k(i,j)$ is found to be:

$$k(i,j) = \frac{\overline{n(i,j)}\sigma^2_{x(i,j)}}{\overline{n(i,j)}^2\sigma^2_{x(i,j)} + \overline{x(i,j)}^2\sigma^2_n)} \tag{3.26}$$

Local statistics calculated from a window centred at location (i,j) is then calculated by using the multiplicative model of equation 3.10, such that the *a priori* mean and variance are:

$$\overline{x(i,j)} = \frac{\overline{z(i,j)}}{\overline{n(i,j)}} \tag{3.27}$$

$$\sigma^2_{x(i,j)} = \frac{\sigma^2_{z(i,j)} + \overline{z(i,j)}^2}{\sigma^2_n + \overline{n(i,j)}^2} - \overline{x(i,j)}^2 \tag{3.28}$$

Following the same procedure, Lee [44] adds the additive noise, $w(i,j)$ to the multiplicative model described in equation 3.10 to derive a similar speckle reduction filter. The computed filter equation is very similar to the filter equation 3.20. The new multiplicative model is:

$$z(i,j) = x(i,j)n(i,j) + w(i,j) \tag{3.29}$$

Assuming that $n(i,j)$, and $w(i,j)$ are independent, and also $E[w(i,j)] = 0$ the linearised image model is found to be:

$$z(i,j) = \overline{n(i,j)}x(i,j) + \overline{x(i,j)}(n(i,j) - \overline{n(i,j)}) + w(i,j) \tag{3.30}$$

The optimal linear estimate, or the filter equation of this new model is:

$$\hat{x}(i,j) = \overline{x(i,j)} + k(i,j)(z(i,j) - \overline{n(i,j)}\overline{x(i,j)} - \overline{w(i,j)}) \tag{3.31}$$

where

$$k(i,j) = \frac{\overline{n(i,j)}\sigma^2_{x(i,j)}}{\overline{x(i,j)}^2\sigma^2_n + \overline{n(i,j)}^2\sigma^2_{x(i,j)} + \sigma^2_w} \tag{3.32}$$

Using the multiplicative model of equation 3.29, the *a priori* mean and variance calculated from the local statistics centred at (i,j) can be found as:

$$\overline{x(i,j)} = \frac{\overline{z(i,j)} - \overline{w(i,j)}}{\overline{n(i,j)}} \tag{3.33}$$

$$\sigma^2_{x(i,j)} = \frac{\sigma^2_{z(i,j)} + \overline{z(i,j)}^2}{\sigma^2_n + \overline{n(i,j)}^2} - \overline{x(i,j)}^2 - \sigma^2_w. \tag{3.34}$$

In further work, Lee [49] uses a linear model where

$$\hat{x} = a\bar{x} + by \tag{3.35}$$

in which $\hat{x}$ is the minimum mean square estimate, and a and b are chosen to minimize the mean square error. This results in a minimum mean square estimate of the form

$$\hat{x}_{i,j} = \bar{x}_{i,j} + k(y_{i,j} - \bar{y}_{i,j}) \tag{3.36}$$

where the gain term $k_{i,j}$ is

$$k_{i,j} = \sigma_{x\ i,j}^{2} / \sigma_{y\ i,j}^{2} \qquad (3.37)$$

The difference between this filter and the previous Lee filter is only in the calculation of the gain term. Lee found that there was little difference between the two filters when using 4-look amplitude images, but the newer Lee filter had significantly improved performance with single look intensity images over the original derivation.

The Lee statistical filter assigns a value to the central pixel that is between the mean of the given window and the observed value. As the local mean value gets larger or the ratio between the local variance and the local mean gets smaller, the output tends to be closer to the mean. This filter was rated very favourably by Durand et al [19] and by Lee et al [49] in terms of performance and efficiency. The previous four filtering methods were also compared by Dewaele et al. [18]. They found that the Lee statistical filter performed well, but preferred the Crimmins filter for preserving edges. The primary drawback of the Lee statistical filter is the over-smoothing of edges. This effect can be seen in Figure 3.2 when compared to the original image in Figure 2.5. The single bright linear feature in Figure 3.2 in the harbour region in the left third of the image is actually two separate targets that have been smoothed together.

In order to overcome the problem of over-smoothing of the edges, Lee further refined the filter to use edge directed windows [43]. In this algorithm, eight non-square windows for eight edge orientations are created within a 7x7 window. The local statistics are calculated using the windows for the edge model selected and then the Lee filter is applied. For homogenous regions, this performs similarly to the original Lee statistical filter, but gives much better performance near edge boundaries [49].

Figure 3.2: Results of Lee Statistical Filter(5x5) Applied to SAR Image

3.2.5 Kuan and Map Filters

Kuan et al. [40] developed an adaptive noise smoothing filter by using the Local Linear Minimum Mean Square Error (LLMMSE) as criteria. His observation model is given by:

$$z = Hx + n \tag{3.38}$$

where

z is the degraded observation,

H is the blurring matrix,

n is the noise that can be signal dependent or signal independent.

The minimum mean square error (MMSE) estimate of x is defined as:

$$\hat{x} = E(x|z) \tag{3.39}$$

By constraining the estimate to be linear, the best linear estimate, or $E(x|z)$ in equation 3.39, is found to be

$$\hat{x} = E(x) + \frac{C_{xz}}{C_{zz}}(z - E(z)). \tag{3.40}$$

By using the observation defined in equation 3.38, the covariances are found to be:

$$\begin{aligned} C_{xz} &= C_{xx}H^T + E[(x - E(x))n^T] && (3.41) \\ C_{zz} &= HC_{xx}H^T + C_{nn} + HE[(x - E(x))n^T] + E[n(x - E(x))^T]H^T && (3.42) \end{aligned}$$

where
C_{nn} is the covariance of n.

By assuming that n and x are independent, such that $E(n|x) = 0$, the covariances of x and z can be simplified to:

$$\begin{aligned} C_{xz} &= C_{xx}H^T && (3.43) \\ C_{zz} &= HC_{xx}H^T + C_{nn}. && (3.44) \end{aligned}$$

By further restricting the observation model in equation 3.38 to be a case of no degradation by blurring, such that $H = I$, and furthermore, the noise, n, is uncorrelated such that $E(n_i n_j) = 0$ for $i \neq j$, then the estimate of equation 3.40 can be written as:

$$\bar{x} = E(x) + \frac{\sigma_x^2}{\sigma_x^2 + \sigma_n^2}[z - E(z)] \tag{3.45}$$

Since the means and variances used in equation 3.45 are ensemble means and ensemble variances of x which are usually not available *a priori* and can only be estimated from the degraded signal, so Kuan further modifies his estimate by using local spatial statistics that are estimated from the degraded signal under a local (scanning) window.

Using local statistics, Kuan provides a more explicit structure of an adaptive noise reduction filter for multiplicative noise. With equation 3.45, the degradation model for the multiplicative noise is written as:

$$z'(i,j) = n(i,j)x(i,j) \tag{3.46}$$

The multiplicative noise, $n(i,j)$ is assumed to be independent of $x(i,j)$ and has stationary mean and variance of:

$$\begin{aligned} E[n(i,j)] &= E(n) && (3.47) \\ E[(n(i,j) - E(n))^2] &= \sigma_n^2 && (3.48) \end{aligned}$$

The normalized observation is defined as:

$$z(i,j) = \frac{z'(i,j)}{E(n)} \tag{3.49}$$

Rewriting equation 3.49 in terms of signal plus signal-dependent additive model as:

$$z(i,j) = x(i,j) + [\frac{n(i,j) - E(n)}{E(n)}] \cdot x(i,j) \tag{3.50}$$

where the noise term is $\frac{n(i,j)-E(u)}{E(u)} \cdot x(i,j)$, the variance of the noise and the variance of $x(i,j)$ become:

$$\begin{aligned} \sigma_{n(i,j)}^2 &= \frac{\sigma_n^2[(E(x(i,j)))^2 + \sigma_{x(i,j)}^2]}{[E(n)]^2} && (3.51) \\ \sigma_{x(i,j)}^2 &= \frac{\sigma_{z(i,j)}^2 - \sigma_n^2[E(z(i,j))^2]/[E(n)]^2}{1 + \sigma_n^2/[E(n)]^2} && (3.52) \end{aligned}$$

Replacing the ensemble statistics by local statistics, the adaptive noise reduction filter for the multiplicative model becomes:

$$\hat{x}(i,j) = \bar{x}(i,j) + \frac{var_x(i,j)[z(i,j) - \bar{x}(i,j)]}{var_x(i,j) + \sigma_n^2[(\bar{x}(i,j))^2 + var_x(i,j)]/[E(n)]^2} \tag{3.53}$$

where $var_x(i,j)$ is the local variance of x measured from a window, and $z(i,j)$ is the normalized observation, and $\sigma_n^2/[E(n)]^2$ is a parameter characterizing the multiplicative noise level.

Although this method is better optimized than Lee's method, the improvement in the results is usually reported as negligible [19], [55].

3.2.6 Maximum *A Posteriori* (MAP) Filter

Kuan et al. [41] further developed a maximum *a posteriori*(MAP) method for speckle filtering. To accommodate for complex signal, a more generic image model is used in the derivation. The observation model is given as:

$$z(m,n) = \sum_{i}\sum_{k} h(m-i, n-k)s(i,j)a(i,j) + v(m,n) \qquad (3.54)$$

where

$v(m,n)$ is the zero-mean complex amplitude additive noise; $a(i,j)$ is the exponential $exp(j\phi(i,k))$.

Using a lexicographic representation, equation 3.54 can be written as:

$$z = Hs + v \qquad (3.55)$$

The MAP filter is formulated by taking an estimate with a constraint to maximize the conditional probability density function of $f(s|z)$ such that

$$f(s|z) = \frac{f(z|s)f(s)}{f(z)} \qquad (3.56)$$

Assuming a non-stationary mean and non-stationary variance Gaussian image model, $f(s)$ is given by:

$$f(s) = \prod_{i=1}^{N^2} \frac{1}{\sqrt{2\pi}\sigma_s} exp-[\frac{(s_i - \overline{s_i})^2}{2\sigma_{s_i}^2}] \qquad (3.57)$$

where $*$ denotes complex conjugate inverse.

Moreover, by taking the assumption that the speckles are uncorrelated and fully developed, the conditional probability $f(z|s)$ becomes

$$f(z|s) = \frac{1}{\pi^{N^2}|Cov_{zz}|} exp[-s^{*} Cov_{zz}^{-1} s] \tag{3.58}$$

where

Cov_{zz} is the covariance of z.

By taking the logarithm of equation 3.56, and differentiating it with respect to s, the MAP equation becomes:

$$\frac{\delta log f(z|s)}{\delta s} + \frac{\delta log f(s)}{\delta s} = 0 \tag{3.59}$$

By substituting in the appropriate probability density functions, the MAP equation can be written as:

$$-h^{T} Cov_{zz}^{-1} h + h^{T} Cov_{zz}^{-1} z z^{*} Cov_{zz}^{-1} h - \frac{1}{\sigma_z^2}(s - \bar{s})|_{s=\hat{s}_{map}} = 0 \tag{3.60}$$

where $*$ denotes complex conjugate inverse.

Although equation 3.60 is solvable with iterative method, it is computationally tedious. The covariance matrix to be inverted is of dimension $N^2 * N^2$, where N is dimension of the image and an optimal direction for updating the estimate is required for each iteration. The LLMMSE filter is used to reduce the computational load of the MAP filter. With the additional assumptions of $\bar{z} = 0$, and $\bar{z} = 0$, equation 3.60 is re-written as:

$$\frac{P_{\bar{s}} - s}{s^2} + \frac{\|s_{LL\hat{M}SE}\|^2}{s^2} - \frac{1}{\sigma_s^2}(s - \bar{s})|_{s=\hat{s}_{MAP}} = 0. \tag{3.61}$$

where

$\hat{s}_{LLMMSE} = s h^{T} Cov_{zz}^{-1} z$,

$\bar{s}$ is the local mean of s,

$P_{\bar{s}}$ is the covariance matrix of the error vector defined by $s - \hat{s}_{LLMMSE}$

The computation and update for the solution of this MAP equation is still complex and time consuming. It was implemented as a recursive filter with its update computed by a Kalman filter using the so called ***reduced update*** strategy.

However, for the multiple look cases, where the magnitude of the speckle is observed and independent, the iterative methods and updates become much simpler.

When the *L*-look image has a symmetrical Beta distribution in a two parameter probability density function such as:

$$f(s) = \frac{\Gamma(2m)}{\Gamma^2(m)}(\frac{s}{2\bar{s}})^{m-1}(1 - \frac{s}{\bar{s}})^{m-1} \tag{3.62}$$

The MAP equation becomes:

$$(L - \alpha + 3)\hat{s}^2 + (\bar{z}(\alpha - 2L + 3) - Lz)\hat{z} + 2Lz\bar{z} = 0 \tag{3.63}$$

where

$\alpha = \frac{1}{C_s 2}$

$C_s^2 = \frac{\sigma_s^2}{\bar{s}^2}$.

The only real positive solution lying between z and $\bar{z}$ is:

$$\hat{s} = \frac{Lz + \bar{z}(2L - \alpha + 3) - \sqrt{(Lz - \bar{z}(2L - \alpha + 3))^2 + 2Lz\bar{z}(2\alpha - 6)}}{2(L - \alpha + 3)} \tag{3.64}$$

Similarly, for those multiple look images which have Gamma distribution as:

$$fs = (\frac{\alpha}{\bar{s}})^{\alpha}\frac{1}{\Gamma(\alpha)}exp(-\alpha\frac{s}{\bar{s}})s^{\alpha-1} \tag{3.65}$$

where

$\bar{s} = \bar{z}$

$\alpha = \frac{1}{C_s^2}$.

In this case, the filter equation is:

$$\alpha \hat{s}^2 + (1 + L - \alpha)\bar{z}\hat{s} - Lz\bar{z} = 0. \tag{3.66}$$

The solution of this equation lying between z and $\bar{z}$ is:

$$\hat{s} = \frac{(\alpha - L - 1)\bar{z} + \sqrt{\bar{z}^2(\alpha - L - 1)^2 + 4\alpha Lz\bar{z}}}{2\alpha} \tag{3.67}$$

3.2.7 Frost and Edge directed Frost Filters

Frost et al. [21] developed a speckle noise reduction filter based on an image model in which the observed radar image is corrupted by multiplicative noise. That is, the backscatter from the earth surface is multiplied by a stationary random process of coherent fading. After that, the image is formed by convolving the product of the backscatter and the random process of coherent fading with the system response function. Frost designed his filter by using a mean square error estimate (MMSE) for the backscatter from the image data. Since the MMSE is predicated on the fact that the signal and the noise are both stationary, his filter cannot handle directly the earth observation images (particularly, the radar images). The statistics of the signal and noise of these images are non-stationary and they vary spatially. In order to circumvent this problem, Frost assumes that the signal is stationary in the wide-sense within a small spatial window. Therefore, the MMSE filter is designed to process on a spatial window of an image which is stationary in the wide sense. The filtering of an image is achieved by moving a processing window over an entire image.

In creating the image model, the image data at location (x, y), $I(x, y)$, is the observed power at that point with a gamma distribution; the noise is a standard χ^2

distribution, such that

$$I(x,y) = [r(x,y) \cdot n(x,y)] * h(x,y) \tag{3.68}$$

where

$h(x,y)$ is the system impulse response,

$r(x,y)$ is the actual desired image

$*$ denotes convolution.

In this model, equation 3.68, it is further assumed under the neighbourhood window, $n(x,y)$ and $r(x,y)$ are both stationary in homogeneous areas.

By assuming that $m(t)$ is the impulse response of the filter to extract $r(x,y)$ from $I(x,y)$, the mean square error, ϵ, is established as follows:

$$\epsilon^2 = E[(r(x,y) - I(x,y) * m(x,y))^2] \tag{3.69}$$

The solution of the MMSE in equation 3.69 can be described in a transfer function:

$$M(f) = \begin{cases} [\frac{\bar{n}S_r(f)}{S_r(f) * S_n(f)}]\frac{1}{H^*(f)} & \text{for } f \neq 0 \\ \frac{1}{\bar{n}} & \text{for } f = 0 \end{cases} \tag{3.70}$$

where

$f = (f_x, f_y)$ is the spatial frequency coordinate, $S_r(f)$ and $S_n(f)$ are the power spectral densities of the reflectivity and the speckle noise process, respectively, H^* is the complex conjugate of the system transfer function, and $\bar{n} = E[n(x,y)]$.

Considering the fact that the filter is to extract the $r(x,y)$ from the intensity $I(x,y)$, and $H(f)$ is a constant during the image formation process, then equation 3.69 can be simplified as:

$$M'(f) = \frac{\bar{n}S_r(f)}{S_r(f) * S_n(f)} \tag{3.71}$$

To solve equation 3.71, $r(x, y)$ is modeled as an standard autoregressive process with autocorrelation function $R_r(\tau)$. The autocorrelation function for the noise process is $R_n(\tau)$. Thus, the autocorrelations functions and the subsequent spectral densities of $r(x, y)$ and the noise can be given as:

$$R_\tau = \sigma_r^2 e^{-a|r|} + \bar{r}^2 \tag{3.72}$$

where $\sigma_r^2, \bar{r}, a$ are the variance, mean and constant of $r(x, y)$. They are dependent on the local terrain categories.

$$S_r(f) = \frac{2\sigma_r^2 a}{a^2 + 4\pi^2 f^2} + \bar{r}^2\delta(f) \tag{3.73}$$

$$R_n(\tau) = \sigma_n^2\delta(\tau) + \bar{n}^2 \tag{3.74}$$

$$S_n(f) = \sigma_n^2 + \bar{n}^2\delta(f) \tag{3.75}$$

.

The impulse response of the filter, $m'(x, y)$, is found to be:

$$m'(x, y) = K_1 \alpha e^{-\alpha|(x,y)|} \tag{3.76}$$

where K_1 is a normalizing constant, and

$$\alpha = \sqrt{2a[\frac{\bar{n}}{\sigma_n}]^2 \cdot [\frac{1}{1 + (\frac{\bar{r}}{\sigma_r})^2}] + a} \tag{3.77}$$

The decay constant α is a function of all the three signal parameters $\sigma_r^2, \bar{r}$, and a. Frost estimated α using local statistics from neighbourhood window and found that

$$\alpha \propto \frac{\sigma_I^2}{\bar{I}^2} \tag{3.78}$$

Thus, the filter equation becomes

$$m'(x, y) = K_1 \exp(-KC_o^2|(x, y)|) \tag{3.79}$$

where K_1 is a normalizing constant, K is the filter parameter and C_o is the locally derived coefficient of variation

$$C_o = \frac{\sigma_r}{\bar{I}} \tag{3.80}$$

This filter performs fairly well in comparison to several of the others described above as illustrated by Shi and Fung [72], but it does fail to model additional additive noise as pointed out by Woods and Biemond [85]. Quelle and Boucher[63] combined the Frost model of SAR imagery with spectral estimation techniques to develop an adaptive Frost filter.

3.2.8 Variations of Local Statistical Filters

There exist many slight variations of the above filters. In considering the filtering of complex images [58], especially those that have meaningful texture, Lopes et al [53] suggest that an ideal filter should estimate the pixel value in a homogeneous area simply by pixel averaging. They argue that in such a situation, the minimum variance unbiased estimator is the mean pixel value. However, in the heterogeneous areas, the filter should smooth speckle and, at the same time preserve the edges and textural information. In this situation, an ideal filter should separate the speckle and the textural information, and subsequently reduce or remove the speckle. But, in the case there is highly speculative reflection and there are isolated point targets, then the assumption of fully developed speckle does not hold. The filter function is not valid in this case, the pixels should not be filtered or modified.

Based on the above observations, Lopes et al [55],[54],[52] defined the criteria where and how the local statistics speckle should operate. They define the criteria in terms of speckle coefficients C_n and C_z. In order to apply these criteria, an image is divided into regions of three classes. The first class corresponds to the homogeneous areas; the second class is the heterogeneous areas; and the third class is the regions containing isolated point targets, which, in this case, the filter should preserve the observed pixel value. The coefficient of variation of the speckle noise is defined as $C_n = \frac{\sigma_n}{\bar{n}}$, the coefficient of variation of the image pixel $C_z = \frac{\sigma_z}{\bar{z}}$, and C_{max} is the threshold above which the image pixel remains unfiltered.

The filtering operation is subsequently changed. The changes to the well known local statistics filter can be summarized as follows:

Enhanced Lee Filter

The filter equation of the Lee Filter is rearranged and expressed in terms of a weighing factor $W(i,j)$ such that:

$$\hat{x}(i,j) = \overline{z(i,j)}W(i,j) + z(i,j)(1 - W(i,j)). \qquad (3.81)$$

where

$$W(i,j) = exp\frac{-K(C_z(i,j) - C_n)}{C_{max} - C_z(i,j)} \qquad (3.82)$$

where $C_z(i,j) = \frac{\sigma_z(i,j)}{\overline{z(i,j)}}$. The rules for the filter becomes:

$$\hat{x}(i,j) = \begin{cases} \overline{z(i,j)} & \text{for } C_z(i,j) \leq C_n \\ \overline{z(i,j)}W(i,j) + z(i,j)(1 - W(i,j)) & \text{for } C_n < C_z(i,j) < C_{max} \\ z(i,j) & \text{for } C_z(i,j) \geq C_{max} \end{cases} \qquad (3.83)$$

Enhanced Frost Filter

By re-arranging the impulse response of the Frost Filter in terms of $C_z, C_{max}, and C_n$, it becomes

$$m(i,j) = K_1[-K func(C_z(i,j), C_{max}, C_n)|(i,j)| \tag{3.84}$$

where $func$ is a decreasing function such that

$$func(C_z) = \begin{cases} 0 & \text{for } C_z(i,j) < C_n \\ \frac{C_z(i,j)-C_n}{C_{max}-C_z(i,j)} & \text{for } C_n \leq C_z(i,j) \leq C_{max} \\ \infty & \text{for } C_z(i,j) > C_{max} \end{cases} \tag{3.85}$$

The filter estimate for the two cases of $C_z(i,j) \geq C_{max}$ and $C_z(i,j) \leq C_n$ is represented by:

$$\hat{x}(i,j) = \begin{cases} z(i,j) & \text{for } C_z(i,j) \geq C_{max} \\ \overline{z(i,j)} & \text{for } C_z \leq C_n \end{cases} \tag{3.86}$$

Enhanced MAP Filter

Lopes et al [55],[54],[52] extend the MAP filter proposed by Kuan [41] to work with Gamma distributed scenes and also propose to restrict the filter to replace the pixels with their estimate only in the areas where $C_n \leq C_z(i,j) \leq C_{max}$ so that the homogenous area will be replaced simply by its mean, while the pixels in textured areas are not modified. In summary, the enhanced filter function for a Gamma distributed scene is described by:

$$\hat{x}(i,j) = \begin{cases} \overline{z(i,j)} & \text{for } C_z(i,j) \leq C_n \\ \frac{(\alpha-m-1)\overline{z(i,j)}+\sqrt{\overline{z(i,j)}^2(\alpha-m-1)^2+4\alpha m\overline{z(i,j)}}}{2\alpha} \cdot z(i,j) & \text{for } C_n < C_z(i,j) < C_{max} \\ z(i,j) & \text{for } C_z(i,j) \geq C_{max} \end{cases} \tag{3.87}$$

where m is the number of looks, $C_{max}(i,j) = \sqrt{2}C_n$, and $\alpha = \frac{1+C_n^2}{C_z^2(i,j)-C_n^2}$.

3.2.9 Other Filters

Arsenault [5] combined the local statistics approach for additive noise with Homomorphic scheme. Based on the signal model of equation 3.88

$$z(i,j) = x(i,j) + Kx(i,j)\eta \tag{3.88}$$

where:

K is a constant, and

η is a Gaussian noise source with zero mean and unity variance.

Based on a film grain model, the Homomorphic transformation is formulated as:

$$G(i,j) = \frac{255}{\ln 256}\ln(x(i,j)+1) \tag{3.89}$$

Once the data is transformed in the new domain, the Lee filter [44] is used to remove the additive noise. The filtered image is then recovered by an inverse Homomorphic transformation.

However, Durand et al. [19] found that this filter performed less satisfactorily than the extended multiplicative noise model derived by Lee [44] discussed above.

Another speckle reduction method that does not use a model of the SAR image is the Crimmins geometric filter [16]. The Crimmins filter uses a morphological process referred to as the complementary eight-hull algorithm to "fill in the narrow valleys and break down the narrow peaks". This algorithm utilizes the correlation between the speckle of adjacent pixels and results in a smoothed image. However, the Crimmins geometric filter does not take into account the multiplicative nature of the speckle noise. Thus, the noise at higher intensities will remain while the values at lower intensities will be overly smoothed. It also requires that the image be detected and mapped to a relatively small dynamic range to work reasonably well.

It is very difficult to filter the speckle and preserve the edges, both Lee and Nezry et al [58][49] proposed the use of multiple pass to filter speckle image. The initial pass is to determine where the edges are located on the image, then various schemes are used to filter out the speckles according to the homogeneity of the locality. Unfortunately, the signal to noise ratio of radar images is very low, normal robust edge detector for optical images does not function well. Different edge detection schemes are proposed and experimented. The success of these filters is dependent on the success of the edge detection process. This is somewhat a catch-22 situation. On one hand, speckle filtering is supposed to reduce the speckle noise in order that subsequent interpretation or classification of the image can be done more efficiently and more accurately. At any rate, this brings out another field of interesting research opportunity: detection of edges in the presence of speckle noise.

This approach is in its infancy. As observed by Lee [49] *the speckle smoothing capability of this filter is somewhat inferior to the straight local statistics filter, because the non-square window contains only a reduced set of pixels in the 7 x 7 window.*

3.3 Kalman Filtering of SAR Images

As mentioned in previous sections, the speckle reduction of SAR images has still not found a robust solution. In chapter 7 we will give a series of results of various filters applied to a series of test images, some of them bearing speckle noise collected from homogeneous areas of real SAR images. The quality of various filters can be observed especially in Figures 7.31 - 7.37. The test image for this test was built using a linear pattern image as shown in Figure 7.29 which was multiplied with a speckle noise as given in Figure 7.30.

From the above sections it can also be seen that each filter introduced a more complicated filtering equation whose complexity increased with the assumed image model. Eventually in the MAP filter Kuan [41, 40] assumed a linear model for the observed image.

The use of linear model infers the investigation of using the best linear estimator for signals embedded in noise which is the Kalman filter. Kalman filtering has been used extensively in processing of 1-D AR processes to achieve a linear estimate of the least square error solution [30]. The Kalman filter was extended to the 2-D case by Habibi [31]. However, the straight application of a Kalman filter to the 2-D case is difficult due to the large computational and spatial requirements. For SAR image filtering the literature mentions the paper by Azimi-Hadjadi et al. [8], despite the fact that in that paper no real SAR image was used to demonstrate the validity of the claims. We can state, as per our literature search, that the first application of Kalman filtering were reported in [26, 27] which was the object of Gary Geling's thesis [24].

The Kalman filtering problem is a problem in two parts; first a linear model is to be identified using one of the many parameter identification methods developed mainly for control systems [51] or others, and secondly, obtain an appropriate discrete Kalman filter (equations) for the model identified in the first part of this procedure. These leave the researcher in this field with a set of degrees of freedom; in other words it is up to the researcher to choose the appropriate model and filter such that the best results are obtained.

Definitely, the experimental part plays a tremendous role in choosing the right version of the model and filter (Kalman). We can state that there are no theoretical guidelines of how to choose the image model and how to apply the most appropriate Kalman filter.

In [24] two main models for speckle reduction in SAR images using Kalman filtering were investigated, mainly a half and a full plane block Kalman filter, which were adaptive versions of the corresponding filters by Azimi-Sadjadi [10, 15]. The best results were obtained for the half plane Kalman filter which introduced a multiplicative noise in the state equation and for the adaptive full plane block Kalman filter in [24]. A comparison with the results obtained by other filters and with the original filters proposed by Azimi-Sadjadi can be found in [24, 26, 27] and in Chapter 7 of this thesis where some tests and results obtained in [24] are extended and brought to a scientific basis. In what follows we will continue, therefore, to investigate the improvements which can be brought to the full plane Kalman filter in various noise conditions. In the end we will sketch an optimal method which will eliminate the guessing of the various noise covariances which have to be a priori known by the researcher $\sigma_u^2, \sigma_v^2, \sigma_x^2, \sigma_\gamma^2$, etc.

In both methods developed by Azimi-Sadjadi and improved by Geling, the observed images are modeled as a linear two dimensional autoregressive (AR) process [36]. It has to be mentioned from the beginning that the complexity of this method implies a large number of computations and, therefore, more computational time and more powerful computers.

However, some reductions with respect to the above complexity were brought to this problem. The large number of computational and spatial demands was first reduced when Woods et al. developed several filters, such as the reduced update Kalman filter (RUPK) [87] [84], that were efficient and could be used to process images that were modeled as linear AR processes. These filters were expanded to include on-line parameter estimation [38], linear space invariant(LSI) blur correction [86], and multiple parallel models for edge preservation [77]. Roesser [68] also derived a single input, single output 2-D state space model that possessed a separable impulse response and divided the state into vertical and horizontal components. Zhang and Steenart [88] presented a high speed Kalman filter with LSI blur correction based on Roesser's model [24]

Azimi-Sadjadi has investigated and experimented a few models for Kalman filters, starting with his researches for his Ph.D. thesis [6]. Thus, Azimi-Sadjadi and King [10] derived a general 2-D recursive multiple input, multiple output system based on the Roesser 2-D state space model. This system took advantage of special block structures to implement efficient 2-D filters by applying fast convolution methods [1]. The concept of a 2-D block processor was extended to Kalman filtering and applied to SAR imagery [7]. In order to model SAR imagery, the speckle noise was approximated by the inclusion of a multiplicative noise term in the equations. The 2-D block Kalman filter also included on-line parameter estimation based on local statistics. The adaptive nature of the on-line parameter estimation allowed the filter to be applied to a globally non-stationary image while assuming only local stationarity of the image within the blocks being processed, and global stationarity of the noise process [9]. Further modifications included the expansion of the region of support to a non-symmetric half plane block with special block attributes that increased the order of the filter [8].

The 2-D adaptive block Kalman filter(ABKF) was demonstrated to reduce speckle on relatively homogenous images. However, several simplifications were made in order to reduce the computational work load for this algorithm. For the case of images with large non-homogenous regions such as urban regions or land/sea boundaries, these simplifications create difficulties and the filter fails to work properly in speckle noise conditions. The main computational burden of the filter in [8] is the calculation of the derivative of the Kalman gain term for the parameter estimation. It was assumed that the gain would converge to its steady state value very quickly, and the gain was set to a constant value after an experimentally determined number of runs. The model also weighted the on-line parameter estimation so that the filter parameters would converge to global steady state values. The combination of selecting a steady state gain and using the steady state filter parameters removes the filter's adaptive capability, leading to blurring at edges and large block effects. The Kalman filter, as presented by Azimi-Sadjadi, also assumes a stationary multiplicative noise condition, i.e. it assumes the multiplicative noise statistics are constant over the entire image [24].

In the next section, the Kalman filter technique developed by G. Geling in [24] with emphasis on the most useful one known as the Full Plane Adaptive Kalman Filter (FPAKF) will be discussed, and references to the improvements designed into this technique, by Geling and Ionescu, in order to apply it to SAR processes will be given.

3.4 Fullplane Kalman filters

3.4.1 A General 2-D Linear Model for Kalman Filtering

Images are two dimensional discrete signals and so must be a linear model which describes the image in terms of inputs, states, and outputs. If each discrete point (pixel) in an image is represented by an observed value $y(i,j) \in \mathcal{I}_{16}$, where i is the pixel direction, j the line direction, and $\mathcal{I}_{16}$ is the intensity, the dynamic linear single-input single-output (SISO) model can be represented as follows [79]:

$$\begin{aligned} x(i+1,j+1) &= a_{0,1}x(i+1,j)+a_{0,2}x(i+1,j-1)+\cdots a_{0,n-1}x(i+1,j-n+1)+ \\ &\quad a_{1,0}x(i,j+1)+a_{1,1}x(i,j)+a_{1,2}x(i,j-1)+\cdots \\ &\quad \vdots \\ &\quad +a_{m-1,0}x(i-m+1,j+1)+a_{m-1,1}x(i-m+1,j)+\cdots \\ &\quad +a_{m-1,n-1}x(i-m+1,j-n+1)+bu(i+1,j+1) \qquad (3.90) \\ y(i+1,j+1) &= cx(i+1,j+1)+dv(i+1,j+1) \qquad (3.91) \end{aligned}$$

where:

x(i+1,j+1)	is the value of the system at location i+1,j+1,
y(i+1,j+1)	is the observed value of the system at location i+1,j+1,
a,b,c and d	are the parameters of the system,
u(i+1,j+1)	is the additive input noise, and
v(i+1,j+1)	is the additive observation noise.

The model above uses a quarter-plane region of support such that the causality is preserved. On the other hand, Kalman filtering is usually limited to the quarter plane or half plane regions of support in 2-D image processing. As a consequence, the pixels adjacent to the pixel being calculated that are in the "future" of the dynamic process are ignored. It results in biasing the estimates directionally.

3.4.2 A Full Plane Semicausal Model for SAR Speckle Reduction

In order to reduce the storage requirements of the filter and the problem of directional biasing, Citrin and Azimi-Sadjadi [15] developed a semi-causal Kalman filter with a full-plane region of support. The filter processes from left to right in strips without using the results of previous passes above the current pass. The mapping for the region of support for this filter is given in Figure 3.3 which is borrowed from [24].

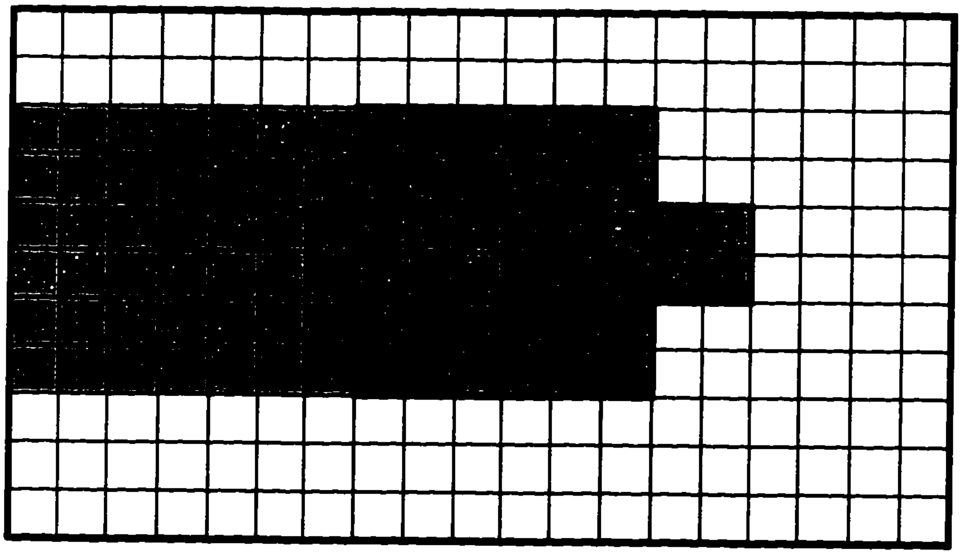

Figure 3.3: Full Plane region of support for 2-D AR image model.

The full plane filter is the combination of four Kalman filters : three employ causal regions of support while the fourth is semi-causal and is dependent on the output of the first three. As shown in Figure 3.3 the linear model contains blocks of pixels instead of pixels. The general linear model will be in this case as given by the equations;

$$X_k = \mathbf{A}\mathbf{X}_{k-1} + \mathbf{B}\mathbf{U}_k \quad \textit{state transition} \tag{3.92}$$

$$Y_k = C\Gamma_k X_k + V_k \quad \textit{observation} \tag{3.93}$$

where A, B, C are matrices whose dimensions depend on the choice of the blocks shown in the Figure 3.3 (their specific structure will be given in details in the next chapter).

The filter has been modified by Gary Geling and D. Ionescu [26] to include the parameter estimation technique given by Ljung and Söderström[51] and by the introduction in the last equation of multiplicative noise matrix Γ such that it can be applied to speckle noise reduction problems. In the remaining part of this thesis, after discussing image models and parameter estimation techniques, the image model will be further refined by the introduction of a multiplicative noise Ψ included in the state transition equation. To bring this model closer to the developments regarding the speckle noise given at the beginning of this section, we will further investigate the effects of considering a Rayleigh, or an exponential distribution for the speckle noise, in the Kalman filter equations. We will gradually introduce these modifications such that all possible noise contributions are inspected. All these filters will be passed through the series of designed tests as presented in Chapter 7. Eventually, the filtering will be done using optimal covariance matrices for the additive noise in the state and in the output. This technique can be applied to all kinds of noise distributions (Rayleigh or exponential), and also to the multiplicative noises. We will develop the optimal procedure for the Gaussian noise assumption only, other combinations following the same path.

3.5 Conclusion

SAR images filtering was the object of a series of researches. Some filters for cleaning a SAR image have been designed and their performance illustrated on some examples of SAR images. This chapter provides a technical review of the digital filters designed to suppress or minimize the effects of speckle on radar imagery. The underlying principles and the equations of these filters are described. The popular and significant speckle suppression filters reviewed are mainly the local statistical filters using fixed size moving windows, homomorphic filters, and the more sophisticated Kalman filters. Most of these filters, other than Kalman filters, are based on simple noise models and different schemes of utilizing local statistics derived from a moving window. The Kalman filters are more elaborate in modelling the image state and different kinds of noise (including the speckle noise, thermal noise etc.). The Kalman filter approach, while being more sophisticated, has suffered from the high demand of computational power. As the computational power increased tremendously in the recent decades, this restriction is aleviated. The capability of the Kalman filter to model more complex noise conditions becomes more attractive to the researchers. The computational barrier has gradually been eroded. This chapter provides, in the last few sections, the descripiton of a few Kalman filters developed for speckle suppression.

Chapter 4

Two Full Plane Kalman Filters for Speckle Noise Reduction in SAR Images

4.1 Introduction

For filtering Gaussian noise in linear systems Kalman and Bucy [30] developed a filter which minimizes the error covariance. Using an optimization technique it is the best of all for the problems which fall in its assumptions.

Kalman filters were tried on images (optical) a long time ago [4] . Azimi-Sadjadi and Bannour claimed in [9] that a Kalman filter which they have developed can be applied to SAR images for speckle reduction. Geling in [24] tested the possibilities of using the above filter for SAR speckle reduction. He showed that, as the filter was designed, it cannot be applied to real SAR images. The image presented by Azimi-

Sadjadi and Bannour in their paper [9] was an optical image on which a known speckle noise was added. Geling in [24] brought a few modifications to the initial filter developed by the above authors. A series of tests and results were presented in his work. The main conclusion was that the Kalman filter, which uses a full plane as a region of support, is the best candidate for being used for speckle reduction in SAR images. Hereafter we will develop further the full plane methodology for the application of the Kalman filter to the speckle noise reduction problem.

4.2 The Full Plane Kalman Filter

4.2.1 Building a Full Plane Image Model

The restrictions imposed on the region of support in order to preserve causality [31],[68],[88], [87] have the drawback of ignoring those pixels adjacent to the pixel being calculated that are in the "future" of the dynamic process. This results in directionally biased estimates and, as a consequence, in asymmetric distortions to the image that greatly detract from the image. On the other hand a non-symmetric region of support requires the states for the entire previous row processed to be saved.

In order to overcome these drawbacks Citrin and Azimi-Sadjadi [15] also developed a semi-causal Kalman filter with a full plane region of support. The filter processes from left to right in strips without using the results of previous passes above the current pass.

The equations and the basic blocks of the full plane filter are given as in Figure 3.3 and as described in Chapter 3. For the ease of reading, the model given in

Chapter 3 is rewritten below as :

$$\begin{aligned} X_k &= \mathbf{A}X_{k-1} + \mathbf{B}U_k \quad \textit{state transition} && (4.1)\\ Y_k &= \mathbf{C}\Gamma_k X_k + V_k \quad \textit{observation} && (4.2) \end{aligned}$$

where A, B, C are matrices whose dimensions depend on the choice of the blocks shown in Figure 3.3; their specific structure will be developed below.

In [15] the model is built based on the assumption that the image blocks on the trailing edge, $\mathbf{X}_0$, $\mathbf{X}_1$, $\mathbf{X}_2$, $\mathbf{X}_3$, and $\mathbf{X}_4$, are copied from the block to their right. Only the remaining blocks $\mathbf{X}_5$, $\mathbf{X}_6$, $\mathbf{X}_7$ and $\mathbf{X}_8$ are related through a 2-D dynamic process equations as expressed by the following set of block-vector equations.

Let $\mathbf{X}_i(k)$ denote the block $\mathbf{X}_i$ at iterative step k, and $\mathbf{X}_i(k-1)$ the block $\mathbf{X}_i$ at iterative step $k-1$, Then,

$$\begin{aligned} \mathbf{X}_0(k) &\Leftarrow \mathbf{X}_1(k-1) && (4.3)\\ \mathbf{X}_1(k) &\Leftarrow \mathbf{X}_5(k-1) && (4.4)\\ \mathbf{X}_2(k) &\Leftarrow \mathbf{X}_3(k-1) && (4.5)\\ \mathbf{X}_3(k) &\Leftarrow \mathbf{X}_7(k-1) && (4.6)\\ \mathbf{X}_4(k) &\Leftarrow \mathbf{X}_6(k-1) && (4.7)\\ A'_{05}\mathbf{X}_5(k) &\Leftarrow A'_{54}\mathbf{X}_4(k-1) + A'_{55}\mathbf{X}_5(k-1) + A'_{56}\mathbf{X}_6(k)(k-1) &&\\ &\quad +A'_{57}\mathbf{X}_7(k-1) + \mathbf{U}_5 && (4.8)\\ A'_{06}\mathbf{X}_6(k) &\Leftarrow A'_{66}\mathbf{X}_6(k-1) + \mathbf{U}_6 && (4.9)\\ A'_{07}\mathbf{X}_7(k) &\Leftarrow A'_{74}\mathbf{X}_4(k-1) + A'_{75}\mathbf{X}_5(k-1) + A'_{76}\mathbf{X}_6(k-1) &&\\ &\quad +A'_{77}\mathbf{X}_7(k-1) + \mathbf{U}_7 && (4.10)\\ A'_{08}\mathbf{X}_8(k) &\Leftarrow A'_{80}\mathbf{X}_0(k-1) + A'_{81}\mathbf{X}_1(k-1) + \ldots + A'_{88}\mathbf{X}_8(k-1) + \mathbf{U}_8 && (4.11) \end{aligned}$$

such that the matrix $\mathbf{A}$ will be given by:

$$\mathbf{A} = \begin{bmatrix} \mathbf{0} & \mathbf{I} & \mathbf{0} & \mathbf{0} & \mathbf{0} & \mathbf{0} & \mathbf{0} & \mathbf{0} & \mathbf{0} \\ \mathbf{0} & \mathbf{0} & \mathbf{0} & \mathbf{0} & \mathbf{0} & \mathbf{I} & \mathbf{0} & \mathbf{0} & \mathbf{0} \\ \mathbf{0} & \mathbf{0} & \mathbf{0} & \mathbf{I} & \mathbf{0} & \mathbf{0} & \mathbf{0} & \mathbf{0} & \mathbf{0} \\ \mathbf{0} & \mathbf{0} & \mathbf{0} & \mathbf{0} & \mathbf{0} & \mathbf{0} & \mathbf{0} & \mathbf{I} & \mathbf{0} \\ \mathbf{0} & \mathbf{0} & \mathbf{0} & \mathbf{0} & \mathbf{0} & \mathbf{0} & \mathbf{I} & \mathbf{0} & \mathbf{0} \\ \mathbf{0} & \mathbf{0} & \mathbf{0} & \mathbf{0} & A_{54} & A_{55} & A_{56} & A_{57} & \mathbf{0} \\ \mathbf{0} & \mathbf{0} & \mathbf{0} & \mathbf{0} & \mathbf{0} & \mathbf{0} & A_{66} & \mathbf{0} & \mathbf{0} \\ \mathbf{0} & \mathbf{0} & \mathbf{0} & \mathbf{0} & A_{74} & A_{75} & A_{76} & A_{77} & \mathbf{0} \\ A_{80} & A_{81} & A_{82} & A_{83} & A_{84} & A_{85} & A_{86} & A_{87} & A_{88} \end{bmatrix} \tag{4.12}$$

A block- state-vector has the structure depicted in the Figure 4.1, where the dimension of each block is consider to be $n \times n = 2 \times 2$,

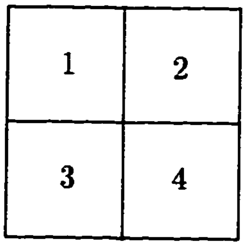

Figure 4.1: Example Mapping of 2-D blocks to Block Vector. Number corresponds to Location in X Vector.

while the $\mathbf{X}_5$, $\mathbf{X}_6$, $\mathbf{X}_7$ and $\mathbf{X}_8$ block-state-vectors are mapped into their parameters of the blocks of the **A** matrix as shown in Figure 4.2

The A' matrices are combined to calculate the state transition equations. One possible choice of input-output model parameters for the parameter estimations and the mapping to the full plane model for $m = 2$ is given below. The a_0 parameter is shown set to -1. According to Geling [24] the intimate structure of the **A** matrix is

1	2	0
3	4	

Mapping for elements 1 & 2 of X_6

5	6	
1	2	0

Mapping for elements 3 & 4 of X_6

7	8	0
9	10	11
12	13	14

Mapping for X_5

20	21	22
17	18	19
15	16	0

Mapping for X_7

23	24	25	26	27
28	29	30	31	32
33	34	0	35	36
37	38	39	40	41
42	43	44	45	46

Mapping for X_8

Figure 4.2: Example Mapping Full Plane Parameters to Each Region of Support. Number corresponds to Location in Parameter Vector.

given by the set of A_{ij} block-matrices:

$$A'_{05} = \begin{bmatrix} -1 & 0 & a_{11} & 0 \\ a_8 & -1 & a_{10} & a_{11} \\ 0 & 0 & -1 & 0 \\ 0 & 0 & a_8 & -1 \end{bmatrix} \text{ and } A'_{55} = \begin{bmatrix} a_7 & a_8 & a_9 & a_{10} \\ 0 & a_7 & 0 & a_9 \\ 0 & 0 & a_7 & a_8 \\ 0 & 0 & 0 & a_7 \end{bmatrix}$$

$$A'_{54} = \begin{bmatrix} a_{12} & a_{13} & 0 & 0 \\ 0 & a_{12} & 0 & 0 \\ a_9 & a_{10} & a_{12} & a_{13} \\ 0 & a_9 & 0 & a_{12} \end{bmatrix} \text{ and } A'_{56} = \begin{bmatrix} a_{14} & 0 & 0 & 0 \\ a_{13} & a_{14} & 0 & 0 \\ a_{11} & 0 & a_{14} & 0 \\ a_{10} & a_{11} & a_{13} & a_{14} \end{bmatrix}$$

$$A'_{06} = \begin{bmatrix} -1 & 0 & 0 & 0 \\ a_2 & -1 & a_4 & 0 \\ 0 & 0 & -1 & 0 \\ a_6 & 0 & a_2 & -1 \end{bmatrix} \text{ and } A'_{66} = \begin{bmatrix} a_1 & a_2 & a_3 & a_4 \\ 0 & a_1 & 0 & a_3 \\ a_5 & a_6 & a_1 & a_2 \\ 0 & a_5 & 0 & a_1 \end{bmatrix}$$

$$A'_{07} = \begin{bmatrix} -1 & 0 & 0 & 0 \\ a_{16} & -1 & 0 & 0 \\ a_{19} & 0 & -1 & 0 \\ a_{18} & a_{19} & a_{16} & -1 \end{bmatrix} \text{ and } A'_{77} = \begin{bmatrix} a_{15} & a_{16} & 0 & 0 \\ 0 & a_{15} & 0 & 0 \\ a_{17} & a_{18} & a_{15} & a_{16} \\ 0 & a_{17} & 0 & a_{15} \end{bmatrix}$$

$$A'_{74} = \begin{bmatrix} a_{20} & a_{21} & a_{17} & a_{18} \\ 0 & a_{20} & 0 & a_{17} \\ 0 & 0 & a_{20} & a_{21} \\ 0 & 0 & 0 & a_{20} \end{bmatrix} \text{ and } A'_{76} = \begin{bmatrix} a_{22} & 0 & a_{19} & 0 \\ a_{21} & a_{22} & a_{18} & a_{19} \\ 0 & 0 & a_{22} & 0 \\ 0 & 0 & a_{21} & a_{22} \end{bmatrix}$$

$$A'_{08} = \begin{bmatrix} -1 & a_{35} & a_{39} & a_{40} \\ a_{34} & -1 & a_{38} & a_{39} \\ a_{30} & a_{31} & -1 & a_{21} \\ a_{29} & a_{30} & a_{34} & -1 \end{bmatrix} \text{ and } A'_{80} = \begin{bmatrix} a_{23} & a_{24} & a_{28} & a_{29} \\ 0 & a_{23} & 0 & a_{28} \\ 0 & 0 & a_{23} & a_{24} \\ 0 & 0 & 0 & a_{23} \end{bmatrix}$$

$$A'_{81} = \begin{bmatrix} a_{25} & a_{26} & a_{30} & a_{31} \\ a_{24} & a_{25} & a_{29} & a_{30} \\ 0 & 0 & a_{25} & a_{26} \\ 0 & 0 & a_{24} & a_{25} \end{bmatrix} \text{ and } A'_{82} = \begin{bmatrix} a_{42} & a_{43} & 0 & 0 \\ 0 & a_{42} & 0 & 0 \\ a_{38} & a_{39} & a_{42} & a_{43} \\ 0 & a_{38} & 0 & a_{42} \end{bmatrix}$$

$$A'_{83} = \begin{bmatrix} a_{44} & a_{45} & 0 & 0 \\ a_{43} & a_{44} & 0 & 0 \\ a_{39} & a_{40} & a_{44} & a_{45} \\ a_{38} & a_{39} & a_{43} & a_{44} \end{bmatrix} \text{ and } A'_{84} = \begin{bmatrix} a_{36} & 0 & a_{41} & 0 \\ a_{35} & a_{36} & a_{40} & a_{41} \\ a_{32} & 0 & a_{36} & 0 \\ a_{31} & a_{32} & a_{35} & a_{36} \end{bmatrix}$$

$$A'_{85} = \begin{bmatrix} a_{27} & 0 & a_{32} & 0 \\ a_{26} & a_{27} & a_{31} & a_{32} \\ 0 & 0 & a_{27} & 0 \\ 0 & 0 & a_{26} & a_{27} \end{bmatrix} \text{ and } A'_{87} = \begin{bmatrix} a_{46} & 0 & 0 & 0 \\ a_{45} & a_{46} & 0 & 0 \\ a_{41} & 0 & a_{46} & 0 \\ a_{40} & a_{41} & a_{45} & a_{46} \end{bmatrix}$$

$$A'_{88} = \begin{bmatrix} a_{33} & a_{34} & a_{37} & a_{38} \\ 0 & a_{33} & 0 & a_{37} \\ a_{28} & a_{29} & a_{33} & a_{34} \\ 0 & a_{28} & 0 & a_{33} \end{bmatrix}$$

$$\mathbf{A}_{54} = -{A'_{05}}^{-1} A'_{54} \tag{4.13}$$

$$\mathbf{A}_{55} = -{A'_{05}}^{-1} A'_{55} \tag{4.14}$$

$$\mathbf{A}_{56} = -{A'_{05}}^{-1} A'_{56} \tag{4.15}$$

$$\mathbf{A}_{57} = 0 \tag{4.16}$$

$$\mathbf{A}_{66} = -{A'_{06}}^{-1} A'_{66} \tag{4.17}$$

$$\mathbf{A}_{74} = -{A'_{07}}^{-1} A'_{74} \tag{4.18}$$

$$\mathbf{A}_{75} = 0 \tag{4.19}$$

$$\mathbf{A}_{76} = -{A'_{07}}^{-1} A'_{76} \tag{4.20}$$

$$\mathbf{A}_{77} = -{A'_{07}}^{-1} A'_{77} \tag{4.21}$$

$$\mathbf{A}_{80} = -{A'_{08}}^{-1} A'_{80} \tag{4.22}$$

$$\mathbf{A}_{81} = -{A'_{08}}^{-1} A'_{81} \tag{4.23}$$

$$\mathbf{A}_{82} = -{A'_{08}}^{-1} A'_{82} \tag{4.24}$$

$$\mathbf{A}_{83} = -{A'_{08}}^{-1} A'_{83} \tag{4.25}$$

$$\mathbf{A}_{84} = -{A'_{08}}^{-1} A'_{84} \tag{4.26}$$

$$\mathbf{A}_{85} = -{A'_{08}}^{-1} A'_{85} \tag{4.27}$$

$$\mathbf{A}_{86} = 0 \tag{4.28}$$

$$\mathbf{A}_{87} = -{A'_{08}}^{-1} A'_{87} \tag{4.29}$$

$$\mathbf{A}_{88} = -{A'_{08}}^{-1} A'_{88} \tag{4.30}$$

The **B** matrix can be obtained directly from the set of equations 4.3-4.11 as:

$$\mathbf{B} = \begin{bmatrix} 0 & 0 & 0 & 0 & 0 & 0 & 0 & 0 & 0 \\ 0 & 0 & 0 & 0 & 0 & 0 & 0 & 0 & 0 \\ 0 & 0 & 0 & 0 & 0 & 0 & 0 & 0 & 0 \\ 0 & 0 & 0 & 0 & 0 & 0 & 0 & 0 & 0 \\ 0 & 0 & 0 & 0 & 0 & 0 & 0 & 0 & 0 \\ 0 & 0 & 0 & 0 & 0 & B_{55} & 0 & 0 & 0 \\ 0 & 0 & 0 & 0 & 0 & 0 & B_{66} & 0 & 0 \\ 0 & 0 & 0 & 0 & 0 & 0 & 0 & B_{77} & 0 \\ 0 & 0 & 0 & 0 & 0 & 0 & 0 & 0 & B_{88} \end{bmatrix} \tag{4.31}$$

where

$$\mathbf{B}_{55} = -{A'_{05}}^{-1} \tag{4.32}$$

$$\mathbf{B}_{66} = -{A'_{06}}^{-1} \tag{4.33}$$

$$\mathbf{B}_{77} = -{A'_{07}}^{-1} \tag{4.34}$$

$$\mathbf{B}_{88} = -{A'_{08}}^{-1} \tag{4.35}$$

while the matrix **C** is given by:

$$\mathbf{C} = \begin{bmatrix} 0 & 0 & 0 & 0 & 0 & \mathbf{I} & 0 & 0 & 0 \\ 0 & 0 & 0 & 0 & 0 & 0 & \mathbf{I} & 0 & 0 \\ 0 & 0 & 0 & 0 & 0 & 0 & 0 & \mathbf{I} & 0 \\ 0 & 0 & 0 & 0 & 0 & 0 & 0 & 0 & \mathbf{I} \end{bmatrix} \tag{4.36}$$

The matrix Γ is the multiplicative noise matrix present in the observation which generates the speckle, and obviously is a square matrix having the dimensions (4 ×

$N)\times(4\times N)$. For the beginning we will assume Γ as produced by a matricial Gaussian noise. Later on we will work out a Kalman filter with other noise assumptions on Γ.

4.2.2 Kalman Filter Equations for a Full Plane Region of Support

The derivation of the Kalman filter equations will be done following the general derivation of the discrete Kalman filter. For the full plane model the equations are similar to the general case, the only difference being the presence of the multiplicative noise Γ. Based on the block state space model given in the equations 4.1 and 4.2

where the noise processes are Gaussian with the statistics as follows

$$
\begin{aligned}
\mathcal{E}[U_k] &= 0 && \textit{process noise} && (4.37)\\
\mathcal{E}[U_k U_{k-l}^T] &= \sigma_u^2 \mathbf{I}\delta_k && && (4.38)\\
\mathcal{E}[V_k] &= 0 && \textit{observation noise} && (4.39)\\
\mathcal{E}[V_k V_{k-l}^T] &= \sigma_v^2 \mathbf{I}\delta_k && && (4.40)\\
\mathcal{E}[\Gamma_k] &= \mu_\gamma && \textit{multiplicative noise} && (4.41)\\
\mathcal{E}[\Gamma_k \Gamma_{k-l}^T] &= \sigma_\gamma^2 \mathbf{I}\delta_k + \mu_\gamma^2 \mathbf{I} && && (4.42)
\end{aligned}
$$

Note that the various noise parameters, u, and v, are independent of the signal, $\mathbf{X}$, and are uncorrelated with respect to each other and with the multiplicative noise Γ.

Using the block form of the filter and following the general procedure shown in detail in [24] which used Grewal and Andrews [30], the Kalman equations for the full plane region of support are as follows:

a priori estimate

$$\begin{aligned} \mathbf{X}_k^{(-)} &= \mathcal{E}[\mathbf{X}_k | \mathbf{X}_{k-1j}^{(+)}] \\ &= \mathbf{A}\mathbf{X}_{k-1}^{(+)} \end{aligned} \tag{4.43}$$

a priori error covariance

$$\begin{aligned} P_k^{(-)} &= \mathcal{E}[(\mathbf{X}_k - \mathbf{X}_k^{(-)})(\mathbf{X}_k - \mathbf{X}_k^{(-)})^T] \\ &= \mathbf{A}P_{k-1}^{(+)}\mathbf{A}^T + \\ &\quad \mathbf{B}\sigma_u^2\mathbf{B}^T \end{aligned} \tag{4.44}$$

innovation

$$\begin{aligned} Z_k &= \mathcal{E}[Y_k - Y_k^{(-)}] \\ &= Y_k - \mathcal{E}[\mathbf{C}\Gamma_k X_k^{(-)} + V_k] \\ &= Y_k - \mu_\gamma \mathbf{C} X_k^{(-)} \end{aligned} \tag{4.45}$$

gain calculation

$$\begin{aligned} R_{z\ k} &= \mathcal{E}[Z_k Z_k^T] \\ &= \mathcal{E}[(\mathbf{C}\Gamma_k X_k + V_k - \mu_\gamma \mathbf{C} X_k^{(-)}) \\ &\quad (\mathbf{C}\Gamma_k X_k + V_k - \mu_\gamma \mathbf{C} X_k^{(+)})^T] \\ &= \mu_\gamma^2 \mathbf{C} P_k^{(-)} \mathbf{C}^T + \sigma_v^2 \mathbf{I} + \ \sigma_\gamma^2(\sigma_{x\ k}^2 + \mu_{x\ k}^2)\mathbf{C}\mathbf{C}^T \end{aligned} \tag{4.46}$$

$$\begin{aligned} K_k &= \mathcal{E}[(X_k - X_k^{(-)}) Z_k^T) R_{z\ k}^{-1} \\ &= \mu_\gamma P_k^{(-)} \mathbf{C}^T R_{z\ k}^{-1} \end{aligned} \tag{4.47}$$

a posteriori estimate

$$X_k^{(+)} = X_k^{(-)} + K_k Z_k \tag{4.48}$$

a posteriori error covariance

$$
\begin{aligned}
P_k^{(+)} &= \mathcal{E}[(X_k - X_k^{(+)})(X_k - X_k^{(+)})^T] \\
&= (\mathbf{I} - \mu_\gamma K_k C) P_k^{(-)} (\mathbf{I} - \mu_\gamma K_k C)^T \\
&\quad + K_k C(\sigma_\gamma^2(\sigma_{x\ k}^2 + \mu_{x\ k}^2))C^T K_k^T + \sigma_v^2 K_{i,j} K_k^T \qquad (4.49) \\
&= (\mathbf{I} - \mu_\gamma K_k C) P_k^{(-)} \qquad (4.50)
\end{aligned}
$$

The values of μ_{x_k} and $\sigma_{x\ k}^2$ used in the calculation of the Kalman filter gain, must be estimated from the local statistics of the image.

4.3 Parameter Estimation

The $(\mathbf{A}, \mathbf{B}, \mathbf{C})$ model used in the calculation of the Kalman filter, have to be identified from image records. For the observed image we will assume that the C matrix is known and as given in 4.36. The **C** matrix can also include known systematic distortions in the imagery.

The parameters of the image model are determined following the recursive prediction error method as presented in [51] and developed in full for the Kalman filter case in [24].

The recursive formula used for the estimate of the parameters are: [51]

$$\hat{\Phi}(t) = \hat{\Phi}(t-1) + \mathcal{L}(t)Z(t) \qquad (4.51)$$

where

$\hat{\Phi}(t)$ is the vector containing the parameter estimates at time t,

$\mathcal{L}(t)$ is the gain for the parameter estimate, and

$Z(t)$ is the innovation or observation error as in (4.45).

In order to derive a model for parameter estimation, a criterion to be minimized is required. A quadratic criterion of the form

$$N(\Phi) = \mathcal{E}[\frac{1}{2}Z^T(t)\Pi^{-1}Z(t)] \tag{4.52}$$

where Π is a positive definite matrix, is often used [51],[8]. It is shown in [51] that the best choice for Π is the true prediction error covariance matrix. It is important to note that this form of criterion gives a substantial penalty for large errors and is sensitive to large measurement errors in the observed process [51].

For such a model of parameter estimation, the criterion may be minimized using the stochastic Newton method. The Newton method is generalized as a successive approximation process of the form

$$f(t+1) = f(t) + k\frac{h(t)}{\frac{d}{dt}h(t)} \tag{4.53}$$

where:

$f(t)$ is the solution,

$h(t)$ is the function being solved, and

k is a gain factor.

Applying this method to solve for the optimal solution to $N(\Phi)$, ie. solving $\frac{dN(\Phi)}{d\Phi} = 0$, gives an equation of the form [51]

$$\begin{aligned} \hat{\Phi}(t) &= \hat{\Phi}(t-1) - \nu(t)\left[\frac{d^2}{d\Phi^2}N(\Phi)\right]^{-1}\left[\frac{d}{d\Phi}N(\Phi)\right]^T & (4.54) \\ &= \hat{\Phi}(t-1) + \nu(t)\left[\frac{d^2}{d\Phi^2}N(\Phi)\right]^{-1}\Delta(t-1)\Pi^{-1}Z(t-1) & (4.55) \end{aligned}$$

where

$\Delta(t)$ is the gradient of the observation error, and

$\nu(t)$ is a time decaying gain factor.

The second derivative, or Hessian, of the criterion can be approximated recursively using the following form [7]:

$$\begin{aligned}\mathcal{R}(t) &\approx \frac{d^2}{d\Phi^2}N(\Phi) &(4.56)\\ \mathcal{R}(t) &= \mathcal{R}(t-1)+\nu(t)[\Delta(t)\Pi^{-1}\Delta^T(t)-\mathcal{R}(t-1)] &(4.57)\end{aligned}$$

The gradient of the observation error can be derived from the Kalman equations (4.45) [7] as

$$\begin{aligned}\Delta(\Phi,t) &= \left[\frac{d}{d\Phi}Y^{(-)}(\Phi,t)\right]^T\\ &= \left[\frac{d}{d\Phi}\mu_\gamma C X^{(-)}(\Phi,t)\right]^T\\ \Delta(\Phi,t) &= [(\mu_\gamma C\Sigma_b(\Phi,t)]^T &(4.58)\end{aligned}$$

where $\Sigma_b(\Phi,t)$ is the derivative of the *a priori* estimate from the Kalman filter (4.43).

$$\Sigma_b(\Phi,t)=\frac{d}{d\Phi}X^{(-)}(\Phi,t) \tag{4.59}$$

The calculation of (4.59) requires the derivative of the Kalman equations (4.43) - (4.50), and it should be noted that the calculation of the derivative of the gain function is computationally intensive [8].

The best estimate for the value Π has been shown to be the covariance of the innovation process $Z(t)$[51]. This covariance is the R_z term used in the formation of the Kalman filter as given in (4.46).

The formula for the calculation of the estimate of the Hessian given in (4.57) is very sensitive to round-off errors. It is desired that an alternative derivation be used that is more numerically stable. Towards this purpose a sequence, $\lambda(t)$, called the forgetting factor is defined. This factor is dependent on the gain sequence, $\nu(t)$, as follows [51]:

$$\lambda(t)=\frac{\nu(t-1)}{\nu(t)}[1-\nu(t)] \tag{4.60}$$

Using this sequence and a new factor $\mathcal{P}(t)$ related to the Hessian by

$$\mathcal{P}(t) = \nu(t)\mathcal{R}^{-1}(t) \tag{4.61}$$

a form of the parameter gain function $\mathcal{L}(t)$ may be written that is more numerically stable[51].

$$\begin{aligned}
\mathcal{L}(t) &= \mathcal{P}(t-1)\Delta(t)[\Delta^T(t)\mathcal{P}(t-1)\Delta(t) + \lambda(t)R_z(t)]^{-1} && (4.62)\\
\mathcal{P}(t) &= [\mathbf{I} - \mathcal{L}(t)\Delta^T(t)]\mathcal{P}(t-1)[\mathbf{I} - \Delta(t)\mathcal{L}^T(t)]/\lambda(t) \\
&\quad + \mathcal{L}(t)R_z(t)\mathcal{L}^T(t) && (4.63)\\
\Phi(t) &= [\Phi(t-1) + \mathcal{L}(t)Z(t)]_{D\mathcal{M}} && (4.64)
\end{aligned}$$

The calculation of the gain must also be modified so that the parameter vector always results in a stable system as indicated by the mapping function in the right-hand side of (4.64) which has been marked as $[\,]_{D\mathcal{M}}$ as specified in [51]. A common method to achieve this is to multiply the gain $\mathcal{L}(t)$ by a weighting factor that decreases from 1 to zero, and to select the greatest factor that results in a choice of parameters that yield to a stable system. The stability of the system may be verified by solving for the eigen values of the solution and ensuring that all are within the unit circle [51]. A priori knowledge of the stable parameter space may also be used to force the parameters to remain in the region that guarantees a stable solution [3].

4.4 Online Parameter Estimation Equations

The Kalman equations have been given in terms of two dimensions, while the parameter estimation is given in the one dimensional terms of the filter. The 2-D terms must be converted into a form compatible with the parameter estimation.

Therefore, a parameter k is defined:

$$k = i * step_i + j * step_j;$$

where $step_i$ and $step_j$ are the number of iterations of the function that occur for each change in i and j respectively. For the block Kalman filter, $step_i$ is 1, and $step_j$ is equal to the number of blocks in one path across the image.

As well, it is necessary to define a sequence for the forgetting factor, $\lambda(t)$. The forgetting factor indicates the rate at which new information overrides the past. This factor should be a low value initially and should approach a value near 1 as the image is processed in order to achieve a stable result. The function

$$\lambda_k = \lambda_{ss} + \lambda_{rate}(\lambda_{k-1} - \lambda_{ss})$$

defines the forgetting factor [51], where λ_{ss} is the steady state value of λ, and λ_{rate} determines the rate at which the $\lambda(t)$ approaches λ_{ss}.

All of the equations required for the online parameter estimation may now be given in terms of the Kalman equations derived earlier [8, 51].

$$\begin{aligned}
k &= i * step_i + j * step_j && (4.65)\\
\lambda_k &= \lambda_{ss} + \lambda_{rate}(\lambda_{k-1} - \lambda_{ss}) && (4.66)\\
\Delta_k^T(\Phi) &= \mu_\gamma C \Sigma_{b(k)}(\Phi) && (4.67)\\
\mathcal{S}_k &= \Delta_k^T(\Phi)\mathcal{P}_{k-1}\Delta_k(\Phi) + \lambda_k R_{z(k)} && (4.68)\\
\mathcal{L}_k &= \mathcal{P}_{k-1}\Delta_k(\Phi)\mathcal{S}_k^{-1} && (4.69)\\
\mathcal{P}_k &= \frac{1}{\lambda_k}(\mathbf{I} - \mathcal{L}_k\Delta_k^T(\Phi))\mathcal{P}_{k-1}(\mathbf{I} - \mathcal{L}_k\Delta_k^T(\Phi))^T + \mathcal{L}_k R_{z(k)}\mathcal{L}_k^T && (4.70)\\
\Phi_k &= [\Phi_{k-1} + \mathcal{L}_k Z_k]_{\mathcal{D}_M} && (4.71)\\
\kappa_k &= \frac{d}{d\Phi}K_k(\Phi) && (4.72)\\
\Sigma_{a(k)}(\Phi) &= \frac{d}{d\Phi}X_k^{(+)}
\end{aligned}$$

$$\begin{aligned}
&= (\mathbf{I} - \mu_\gamma K_k(\Phi) C)\Sigma_{b(k)}(\Phi) + \kappa_k Z_k(\Phi) && (4.73)\\
\Sigma_{b(k+1)}(\Phi) &= \frac{d}{d\Phi} X_k^{(-)} \\
&= \mathbf{A}(\Phi)\mathbf{\Sigma}_{a(k)}(\Phi) + \frac{d\mathbf{A}(\Phi)}{d\Phi} X_{k-1}^{+} && (4.74)
\end{aligned}$$

The derivative of the Kalman filter gain K_k is calculated as follows:

$$\begin{aligned}
\frac{d}{d\Phi} K_k(\Phi) &= \mu_\gamma \frac{d}{d\Phi}(P_k^{(-)} \mathbf{C}^T R_{z\ k}^{-1}) \\
&= \mu_\gamma \frac{dP_k^{(-)}}{d\Phi} \mathbf{C}^T R_{z\ k}^{-1} + \mu_\gamma P_k^{(-)} \mathbf{C}^T \frac{dR_{z\ k}^{-1}}{d\Phi} && (4.75)\\
\frac{dP_k^{(-)}}{d\Phi} &= \frac{d}{d\Phi}[\mathbf{A} P_{k-1}^{(+)} \mathbf{A}^T + \mathbf{B}\sigma_u^2 \mathbf{B}^T] \\
&= (\frac{d}{d\Phi}\mathbf{A}) P_{k-1}^{(+)} \mathbf{A}^T + \mathbf{A} P_{k-1}^{(+)} \frac{d}{d\Phi}\mathbf{A}^T + \\
&\quad \mathbf{A}(\frac{d}{d\Phi} P_{k-1}^{(+)})\mathbf{A}^T + (\frac{d}{d\Phi}\mathbf{B})\sigma_u^2 \mathbf{B}^T + \mathbf{B}\sigma_u^2(\frac{d}{d\Phi}\mathbf{B}^T) && (4.76)\\
\frac{dP_k^{(+)}}{d\Phi} &= -\mu_\gamma K_k \mathbf{C} \frac{dP_k^{(-)}}{d\Phi} && (4.77)
\end{aligned}$$

In the previous set of equations the derivative of the matrix **A** with respect to its own elements contained as components in the parameter $\mathbf{\Phi}$ has to be calculated. This is done as follows:

$$\frac{d}{d\Phi_i}\mathbf{A} = \begin{bmatrix} 0 & 0 & 0 & 0 & 0 & 0 & 0 & 0 & 0 \\ 0 & 0 & 0 & 0 & 0 & 0 & 0 & 0 & 0 \\ 0 & 0 & 0 & 0 & 0 & 0 & 0 & 0 & 0 \\ 0 & 0 & 0 & 0 & 0 & 0 & 0 & 0 & 0 \\ 0 & 0 & 0 & 0 & 0 & 0 & 0 & 0 & 0 \\ 0 & 0 & 0 & 0 & \frac{d}{d\Phi_i}A_{54} & \frac{d}{d\Phi}A_{55} & \frac{d}{d\Phi}A_{56} & 0 & 0 \\ 0 & 0 & 0 & 0 & 0 & 0 & \frac{d}{d\Phi}A_{66} & 0 & 0 \\ 0 & 0 & 0 & 0 & \frac{d}{d\Phi_i}A_{74} & 0 & \frac{d}{d\Phi_i}A_{76} & \frac{d}{d\Phi_i}A_{77} & 0 \\ \frac{d}{d\Phi_i}A_{80} & \frac{d}{d\Phi_i}A_{81} & \frac{d}{d\Phi_i}A_{82} & \frac{d}{d\Phi_i}A_{83} & \frac{d}{d\Phi_i}A_{84} & \frac{d}{d\Phi_i}A_{85} & 0 & \frac{d}{d\Phi_i}A_{87} & \frac{d}{d\Phi_i}A_{88} \end{bmatrix} \tag{4.78}$$

The expressions for each the above $\frac{d}{d\Phi_i}A_{kl}$ will be calculated according to their definition relations given in 4.13 to 4.30 as in the following:

$$\begin{aligned} \frac{d}{d\Phi_i}\mathbf{A}_{kl} &= -\frac{d}{d\Phi_i}{A'_{0k}}^{-1}A'_{kl} - A'_{0k}\frac{d}{d\Phi_i}A'_{kl} \\ &= {A'_{0k}}^{-1}\frac{d}{d\Phi_i}A'_{0k}{A'_{0k}}^{-1}A'_{kl} - {A'_{0k}}^{-1}\frac{d}{d\Phi_i}A'_{kl} \end{aligned} \tag{4.79}$$

Finally the derivatives for each A_{kl} will be calculated as in the following example where the derivative of A'_{05} will be taken with respect to a_{10}.

$$\frac{d}{da_{10}}\mathbf{A}_{05} = \begin{bmatrix} 0 & 0 & 0 & 0 \\ 0 & 0 & 1 & 0 \\ 0 & 0 & 0 & 0 \\ 0 & 0 & 0 & 0 \end{bmatrix}$$

Similarly the derivative of **B** with respect of Φ is given by :

$$\mathbf{B} = \begin{bmatrix} 0 & 0 & 0 & 0 & 0 & 0 & 0 & 0 & 0 \\ 0 & 0 & 0 & 0 & 0 & 0 & 0 & 0 & 0 \\ 0 & 0 & 0 & 0 & 0 & 0 & 0 & 0 & 0 \\ 0 & 0 & 0 & 0 & 0 & 0 & 0 & 0 & 0 \\ 0 & 0 & 0 & 0 & 0 & 0 & 0 & 0 & 0 \\ 0 & 0 & 0 & 0 & 0 & \frac{d}{d\Phi_i}\mathbf{B}_{55} & 0 & 0 & 0 \\ 0 & 0 & 0 & 0 & 0 & 0 & \frac{d}{d\Phi_i}\mathbf{B}_{66} & 0 & 0 \\ 0 & 0 & 0 & 0 & 0 & 0 & 0 & \frac{d}{d\Phi_i}\mathbf{B}_{77} & 0 \\ 0 & 0 & 0 & 0 & 0 & 0 & 0 & 0 & \frac{d}{d\Phi_i}\mathbf{B}_{88} \end{bmatrix} \tag{4.80}$$

The initial conditions required for the parameter estimation are Φ_0, $\mathcal{R}_0$, λ_0, λ_{rate}, λ_{ss}, and $\Sigma_a(0)$.

As final and general comments which we found very interesting in Geling's [24] work we will mention the following:

- the filter requires no history from each pass through the image, left to right.
- the filter processes only one strip at a time, using the data from three strips from the image. Only the centre strip from each scan through the image is saved.

From the original paper of Azimi-Sadjadi [15] we retained the fact that the filter has a superior SNR as compared with other Kalman filters implementations such as those tried in [31],[68],[88],[87].

The above reasons made us choose to do further research on this subject and apply more advanced Kalman filtering techniques using the Full-Plane Block Adaptive Model (FPBAM).

Reviewing the development of the original FPBKF by Azimi-Sadjadi [8] and testing it over the Victoria images, Geling [24] mentioned that the derived Kalman filter is adaptive only in terms of a variable parameter system and even this condition is weakened when the filter is used to determine a steady state solution for both the Kalman gain and the parameters. The next sections deal with the development of a modified adaptive block Kalman filter for the fullplane case. This filter, modified by Geling [24, 26, 27] so that it becomes truly adaptive over the entire image by evaluating the multiplicative noise assumption for each set of blocks processed, will be further modified by assuming that there is a multiplicative noise in the state of this filter. This will allow the filter to better follow the large variations found in a "speckled" image of urban regions such as that found in the test image of Victoria, B.C., especially when edges have to be preserved.

4.5 Adaptive Kalman Filters

An adaptation index was introduced by Geling in [24] in the structure of the full plane Kalman filter which he applied to the reduction of the speckle noise in SAR image. He got his inspiration from a series of works [44],[19],[40] where this method was justified. It was shown that, over homogeneous regions, the speckle statistics of SAR imagery remain stationary and close to the theoretical values of $1/\sqrt{M}$; where M is the number of looks. However, in areas with strong point reflectors, such as urban regions, the assumption of fully developed speckle is no longer true. To prove this he considered the observation effected by a multiplicative noise as given in the relationship:

$$Y_k = C\Gamma_k X_k + V_k \quad \textit{observation} \tag{4.81}$$

with the following multiplicative noise conditions:

$$\begin{aligned} \mathcal{E}[\Gamma_k] &= \mu_\gamma & \textit{multiplicative noise} \qquad (4.82) \\ \mathcal{E}[\Gamma_k \Gamma_{k-1}^T] &= \sigma_\gamma^2 \mathbf{I} \delta_{k,l} + \mu_\gamma^2 \mathbf{I} & (4.83) \end{aligned}$$

If it is assumed that the statistics of the multiplicative noise are non-stationary over the entire image, then a variable value of σ_γ^2 must be considered.

Following Lopes et al.[55] a criteria to assess the validity of the multiplicative noise assumption for use in many SAR imagery filters was developed. This criteria, known as the coefficient of variation, C_o, is the ratio of the square root of the variance of a region to the mean of the region. For a homogeneous region, this coefficient is also known as the speckle index. This parameter can be used to modify the multiplicative noise term in the state observation equation (4.2).

$$C_o = \frac{\sigma_{y\ k}}{\mu_{y\ k}} \tag{4.84}$$

For regions where the multiplicative noise assumption is valid, the algorithm may be left unchanged. For regions where the coefficient of variation exceeds a given limit, the multiplicative noise assumption is deemed invalid and must be relaxed. Two values must be defined: σ_γ^2 is the value of the multiplicative noise variance over the majority of the image and is typically $\sim 1/\sqrt{M}$; $\sigma_{\gamma\ k}^2$ is a localized value of the multiplicative noise variance that is calculated for each iteration. For a smooth decrease in the effect of this variation a linear decay function, $f(C_o)$, is defined.

$$f(C_o) = \begin{cases} 1 & If\ C_o \leq C_{omax1} \\ \frac{C_{omax2} - C_o}{C_{omax2} - C_{omax1}} & if\ C_{omax1} < C_o < C_{omax2} \\ 0 & \text{otherwise} \end{cases} \tag{4.85}$$

The decay function may now be applied to the multiplicative noise term, $\sigma_{\gamma\ k}$ so that the value of the noise term will be decreased as the assumption becomes less likely, until the multiplicative noise parameter is set to zero at C_{omax2}.

$$\sigma_{\gamma\ k} = f(C_o)\sigma_\gamma \tag{4.86}$$

As well, the parameter estimation must be reduced or terminated for the iteration when the model assumptions no longer hold. This will prevent the parameters from being affected by the errors created by applying the model to localized regions of images that do not fit the model. Consequently, the calculation of the parameter vector in (4.71) must be modified as given in (4.87).

$$\Phi_k = [\Phi_{k-1} + f(C_o)\mathcal{L}_k Z_k]_{\mathcal{D}_M} \tag{4.87}$$

The effect of this modification can be determined by examining the formulation of the gain in (4.47) and (4.46). By setting the multiplicative noise variance term, σ_γ, to zero the value of the gain, K, will have a larger magnitude allowing the filter to better track the change in the image. The parameter estimation is halted so that any large transients are not introduced into the parameter vector.

The values for C_{omax} must be chosen so that the Kalman filter is capable of following the changes in the image over highly variable areas without under-smoothing more homogeneous regions. For an intensity image, the values should be larger than the expected value over a homogeneous region of $C_o = 1/\sqrt{M}$. Lopes et al.[55] suggest a value of $C_{omax} = \sqrt{1 + 2/M}$ for an intensity image. For a one-look intensity image, this results in a value of $C_{omax} = 1.73$.

4.6 A Kalman Filter with State Multiplicative Noise Parameters

Urban regions tend to consist of complicated regions that vary quickly from strong point reflectors to "dark" regions caused by building shadows or multi-path effects on the radar. In order to model this phenomenon, it has been proposed that the change in the radar response between adjacent regions may be related using a multiplicative noise term in the state transition equation. The use of a multiplicative noise parameter in the dynamic equation would allow the filter to follow the image in regions of fast change such as sharp edges. These modified block dynamic equations would be expressed as

$$\begin{aligned} X_k &= \mathbf{A}\Psi X_{k-1} + \mathbf{B}U_k \quad \textit{state transition} && (4.88) \\ Y_k &= \mathbf{C}\Gamma X_k + V_k \quad \textit{observation} && (4.89) \end{aligned}$$

where the matrices $\mathbf{A}, \mathbf{B}$, and $\mathbf{C}$ are the same as in section 4.1 and where the noise process Ψ is Gaussian with the following statistics:

$$\begin{aligned} \mathcal{E}[\Psi_k] &= 1 \quad \textit{multiplicative state noise} && (4.90) \\ \mathcal{E}[\Psi_k \Psi_{k-l}^T] &= \sigma_\psi^2 \mathbf{I}\delta_k + \mathbf{I} && (4.91) \end{aligned}$$

and the remaining noise parameters are

$$\begin{aligned} \mathcal{E}[U_k] &= 0 \quad \textit{process noise} && (4.92) \\ \mathcal{E}[U_k U_{k-l}^T] &= \sigma_u^2 \mathbf{I}\delta_k && (4.93) \\ \mathcal{E}[V_k] &= 0 \quad \textit{observation noise} && (4.94) \\ \mathcal{E}[V_k V_{k-l}^T] &= \sigma_v^2 \mathbf{I}\delta_k && (4.95) \\ \mathcal{E}[\Gamma_k] &= \mu_\gamma \quad \textit{multiplicative noise} && (4.96) \end{aligned}$$

$$\mathcal{E}[\Gamma_k \Gamma_{k-l}^T] = \sigma_\gamma^2 \mathbf{I}\delta_k + \mu_\gamma^2 \mathbf{I} \tag{4.97}$$

Note that the various noise parameters, u, and v, are independent of the signal, $\mathbf{X}$, and are uncorrelated to each other.

We also assume that the multiplicative noise parameters Ψ, are independent of the signal, $\mathbf{X}$, and the other noise parameters, Γ, U, and V.

The local statistics of the image model are also defined for the state variable X as

$$\mathcal{E}[X_k] = \mu_{x\ k} \tag{4.98}$$

$$\mathcal{E}[X_k X_{k-l}^T] = \sigma_{x\ k}^2 \mathbf{I}\delta_k + \mu_{x\ k}^2 \mathbf{I} \tag{4.99}$$

The resulting dynamic model is given as a block diagram in Figure 4.3. Recall that the term z_x^{-1} is the shift operators.

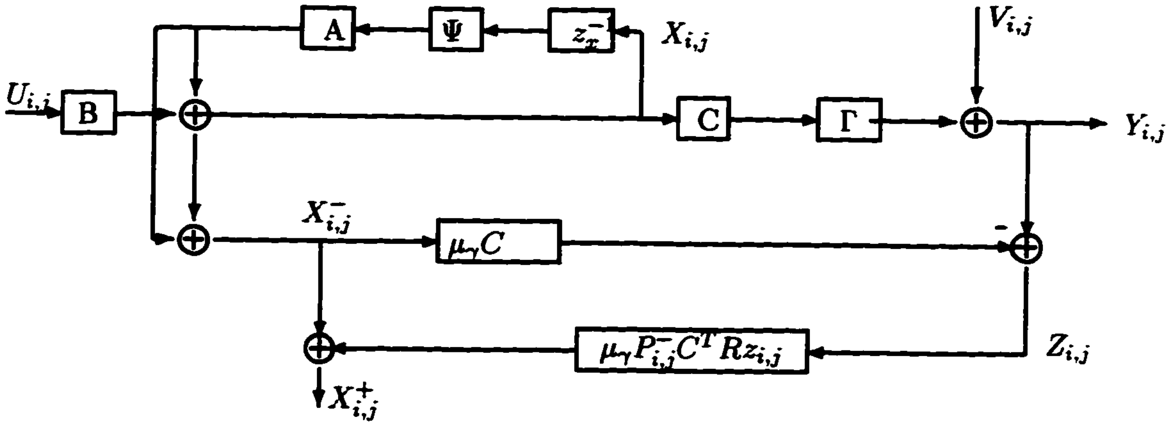

Figure 4.3: Block Diagram of Modified Fullplane Block Kalman Filter.

The re-evaluation of each of the Kalman equations is given here to determine the effects of including a multiplicative noise term, Ψ, in the state transition equation.

a priori estimate

$$\begin{aligned}
\mathbf{X}_k^{(-)} &= \mathcal{E}[\mathbf{X}_k|\mathbf{X}_{k-1}] \\
&= \mathcal{E}[\mathbf{A}\mathbf{\Psi}\mathbf{X}_{k-1} + \mathbf{B}\mathbf{U}_k] \\
&\quad \mathbf{\Psi} \text{ and } \mathbf{X} \text{ are independent, therefore} \\
\mathcal{E}[\mathbf{\Psi}\mathbf{X}] &= \mathcal{E}[\mathbf{\Psi}]\mathcal{E}[\mathbf{X}] \;=\; \mathcal{E}[\mathbf{X}] \\
&\quad \text{Recall } \mathcal{E}[U_k] = 0, \text{ giving} \\
\mathbf{X}_k^{(-)} &= \mathbf{A}\mathbf{X}_{k-1}^{(+)} \qquad (4.100)
\end{aligned}$$

The sub-optimal estimator for this case may be expressed as a function of the *a priori* estimate, $X_k^{(-)}$, and the observation, $\mathbf{Y}$ in the form:

$$\mathbf{X}_k^{(+)} = K_k^1 \mathbf{X}_k^{(-)} + \bar{K}_k \mathbf{Y}_k \qquad (4.101)$$

The orthogonality condition [30] must be met to determine the minimum mean squared error. This can be written as

$$\mathcal{E}[(\mathbf{X}_k - \mathbf{X}_k^{(+)})\mathbf{Y}_l^T] = 0 \qquad 1 \le l < k \qquad (4.102)$$

Using this relationship and the fact that $\mathcal{E}[V_i Y_l] = 0$ for $l < kj$, the expression for the factor K_k^1 may be derived.

$$\begin{aligned}
\mathcal{E}[X_k Y_l^T - X_k^{(+)} Y_l^T] &= 0 \\
&\text{substituting (4.101)} \\
\mathcal{E}[X_k Y_l^T - K_k^1 X_k^{(-)} Y_l^T - \bar{K}_k Y_k Y_l^T] &= 0 \\
&\text{substituting (4.89)}
\end{aligned}$$

$$\begin{aligned}
\mathcal{E}[X_kY_l^T - K_k^1X_k^{(-)}Y_l^T - \bar{K}_kC\Gamma X_kY_l^T - \bar{K}_kV_kY_l^T] &= 0 \\
\mathcal{E}[X_kY_l^T - K_k^1X_k^{(-)}Y_l^T - \bar{K}_kC\Gamma X_kY_l^T] &= 0 \\
\mathcal{E}[(\mathbf{I} - \bar{K}_kC\Gamma)X_kY_l^T - K_k^1X_k^{(-)}Y_l^T &= 0 \\
\mathcal{E}[(\mathbf{I} - \bar{K}_kC\Gamma - K_k^1)X_kY_l^T - K_k^1((X_k^{(-)} - X_k)Y_l^T] &= 0 \\
&\text{using (4.102)} \\
\mathcal{E}[(\mathbf{I} - \bar{K}_kC\Gamma - K_k^1)X_kY_l^T] &= 0 \\
(\mathbf{I} - \bar{K}C\mathcal{E}[\Gamma] - K_k^1)\mathcal{E}[X_kY_l^T] &= 0 \\
(\mathbf{I} - \bar{K}C\mu_\gamma - K_k^1)\mathcal{E}[X_kY_l^T] &= 0 \qquad (4.103)
\end{aligned}$$

This restriction will remain true if the first portion of the expression is zero. Therefore

$$K_k^1 = \mathbf{I} - \bar{K}_kC\mu_\gamma \qquad (4.104)$$

where $\bar{K}_k$ is the Kalman gain and will be simplified to K_k from now on.

Now the estimator, $X_k^{(+)}$ is expressed as

$$\begin{aligned}
X_k^{(+)} &= (\mathbf{I} - K_kC\mu_\gamma)X_k^{(-)} + K_kY_k \\
&= X_k^{(-)} + K_k(Y_k - C\mu_\gamma X_k^{(-)}) \qquad (4.105)
\end{aligned}$$

Using the definition of the innovation

$$Z_k = Y_k - C\mu_\gamma X_k^{(-)} \qquad (4.106)$$

the *a posteriori* estimate now assumes the standard Kalman filter form

$$X_k^{(+)} = X_k^{(-)} + K_kZ_k \qquad (4.107)$$

Using the orthogonality condition again, the two equations

$$\begin{aligned}
\mathcal{E}[(X_k - X_k^{(+)})Y_k^T] &= 0 \\
\mathcal{E}[(X_k - X_k^{(+)})(C\mu_\gamma X_k^{(-)})^T] &= 0
\end{aligned}$$

may be combined to give

$$\mathcal{E}[(X_k - X_k^{(+)})(Y_k - C\mu_\gamma X^{(-)})^T] = 0 \tag{4.108}$$

This equation may be arranged using (4.105), (4.89), and the definition for $P_k^{(-)}$ to determine an expression for the Kalman gain

$$\begin{aligned}
0 &= \mathcal{E}[(X_k - X_k^{(-)} - KY_k + KC\mu_\gamma X_k^{(-)})(Y_k - C\mu_\gamma X^{(-)})^T] \\
0 &= \mathcal{E}[((X_k - X_k^{(-)}) - K(C\Gamma X_k + V_k) + KC\mu_\gamma X_k^{(-)}) \\
&\quad (C\Gamma X_k + V_k - C\mu_\gamma X^{(-)})^T] \\
0 &= \mathcal{E}[(X_k - X_k^{(-)}){X_k}^T\Gamma^T C^T - \\
&\quad (X_k - X_k^{(-)})(X_k^{(-)})^T\mu_\gamma C^T + \\
&\quad (X_k - X_k^{(-)}){V_k}^T - \\
&\quad KC(\Gamma X_k - \mu_\gamma X_k^{(-)}){X_k}^T\Gamma^T C^T + \\
&\quad KC(\Gamma X_k - \mu_\gamma X_k^{(-)})(X_k^{(-)})^T\mu_\gamma C^T - \\
&\quad KC(\Gamma X_k - \mu_\gamma X_k^{(-)}){V_k}^T - \\
&\quad KV_k{X_k}^T\Gamma^T C^T + KV_k(X_k^{(-)})^T\mu_\gamma C^T - KV_kV_k^T]
\end{aligned} \tag{4.109}$$

$$\begin{aligned}
0 &= \mathcal{E}[(X_k - X_k^{(-)})(X_k - X_k^{(-)})^T]\mu_\gamma C^T + \mathcal{E}[(X_k - X_k^{(-)})]\mathcal{E}[V_k] - \\
&\quad KC\mathcal{E}[\Gamma X_k{X_k}^T\Gamma^T - \mu_\gamma X_k^{(-)}{X_k}^T\Gamma^T - \\
&\quad \Gamma X_k{X_k^{(-)}}^T\mu_\gamma + \mu_\gamma X_k^{(-)}{X_k^{(-)}}^T\mu_\gamma]C^T - \\
&\quad KC\mathcal{E}[\Gamma X_k - \mu_\gamma X_k^{(-)}]\mathcal{E}[{V_k}^T] - \\
&\quad K\mathcal{E}[V_k]\mathcal{E}[{X_k}^T\Gamma^T]C^T + K\mathcal{E}[V_k][(X_k^{(-)})^T]\mu_\gamma C^T - K\mathcal{E}[V_kV_k^T]
\end{aligned} \tag{4.110}$$

Simplifying the expectation expressions and substituting for the expression of $P_{i,j}^{(-)}$ gives

$$\begin{aligned}
0 &= P_k^{(-)}\mu_\gamma C^T - \\
&\quad KC\mathcal{E}[\Gamma X_k{X_k}^T\Gamma^T]C^T -
\end{aligned}$$

$$\begin{aligned}
& KC\mu_\gamma P_k^{(-)}\mu_\gamma C^T + \\
& KC\mu_\gamma \mathcal{E}[X_k X_k^T]\mu_\gamma C^T - \\
& K\mathcal{E}[V_k V_k^T] && (4.111) \\
0 \;=\; & \mu_\gamma P_k^{(-)} C^T - \\
& KC((\sigma_\gamma^2 + \mu_\gamma^2)(\sigma_x^2 + \mu_x^2))C^T - \\
& KC\mu_\gamma^2 P_{i,j}^{(-)} C^T + \\
& KC(\mu_\gamma^2(\sigma_x^2 + \mu_x^2))C^T \\
& -K\sigma_v^2 && (4.112) \\
0 \;=\; & \mu_\gamma P_k^{(-)} C^T - K(C\sigma_\gamma^2(\sigma_x^2 + \mu_x^2)C^T + \mu_\gamma^2 C P_k^{(-)} C^T + \sigma_v^2 \mathbf{I}) && (4.113)
\end{aligned}$$

Rearranging for the Kalman gain results in

$$K = P_k^{(-)} C^T \mu_\gamma [\mu_\gamma^2 C P_k^{(-)} C^T + C\sigma_\gamma^2(\sigma_x^2 + \mu_x^2)C^T + \sigma_v^2 \mathbf{I}]^{-1} \tag{4.114}$$

$$R_z = \mu_\gamma^2 C P_k^{(-)} C^T + C\sigma_\gamma^2(\sigma_x^2 + \mu_x^2)C^T + \sigma_v^2 \mathbf{I} \tag{4.115}$$

$$K = P_k^{(-)} C^T \mu_\gamma R_z^{-1} \tag{4.116}$$

To derive the *a posteriori* error covariance,

$$\begin{aligned}
P_k^{(+)} &= \mathcal{E}[(X_k - X_k^{(+)})(X_k - X_k^{(+)})^T] \\
& \quad \text{substituting in (4.105)} \\
P_k^{(+)} &= \mathcal{E}[(X_k - (\mathbf{I} - KC\mu_\gamma)X_k^{(-)} - KY_k)(X_k - (\mathbf{I} - KC\mu_\gamma)X_k^{(-)} - KY_k)^T] \\
&= \mathcal{E}[X_k(X_k^T - (X_k^{(-)})^T(\mathbf{I} - \mu_\gamma CK)^T - (K(C\Gamma X_k + V_k))^T)] - \\
& \quad \mathcal{E}[(\mathbf{I} - KC\mu_\gamma)X_k^{(-)}(X_k^T - (X_k^{(-)})^T(\mathbf{I} - \mu_\gamma CK)^T - (K(C\Gamma X_k + V_k))^T)] - \\
& \quad \mathcal{E}[KC\Gamma X_k(X_k^T - (X_k^{(-)})^T(\mathbf{I} - \mu_\gamma CK)^T - (K(C\Gamma X_k + V_k))^T)] - \\
& \quad \mathcal{E}[KV_k(X_k^T - (X_k^{(-)})^T(\mathbf{I} - \mu_\gamma CK)^T - (K(C\Gamma X_k + V_k))^T)] && (4.117) \\
&= \mathcal{E}[(\mathbf{I} - KC\Gamma)X_k X_k^T(\mathbf{I} - KC\Gamma)^T] -
\end{aligned}$$

$$\begin{aligned}
&\mathcal{E}[(\mathbf{I} - KC\Gamma)X_k^{(-)}X_k^T(\mathbf{I} - KC\mu_\gamma)^T] - \\
&\mathcal{E}[(\mathbf{I} - KC\mu_\gamma)X_k^{(-)}X_k^T(\mathbf{I} - KC\Gamma)^T] + \\
&\mathcal{E}[(\mathbf{I} - KC\mu_\gamma)X_k^{(-)}(X_k^{(-)})^T(\mathbf{I} - KC\mu_\gamma)^T] + \\
&\mathcal{E}[KV_kV_k^TK^T] \qquad (4.118)
\end{aligned}$$

Now adding extra terms to complete the expression for $(X_k - X_k^{(-)})(X_k - X_k^{(-)})^T$, the equation becomes

$$\begin{aligned}
P_k^{(+)} &= (\mathbf{I} - KC\mu_\gamma)\mathcal{E}[(X_k - X_k^{(-)})(X_k - X_k^{(-)})^T](\mathbf{I} - KC\mu_\gamma) + \\
&\quad KC\mathcal{E}[\Gamma X_k X_{i,j}^T \Gamma^T]C^TK^T - KC\mu_\gamma\mathcal{E}[X_kX_k^T]\mu_\gamma C^TK^T + \\
&\quad K\mathcal{E}[V_kV_k^T]K^T
\end{aligned}$$

The expression for $P_k^{(-)}$ may now be substituted, and the expectations replaced by their values so that

$$\begin{aligned}
P_k^{(+)} &= (\mathbf{I} - \mu_\gamma KC)P_k^{(-)}(\mathbf{I} - \mu_\gamma KC)^T + \\
&\quad KC(\sigma_\gamma^2(\sigma_x^2 + \mu_x^2))C^TK^T + \\
&\quad K\sigma_v^2K^T \qquad (4.119) \\
&= (\mathbf{I} - \mu_\gamma KC)P_k^{(-)} - \mu_\gamma P_{i,j}^{(-)}C^TK^T + \\
&\quad KC(\sigma_\gamma^2(\sigma_x^2 + \mu_x^2))C^TK^T + \\
&\quad K(CP_k^{(-)}C^T + \sigma_v^2\mathbf{I})K^T \qquad (4.120)
\end{aligned}$$

By substituting the expression for $\mu_\gamma P_k^{(-)}C^T$ from (4.113) into the above equation, the expression simplifies to

$$P_k^{(+)} = (\mathbf{I} - \mu_\gamma KC)P_k^{(-)} \qquad (4.121)$$

The expression for the *a priori* error covariance

$$P_k^{(-)} = \mathcal{E}[(X_k - X_k^{(-)})(X_k - X_k^{(-)})^T]$$

is now determined by substituting the expressions for X_k and $X_k^{(-)}$ and expanding the resulting expression.

$$\begin{aligned} P_k^{(-)} &= \mathcal{E}[(\mathbf{A}\Psi X_{k-1} + BU_k - \mathbf{A}X_{k-1}^{(+)}) \\ &\quad (\mathbf{A}\Psi X_{k-1} + BU_k - \mathbf{A}X_{k-1}^{(+)})^T] \\ &= \mathcal{E}[\mathbf{A}\Psi X_{k-1}X_{k-1}^T\Psi^T A^T + \mathbf{A}\Psi X_{k-1}U_k^T B^T - \\ &\quad \mathbf{A}\Psi X_{k-1}X_{k-1}^{(+)^T}\mathbf{A}^T + \\ &\quad BU_k X_{k-1}^T\Psi^T\mathbf{A}^T + BU_kU_k^T B^T - \\ &\quad BU_k X_{k-1}^{(+)^T} A^T - \\ &\quad \mathbf{A}X_{k-1}^{(+)}X_{k-1}^T\Psi^T\mathbf{A}^T - \mathbf{A}X_{k-1}^{(+)}U_k^T B^T + \\ &\quad \mathbf{A}X_{k-1}^{(+)}X_{k-1}^{(+)^T}\mathbf{A}^T] \end{aligned} \tag{4.122}$$

Substituting the expressions for the earlier $P_k^{(+)}$ and the cross covariance term, the equation now becomes

$$\begin{aligned} P_k^{(-)} &= \mathbf{A}P_{k-1}^{(+)}\mathbf{A}^T + \mathbf{A}\mathcal{E}[\Psi X_{k-1}X_{k-1}^T\Psi^T]\mathbf{A}^T - \mathbf{A}\mathcal{E}[X_{k-1}X_{k-1}^T]\mathbf{A}^T + \\ &\quad B\mathcal{E}[U_kU_k^T]B^T \end{aligned} \tag{4.123}$$

Since the multiplicative noise, Ψ, and the original image, X, are independent, the result of the combined expectation can be expressed as

$$\mathcal{E}[\Psi X_{k-1}X_{k-1}^T\Psi^T] = \sigma_\psi^2(\sigma_x^2 + \mu_x^2) + \sigma_x^2 + \mu_x^2 \tag{4.124}$$

Recall that

$$\mathcal{E}[X_{k-1}X_{k-1}^T] = \sigma_x^2 + \mu_x^2 \tag{4.125}$$

resulting in the final expression for the *a priori* error covariance of

$$\begin{aligned} P_k^{(-)} &= \mathbf{A}P_{k-1}^{(+)}\mathbf{A}^T + \mathbf{A}(\sigma_\psi^2(\sigma_x^2 + \mu_x^2))\mathbf{A}^T + \\ &\quad \mathbf{B}\sigma_u^2\mathbf{B}^T \end{aligned} \tag{4.126}$$

The above derivations show that only the *a priori* error covariance term changes when the multiplicative noise mean of one is included in the model. The formulation of the recursive parameter estimation remains the same, with only the derivative of *a priori* covariance changing to reflect the new equations. Due to these new terms, the Kalman gain becomes more sensitive to the local statistics. The *a priori* covariance will become larger as a result of these new terms, but as it appears in the gain equation as a multiplicative term and as part of the inverse of R_z, as shown in (4.115), the gain will become slightly larger. In homogeneous regions and regions of low mean value, the effect of the multiplicative noise term in the state transition matrix will be negligible, and the effects should only become noticeable in regions of greater variance and mean. Although there is no proven method to choose the value of the multiplicative noise variance, it should be less than one to maintain the stability of the filter. In the tests presented in Chapter 7 the value is chosen less than 0.25 to avoid the saturation of the filter which would be caused by the presence of too much noise in the model.

4.7 Online Parameter Estimation Equations for the State Multiplicative Noise Case

The online model identification equations for the full plane case given above 4.65 - 4.74 are preserved for the state multiplicative noise case; the only difference is in the derivative of the Kalman filter gain, especially when calculating the derivative for the *a priori* error covariance. For this latter equation the derivative is given by:

$$\begin{aligned}\frac{dP_k^{(-)}}{d\Phi} &= \frac{d}{d\Phi}[\mathbf{A}P_{k-1}^{(+)}\mathbf{A}^T + \mathbf{A}(\sigma_\psi^2(\sigma_x^2 + \mu_x^2))\mathbf{A}^T + \\ &\quad \mathbf{B}\sigma_u^2\mathbf{B}^T]\end{aligned}$$

$$\begin{aligned} &= \frac{d}{d\Phi}\mathbf{A}P_{k-1}^{(+)}\mathbf{A}^T + \mathbf{A}P_{k-1}^{(+)}\frac{d}{d\Phi}\mathbf{A}^T + \\ &\quad \frac{d}{d\Phi}\mathbf{A}(\sigma_\psi^2(\sigma_x^2+\mu_x^2))\mathbf{A}^T + \mathbf{A}(\sigma_\psi^2(\sigma_x^2+\mu_x^2))\frac{d}{d\Phi}\mathbf{A}^T + \\ &\quad \mathbf{A}\frac{d}{d\Phi}P_{k-1}^{(+)}\mathbf{A}^T + \frac{d}{d\Phi}\mathbf{B}\sigma_u^2\mathbf{B}^T + \mathbf{B}\sigma_u^2\frac{d}{d\Phi}\mathbf{B}^T \qquad (4.127) \\ & \qquad (4.128) \end{aligned}$$

The initial conditions required for the parameter estimation are the same as above: Φ_0, $\mathcal{R}_0$, λ_0, λ_{rate}, λ_{ss}, and $\Sigma_a(0)$.

4.8 Conclusions

In this chapter the starting point of a Kalman filtering technique for speckle reduction in SAR images has been introduced. This refers to the work presented in [24] which was inspired by the work of Citrin and Azimi-Sadjadi [15] to which a series of corrections have been brought by Geling. Corrections to the work of Geling have been brought in Section 1 of this chapter. In section two of the present chapter, a new Kalman filter technique for the case of a state multiplicative noise has been proposed; the modification of the parameter estimation technique has been developed accordingly. The motivation of choosing the full plane model resides in the fact of a good return and the absence of the box effect around edges. The latter is produced by the two dimensional block which scans the region of support [9]. In the next chapter two new Kalman filtering techniques will developed: a Kalman filter for Markov noise components in the observation and a Kalman filter for a dynamic state multiplicative noise.

Chapter 5

Kalman Filters with Non-Gaussian Noise for Speckle Reduction

5.1 Introduction

As mentioned in Chapter 2 the speckle noise can be characterized either by exponential or Rayleigh distributions if the one look or the raw complex signal are dealt with, respectively, when applying the Kalman filter for restoring SAR images.

The Kalman filter was designed assuming that Gaussian noise is applied in the state and in the observation equations. A series of papers [49] discussed the presence of a multiplicative noise component in the observations such that the effect of the speckle noise in a real image can be modeled through the following equation:

$$Y_k = C\Gamma_k X_k + V_k \tag{5.1}$$

In some papers the V_k component is not considered in order to facilitate the construction of a fast algorithm which can filter out the speckle to some degree. Some other filters contain this component. In all papers it is agreed on the fact that the speckle has an exponential or Rayleigh distribution. Same references agree on the fact that the multiplicative noise in the observation should be Gaussian such that its final effect becomes closer to the exponential distribution.

In what follows we will keep the Gaussian character of the multiplicative noise valid, however we will modify the hypothesis made on the character of the additive noise in the observation such that the exponential character of the speckle should not be altered by an additive Gaussian noise present in the observation. It is also interesting to study the effect of a Markov noise in the state equation as a multiplicative noise factor. We will, therefore, dedicate this chapter to the study of the effects of Markov noises in the Kalman filter equations especially for the full plane model for SAR images.

Thus, in this chapter two suboptimal Kalman filters for SAR images will be developed following a known methodology for the derivation of Kalman equations when the noise is Markov. The method will take care of the Full Plane Model in both conditions: with and without multiplicative state noise. The adaptive correction to the Kalman filter technique will also be preserved.

5.2 A Kalman Filter for Speckle Noise Reduction in SAR Images Using Markov Noise in the Observation

A series of Kalman filters can be developed if the Gaussian noise hypothesis is dropped. In other words, the noise input variables such as U_k or the noise disturbance variables V_k are not Gaussian but other types. In what follows we will consider in the first step that the output noise (disturbance) has a Markov distribution. However, we will not consider that the input variable U_k follows this distribution, rather we will develop a Kalman filter for a state multiplicative Markov noise.

To this end the full plane model for the dynamic (state) equations of the SAR image will be again considered.

$$\begin{aligned} X_k &= \mathbf{A}X_{k-1} + \mathbf{B}U_k \quad \textit{state transition} && (5.2)\\ Y_k &= \mathbf{C}\Gamma_k X_k + V_k \quad \textit{observation} && (5.3)\end{aligned}$$

To the above set of equations, the equation which describes the dynamic of the Markov noise signal V_k is added.

$$V_{k+1} = \mathbf{F}V_k + \eta_{k+1} \quad \textit{Markov observation noise} \tag{5.4}$$

where $\mathbf{F}$ is a matrix of $(4 \times N) \times (4 \times N)$ which characterizes the dynamic of the Markov noise.

Substituting V_k from this last equation into 5.3 and making the notation:

$$\bar{\mathbf{C}}_k = \mathbf{C}_{k+1}\Gamma\mathbf{A}_k - \mathbf{F}_k\mathbf{C}_k\Gamma \tag{5.5}$$

the following set of equations for the SAR image model with an output Markov noise are obtained:

$$\begin{aligned} X_k &= \mathbf{A}\mathbf{X}_{k-1} + \mathbf{B}\mathbf{U}_k && \textit{state transition} && (5.6) \\ \bar{Y}_k &= \bar{\mathbf{C}}_k X_k + \eta_{k+1} + \mathbf{C}\Gamma\mathbf{U}_{k+1} && \textit{observation} && (5.7) \end{aligned}$$

with the initial conditions:

$$\bar{Y}_0 = \bar{\mathbf{C}}_0 X_0 + V_0 = Y_0 \qquad (5.8)$$

where

$$\bar{Y}_k = Y_{k+1} - \mathbf{F}Y_k \qquad (5.9)$$

The innovation process is now given by:

$$Z_k = \bar{Y}_k - \bar{\mathbf{C}}_k X_k^{(-)} \qquad (5.10)$$

$$Z_k = (\bar{\mathbf{C}}_k X_k + \eta_{k+1} + \mathbf{C}_k\Gamma_k\mathbf{U}_{k+1}) - \bar{\mathbf{C}}X_k^{(-)} \qquad (5.11)$$

The use of a Markov noise in the output modifies the expression of the observation and innovation; the observation becomes a dynamic system as well. The final expression of the Kalman filter gain will also be affected by these changes.

The noise process will be now characterized by the following statistics:

$$\begin{aligned} \mathcal{E}[U_k] &= 0 && \textit{process noise} && (5.12) \\ \mathcal{E}[U_k U_{k-l}^T] &= \sigma_u^2 \mathbf{I}\delta_l && && (5.13) \end{aligned}$$

$$\begin{aligned}
\mathcal{E}[V_k] &= 0 && \textit{observation noise} && (5.14)\\
\mathcal{E}[\eta_k \eta_{k-l}^T] &= \sigma_\eta^2 \mathbf{I}\delta_l && && (5.15)\\
\mathcal{E}[\Gamma_i] &= \mu_\gamma && \textit{multiplicative noise} && (5.16)\\
\mathcal{E}[\Gamma_k \Gamma_{kl}^T] &= \sigma_\gamma^2 \mathbf{I}\delta_{k,l} + \mu_\gamma^2 \mathbf{I} && && (5.17)
\end{aligned}$$

Note that the various noise parameters, u, v, and η are independent of the signal $\mathbf{X}$, as well as the stochastic signal η which is independent of the signal V_k, and are uncorrelated with respect to each other and with the multiplicative noise Γ.

Using the block form of the filter and following the general procedure shown in detail in [24] in which the calculation of the Kalman filter equations were obtained by following the procedure used in Grewal and Andrews [30], the Kalman equations for the full plane region of support with output Markov noise are as follows:
a priori estimate

$$\begin{aligned}
\mathbf{X}_k^{(-)} &= \mathcal{E}[\mathbf{X}_k | \mathbf{X}_{k-1}^{(+)}]\\
&= \mathbf{A}\mathbf{X}_{k-1}^{(+)} \qquad (5.18)
\end{aligned}$$

a priori error covariance

$$\begin{aligned}
P_k^{(-)} &= \mathcal{E}[(\mathbf{X}_k - \mathbf{X}_k^{(-)})(\mathbf{X}_k - \mathbf{X}_k^{(-)})^T]\\
&= \mathbf{A}P_{k-1}^{(+)}\mathbf{A}^T +\\
&\quad \mathbf{B}\sigma_u^2\mathbf{B}^T \qquad (5.19)
\end{aligned}$$

As expected, the a priori error covariance is not affected by the Markov noise present in the observation.

innovation:

$$Z_k = [\bar{\mathbf{Y}}_k - \bar{\mathbf{C}}_k X_k^{(-)}]$$

$$Z_k = (\bar{\mathbf{C}}_k X_k + \eta_{k+1} + \mathbf{C}_k \Gamma_k \mathbf{U}_{k+1}) - \bar{\mathbf{C}}_k X_k^{(-)} \tag{5.20}$$

covariance calculation

$$\begin{aligned} R_{z\ k} &= \mathcal{E}[Z_k Z_k^T] \\ &= \mathcal{E}[(\bar{\mathbf{C}}_k X_k + \eta_{k+1} + \mathbf{C}_k \Gamma_k \mathbf{U}_{k+1} - \bar{\mathbf{C}}_k X_k^{(-)}) \\ &\quad (\bar{\mathbf{C}}_k X_k + \eta_{k+1} + \mathbf{C}_k \Gamma_k \mathbf{U}_{k+1} - \bar{\mathbf{C}}_k X_k^{(-)})^T] \\ &= \mathcal{E}[\bar{\mathbf{C}}_k X_k X_k^T \bar{\mathbf{C}}_k^T] - \mathcal{E}[\bar{\mathbf{C}}_k X_k X_k^{(-)^T} \bar{\mathbf{C}}_k^T] - \\ &\quad \mathcal{E}[\bar{\mathbf{C}}_k X_k^{(-)} {X_k}^T \bar{\mathbf{C}}_k^T] + \mathcal{E}[\bar{\mathbf{C}}_k X_k^{(-)} X_k^{(-)^T} \bar{\mathbf{C}}_k^T] + \\ &\quad \mathcal{E}[\eta_{k+1} \eta_{k+1}^T] + \mathbf{C}_k \mathcal{E}[\Gamma_k \mathbf{U}_{k+1} \mathbf{U}_{k+1}^T \Gamma_k^T] \mathbf{C}_k^T \\ &= \mu_\gamma^2 (\mathbf{C}_{k+1} \mathbf{A}_k - \mathbf{F}_k \mathbf{C}_k) P_k^{(-)} (\mathbf{C}_{k+1} \mathbf{A}_k - \mathbf{F}_k \mathbf{C}_k)^T \\ &\quad + \sigma_\eta^2 \mathbf{I} + \mathbf{C}_k [\sigma_u^2 (\sigma_\gamma^2 + \mu_\gamma^2)] \mathbf{C}_k^T \end{aligned} \tag{5.21}$$

Kalman gain

$$\begin{aligned} K_k &= \mathcal{E}[(X_k - X_k^{(-)}) Z_k^T] R_{z\ k}^{-1} \\ &= \mathcal{E}[(X_k - X_k^{(-)})(\bar{\mathbf{C}}_k X_k + \eta_{k+1} + \mathbf{C}_k \Gamma_k \mathbf{U}_{k+1} - \bar{\mathbf{C}} X_k^{(-)})^T] R_{z\ k}^{-1} \\ &= \mu_\gamma P_k^{(-)} (\mathbf{C}_{k+1} \mathbf{A}_k - \mathbf{F}_k \mathbf{C}_k)^T R_{z\ k}^{-1} \end{aligned} \tag{5.22}$$

a posteriori estimate

$$X_k^{(+)} = X_k^{(-)} + K_k Z_k \tag{5.23}$$

Before the derivation of the *a posteriori* error covariance, a useful expression is derived using the orthogonality principle below:

$$0 = \mathcal{E}[(X_k - X_k^{(+)}) Z_k^T]$$

$$\begin{aligned} 0 &= \mathcal{E}[(X_k - X_k^{(-)} - K_k Z_k) Z_k^T] \\ 0 &= \mathcal{E}[(X_k - X_k^{(-)}) Z_k^T] - \mathcal{E}[K_k Z_k Z_k^T] \end{aligned} \tag{5.24}$$

That is:

$$\mathcal{E}[(X_k - X_k^{(-)}) Z_k^T] = \mathcal{E}[K_k Z_k Z_k^T] \tag{5.25}$$

a posteriori error covariance

$$\begin{aligned} P_k^{(+)} &= \mathcal{E}[(X_k - X_k^{(+)})(X_k - X_k^{(+)})^T] \\ &= \mathcal{E}[((X_k - X_k^{(-)}) - K_k Z_k) \\ &\quad ((X_k - X_k^{(-)}) - K_k Z_k)^T] \\ &= P_k^{(-)} - \mathcal{E}[(X_k - X_k^{(-)}) Z_k^T K_k^T] - \\ &\quad \mathcal{E}[K_k Z_k (X_k - X_k^{(-)})^T] + K_k \mathcal{E}[Z_k Z_k^T] K_k^T \\ &= [I - \mu_\gamma K_k (\mathbf{C}_{k+1} \mathbf{A}_k - \mathbf{F}_k \mathbf{C}_k)] P_k^{(-)} \end{aligned} \tag{5.26}$$

The values of μ_{x_k} and $\sigma_{x\ k}^2$ used in the calculation of the Kalman filter gain must be estimated from the local statistics of the image.

The parameter estimation process is not affected by the presence of the Markov noise in the observation. It is easy to see that the parameter estimation process is affected by the Kalman gain only through its derivative with respect to the system parameters, i.e. the elements of the matrix **A** only. Thus, there are only the derivatives if **A** and **B** which have to be derived. However, the presence of the Markov output noise does not entail a modification of the above matrices.

5.3 Online Parameter Estimation Equations

Due to the Markov noise in the output equation of the state space model of the observed image, the equations required for the online parameter estimation have to be altered by the introduction of the new **C** matrix of equation 5.5. As it was given in chapter 4 they may be given in terms of the corresponding Kalman equations.

$$\begin{aligned}
k &= i * step_i + j * step_j && (5.27)\\
\lambda_k &= \lambda_{ss} + \lambda_{rate}(\lambda_{k-1} - \lambda_{ss}) && (5.28)\\
\Delta_k^T(\Phi) &= \mu_\gamma(\mathbf{CA} - \mathbf{FC})\Sigma_{b(k)}(\Phi) && (5.29)\\
\mathcal{S}_k &= \Delta_k^T(\Phi)\mathcal{P}_{k-1}\Delta_k(\Phi) + \lambda_k R_{z(k)} && (5.30)\\
\mathcal{L}_k &= \mathcal{P}_{k-1}\Delta_k(\Phi)\mathcal{S}_k^{-1} && (5.31)\\
\mathcal{P}_k &= \frac{1}{\lambda_k}(\mathbf{I} - \mathcal{L}_k\Delta_k^T(\Phi))\mathcal{P}_{k-1}(\mathbf{I} - \mathcal{L}_k\Delta_k^T(\Phi))^T + \mathcal{L}_k R_{z(k)}\mathcal{L}_k^T && (5.32)\\
\Phi_k &= [\Phi_{k-1} + \mathcal{L}_k Z_k]_{\mathcal{D}_M} && (5.33)\\
\kappa_k &= \frac{d}{d\Phi}K_k(\Phi) && (5.34)\\
\Sigma_{a(k)}(\Phi) &= \frac{d}{d\Phi}X_k^{(+)} \\
&= (\mathbf{I} - \mu_\gamma K_k(\Phi)(\mathbf{CA} - \mathbf{FC}))\Sigma_{b(k)}(\Phi) + \kappa_k Z_k(\Phi) && (5.35)\\
\Sigma_{b(k+1)}(\Phi) &= \frac{d}{d\Phi}X_k^{(-)} \\
&= \mathbf{A}(\Phi)\mathbf{\Sigma}_{a(k)}(\Phi) + \frac{d\mathbf{A}(\Phi)}{d\Phi}X_{k-1}^{+} && (5.36)
\end{aligned}$$

The derivative of the Kalman filter gain K_k is calculated as follows:

$$\frac{d}{d\Phi}K_k(\Phi) = \mu_\gamma\frac{d}{d\Phi}(P_k^{(-)}(\mathbf{CA} - \mathbf{FC})^T R_{z\ k}^{-1})$$

$$
\begin{aligned}
&= \mu_\gamma \frac{dP_k^{(-)}}{d\Phi}(\mathbf{CA}-\mathbf{FC})^T R_{z\ k}^{-1} + \\
&\quad \mu_\gamma P_k^{(-)} \mathbf{C} \frac{dA}{d\Phi}^T R_{z\ k}^{-1} + \\
&\quad \mu_\gamma P_k^{(-)} (\mathbf{CA}-\mathbf{FC})^T \frac{dR_{z\ k}^{-1}}{d\Phi} && (5.37) \\
\frac{dP_k^{(-)}}{d\Phi} &= \frac{d}{d\Phi}[\mathbf{A}P_{k-1}^{(+)}\mathbf{A}^T + \mathbf{B}\sigma_u^2\mathbf{B}^T] \\
&= (\frac{d}{d\Phi}\mathbf{A})P_{k-1}^{(+)}\mathbf{A}^T + \mathbf{A}P_{k-1}^{(+)}\frac{d}{d\Phi}\mathbf{A}^T + \\
&\quad \mathbf{A}(\frac{d}{d\Phi}P_{k-1}^{(+)})\mathbf{A}^T + (\frac{d}{d\Phi}\mathbf{B})\sigma_u^2\mathbf{B}^T + \\
&\quad \mathbf{B}\sigma_u^2\frac{d}{d\Phi}\mathbf{B}^T && (5.38) \\
\frac{dP_k^{(+)}}{d\Phi} &= -\mu_\gamma(\frac{dK_k}{d\Phi})(\mathbf{CA}-\mathbf{FC})P_k^{(-)} - \\
&\quad \mu_\gamma K_k(\mathbf{CA}-\mathbf{FC})\frac{dP_k^{(-)}}{d\Phi} - \\
&\quad \mu_\gamma K_k\mathbf{C}(\frac{d\mathbf{A}}{d\Phi})P_k^{(-)} && (5.39)
\end{aligned}
$$

The initial conditions required for the parameter estimation are the same as given in chapter 4. Φ_0, $\mathcal{R}_0$, λ_0, λ_{rate}, λ_{ss}, and $\Sigma_a(0)$.

5.4 A Kalman Filter for SAR Speckle Reduction with Markov State Noise

As mentioned before, the Markov noise can be present in the output of the system but might be present in the state equation as a multiplicative Markov noise. We will study hereafter the modifications which have to be brought to the original Kalman filter such that it can also filter this type of noise.

The state equations model for the SAR image is similar to the model presented in Section 2 of Chapter 4, i.e.:

$$\begin{aligned} X_k &= \mathbf{A}\Psi X_{k-1} + \mathbf{B}U_k \quad \textit{state transition} && (5.40) \\ Y_k &= \mathbf{C}\Gamma X_k + V_k \quad \textit{observation} && (5.41) \end{aligned}$$

where the matrices $\mathbf{A}, \mathbf{B}$, and $\mathbf{C}$ are the same as in section 4.1 and where the noise process Ψ is described by the following dynamic equation:

$$\begin{aligned} \Psi_k &= \Pi\Psi_{k-1} + \Xi\mathbf{W}_k \\ & \quad \textit{state multiplicative noise transition} && (5.42) \end{aligned}$$

where Π and Ξ are state transition and input matrices describing the dynamics of the state multiplicative noise component and $\mathbf{W}$ is a Gaussian noise matrix. The latter has the following noise characteristics:

$$\begin{aligned} \mathcal{E}[\mathbf{W}_k] &= 0 \\ & \quad \textit{state additive noise of the multiplicative state noise} \\ \mathcal{E}[\mathbf{W}_k\mathbf{W}_{k-l}^T] &= \sigma_W^2\mathbf{I}\delta_k + \mathbf{I} && (5.43) \end{aligned}$$

The remaining noise parameters are:

$$\begin{aligned} \mathcal{E}[U_k] &= 0 \quad \textit{process noise} && (5.44) \\ \mathcal{E}[U_kU_{k-l}^T] &= \sigma_u^2\mathbf{I}\delta_k && (5.45) \\ \mathcal{E}[V_k] &= 0 \quad \textit{observation noise} && (5.46) \\ \mathcal{E}[V_kV_{k-l}^T] &= \sigma_v^2\mathbf{I}\delta_k && (5.47) \end{aligned}$$

$$\begin{aligned} \mathcal{E}[\Gamma_k] &= \mu_\gamma \qquad\qquad \textit{multiplicative noise} && (5.48)\\ \mathcal{E}[\Gamma_k \Gamma_{k-l}^T] &= \sigma_\gamma^2 \mathbf{I}\delta_k + \mu_\gamma^2 \mathbf{I} && (5.49)\\ \mathcal{E}[\Psi] &= 1 && (5.50) \end{aligned}$$

Note that the various noise parameters, U, V, and $\mathbf{W}$, are independent of the signal, $\mathbf{X}$, and are uncorrelated to each other.

We also assume that the multiplicative noise parameters, Ψ, are independent of the signal, $\mathbf{X}$, and the other noise parameters, $\mathbf{W}$, Γ, U, and V.

The local statistics of the image model for the state variable X are as defined in Chapter 4.

The re-evaluation of each of the Kalman equations is given below in order to determine the effects of including a dynamic (Markov) multiplicative noise term, Ψ, in the state transition equation.

a priori estimate

$$\begin{aligned} \mathbf{X}_k^{(-)} &= \mathcal{E}[\mathbf{X}_k | \mathbf{X}_{k-1}] \\ &= \mathcal{E}[\mathbf{A}\Psi_k X_{k-1} + \mathbf{B}U_k] \\ &= \mathcal{E}[\mathbf{A}(\Pi\Psi_{k-1} + \Xi\mathbf{W}_k)X_{k-1} + \mathbf{B}U_k] \\ &= \mathcal{E}[\mathbf{A}\Pi\Psi_{k-1}X_{k-1} + \mathbf{A}\Xi\mathbf{W}_k X_{k-1} + \mathbf{B}U_k] \\ &\quad \Psi,\mathbf{W} \text{ and } \mathbf{X} \text{ are independent and/or uncorrelated, therefore,} \\ \mathcal{E}[\Psi\mathbf{X}] &= \mathcal{E}[\Psi]\mathcal{E}[\mathbf{X}] = \mathcal{E}[\mathbf{X}] \\ &\quad \text{Recall } \mathcal{E}[U_k] = 0, \text{ giving} \\ \mathbf{X}_k^{(-)} &= \mathbf{A}\Pi\mathbf{X}_{k-1}^{(+)} && (5.51) \end{aligned}$$

The sub-optimal estimator for this case will be described by the following expressions:

the innovation

$$Z_k = Y_k - \mathbf{C}\mu_\gamma X_k^{(-)} \tag{5.52}$$

the *a posteriori* estimate

$$X_k^{(+)} = X_k^{(-)} + K_k Z_k \tag{5.53}$$

the Kalman filter gain remains as in Chapter 4:

$$K = P_k^{(-)} C^T \mu_\gamma [\mu_\gamma^2 C P_k^{(-)} C^T + C\sigma_\gamma^2(\sigma_x^2 + \mu_x^2)C^T + \sigma_v^2 \mathbf{I}]^{-1} \tag{5.54}$$

as well the expression for R_z

$$R_z = \mu_\gamma^2 C P_k^{(-)} C^T + C\sigma_\gamma^2(\sigma_x^2 + \mu_x^2)C^T + \sigma_v^2 \mathbf{I} \tag{5.55}$$

Therefore, as in Chapter 4 we will have:

$$K = P_k^{(-)} C^T \mu_\gamma R_z^{-1} \tag{5.56}$$

The expression for the *a priori* error covariance

$$P_k^{(-)} = \mathcal{E}[(X_k - X_k^{(-)})(X_k - X_k^{(-)})^T]$$

is now determined by substituting the expressions for X_k and $X_k^{(-)}$ and expanding the resulting expression.

$$
\begin{aligned}
P_k^{(-)} &= \mathcal{E}[(\mathbf{A}\boldsymbol{\Psi}_k X_{k-1} + BU_k - \mathbf{A}\boldsymbol{\Pi} X_{k-1}^{(+)}) \\
&\quad (\mathbf{A}\boldsymbol{\Psi}_k X_{k-1} + BU_k - \mathbf{A}\boldsymbol{\Pi} X_{k-1}^{(+)})^T] \qquad (5.57) \\
&= \mathcal{E}[(\mathbf{A}(\boldsymbol{\Pi}\boldsymbol{\Psi}_{k-1} + \boldsymbol{\Xi}\mathbf{W}_k)X_{k-1} + BU_k - \mathbf{A}\boldsymbol{\Pi} X_{k-1}^{(+)}) \\
&\quad \mathcal{E}[(\mathbf{A}(\boldsymbol{\Pi}\boldsymbol{\Psi}_{k-1} + \boldsymbol{\Xi}\mathbf{W}_k)X_{k-1} + BU_k - \mathbf{A}\boldsymbol{\Pi} X_{k-1}^{(+)})^T] \\
&= \mathcal{E}[\mathbf{A}\boldsymbol{\Pi}\boldsymbol{\Psi}_{k-1}X_{k-1}X_{k-1}^T\boldsymbol{\Psi}^T\boldsymbol{\Pi}^T\mathbf{A}^T + \mathbf{A}\boldsymbol{\Pi}\boldsymbol{\Psi}_{k-1}X_{k-1}X_{k-1}^T\mathbf{W}_k^T\boldsymbol{\Xi}^T\mathbf{A}^T + \\
&\quad \mathbf{A}\boldsymbol{\Pi}\boldsymbol{\Psi}_{k-1}X_{k-1}U_k^T\mathbf{B}^T - \mathbf{A}\boldsymbol{\Pi}\boldsymbol{\Psi}_{k-1}X_{k-1}X_{k-1}^{(+)^T}\boldsymbol{\Pi}^T\mathbf{A}^T + \\
&\quad \mathbf{A}\boldsymbol{\Xi}\mathbf{W}_kX_{k-1}X_{k-1}^T\boldsymbol{\Psi}_{k-1}^T\boldsymbol{\Pi}^T\mathbf{A}^T + \mathbf{A}\boldsymbol{\Xi}\mathbf{W}_kX_{k-1}X_{k-1}^T\mathbf{W}_k^T\boldsymbol{\Xi}^T\mathbf{A}^T + \\
&\quad \mathbf{A}\boldsymbol{\Xi}\mathbf{W}_kX_{k-1}U_k^T\mathbf{B}^T - \mathbf{A}\boldsymbol{\Xi}\mathbf{W}_kX_{k-1}X_{k-1}^{(+)^T}\boldsymbol{\Pi}^T\mathbf{A}^T + \\
&\quad \mathbf{B}U_kX_{k-1}^T\boldsymbol{\Psi}_{k-1}^T\boldsymbol{\Pi}^T\mathbf{A}^T + \mathbf{B}U_kX_{k-1}^T\mathbf{W}_k^T\boldsymbol{\Xi}^T\mathbf{A}^T + \\
&\quad \mathbf{B}U_kU_k^T\mathbf{B}^T - \mathbf{B}U_kX_{k-1}^{(+)^T}\boldsymbol{\Pi}^T\mathbf{A}^T - \\
&\quad \mathbf{A}\boldsymbol{\Pi}X_{k-1}^{(+)}X_{k-1}^T\boldsymbol{\Psi}_{k-1}^T\boldsymbol{\Pi}^T\mathbf{A}^T - \mathbf{A}\boldsymbol{\Pi}X_{k-1}^{(+)}X_{k-1}^T\mathbf{W}_k^T\boldsymbol{\Xi}^T\mathbf{A}^T - \\
&\quad \mathbf{A}\boldsymbol{\Pi}X_{k-1}^{(+)}U_k^T\mathbf{B}^T + \mathbf{A}\boldsymbol{\Pi}X_{k-1}^{(+)}X_{k-1}^{(+)^T}\boldsymbol{\Pi}^T\mathbf{A}^T] \\
&= \mathcal{E}[\mathbf{A}\boldsymbol{\Pi}\boldsymbol{\Psi}_{k-1}X_{k-1}X_{k-1}^T\boldsymbol{\Psi}^T\boldsymbol{\Pi}^T\mathbf{A}^T - \mathbf{A}\boldsymbol{\Pi}\boldsymbol{\Psi}_{k-1}X_{k-1}X_{k-1}^{(+)^T}\boldsymbol{\Pi}^T\mathbf{A}^T + \\
&\quad \mathbf{A}\boldsymbol{\Xi}\mathbf{W}_kX_{k-1}X_{k-1}^T\mathbf{W}_k^T\boldsymbol{\Xi}^T\mathbf{A}^T + \mathbf{B}U_kU_k^T\mathbf{B}^T - \\
&\quad \mathbf{A}\boldsymbol{\Pi}X_{k-1}^{(+)}X_{k-1}^T\boldsymbol{\Psi}_{k-1}^T\boldsymbol{\Pi}^T\mathbf{A}^T + \mathbf{A}\boldsymbol{\Pi}X_{k-1}^{(+)}X_{k-1}^{(+)^T}\boldsymbol{\Pi}^T\mathbf{A}^T] \qquad (5.58)
\end{aligned}
$$

Proceeding as shown in Chapter 4 by substituting the expressions for the earlier $P_k^{(+)}$ and the cross covariance term, the equation now becomes:

$$
\begin{aligned}
P_k^{(-)} &= \mathbf{A}\boldsymbol{\Pi}P_{k-1}^{(+)}\boldsymbol{\Pi}^T\mathbf{A}^T + \mathbf{A}\boldsymbol{\Pi}\mathcal{E}[\boldsymbol{\Psi}X_{k-1}X_{k-1}^T\boldsymbol{\Psi}^T]\boldsymbol{\Pi}^T\mathbf{A}^T - \\
&\quad \mathbf{A}\boldsymbol{\Pi}\mathcal{E}[X_{k-1}X_{k-1}^T]\boldsymbol{\Pi}^T\mathbf{A}^T + B\mathcal{E}[UU^T]B^T + \\
&\quad \mathbf{A}\boldsymbol{\Xi}\mathcal{E}[\mathbf{W}_kX_{k-1}X_{k-1}^T\mathbf{W}_k^T]\boldsymbol{\Xi}^T\mathbf{A}^T \qquad (5.59)
\end{aligned}
$$

Since the multiplicative noise, $\boldsymbol{\Psi}$, and the original image, X, are independent, the result of the combined expectation can be expressed as

$$\mathcal{E}[\Psi X_{k-1} X_{k-1}^T \Psi^T] = \sigma_\psi^2(\sigma_x^2 + \mu_x^2) + \sigma_x^2 + \mu_x^2 \tag{5.60}$$

Recall that

$$\mathcal{E}[X_{k-1} X_{k-1}^T] = \sigma_x^2 + \mu_x^2 \tag{5.61}$$

and

$$\mathcal{E}[\mathbf{W}_k X_{k-1} X_{k-1}^T \mathbf{W}_k^T] = \sigma_w^2(\sigma_x^2 + \mu_x^2) + \sigma_x^2 + \mu_x^2 \tag{5.62}$$

resulting in the final expression for the *a priori* error covariance of

$$\begin{aligned} P_k^{(-)} &= \mathbf{A}\Pi P_{k-1}^{(+)} \Pi^T \mathbf{A}^T + \mathbf{A}\Pi[\sigma_\psi^2(\sigma_x^2 + \mu_x^2)]\Pi^T \mathbf{A}^T + \\ &\quad \mathbf{A}\Xi[\sigma_w^2(\sigma_x^2 + \mu_x^2) + \sigma_x^2 + \mu_x^2]\Xi^T \mathbf{A}^T + \mathbf{B}\sigma_u^2 \mathbf{B}^T \end{aligned} \tag{5.63}$$

As expected only the *a priori* error covariance term changes when the multiplicative noise mean of one is included in the model. This implies again changing only the derivative of *a priori* covariance in the recursive parameter estimation equations.

5.5 Modifications for the Online Parameter Estimation Equations

From the development given in Chapter 4, the only modifications needed to adapt the online identification equations to the case of dynamic state multiplicative noise are in the expression of the derivative of the *a priori* covariance estimate. They will be given by the following expression:

$$
\begin{aligned}
\frac{dP_k^{(-)}}{d\Phi} &= \frac{d}{d\Phi}[\mathbf{A}\Pi P_{k-1}^{(+)}\Pi^T\mathbf{A}^T + \mathbf{A}\Pi(\sigma_\psi^2(\sigma_x^2+\mu_x^2))\Pi^T\mathbf{A}^T + \\
&\quad \mathbf{A}\Xi[\sigma_w^2(\sigma_x^2+\mu_x^2)+\sigma_x^2+\mu_x^2]\Xi^T\mathbf{A}^T + \mathbf{A}\Xi[\sigma_w^2(\sigma_x^2+\mu_x^2)+\sigma_x^2+\mu_x^2]\Xi^T\mathbf{A}^T + \mathbf{B}\sigma_u^2\mathbf{B}^T] \\
&= (\frac{d}{d\Phi}\mathbf{A}\Pi)P_{k-1}^{(+)}\Pi^T\mathbf{A}^T + \mathbf{A}\Pi P_{k-1}^{(+)}\frac{d}{d\Phi}(\Pi^T\mathbf{A}^T) + \\
&\quad (\frac{d}{d\Phi}\mathbf{A}\Pi)(\sigma_\psi^2(\sigma_x^2+\mu_x^2))\Pi^T\mathbf{A}^T + \mathbf{A}\Pi(\sigma_\psi^2(\sigma_x^2+\mu_x^2))(\frac{d}{d\Phi}\Pi^T\mathbf{A}^T) + \\
&\quad \mathbf{A}\Pi(\frac{d}{d\Phi}P_{k-1}^{(+)})\Pi^T\mathbf{A}^T + (\frac{d}{d\Phi}\mathbf{B})\sigma_u^2\mathbf{B}^T + \mathbf{B}\sigma_u^2(\frac{d}{d\Phi}\mathbf{B}^T) + \\
&\quad (\frac{d}{d\Phi}\mathbf{A}\Xi)[\sigma_w^2(\sigma_x^2+\mu_x^2)+\sigma_x^2+\mu_x^2]\Xi^T\mathbf{A}^T + \\
&\quad \mathbf{A}\Xi[\sigma_w^2(\sigma_x^2+\mu_x^2)+\sigma_x^2+\mu_x^2](\frac{d}{d\Phi}\Xi^T\mathbf{A}^T) \qquad (5.64)
\end{aligned}
$$

The initial conditions required for the parameter estimation are the same as those given in chapter 4. Φ_0, $\mathcal{R}_0$, λ_0, λ_{rate}, λ_{ss}, and $\Sigma_a(0)$.

5.6 Conclusions

This chapter introduced two new filters for speckle reduction in SAR images. Both filters are based on a Kalman estimation technique; the presence of the noise components having a distribution other than Gaussian imposes the modification of the Kalman filter and also the modification of the parameter estimation set of equations. Two main problems have been considered: the presence of a Markov noise in the observation equation and the case of a colored multiplicative noise in the state equation. There are, of course, many other cases to be considered such as the presence of a Markov noise in the state equation (for the additive noise component), both additive noises Markov, etc. We have selected only the main cases taking into account that the final behaviour of the observation has to obey an exponential distribution. Although the development of the set of the equations for the Kalman filter and for the parameter estimation for the remaining cases might not be trivial, it follows the pattern described in this chapter; future developments, therefore, can be approached following the guidelines presented above. In the next chapter an optimization technique for the determination of the noise parameters will be developed. It is very well known that the Kalman filter is extremely sensitive to the variation of parameters. It is also known that the Kalman filter performance depends tremendously on the choice of the noise parameters. We will develop in the next chapter an optimal methodology for establishing the noise parameters for filtering a given signal.

Chapter 6

An Optimized Full Plane Modified Kalman Filter

6.1 Introduction

In the Kalman filter model, both additive noises have been assumed to be Gaussian; moreover, their covariances have been assumed known. It is a very well known fact that the Kalman filter performance depends very much on both these two matrices:

$$\begin{aligned} \mathcal{E}[U_k U_{k-l}^T] &= \sigma_u^2 \mathbf{I} \delta_k \\ \mathcal{E}[V_k V_{k-l}^T] &= \sigma_v^2 \mathbf{I} \delta_k \end{aligned} \tag{6.1}$$

Small changes in the numerical values of the elements of the above matrices bring strong changes in the quality of the filtered image. With an appropriate value for the parameters of the two matrices the images are smoothed according to the Gaussian law. If, in the real image, a small change occurs in the values of σ_u^2 or σ_v^2, the behaviour of the filter deteriorates, over smoothing the image. To reduce the over smoothing trend, the Kalman filter is modified so that it does not require any assumptions on the state transition and state observation additive noises. At every step of the filter the noise will be approximated so as to reduce further the speckle noise.

6.2 An Optimal Technique for Determining the Noise Parameters of the Kalman Filter

6.2.1 The Image Model

In what follows we will again consider the problem developed in section 4.4 of chapter 4. The model of the SAR image will be, therefore, given by the following equations:

$$\begin{aligned} \mathbf{X}_k &= \mathbf{A}\Psi\mathbf{X}_{k-1} + \mathbf{B}\mathbf{U}_{k-1} && \textit{state transition} \\ \mathbf{Y}_k &= C\Gamma\mathbf{X}_k + V_k && \textit{observation} \end{aligned} \tag{6.2}$$

where the noise process Ψ is Gaussian with the following statistics:

$$\begin{aligned} \mathcal{E}[\Psi_k] &= 1 && \textit{multiplicative state noise} \\ \mathcal{E}[\Psi_k\Psi_{k-l}^T] &= \sigma_\psi^2\mathbf{I}\delta_{k,l} + \mathbf{I} \end{aligned}$$

and the remaining noise parameters are

$$\mathcal{E}[U_k] = 0 \qquad \textit{process noise} \tag{6.3}$$

$$\mathcal{E}[U_k U_{k-l}^T] = \sigma_u^2 \mathbf{I} \delta_k \tag{6.4}$$

$$\mathcal{E}[V_k] = 0 \qquad \textit{observation noise} \tag{6.5}$$

$$\mathcal{E}[V_k V_{k-l}^T] = \sigma_v^2 \mathbf{I} \delta_k \tag{6.6}$$

$$\mathcal{E}[\Gamma_k] = \mu_\gamma \qquad \textit{multiplicative noise}$$

$$\mathcal{E}[\Gamma_k \Gamma_{k-l}^T] = \sigma_\gamma^2 \mathbf{I} \delta_{k,l} + \mu_\gamma^2 \mathbf{I}$$

6.2.2 Transforming the Filtering Problem into a Control Problem

However, in the development of the Kalman filter equations, the noise parameters, that is the process noise and the observation correlations, will now be considered unknown. In other words, although the equations of the filter remain the same, as in the previous development given in section 4.4 :

$$\begin{aligned}
P_k^{(-)} &= \mathbf{A} P_{k-1}^{(+)} \mathbf{A}^T + \mathbf{A}(\sigma_\psi^2(\sigma_x^2 + \mu_x^2))\mathbf{A}^T + \mathbf{B}\sigma_u^2 \mathbf{B}^T \\
R_z &= \mu_\gamma^2 C P_k^{(-)} C^T + C\sigma_\gamma^2(\sigma_x^2 + \mu_x^2) C^T + \sigma_v^2 \mathbf{I} \\
K &= P_k^{(-)} C^T \mu_\gamma R_z^{-1} \\
P_k^{(+)} &= (\mathbf{I} - \mu_\gamma K C) P_k^{(-)}
\end{aligned}$$

The difference here consists in considering the expressions which characterize the two additive noises:

$$\mathcal{E}[U_k U_{k-l}^T] = \sigma_u^2 \mathbf{I} \delta_k \tag{6.7}$$

$$\mathcal{E}[V_k V_{k-l}^T] = \sigma_v^2 \mathbf{I} \delta_k \tag{6.8}$$

$$\tag{6.9}$$

as unknowns. It is, therefore, necessary to establish a new procedure which can determine, based on a supplementary criterion (say a cost function again!), which are the best values for these unknowns such that this new criterion becomes minimum with respect to $\sigma_u^2 \mathbf{I}\delta_k$ and $\sigma_v^2 \mathbf{I}\delta_k$ and maximum with respect to the Kalman filter gain K.

Let's define $\tilde{X}_j = X_j - \hat{X}_j$ where $\hat{X}_j$ is the estimate

$$\begin{aligned} \hat{X}_j &= A\Psi\hat{X}_{j-1} + K_j[Y_{j-1} - \mu_\gamma C\hat{X}_{j-1}] \\ Y_{j-1} &= C\Gamma X_{j-1} + V_{j-1} \end{aligned}$$

Since

$$X_j - \hat{X}_j = \tilde{X}_j$$

it follows that:

$$\begin{aligned} \tilde{X}_j &= A\Psi X_{j-1} + BU_{j-1} - A\Psi\hat{X}_{j-1} - K_j[Y_{j-1} - \mu_\gamma C\hat{X}_{j-1}] \\ &= A\Psi(X_{j-1} - \hat{X}_{j-1}) + BU_{j-1} - K_j[C\Gamma X_{j-1} + V_{j-1} - \mu_\gamma C\hat{X}_{j-1}] \\ &= (A\Psi - K_jC\Gamma)(X_{j-1} - \hat{X}_{j-1}) + BU_{j-1} - K_jV_{j-1} \\ \tilde{X}_j &= (A\Psi - K_jC\Gamma)\tilde{X}_{j-1} + BU_{j-1} - K_jV_{j-1} \qquad (6.10) \end{aligned}$$

Defining now

$$\mathbf{X}_j = \begin{bmatrix} X_j \\ \tilde{X}_j \end{bmatrix} = \begin{bmatrix} A\Psi & 0 \\ 0 & A\Psi - K_jC\Gamma \end{bmatrix} \mathbf{X}_{j-1} + \begin{bmatrix} B & 0 \\ B & -K_j \end{bmatrix} \mathbf{U}_{j-1}$$

where $\mathbf{U}_{j-1} = \begin{bmatrix} U_{j-1} \\ V_{j-1} \end{bmatrix}$

One obtains the following set of equations for the new image model:

$$\mathbf{X}_j = \bar{A}\mathbf{X}_{j-1} + \bar{B}\mathbf{U}_{j-1} \qquad (6.11)$$

where

$$\bar{A} = \begin{bmatrix} A\Psi & 0 \\ 0 & A\Psi - K_j C\Gamma \end{bmatrix} \tag{6.12}$$

and

$$\bar{B} = \begin{bmatrix} B & 0 \\ B & -K_j \end{bmatrix} \tag{6.13}$$

Using this new model we have to find the matrices $\mathbf{U}_k$ and $\mathbf{V}_k$ such that the estimate of the error is minimum. At the same time, the same estimate has to be maximum with respect to the Kalman filter gain [60, 61]. This new problem is similar to finding the input function for a linear quadratic Gaussian regulator [74]. In other words, the estimation problem, which has been solved in Chapters 4 and 5, turned into a control problem for the image we want to filter. In this new control problem the state vector is the image state vector of equation 6.2 extended by the error vector, expressed as a difference between the image state vector and its estimate 6.2.2. In what follows, a cost function will be attached to this new vector. The problem to be solved is finding the control:

$$\mathbf{U}_{j-1} = \begin{bmatrix} U_{j-1} \\ V_{j-1} \end{bmatrix}$$

such that the cost index reaches its minimum with respect to it and at the same time a maximum with respect to K.

6.2.3 Defining a Cost Index

The most natural way to introduce a cost index is to impose a minimum on the error covariance, in other words:

$$J(Q_u, Q_v, K_k) = \mathcal{E}[\bar{X}^T(Tn)\bar{X}(Tn)]$$

where $Tn = nj$

As stated above, solving the filtering problem with unknown noise parameters is equivalent to solve the following control problem:

Given:

$$\mathbf{X}_j = \bar{A}\mathbf{X}_{j-1} + \bar{B}\mathbf{U}_{j-1} \tag{6.14}$$

Find $\bar{\mathbf{U}}_{(j-1)}$ such that

$$J(Q_u, Q_v, K_k) = \mathcal{E}[\bar{X}^T(Tn)\bar{X}(Tn)]$$

reaches a minimum.

In order to optimize this linear control system, we have to minimize J with respect to Qu and Qv, and to maximize it with respect to K. In other terms, we aim at finding Qu, Qv which minimize J, and K which maximize J. Let $\bar{P}_j = \mathcal{E}\{\mathbf{X}_{i,j}\mathbf{X}_{i,j}^T\}$ then $J = \mathcal{E}\{\bar{X}_{Tn}^T\bar{X}_{Tn}\} = tr\{\bar{H}\bar{P}_{nj})\}$

where $\bar{H} = \begin{bmatrix} 0 & 0 \\ 0 & U \end{bmatrix}$ and U can be chosen as being the identity matrix.

Let's represent $\bar{P}$ as : $\begin{bmatrix} P_{1_{nj}} & P_{2_{nj}} \\ P_{3_{nj}} & P_{4_{nj}} \end{bmatrix}$

Then $\bar{H}\bar{P}_{nj} = \begin{bmatrix} 0 & 0 \\ 0 & P_{4_{nj}} \end{bmatrix}$

With this in mind one obtains :

$$J = tr(\bar{H}\bar{P}_{nj}) = tr(P_{4_{nj}}) \tag{6.15}$$

6.2.4 A Riccati Equation and its Solution

The expression of $\bar{P}_{nj}$ can be written as following :

$$\bar{P}_{nj} = \mathcal{E}\{\mathbf{X}_{nj}\mathbf{X}_{nj}^T\} = \bar{A}\bar{P}_{(nj-1)}\bar{A}^T + \bar{B}\Lambda\bar{B}^T$$

This is known as a Riccati equation, it allows one to calculate $\bar{P}_{nj}$.

$$\begin{aligned}
\bar{P}_{nj} &= \begin{bmatrix} P_{1_{nj}} & P_{2_{nj}} \\ P_{3_{nj}} & P_{4_{nj}} \end{bmatrix} \\
&= \begin{bmatrix} A\Psi & 0 \\ 0 & A\Psi - KC\Gamma \end{bmatrix} \begin{bmatrix} P_{1_{(nj-1)}} & P_{2_{(nj-1)}} \\ P_{3_{(nj-1)}} & P_{4_{(nj-1)}} \end{bmatrix} \begin{bmatrix} \Psi^T A^T & 0 \\ 0 & \Psi^T A^T - \Gamma^T C^T K^T \end{bmatrix} \\
&\quad + \begin{bmatrix} B & 0 \\ B & K_j \end{bmatrix} \begin{bmatrix} Qu & 0 \\ 0 & Qv \end{bmatrix} \begin{bmatrix} B^T & B^T \\ 0 & K_j^T \end{bmatrix}
\end{aligned}$$

Since $P_2 = P_3$ (due to the condition to Riccati's solution existence) it becomes

$$\begin{aligned}
P_{1_{nj}} &= A\Psi P_{1_{nj-1}}\Psi^T A^T + BQuB^T \\
P_{2_{nj}} &= A\Psi P_{2_{nj-1}}(\Psi^T A^T - \Gamma^T C^T K^T) + BQuB^T \\
&= (A\Psi - KC\Gamma)P_{2_{nj-1}}\Psi^T A^T + BQuB^T \\
P_{4_{nj}} &= (A\Psi - KC\Gamma)P_{4_{nj-1}}(\Psi^T A^T - \Gamma^T C^T K^T) + BQuB^T + KQvK^T
\end{aligned}$$

Writing $P_{4_{nj}}$ in terms of elements, it can be represented as following :

$$\begin{aligned} P_{4_{xy}}^{nj} &= \sum_i \sum_k (\sum_m a_{xm} \Psi_{mi} - \sum_m \sum_n K_{xm} C_{mn} \Gamma_{ni}) \\ & P_{4_{ik}}^{(nj-1)} (\sum_m \Psi_{mk} a_{ym} - \sum_m \sum_n \Gamma_{mk} C_{nm} K_{yn}) + \\ & (\sum_i \sum_k b_{xi} Qu_{ik} b_{yk} + \sum_i \sum_k K_{xi} Qv_{ik} K_{yk} \end{aligned}$$

So that,

$$\begin{aligned} J &= tr(P_4) = \sum_x P_{4_{xx}}^{j} \\ &= \sum_i \sum_k (\sum_m a_{xm} \Psi_{mi} - \sum_m \sum_n K_{xm} C_{mn} \Gamma_{ni}) \\ & P_{4_{ik}}^{(nj-1)} (\sum_m \Psi_{mk} a_{xm} - \sum_m \sum_n \Gamma_{mk} C_{nm} K_{xn}) + \\ & (\sum_i \sum_k b_{xi} Qu_{ik} b_{xk} + \sum_i \sum_k K_{xi} Qv_{ik} K_{xk} \end{aligned}$$

6.3 The Gradient of the Cost Index

The solution to the initial control problem is now given by the solution of the minimax problem set on the cost index J expressed as a trace operator on a matrix expression. In other words an extremum of matrix function which depends on unknown matrices Q_u and Q_v has to be found.

The solution to this problem has been shown in [35] for the continuous case. However, the existence conditions remain the same as in [35]. It has been shown that for a matrix function over matrices the gradient exists and can be calculated by weak or strong derivative procedures. The Gâteaux derivative (see appendix A) is preferable because it is easier to use in a computer program.

We aim at minimizing J with respect to Qu and Qv and maximize it with respect to K.

Therefore the main problem in solving the filtering problem under unknown noise conditions is to find the gradient of J with respect to the unknowns Q_u, Q_v, and K. For this reason it is necessary to find the derivatives of J with respect to the above mentioned variables.

The existence of the derivatives (gradient) was proven in [35] according to the following lemma: Lemma 6.1: Let $f(K)$, $d(K)$, and K be matrices with suitable dimensions. Given the functional $J(K) = tr.(f(K))$, if $tr.(f(K + \Delta K) - f(K)) = tr.(d(K)\Delta K)$ for any ΔK, then the Gâteaux derivative of $J(K)$ is as follows:

$$\nabla J(K) = d^T(K)$$

using this result one can adapt Theorem 3.1 from [35] as follows:

Theorem 6.1: Denote $\kappa \stackrel{def}{=} \{(Q_u, Q_v, K) \in R^{9N \times 9N} \times R^{4N \times 4N} \times R^{9N \times 4N} | \bar{A}(K)$ *is asymptotically stable*$\}$, given the functional $J(Q_u, Q_v, K)$ in 6.15. Then, the Gâteaux derivative $\nabla J(Q_u, Q_v, K)$ exists on (Q_u, Q_v, K) and is as follows:

$$\nabla J(Q_u, Q_v, K) = \nabla(tr(P_4(Q_u, Q_v, K)))$$

where the derivatives of P_4 with respect to K, Q_u, and Q_v are calculated as follows:.

$$\begin{aligned} \frac{dP_{4xy}^{\,nj}}{dK_{st}} &= -\sum_i \sum_k (\sum_m \sum_n \frac{dK_{xm}}{K_{st}} C_{mn}\Gamma_{ni}) \\ & P_{4ik}^{(nj-1)}(\sum_m \Psi_{mk} a_{ym} - \sum_m \sum_n \Gamma_{mk} C_{nm} K_{yn}) + \\ & \sum_i \sum_k (\sum_m a_{xm}\Psi_{mi} - \sum_m \sum_n K_{xm} C_{mn}\Gamma_{ni}) \end{aligned}$$

$$\begin{aligned}
&\frac{dP_{4_{xy}}^{(nj-1)}}{dK_{st}}(\sum_m \Psi_{mk}a_{ym} - \sum_m \sum_n \Gamma_{mk}C_{nm}K_{yn}) - \\
&\sum_i \sum_k (\sum_m a_{xm}\Psi_{mi} - \sum_m \sum_n K_{xm}C_{mn}\Gamma_{ni}) \\
&P_{4_{ik}}^{(nj-1)}(\sum_m \sum_n \Gamma_{mk}C_{nm}\frac{dK_{yn}}{dK_{st}}) + \\
&\sum_i \sum_k \frac{dK_{xi}}{dK_{st}}Qv_{ik}K_{yk} + \sum_i \sum_k K_{xi}Qv_{ik}\frac{dK_{yk}}{dK_{st}}
\end{aligned}$$

but: $\frac{dK_{ij}}{dK_{st}} = \begin{cases} 1 \; when \; i = s \; and \; j = t \\ 0 \; else \end{cases}$

Thus when $x = s$ and $y \neq s$

$$\begin{aligned}
\frac{dP_{4_{xy}}^{nj}}{dK_{st}} = &-\sum_i \sum_k (\sum_n C_{tn}\Gamma_{ni})P_{4_{ik}}^{(nj-1)}(\sum_m \Psi_{mk}a_{ym} - \sum_m \sum_n \Gamma_{mk}C_{nm}K_{yn}) + \\
&\sum_i \sum_k (\sum_m a_{xm}\Psi_{mi} - \sum_m \sum_n K_{xm}C_{mn}\Gamma_{ni}) \\
&\frac{dP_{4_{xy}}^{(nj-1)}}{dK_{st}}(\sum_m \Psi_{mk}a_{ym} - \sum_m \sum_n \Gamma_{mk}C_{nm}K_{yn}) + \\
&\sum_k Qv_{tk}K_{yk}
\end{aligned}$$

when $x \neq s$ and $y = s$

$$\begin{aligned}
\frac{dP_{4_{xy}}^{nj}}{dK_{st}} = &\sum_i \sum_k (\sum_m a_{xm}\Psi_{mi} - \sum_m \sum_n K_{xm}C_{mn}\Gamma_{ni}) \\
&\frac{dP_{4_{xy}}^{(nj-1)}}{dK_{st}}(\sum_m \Psi_{mk}a_{ym} - \sum_m \sum_n \Gamma_{mk}C_{nm}K_{yn}) - \\
&\sum_i \sum_k (\sum_m a_{xm}\Psi_{mi} - \sum_m \sum_n K_{xm}C_{mn}\Gamma_{ni}) \\
&P_{4_{ik}}^{(nj-1)}(\sum_m \Gamma_{mk}C_{tm}) + \\
&\sum_i K_{xi}Qv_{it}
\end{aligned}$$

when $x \neq s$ and $y \neq s$

$$\begin{aligned}
\frac{dP_{4_{xy}}^{nj}}{dK_{st}} = & -\sum_i \sum_k (\sum_n C_{tn}\Gamma_{ni}) P_{4_{ik}}^{(nj-1)} (\sum_m \Psi_{mk} a_{ym} - \sum_m \sum_n \Gamma_{mk} C_{nm} K_{yn}) + \\
& \sum_i \sum_k (\sum_m a_{xm} \Psi_{mi} - \sum_m \sum_n K_{xm} C_{mn} \Gamma_{ni}) \\
& \frac{dP_{4_{xy}}^{(nj-1)}}{dK_{st}} (\sum_m \Psi_{mk} a_{ym} - \sum_m \sum_n \Gamma_{mk} C_{nm} K_{yn}) + \\
& \sum_i \sum_k (\sum_m a_{xm} \Psi_{mi} - \sum_m \sum_n K_{xm} C_{mn} \Gamma_{ni}) \\
& P_{4_{ik}}^{(nj-1)} (\sum_m \Gamma_{mk} C_{tm}) + \\
& \sum_i K_{xi} Qv_{it} + \sum_k Qv_{tk} K_{yk}
\end{aligned}$$

when $x = s$ and $y = s$

$$\begin{aligned}
\frac{dP_{4_{xy}}^{nj}}{dK_{st}} = & \sum_i \sum_k (\sum_m a_{xm} \Psi_{mi} - \sum_m \sum_n K_{xm} C_{mn} \Gamma_{ni}) \\
& \frac{dP_{4_{xy}}^{(nj-1)}}{dK_{st}} (\sum_m \Psi_{mk} a_{ym} - \sum_m \sum_n \Gamma_{mk} C_{nm} K_{yn})
\end{aligned}$$

Similarly,

$$\begin{aligned}
\frac{dP_{4_{xy}}^{nj}}{dU_{st}} = & \sum_i \sum_k (\sum_m a_{xm} \Psi_{mi} - \sum_m \sum_n K_{xm} C_{mn} \Gamma_{ni}) \\
& \frac{dP_{4_{xy}}^{(nj-1)}}{dU_{st}} (\sum_m \Psi_{mk} a_{ym} - \sum_m \sum_n \Gamma_{mk} C_{nm} K_{yn}) + \\
& b_{xs} b_{yt}
\end{aligned}$$

and,

$$\begin{aligned}
\frac{dP_{4_{xy}}^{nj}}{dV_{st}} = & \sum_i \sum_k (\sum_m a_{xm} \Psi_{mi} - \sum_m \sum_n K_{xm} C_{mn} \Gamma_{ni}) \\
& \frac{dP_{4_{xy}}^{(nj-1)}}{dV_{st}} (\sum_m \Psi_{mk} a_{ym} - \sum_m \sum_n \Gamma_{mk} C_{nm} K_{yn}) + \\
& K_{xs} K_{yt}
\end{aligned}$$

The three derivatives are used to obtain the extremum points of J with respect to Q_u, Q_v, and K following a nonlinear programming algorithm such as Kuhn-Tucker [11].

It was also shown in [35] that the extremal point of the above functional exists. This is justified by the following lemmas and theorem:

Lemma 6.2: For the given functional $J(Q_u, Q_v, K)$ in 6.15 , there holds that

$$J(K+H) - J(K) = \langle \nabla J(K), H \rangle \quad for\ all\ K, H \in \kappa \tag{6.16}$$

where $\langle . \rangle$ denotes the inner product operator.

Furthermore, the Gâteaux derivative of $J(Q_u, Q_v, K)$ is independent of (Q_u, Q_v, K), that is, for all $K, H, G \in \kappa$, there holds that:

$$\langle \nabla J(K+G), H \rangle = \langle \nabla J(K), H \rangle \tag{6.17}$$

Theorem 6.2: Given the functional $J(Q_u, Q_v, K)$ in 6.15, then the necessary and sufficient condition for (Q_u, Q_v, K) to be an optimal solution is that for all $K \in \kappa$, there holds that:

$$\langle \nabla J(K^*), K - K^* \rangle \geq 0.$$

Corollary 6.1: The optimal solution K^* obtained by using Theorem 6.2 is unique if and only if there holds that:

$$\langle \nabla J(K^*), K - K^* \rangle > 0$$

for all $K \in \kappa$ and $K \neq K^*$.

One of the most basic problems is the existence of solutions to the optimal problem. The results are as follows:

Theorem 6.3: Given $J(K)$ in 6.15. Then, there exists a matrix $K^* \in M_s$ such that:

$$J(K^*) = \min_{K \in M_s} J(K)$$

where M_s is any closed subset of κ.

It is also worthwhile to note the following results given in [35]

Remark 6.1: Obviously, κ is not a closed set in $R^{N \times M}$. However, for any $\epsilon > 0$, the subset

$$\kappa_\epsilon \overset{def}{=} \{K \in R^{N \times M} \mid \sigma(\bar{A}(K)) \subseteq (-\infty, -\epsilon]\} \tag{6.18}$$

is a closed subset of κ. In fact, κ_ϵ is compact and therefore is closed. Hence, it is of practical interest to compute the optimal solution on the subset κ_ϵ for the given machine error $\epsilon > 0$.

Remark 4.2: In the computation of minimizing $J(K)$, one has to choose the feasible initial matrix K_0 such that $K_0 \in \kappa$. If Lemma 6.1 holds, then there always exists a feasible initial matrix K_0 for this optimization problem.

Based on the above there is always a solution to this problem which will provide optimal Q_u, Q_v and K. The calculated noises and gain are then introduced as values in the full plane modified Kalman filter and recalculated at each step of the filter.

These changes result in a better adaptation of the filter to any type of region, homogeneous regions as well as highly contrasted ones, because it estimates the exact speckle noise of each region of the image instead of assuming that this noise is Gaussian over the entire image.

Moreover, in the FABKF processed images the mean is reduced by an amount usually proportional to the amount of smoothing done by the filter. This is due to the Gaussian noise assumption in the derivation of the Kalman filter. The filter smoothes the low probability, higher intensity pixels in the image so that they fit within the envelope of the given Gaussian noise distribution. With a Kalman filter under unknown noise conditions this smoothing is reduced.

6.4 An Optimization Algorithm for Determining the Noise Parameters of the Kalman Filter for SAR Speckle Reduction

The program flowchart is shown in figures 6.1 and 6.2. After the initialization step is completed the filter calculates the Kalman gain. Then it calls the optimal point routine with the noises and the Kalman gain as arguments. This routine requires :

- a golden section routine
- a routine to calculate P and its derivatives
- a routine to calculate J and its gradient
- a routine to calculate the norm J and and of its gradient
- a routine to calculate the proximity of the gradient of J to the origin

The optimal point that we are looking for has to be a minimum of J with respect to Qu, and Qv, and a maximum of J with respect to the Kalman gain K. The routine calls then the Kalman filter function with these new values as parameters. This cycle is repeated at each step of the filter.

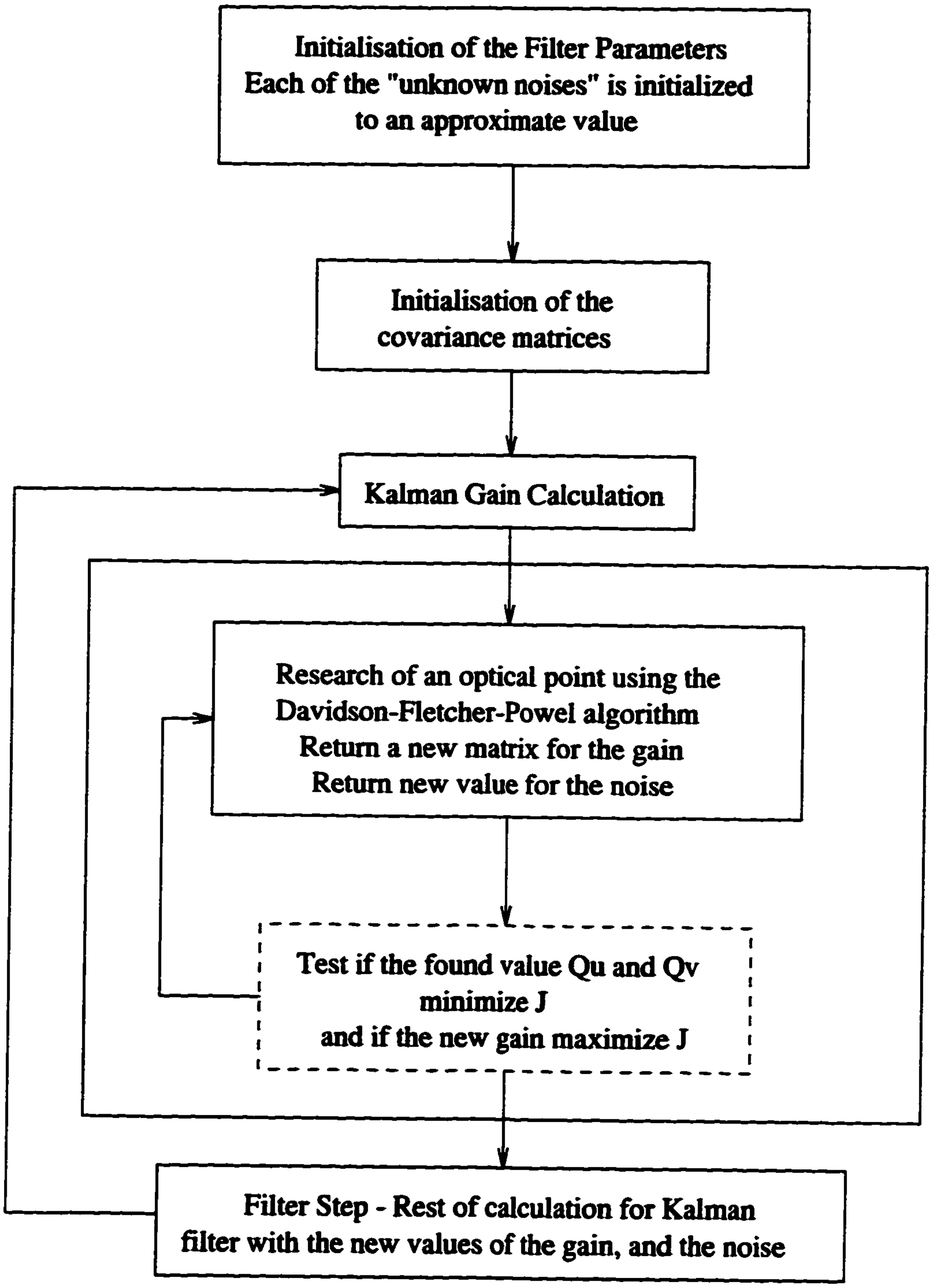

Figure 6.1: Program flowchart for the full plane Kalman filter under the condition of unknown noise values.

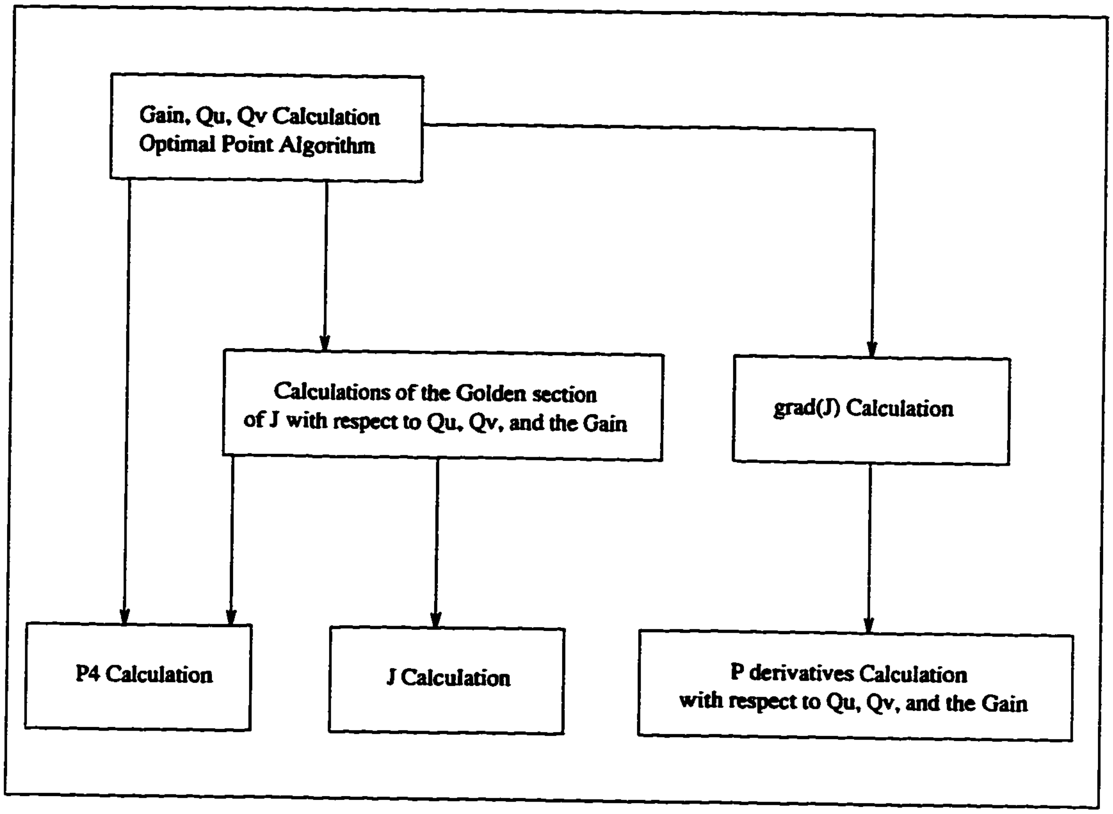

Figure 6.2: Links between the needed programs for the full plane Kalman filter under the condition of unknown noise values.

$$H(K,\Lambda,\Gamma) = (\bar{A}(\Gamma)\bar{P}(k-1)\bar{A}^T(\Gamma) + \bar{B}\Lambda\bar{B}^T)F \tag{6.19}$$

where

$$F = \begin{bmatrix} F_{11} & 0 \\ 0 & F_{22} \end{bmatrix} \tag{6.20}$$

and

$$F_{11}(T_n) = \quad 0 \tag{6.21}$$

$$F_{11}(k) = \quad -\bar{A}^T(\Gamma)F_{11}(k-1)\bar{A}(\Gamma) \tag{6.22}$$

$$F_{22}(T_n) = \quad 0 \tag{6.23}$$

$$F_{22}(k) = \quad (K^*C - \bar{A}(\Gamma))^T F_{22}(k-1)A(\Gamma) \tag{6.24}$$

and Γ is given by the following conjugate gradient algebra:

$$\delta H \geq 0 \tag{6.25}$$

Choose an initial $\Gamma = \Gamma_0$

Step 1.

$j = 0$

Step 2.

Calculate $g_k = \nabla H(\Gamma_k)$

If $\|g_k\| = 0 \Longrightarrow \Gamma^* = \Gamma_k$ and STOP.

else

$h_k = -g_k$ and go to Step 3.

Step 3.

Determine $\alpha_k = alpha^*$ from *Golden section algorithm*

Step 4.

Put $\Gamma_{k+1} = \Gamma_k + \alpha_k h_k$ and $k \leftarrow k + 1$ and go to Step 2.

Stop when $\|g_k\| \cong (\epsilon)$

Golden Section Algorithm

Given $c > 0$ and $\epsilon > 0$ and $0 < c < 1$

$F \triangleq (3 - \sqrt{5})/2 = 0.382$ and $\epsilon = 1 - F$

Step 1. Calculate

$$\theta(c) = H(\Gamma_k + \alpha h_k) - H(\Gamma_k)|_{\alpha=c} \tag{6.26}$$

Step 2.

If $\theta(c) \geq 0$, put $a_0 = 0, b_0 = c$ and go to Step 7.

Step 3.

Put $l = 1$ and $d_1 = c$

Step 4.

Put $d_{l+1} = d_l + c$

Step 5.

Calculate $\theta(d_{l+1})$

Step 6.

If $\theta(d_{l+1} \geq \theta(d_l)$ then put $a_0 = d_{l-1}$ and $b_0 = d_{l+1}$ and Go to Step 7.

else make $j \leftarrow j + 1$ and Go to Step 4.

Step 7.

Put $i = 0$

Step 8.

Calculate $L_i = b_i - a_i$. If $L_i \leq \epsilon$ put $\alpha^* = a_i + b_i$ and STOP.

else Go to Step 9.

Step 9.

Calculate $u_i = a_i + FL_i$ and $v_i = a_i + GL_i$ and $\theta(U_i), \theta(v_i)$

Step 10.

If $\theta(U_i) < \theta(v_i)$ then $a_{i+1} = a_i, b_{i+1} = v_i$ and do $i \leftarrow i+1$ and Go to Step 8.
else $a_{i+1} = u_i$, $b_{i+1} = b_i$ and do $i \leftarrow i+1$ and go to Step 8.

For Λ

$$tr(\bar{B}^*(\Lambda^* - \Lambda)\bar{B}^{*T}F) \geq 0 \tag{6.27}$$

$\bar{B}^*$ corresponds to $\bar{B}$ for K^* given by:

$$K^*(k) = \mu_\gamma^* P_b^*(k) C^T R_Z^{*-1}(k) \tag{6.28}$$

where μ_γ^* is derived from Γ^* of the optimum parameter of the gradient algorithm with an initial guess for Q_u.

$$tr \begin{bmatrix} B & 0 \\ B & K(k)D \end{bmatrix} \begin{bmatrix} \Omega^* - \Omega & 0 \\ 0 & \Delta^* - \Delta \end{bmatrix} \begin{bmatrix} B^T & B^T \\ 0 & D^T K(k) \end{bmatrix} \geq 0 \tag{6.29}$$

6.5 Conclusions

In this section a new technique for finding the noise parameters has been proposed. This technique is based on a known method of transforming the filtering problem into a control problem. Following the methodology for designing optimal controllers, a mathematical expression for the quality index (the linear functional which measures the degree of efficiency of the controller) is found. This expression is then optimized with respect to the noise parameters and to the Kalman filter gain. In the next chapters we will present some results in filtering speckle noise components in SAR images, comparison of different filters used to this end and some test techniques for filters for speckle noise reduction.

Chapter 7

Results and Performance Evaluation

7.1 Principles of Evaluations

In order to compare various speckle reduction filters, some principles or criteria which are used to evaluate the performance of the filters under test are required. In an effort to establish the criteria, we have developed a methodology for testing filters for SAR imagery [72]. The evaluation methods developed in [72] were published simultaneously and independently of [49]; in the latter Lee showed results of speckle reduction by various filters for speckle reduction without giving test and evaluation criteria for the quality of SAR speckle reduction filters. In [72] we have proposed, for the first time in the domain literature, a set of test images and a set of criteria for filter behavior interpretation. This methodology was expanded on Kalman filters in [22]. The criteria for evaluating the quality of various speckle reduction filters are:

- the mean tonal value,
- the ability of speckle smoothing,
- the edge preservation,
- the angle preservation,
- the point target preservation,
- the slope of the step response,
- filter response to linear patterns.

A good filter should keep the mean tonal value unchanged after filtering. This factor is measured by the bias. The ability of speckle smoothing relates to the radiometric resolution and is measured by the equivalent number of looks (ENL). The bias and the ENL are good indicators of the capability of the filters to smoothing for homogeneous areas. For texture preservation abilities (which is highly demanded for a good adaptive filter), the filters are to be tested with simulated SAR images containing features such as edges, a point target, linear and angular shapes.

The filters to be compared are: Lee, Kuan, Enhanced Lee, Frost, Enhanced Frost, Gamma MAP, and Kalman filters. In order to facilitate the comparison, a BOX filter is included, which is a low pass filter that replaces the center pixel of a scanning window with the average value of all the pixels in the window. The damping factor K, for the Frost, the Enhanced Lee and the Enhanced Frost are chosen to be 1. Since the test images are all single look intensity images, we have $C_n = \sqrt{L} = 1$. For the enhanced Lee and Enhanced Frost filters, $C_{max} = \sqrt{1 + 2/m} = \sqrt{3}$ is chosen. For the Gamma MAP Filter, $C_{max} = \sqrt{2}C_n$.

7.1.1 Homogeneous Areas

Two parts of homogeneous areas of an image are put together to form a test image (Figure 7.1). These two parts are from two areas of water bodies of different intensities from a single look ERS-1 SAR image. The statistics of these two homogeneous areas are calculated from the two areas of 256 pixels by 1024 lines. The results are shown in Table 7.1.

	Mean	Mean(dB)	Variance (dB)	C_n	ENL
Area 1	972.30	59.756	120.07	1.032	0.9382
Area 2	2395.22	67.587	135.61	1.025	0.9512

Table 7.1: Statistics of the areas on the test image

The histogram of homogeneous area 1 and the corresponding theoretical exponential distribution with mean at 972.31 are shown for comparison in Figure 7.2 and in Figure 7.3 respectively. From these two figures, one can see that the two histograms obey the same distribution law, i.e. the distribution of the homogeneous area is exponential.

Similarly, Figure 7.4 shows the histogram of the homogeneous area 2 (which has a mean of 2395.22). It is compared with the theoretical exponential distribution of mean 2395.22 (Figure 7.5). Again, they agree well.

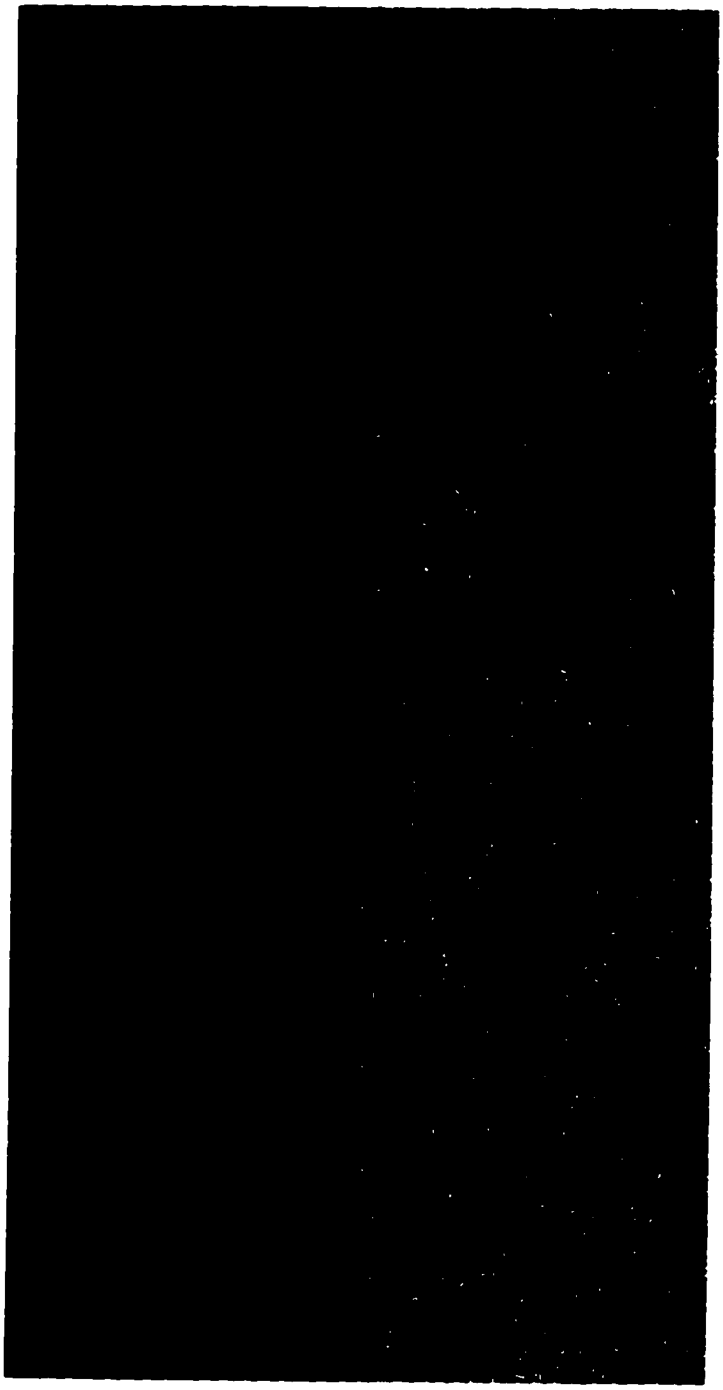

Figure 7.1: Test image created by putting together two homogeneous areas

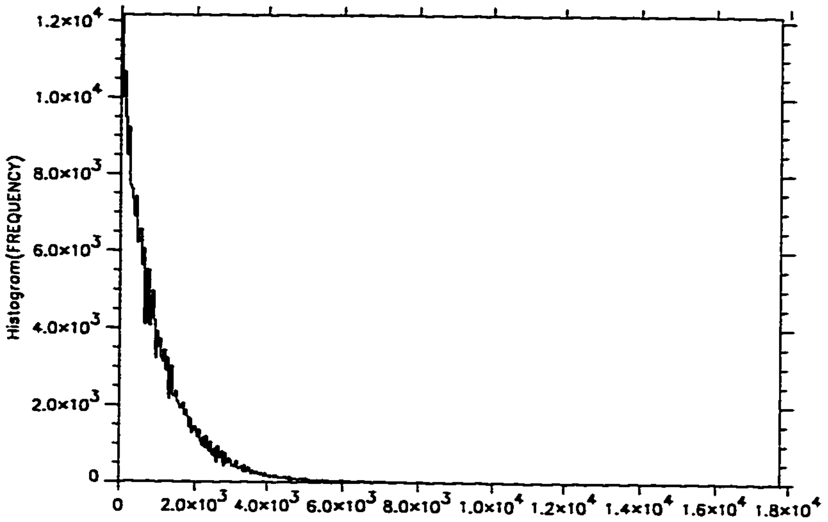

Figure 7.2: The normalized histogram of the homogeneous test area no. 1 (with mean = 972.31).

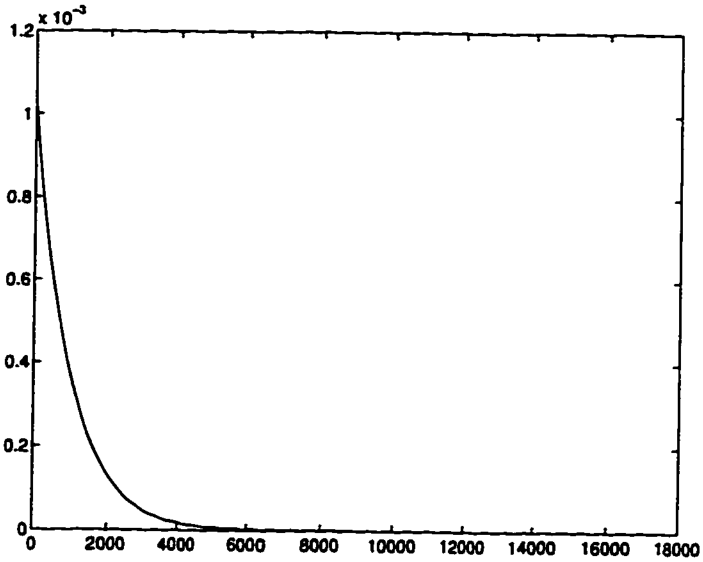

Figure 7.3: The theoretical exponential distribution with mean at 972.31.

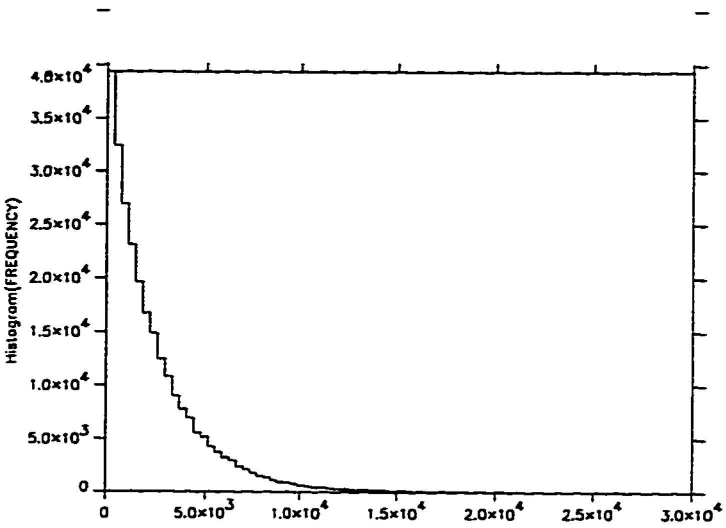

Figure 7.4: The normalized histogram of the homogeneous test area no. 2 (with mean at 2395.22) .

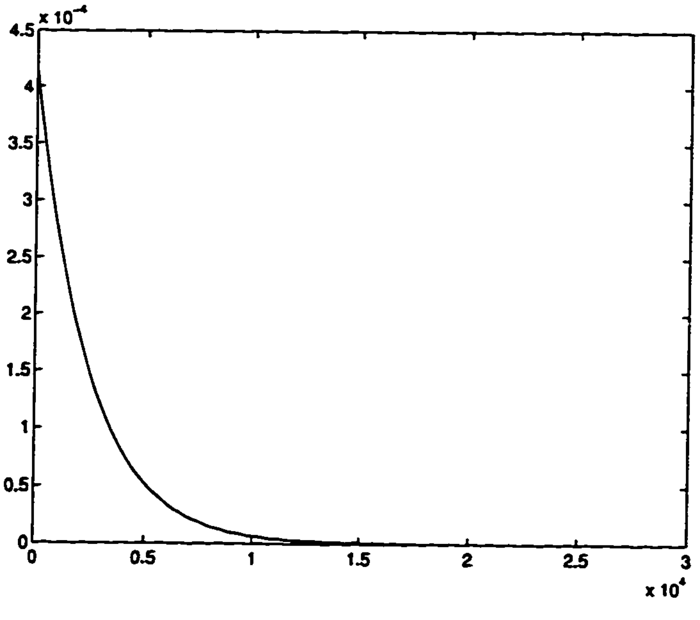

Figure 7.5: The theoretical exponential distribution with mean at 2395.22.

7.2 Test Results on Filters for Speckle Noise Reduction

In what follows, a series of filters for speckle noise reduction, such as Box, Lee, enhanced Lee, Kuan, enhanced Kuan (Gamma MAP filter) , Frost and enhanced Frost, will be tested against various artifact images. Each image tests the performance of the above filters with respect to a given criterion such as: step response (homogeneous area), angular patterns, point target response ("impulse response"), and linear pattern. The results of applying the filters to the combined homogeneous test image are given in Tables 7.2 and 7.13.

The evaluation criteria used to interpret the filtering quality of the above filters are the bias, C_n and the Equivalent Number of Looks (ENL). The bias is expressed as

$$Bias = 20log(\frac{\mu_a}{\mu_b}) \tag{7.1}$$

where μ_b is the mean of the image before filtering, and μ_a is the mean after filtering.

The Equivalent Number of Look (ENL) is a measure of smoothness given by

$$ENL = \frac{\mu^2}{\sigma^2} \tag{7.2}$$

where μ and σ are computed from the filtered image.

The factor C_n is the speckle index, and is related to ENL as in:

$$C_n = \frac{1}{\sqrt{ENL}} = \frac{\sigma}{\mu} \tag{7.3}$$

Box Filter						
	Area 1			Area 2		
Size of the Window	Bias (dB)	C_n	ENL	Bias (dB)	C_n	ENL
3 x 3	$+4.95x10^{-5}$	0.5736	3.04	$+4.84x10^{-6}$	0.5724	3.05
5 x 5	$+2.15x10^{-4}$	0.3827	6.83	$+9.35x10^{-5}$	0.3842	6.78
7 x 7	$+7.70x10^{-4}$	0.2898	11.91	$+2.74x10^{-4}$	0.2932	11.63
9 x 9	$+3.29x10^{-4}$	0.2369	17.82	$+4.67x10^{-4}$	0.2407	17.26
11 x 11	$-5.54x10^{-4}$	0.2029	24.30	$+3.84x10^{-4}$	0.2069	23.36
13 x 13	$-1.31x10^{-3}$	0.1793	31.12	$+1.38x10^{-4}$	0.1838	29.60
15 x 15	$-1.93x10^{-3}$	0.1622	38.03	$-3.62x10^{-5}$	0.1671	35.81
17 x 17	$-2.44x10^{-3}$	0.1494	44.82	$-2.85x10^{-4}$	0.1544	41.95
19 x 19	$-2.84x10^{-3}$	0.1396	51.33	$-4.67x10^{-4}$	0.1445	47.87

Table 7.2: Statistics of the smoothed areas by box filter

As shown in Table 7.2, the Box filter does its job of smoothing the data. As the window size increases, the smoothing factor increases. It is also evident that the smoothing is really a factor of the window sizes for both areas. As a result, it attains an ENL close to 50 for 19 x 19 window. Of course, this gain of smoothness is at the expense of edges and point targets.

Lee Filter						
	Area 1			Area 2		
Size of the Window	Bias (dB)	C_n	ENL	Bias (dB)	C_n	ENL
3 x 3	-1.76	1.4347	0.49	-1.78	1.4649	0.47
5 x 5	$-2.59x10^{-1}$	0.6583	2.31	$-2.72x10^{-1}$	0.6709	2.22
7 x 7	$-7.35x10^{-2}$	0.4678	4.57	$-7.25x10^{-2}$	0.4728	4.47
9 x 9	$-2.38x10^{-2}$	0.3736	7.16	$-2.56x10^{-2}$	0.3762	7.07
11 x 11	$-8.17x10^{-3}$	0.3158	10.03	$-1.04x10^{-2}$	0.3181	9.88
13 x 13	$-4.43x10^{-3}$	0.2758	13.15	$-4.25x10^{-3}$	0.2779	12.95
15 x 15	$-2.28x10^{-3}$	0.2478	16.28	$+2.13x10^{-3}$	0.2487	16.17
17 x 17	$-2.76x10^{-3}$	0.2272	19.38	$+3.12x10^{-3}$	0.2267	19.46
19 x 19	$-1.38x10^{-3}$	0.2111	22.45	$+3.12x10^{-3}$	0.2091	22.86

Table 7.3: Statistics of the smoothed areas by Lee filter

The smoothing by the Lee filter is very gradual. The effect of the 3 x 3 filter is very limited. The effect of smoothing is very low for 3 x 3 when compared to the Box filter. Once the window size is increased to 5 x 5 and beyond, it is about half as effective as the Box filter.

Kuan Filter						
	Area 1			Area 2		
Size of the Window	Bias (dB)	C_n	ENL	Bias (dB)	C_n	ENL
3 x 3	$-8.34x10^{-1}$	0.7572	1.74	$-8.46x10^{-1}$	0.7665	1.70
5 x 5	$-1.28x10^{-1}$	0.4588	4.75	$-1.35x10^{-1}$	0.4635	4.65
7 x 7	$-3.63x10^{-2}$	0.3417	8.56	$-3.61x10^{-2}$	0.3453	8.39
9 x 9	$-1.22x10^{-2}$	0.2768	13.05	$-1.25x10^{-2}$	0.2804	12.72
11 x 11	$-4.36x10^{-3}$	0.2358	17.99	$-4.99x10^{-3}$	0.2395	17.43
13 x 13	$-2.87x10^{-3}$	0.2075	23.23	$-2.06x10^{-3}$	0.2112	22.41
15 x 15	$-2.10x10^{-3}$	0.1873	28.49	$+1.05x10^{-3}$	0.1908	27.47
17 x 17	$-2.60x10^{-3}$	0.1723	33.67	$+1.42x10^{-3}$	0.1754	32.52
19 x 19	$-2.11x10^{-3}$	0.1607	38.73	$+1.33x10^{-3}$	0.1632	37.56

Table 7.4: Statistics of the smoothed areas by Kuan filter

The Kuan filter does a better job for a 3x3 window than the Lee filter. Its ENL is more than 3 times of the Lee filter. It does a better job for the homogeneous than the Lee filter for window sizes above 5 x 5. However, it does not have the same level of smoothing as the Box filter.

Enhanced Lee Filter ($K = 0.1$)						
	Area 1			Area 2		
Size of the Window	Bias (dB)	C_n	ENL	Bias (dB)	C_n	ENL
3 x 3	$-1.91x10^{-2}$	0.5756	3.02	$-1.67x10^{-2}$	0.5742	3.03
5 x 5	$-1.91x10^{-2}$	0.3854	6.73	$-1.53x10^{-2}$	0.3866	6.69
7 x 7	$-6.59x10^{-3}$	0.2947	11.51	$-5.68x10^{-3}$	0.2958	11.43
9 x 9	$-2.89x10^{-4}$	0.2460	16.52	$-1.58x10^{-3}$	0.2425	17.00
11 x 11	$+5.74x10^{-4}$	0.2131	22.01	$-2.17x10^{-4}$	0.2081	23.09
13 x 13	$-1.15x10^{-3}$	0.1845	29.37	$-9.34x10^{-5}$	0.1846	29.33
15 x 15	$-1.99x10^{-3}$	0.1643	37.03	$-6.20x10^{-5}$	0.1678	35.52
17 x 17	$-2.54x10^{-3}$	0.1508	43.98	$-2.30x10^{-4}$	0.1550	41.64
19 x 19	$-2.82x10^{-3}$	0.1406	50.58	$-4.05x10^{-4}$	0.1450	47.56

Table 7.5: Statistics of the smoothed areas by Enhanced Lee filter with K = 0.1

The enhanced Lee filter uses a speckle index of the (unfiltered) input data to direct its filtering function for the homogeneous area. However, this is affected by the selection of the K value. In this combination, with $K = 0.1$, it does a good job. It matches the Box filter because the enhanced Lee filter uses the Box filter once the speckle index is found to be below a given speckle index. Unfortunately, both K and the value which determines the homogeneity of the areas must be found experimentally.

Enhanced Lee Filter ($K = 1.0$)						
	Area 1			Area 2		
Size of the Window	Bias (dB)	C_n	ENL	Bias (dB)	C_n	ENL
3 x 3	$-1.09x10^{-1}$	0.5873	2.90	$-9.87x10^{-2}$	0.5846	2.93
5 x 5	$-9.24x10^{-2}$	0.4174	5.74	$-8.25x10^{-2}$	0.4142	5.83
7 x 7	$-3.27x10^{-2}$	0.3480	8.26	$-3.13x10^{-2}$	0.3418	8.56
9 x 9	$-8.64x10^{-3}$	0.3013	11.02	$-1.23x10^{-2}$	0.2933	11.62
11 x 11	$-2.11x10^{-3}$	0.2660	14.14	$-4.20x10^{-3}$	0.2558	15.28
13 x 13	$-1.91x10^{-3}$	0.2395	17.44	$-1.85x10^{-3}$	0.2271	19.39
15 x 15	$-7.66x10^{-4}$	0.2193	20.79	$-2.31x10^{-4}$	0.2052	23.74
17 x 17	$-2.23x10^{-3}$	0.2018	24.55	$+3.80x10^{-4}$	0.1884	28.17
19 x 19	$-2.23x10^{-3}$	0.1878	28.36	$+4.14x10^{-4}$	0.1749	32.67

Table 7.6: Statistics of the smoothed areas by Enhanced Lee filter with K = 1.0

With $K = 1$, the enhanced Lee filter does not have a good smoothing quality as in case of $K = 0.1$. The smoothing effect is now lower than the Box filter, but it is comparable with the Kuan filter.

Enhanced Lee Filter (K = 10)						
	Area 1			Area 2		
Size of the Window	Bias (dB)	C_n	ENL	Bias (dB)	C_n	ENL
3 x 3	$-2.94x10^{-1}$	0.6268	2.55	$-2.78x10^{-1}$	0.6219	2.59
5 x 5	$-2.04x10^{-1}$	0.5680	3.10	$-1.92x10^{-1}$	0.5524	3.28
7 x 7	$-7.12x10^{-2}$	0.5750	3.02	$-6.09x10^{-2}$	0.5546	3.25
9 x 9	$-2.18x10^{-2}$	0.5682	3.10	$-3.38x10^{-2}$	0.5417	3.41
11 x 11	$-2.22x10^{-3}$	0.5520	3.28	$-1.58x10^{-2}$	0.5272	3.60
13 x 13	$-2.14x10^{-3}$	0.5369	3.47	$-5.79x10^{-3}$	0.5144	3.78
15 x 15	$+2.06x10^{-3}$	0.5257	3.62	$-2.00x10^{-4}$	0.5002	4.00
17 x 17	$-1.12x10^{-3}$	0.5139	3.79	$+5.38x10^{-3}$	0.4870	4.22
19 x 19	$+4.27x10^{-3}$	0.5029	3.95	$+9.47x10^{-3}$	0.4752	4.43

Table 7.7: Statistics of the smoothed areas by Enhanced Lee filter with K = 10

The value $K = 10$ is too large for the Enhanced Lee filter 7.7. Its ability to smooth out noise in homogeneous areas is lost. Increasing the window size does not improve much on its ability of smoothing. However, it does a respectable job for a small 3 x 3 window. In fact, it is comparable in smoothing in a window of size 3 x 3, with all the other other tested filters.

Frost Filter ($K = 0.1$)						
	Area 1			Area 2		
Size of the Window	Bias (dB)	C_n	ENL	Bias (dB)	C_n	ENL
3 x 3	$-1.03x10^{-2}$	0.5760	3.01	$-9.98x10^{-3}$	0.5748	3.03
5 x 5	$-8.76x10^{-3}$	0.3872	6.67	$-8.46x10^{-3}$	0.3885	6.63
7 x 7	$-4.21x10^{-3}$	0.2948	11.50	$-4.53x10^{-3}$	0.2980	11.26
9 x 9	$-2.00x10^{-3}$	0.2418	17.10	$-2.18x10^{-3}$	0.2456	16.58
11 x 11	$-1.65x10^{-3}$	0.2077	23.18	$-1.10x10^{-3}$	0.2118	22.29
13 x 13	$-1.80x10^{-3}$	0.1842	29.47	$-5.00x10^{-4}$	0.1887	28.09
15 x 15	$-1.86x10^{-3}$	0.1672	35.75	$-1.55x10^{-4}$	0.1720	33.78
17 x 17	$-1.91x10^{-3}$	0.1546	41.87	$-1.34x10^{-4}$	0.1595	39.31
19 x 19	$-1.97x10^{-3}$	0.1448	47.69	$-1.29x10^{-4}$	0.1498	44.57

Table 7.8: Statistics of the smoothed areas by Frost filter with K = 0.1

The basic Frost filter operates well for homogeneous areas. As shown in Table 7.8, its performance is comparable to the Box filter one. It does not need to use the speckle indicator as the other enhanced speckle filters. In our test, it outperforms the basic Lee filter. However, the filter depends on the value of K as well.

Frost Filter (K = 1)						
	Area 1			Area 2		
Size of the Window	Bias (dB)	C_n	ENL	Bias (dB)	C_n	ENL
3 x 3	$-1.43x10^{-1}$	0.6140	2.65	$-1.37x10^{-1}$	0.6112	2.68
5 x 5	$-8.78x10^{-2}$	0.4897	4.17	$-8.51x10^{-2}$	0.4858	4.24
7 x 7	$-3.12x10^{-2}$	0.4543	4.85	$-3.11x10^{-2}$	0.4480	4.98
9 x 9	$-8.35x10^{-3}$	0.4397	5.17	$-1.04x10^{-2}$	0.4316	5.37
11 x 11	$-1.19x10^{-3}$	0.4315	5.37	$-2.80x10^{-3}$	0.4232	5.58
13 x 13	$+3.92x10^{-4}$	0.4269	5.49	$-4.76x10^{-4}$	0.4191	5.69
15 x 15	$+8.57x10^{-4}$	0.4249	5.54	$+1.39x10^{-3}$	0.4169	5.75
17 x 17	$-5.11x10^{-5}$	0.4235	5.58	$+1.93x10^{-3}$	0.4155	5.79
19 x 19	$+2.57x10^{-4}$	0.4225	5.60	$+1.84x10^{-3}$	0.4147	5.82

Table 7.9: Statistics of the smoothed areas by Frost filter with K = 1

When $K = 1$, the performance of the Frost filter stays more or less around an ENL of 5 for windows larger than 5 x 5. It is obvious that this filter is dependent on setting the value of K. In our test cases, it performs best for homogeneous areas when $K = 0.1$.

Frost Filter (K = 10)						
	Area 1			Area 2		
Size of the Window	Bias (dB)	C_n	ENL	Bias (dB)	C_n	ENL
3 x 3	$-1.31x10^{-1}$	0.9960	1.01	$-1.35x10^{-1}$	0.9878	1.02
5 x 5	$-2.62x10^{-4}$	1.0263	0.95	$-1.06x10^{-3}$	1.0188	0.96
7 x 7	$-8.35x10^{-4}$	1.0304	0.94	$-2.88x10^{-6}$	1.0232	0.96
9 x 9	$+5.96x10^{-6}$	1.0315	0.94	$-2.63x10^{-5}$	1.0243	0.95
11 x 11	$+5.36x10^{-5}$	1.0319	0.94	$-1.05x10^{-5}$	1.0247	0.95
13 x 13	$+4.68x10^{-5}$	1.0320	0.94	$-1.02x10^{-5}$	1.0249	0.95
15 x 15	$+4.65x10^{-5}$	1.0321	0.94	$-7.19x10^{-6}$	1.0250	0.95
17 x 17	$+4.75x10^{-5}$	1.0322	0.94	$-3.22x10^{-6}$	1.0251	0.95
19 x 19	$+4.53x10^{-5}$	1.0322	0.95	$-2.82x10^{-6}$	1.0251	0.95

Table 7.10: Statistics of the smoothed areas by Frost filter with K = 10

When $K = 10$, its performance deteriorates as the window size increases. i.e. the performance decreases to a level of approximately 1 look, which means no improvement at all. The three test cases show that this filter should operate with a $K = 1$ for homogeneous areas.

Enhanced Frost Filter (K = 0.1)						
	Area 1			Area 2		
Size of the Window	Bias (dB)	C_n	ENL	Bias (dB)	C_n	ENL
3 x 3	$-6.45x10^{-3}$	0.5745	3.03	$-5.37x10^{-3}$	0.5731	3.04
5 x 5	$-1.04x10^{-2}$	0.3840	6.78	$-7.84x10^{-3}$	0.3854	6.73
7 x 7	$-4.65x10^{-3}$	0.2929	11.68	$-3.95x10^{-3}$	0.2942	11.55
9 x 9	$+2.96x10^{-4}$	0.2448	16.68	$-1.29x10^{-3}$	0.2413	17.17
11 x 11	$+8.30x10^{-4}$	0.2118	22.30	$-4.66x10^{-4}$	0.2073	23.27
13 x 13	$-1.57x10^{-3}$	0.1813	30.43	$-2.04x10^{-4}$	0.1841	29.51
15 x 15	$-2.15x10^{-3}$	0.1627	37.79	$-1.66x10^{-4}$	0.1673	35.71
17 x 17	$-2.36x10^{-3}$	0.1497	44.64	$-3.56x10^{-4}$	0.1546	41.84
19 x 19	$-2.70x10^{-3}$	0.1398	51.18	$-4.80x10^{-4}$	0.1447	47.76

Table 7.11: Statistics of the smoothed areas by Enhanced Frost filter with K = 0.1

This Enhanced Frost does have a good performance which is comparable to the Box Filter. It uses a speckle index to identify homogeneous areas and then it does the area filtering by averaging. However, this is not strictly the performance of the filter itself. It is actually the Box filter in some sense.

Enhanced Frost Filter (K = 1)						
	Area 1			Area 2		
Size of the Window	Bias (dB)	C_n	ENL	Bias (dB)	C_n	ENL
3 x 3	$-4.36x10^{-2}$	0.5789	2.98	$-3.84x10^{-2}$	0.5770	3.00
5 x 5	$-5.90x10^{-2}$	0.3958	6.38	$-5.13x10^{-2}$	0.3954	6.40
7 x 7	$-2.88x10^{-2}$	0.3148	10.09	$-2.73x10^{-2}$	0.3120	10.28
9 x 9	$-1.23x10^{-2}$	0.2638	14.36	$-1.27x10^{-2}$	0.2597	14.83
11 x 11	$-6.16x10^{-3}$	0.2308	18.78	$-5.86x10^{-3}$	0.2216	20.37
13 x 13	$-4.51x10^{-3}$	0.2069	23.36	$-2.43x10^{-3}$	0.1950	26.31
15 x 15	$-2.76x10^{-3}$	0.1855	29.06	$-7.19x10^{-4}$	0.1761	32.24
17 x 17	$-2.14x10^{-3}$	0.1682	35.36	$-6.42x10^{-4}$	0.1620	38.08
19 x 19	$-1.52x10^{-3}$	0.1546	41.86	$-6.57x10^{-4}$	0.1512	43.72

Table 7.12: Statistics of the smoothed areas by the Enhanced Frost filter with K = 1

The K does affect the performance of the Enhanced Frost filter. When $K = 1$, its performance is lowered by a small amount when compared to the case when $K = 0.1$. In fact, the Frost filter performs very well without the use of the speckle index (see Table 7.8.

Enhanced Frost Filter ($K = 10$)						
	Area 1			Area 2		
Size of the Window	Bias (dB)	C_n	ENL	Bias (dB)	C_n	ENL
3 x 3	$-2.28x10^{-1}$	0.6116	2.67	$-2.12x10^{-1}$	0.6070	2.71
5 x 5	$-1.89x10^{-1}$	0.5202	3.70	$-1.79x10^{-1}$	0.5070	3.89
7 x 7	$-7.61x10^{-2}$	0.5119	3.82	$-7.03x10^{-2}$	0.4948	4.09
9 x 9	$-2.18x10^{-2}$	0.4961	4.06	$-3.58x10^{-2}$	0.4728	4.47
11 x 11	$-3.69x10^{-3}$	0.4700	4.53	$-1.59x10^{-2}$	0.4489	4.96
13 x 13	$-6.97x10^{-4}$	0.4456	5.04	$-9.17x10^{-3}$	0.4279	5.46
15 x 15	$+3.80x10^{-3}$	0.4264	5.50	$-1.30x10^{-3}$	0.4074	6.02
17 x 17	$+5.68x10^{-3}$	0.4078	6.01	$+4.06x10^{-3}$	0.3865	6.69
19 x 19	$+1.02x10^{-2}$	0.3920	6.51	$+9.12x10^{-3}$	0.3673	7.41

Table 7.13: Statistics of the smoothed areas by Enhanced Frost filter with K = 10

The effect of a large K value is clearly shown in this test case. The increase in window size does not help the smoothing. In fact the bias is bigger than the other cases and the ENL is much lower than the other cases for large window size.

For the Kalman filters the results are as given in the following table:

7.2.1 Edges

Edge is an important feature for evaluating digital filters. A desired feature of a speckle reduction filter is the preservation of the position and the sharpness (or slope) of the edge. An expected edge in an image should not be shifted or blurred after the filter operation is complete. Unfortunately, most of the filters either blur

	Image A				Image B			
Filter	Mean	Variance	Bias(dB)	ENL	Mean	Variance	Bias(dB)	ENL
None	942	9.18e5		0.97	2537	6.699e6		0.96
FABKF, $\sigma_v^2 = 3.0e4$	877	8.99e4	-6.2e-1	8.6	2703	8.65e5	5.5e-1	8.4
FABKF, $\sigma_v^2 = 3.0e5$	843	1.85e5	-9.6e-1	3.8	2753	1.17e6	7.1e-1	6.5
FABKF, $\sigma_v^2 = 3.0e6$	896	5.54e5	-4.3e-1	1.4	2543	2.07e6	2.1e-2	3.1
SMABKF, $\sigma_v^2 = 3.0e4$	875	7.88e4	-23.9e-1	10.5	2344	4.34e5	-5.6	11.7
SMABKF, $\sigma_v^2 = 3.0e5$	935	3.591e5	-19.9e-1	11.5	2361	6.0e5	-5.0e-1	19.55
SMABKF, $\sigma_v^2 = 3.0e6$	975	7.72e5	-9.4e-1	1.5	2417	2.54e6	-4.2e-1	13.8
MMABKF, $\sigma_v^2 = 3.0e4$	850	6.88e4	-8.9e-1	10.5	2351	3.74e5	5.6	12.7
MMABKF, $\sigma_v^2 = 3.0e5$	922	1.91e5	-11.9e-1	15.5	2384	6.5e5	4.50e-1	19.55
MMABKF, $\sigma_v^2 = 3.0e6$	927	5.72e5	-11.4e-1	10.5	2417	1.34e6	3.2e-1	13.8

Table 7.14: Speckle Reduction Performance of Kalman Filters; Full Plane (FABKF), State Multiplicative Noise Kalman Filter (SMABKF), and Markov State Multiplicative Noise Kalman Filter (MMABKF)

or shift the location of edges.

The test image constructed for this test is similar to the combined homogeneous areas given in the last section. It is formed by combining two homogeneous areas. The resultant image has 512 pixels by 1024 lines. The left half occupies 256 pixels by 1024 lines with a mean intensity value of 973.31; the other half has the same size but with a mean intensity value of 2395.22. As a result, there is a sharp edge dividing the two homogeneous areas.

A reference profile is then created to measure the performance of different filters. It is created by averaging the test image column-wise (thus creating a profile of 512 pixels as shown in Figure 7.7). The average of the higher intensity half (i.e. the right half) is 2395.22 (which is called the upper baseline). The average of the lower intensity half (the left side) is 972.31(which is called the lower baseline). Therefore, the value at the mid-slope between the upper and the lower baseline is 1683.77; and the pixel value at this mid-slope is at 255.5.

The reference slope is defined to be the ratio of the distance between the two baselines to the extent that it covers in the pixel domain. For the ease of computation, we select the slope between the lines labeled d and b for the estimation, where the slope is found to be linear in all of the filtered results. The line d is located at intensity value of 2252.93, which is equal to the intensity at e lowered by 10% of the "length" between lines a and e. Similarly, line b is at 1256.88, which is equal to the value at a plus 20% of the "length" between lines a and e. Figure 7.7 shows the relative positions of the lines a, b, c, d, e. The slope of an edge filtered using the box filter is superimposed for illustration. The numerical results computed from the filtered images of the different filters are tabulated in Table 7.15, with the corresponding image files shown in the following figures 7.8, 7.9, 7.10, 7.11, 7.12, 7.13, 7.14, 7.15, 7.16.

With reference to Table 7.15, most of the filters do not shift the given edge in the filtered image. However, when the window size exceeds 9, the Box filter, the Enhanced Lee (K=0.1), the Frost(K=0.1) and the enhanced Frost (K=0.1) filters shift the edge on the filtered image by 1 pixel. But, in general, the Frost filter with $K = 1$ has the best result. Close by are the Lee, Kuan, Enhanced Frost ($K = 1$) and the Gamma MAP filters. Following on then is the Enhanced Lee Filter with ($K = 1$). Even though the Enhanced Lee (K=0.1), enhanced Frost (K+0.1) and Frost filters function well with the homogeneous areas, they are ranked in the bottom group in the edge test. From this test, it seems that the optimal value for K for all these filters is K=1.

The filtered response of a Kalman filter to a step edge is illustrated by an average contour line at ±1% around the maximum and minimum values and at 10% and 90% between the maximum and minimum values. This indicates the degree of overshoot and undershoot in the filter output and is shown in Figure 7.17.

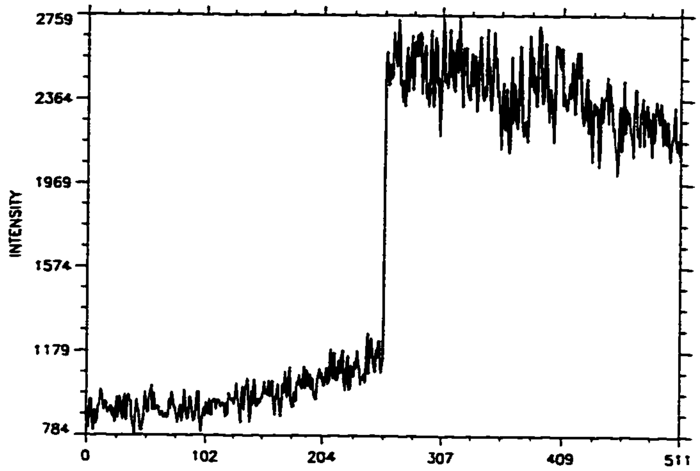

Figure 7.6: The input image profile of the step edge generated from the homogeneous test image. It is used to test the step response of the speckle reduction filters

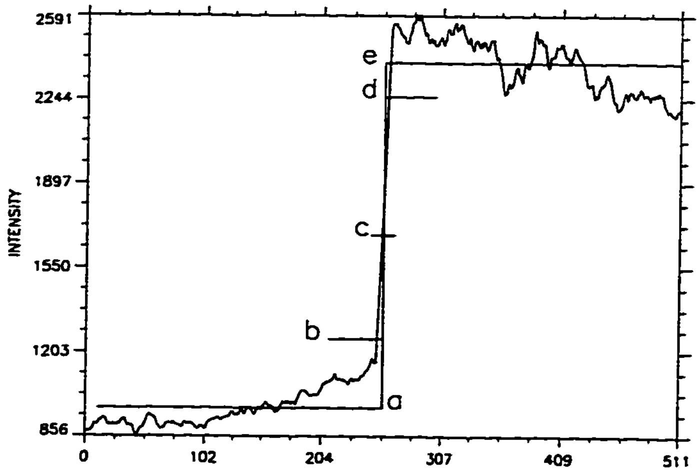

Figure 7.7: Diagram showing how the slope is computed. Superimposed on it is a filtered profile by using a Box filter with a scanning window of 11 x 11.

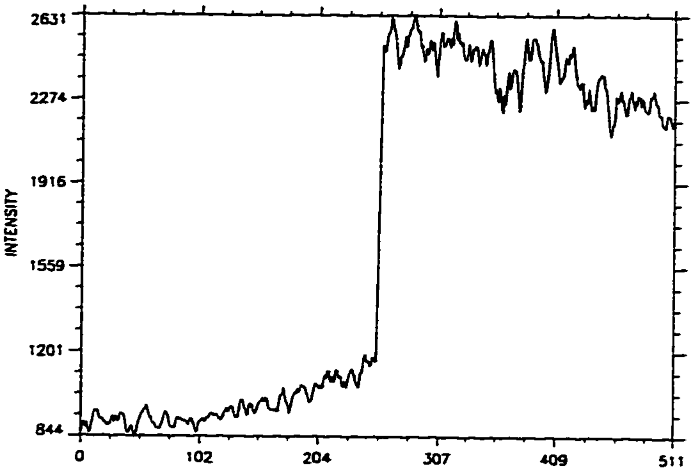

Figure 7.8: The filtered response to a step edge by the Box Filter with a 5x5 scanning window

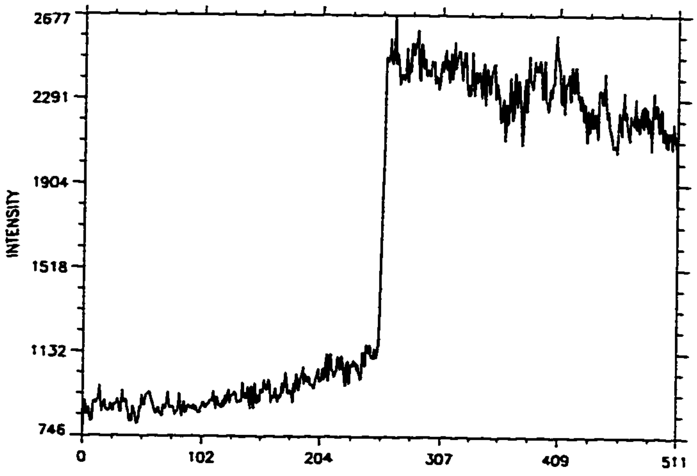

Figure 7.9: The filtered response to a step edge by the Lee Filter with a 5x5 scanning window

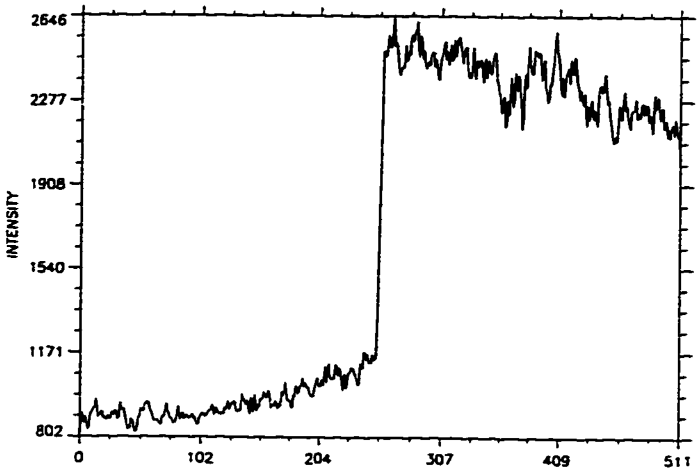

Figure 7.10: The filtered response to a step edge by the Kuan Filter with a 5x5 scanning window

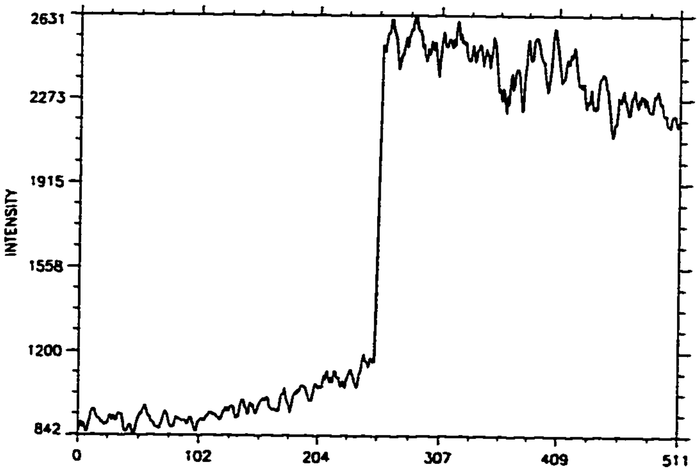

Figure 7.11: The filtered response to a step edge by the Enhanced Lee Filter (K=0.1) with a 5x5 scanning window

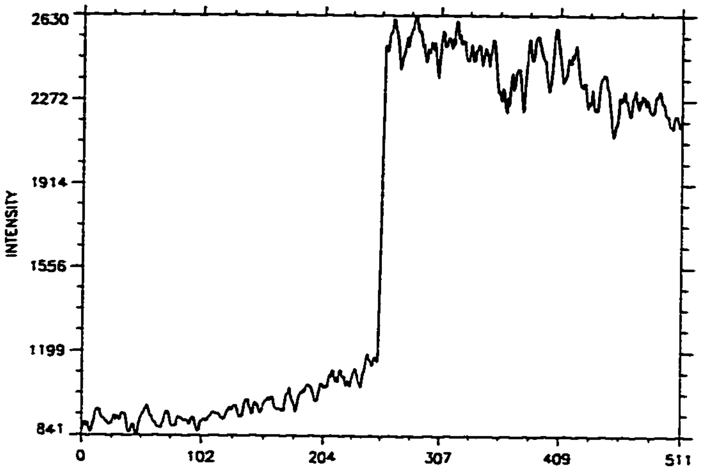

Figure 7.12: The filtered response to a step edge by the Frost Filter (K=0.1) with a 5x5 scanning window

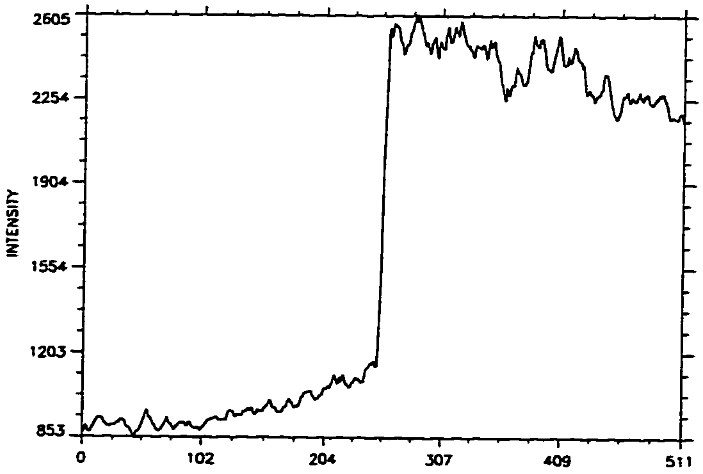

Figure 7.13: The filtered response to a step edge by the Frost Filter (K=1) with a 5x5 scanning window

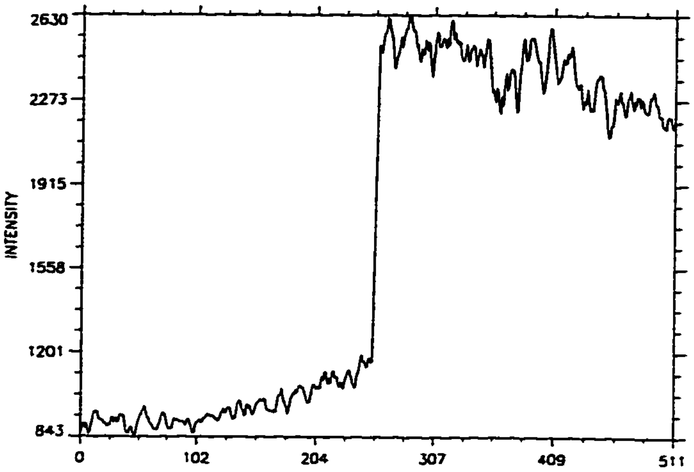

Figure 7.14: The filtered response to a step edge by the Enhanced Frost Filter (K=0.1) with a 5x5 scanning window

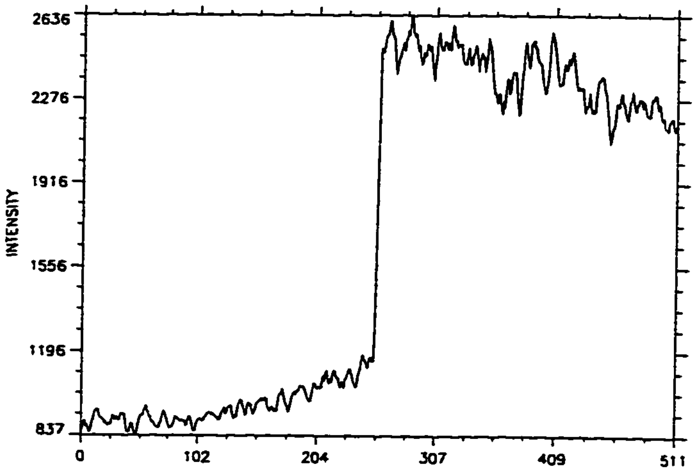

Figure 7.15: The filtered response to a step edge by the Enhanced Frost Filter (K=1) with a 5x5 scanning window

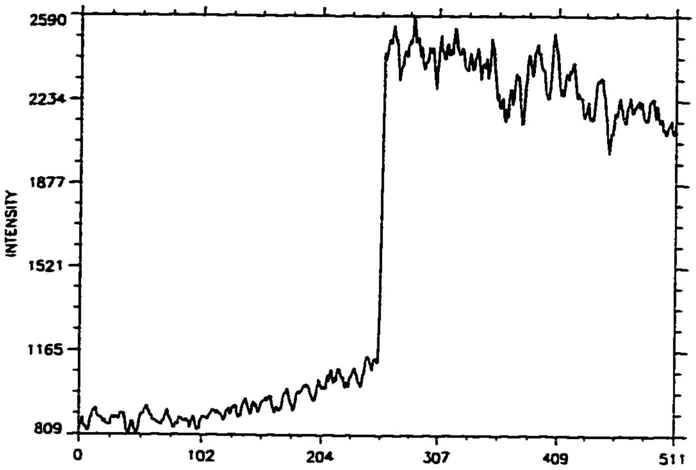

Figure 7.16: The filtered response to a step edge by the Gamma Filter with a 5x5 scanning window

A synoptic presentation of the quality of responses of various filters for speckle noise reduction to a step function in terms of mid-point and slope is given in the next table.

A similar table was built for the results obtained by filtering the slope-test image of 7.1 using the Kalman filter. There are differences in the structure of this table as compared to the previous one due to other parameters that had to be considered while experimenting with the Kalman filter.

Calculation of Mid-Point, and Slope										
Window Size		$3x3$	$5x5$	$7x7$	$9x9$	$11x11$	$13x13$	$15x15$	$17x17$	$19x19$
Box	M.P.	255	255	255	254	254	254	254	254	253
	Slope	332.0	199.2	142.3	124.5	99.60	90.55	83.00	76.62	66.4
Lee	M.P.	256	255	255	255	255	255	255	255	255
	Slope	76.62	199.2	142.3	124.5	110.7	99.60	90.55	76.62	76.62
Kuan	M.P.	255	255	255	255	255	255	255	255	254
	Slope	249.0	199.2	142.3	124.5	110.7	90.55	83.00	76.62	66.40
E. Lee K=0.1	M.P.	255	255	255	255	254	254	254	254	254
	Slope	569.2	66.96	59.91	59.91	54.21	51.74	47.43	47.43	43.78
E. Lee K=1	M.P.	255	255	255	255	255	255	255	255	255
	Slope	379.4	66.96	59.91	56.92	54.21	51.74	49.49	47.43	51.74
Frost K=0.1	M.P.	255	255	255	255	254	254	254	254	254
	Slope	569.2	63.24	59.91	59.91	56.92	51.74	51.74	49.49	49.49
Frost K=1	M.P.	255	255	255	255	255	255	255	255	255
	Slope	332.0	249.0	199.2	199.2	199.2	199.2	199.2	199.2	199.2
E. Frost K=0.1	M.P.	255	255	255	255	254	254	254	254	254
	Slope	66.96	63.24	59.91	59.91	54.21	51.74	47.43	47.43	43.78
E. Frost K=1	M.P.	255	255	255	255	255	255	255	255	255
	Slope	332.0	199.2	142.3	142.3	110.7	99.6	99.6	83.0	83.0
Γ MAP	M.P.	255	256	256	256	256	256	256	256	256
	Slope	249.0	249.0	166.0	124.5	110.7	110.7	90.55	83.0	76.62

Table 7.15: Responses of the test filters to a step function in terms of mid-point and slope.

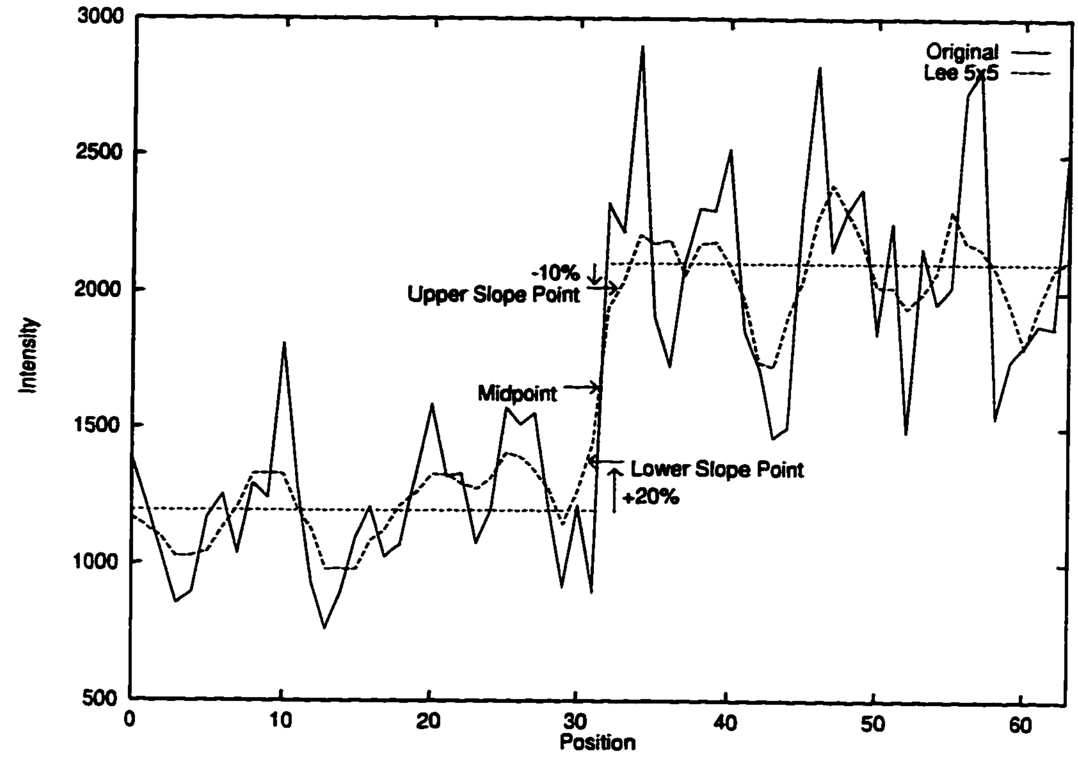

Figure 7.17: The filtered response to a step edge by the Kalman Filter.

7.2.2 Point Target

In general, corner reflectors, natural and man-made objects with angular shapes show up clearly on the microwave image with strong responses. Some of these targets are relatively small, occupying one to a few pixels, yet they are objects to be studied or located (such as the case of ship detection [20], [82]). Speckle reduction filter must preserve them. In this test, we examine the ability of preservation and conditioning of the point targets by the speckle filters.

A test image is created by first designing a point target without noise (Figure 7.18). Speckle noise, modeled after the RADARSAT SAR "fine" mode beam pattern and the associated response of the signal processor, was generated and inserted into

Calculation of Mid-Point, and Slope				
Block size		$1x1$	$2x2$	$3x3$
Kalman FABKF	M.P.	64	64	65
$\sigma_u^2 = 3.0e6$	Slope	452.5	390	385
Kalman MMFABKF	M.P.	64.5	65	63.9
$\sigma_u^2 = 3.0e6$	Slope	831	732	695
Kalman OFABKF	M.P.	64	65.5	64.2
$\sigma_u^2 = 3.0e6$	Slope	895	850	745

Table 7.16: Responses of the Kalman filters to a step function in terms of mid-point and slope

the image (Figure 7.19). The point target is a 3 x 3 pulse in the middle of a flat background. The intensity of the point target is set to 16900, while its background to 2704 (i.e. 15.92 dB).

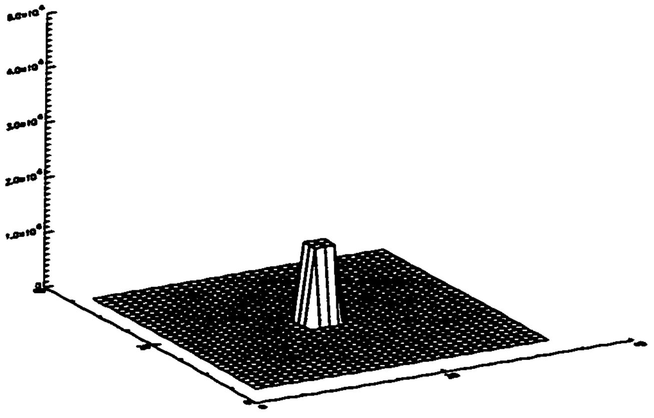

Figure 7.18: The simulated point target before multiplicative speckle noise is injected.

While all of the above filters greatly reduce the level of noise in the original image, the three modified Kalman filters all preserve the point target at values near the original. Of the all Kalman filters, the full plane (FABKF) results are the best compromise of smoothing the homogeneous region while maintaining the point target. The introduction of the state multiplicative noise in the state model of the Kalman filter preserves the point target better; it smoothes the homogeneous region the least while maintaining the shape and location of the point target.

It is interesting to note that the adaptation criteria plays an important role in preserving the point target while the state transition noise, σ_u^2, is not as important.

The above facts are shown in Figure 7.28 where the results of the MFABKF with various coefficient of variation threshold values, Cr_{max}, are given. When Cr_{max} is set to 3.5 or higher, the entire point is filtered out.

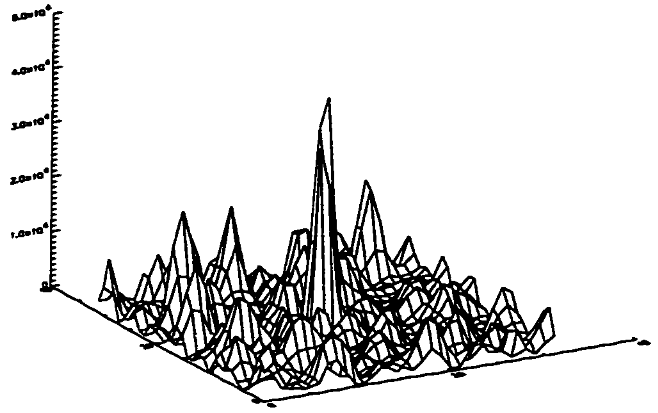

Figure 7.19: The simulated point target after speckle noise is injected. The speckle noise is modeled after the RADARSAT fine mode beam pattern and its corresponding signal processor

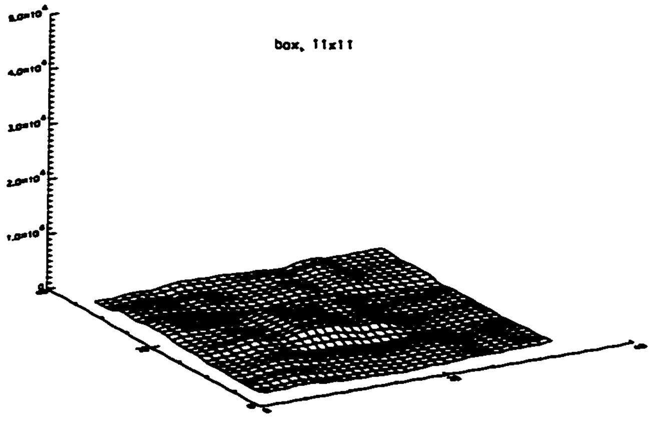

Figure 7.20: The result of filtering the noisy speckled point target by the Box Filter with a 11 x 11 scanning window

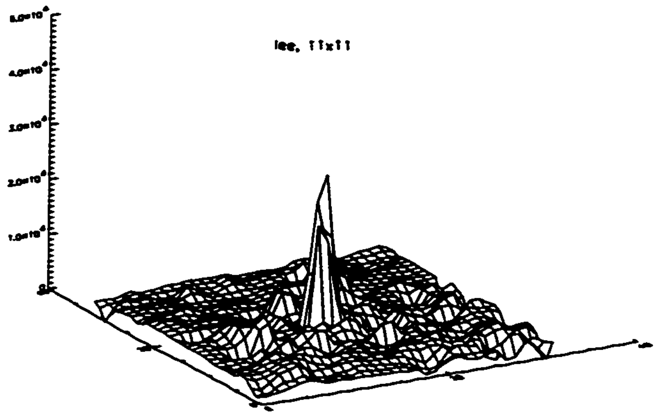

Figure 7.21: The result of filtering the noisy speckled point target by the Lee Filter with a 11 x 11 scanning window

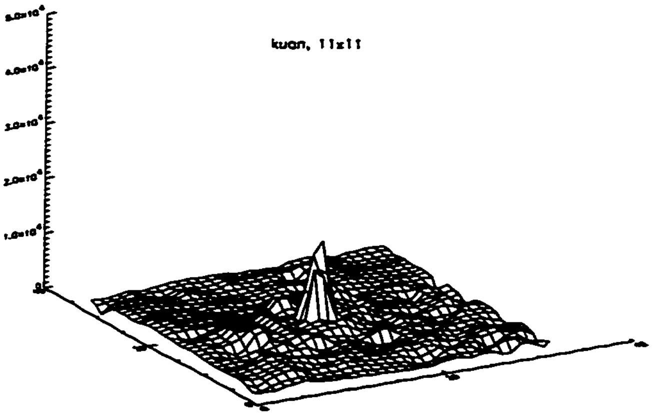

Figure 7.22: The result of filtering the noisy speckled point target by the Kuan Filter with a 11 x 11 scanning window

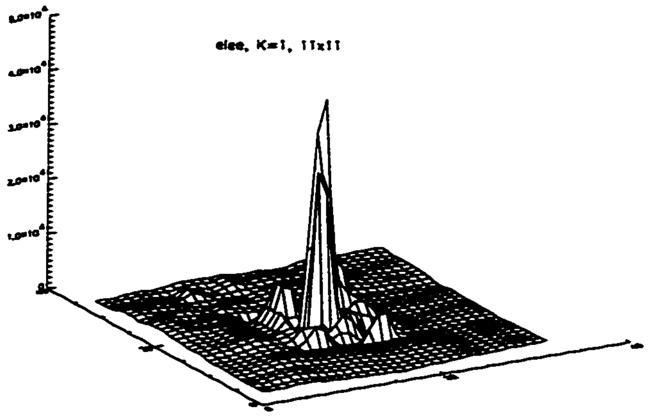

Figure 7.23: The result of filtering the noisy speckled point target by the Enhanced Lee Filter (K=1) with a 11 x 11 scanning window

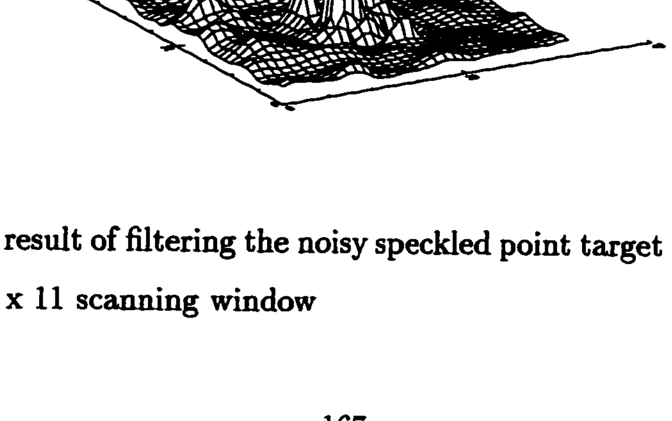

Figure 7.24: The result of filtering the noisy speckled point target by the Frost Filter (K=1) with a 11 x 11 scanning window

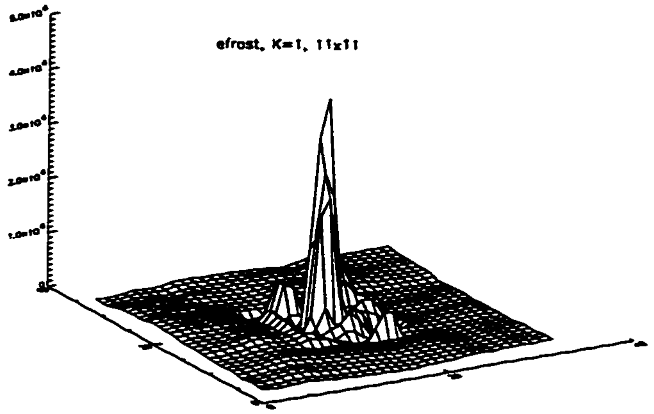

Figure 7.25: The result of filtering the noisy speckled point target by the Enhanced Frost Filter (K=1) with a 11 x 11 scanning window

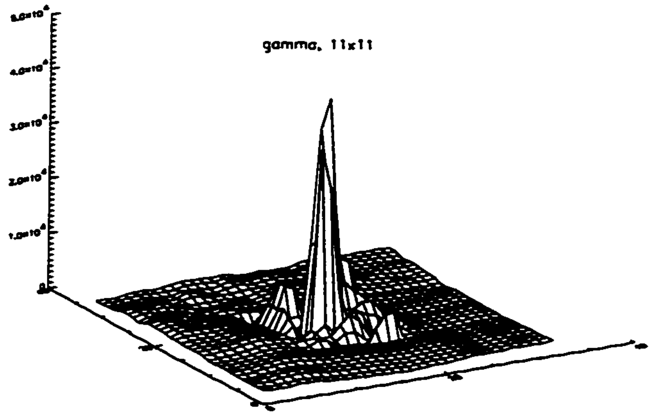

Figure 7.26: The result of filtering the noisy speckled point target by the Gamma Filter with a 11 x 11 scanning window

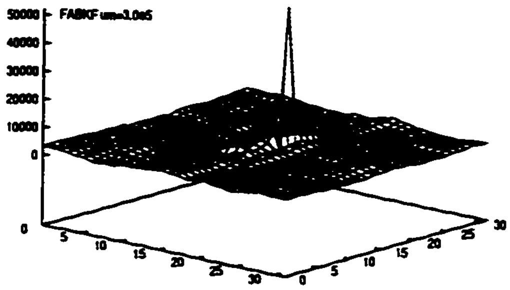

Figure 7.27: Results of Kalman Filters on Noisy Point Target.

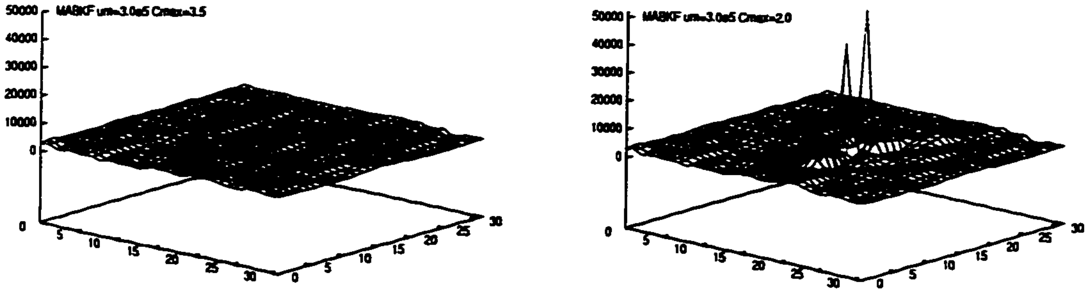

(a)

(b)

Figure 7.28: Comparison of Results of Kalman filters Filter with Varying Cr_{max} on Noisy Point Target.

7.2.3 Linear Structures

The objective of this test is to find out how well the speckle filters will restore linear features from speckle; and also by how much they can restore the fine structures in linear features.

Creating a Linear Pattern Test Image

As shown in Figure 7.29, once again we use a simulated one look fine mode RADARSAT image consisting of a test pattern in an image of size 1024 pixels by 1024 lines. The test pattern consists of 8 x 8 (64) sub-images of 128 pixels by 128 pixels. The sub-image consists of alternate rows of pixels of different intensities. The width of the rows in each sub-image stays the same, but increases from sub-image to sub-image (starting with one pixel and ending with a width of 8 pixels). The contrast between the bright and the dark pixel rows is set to 4 (i.e. 12.04 dB).

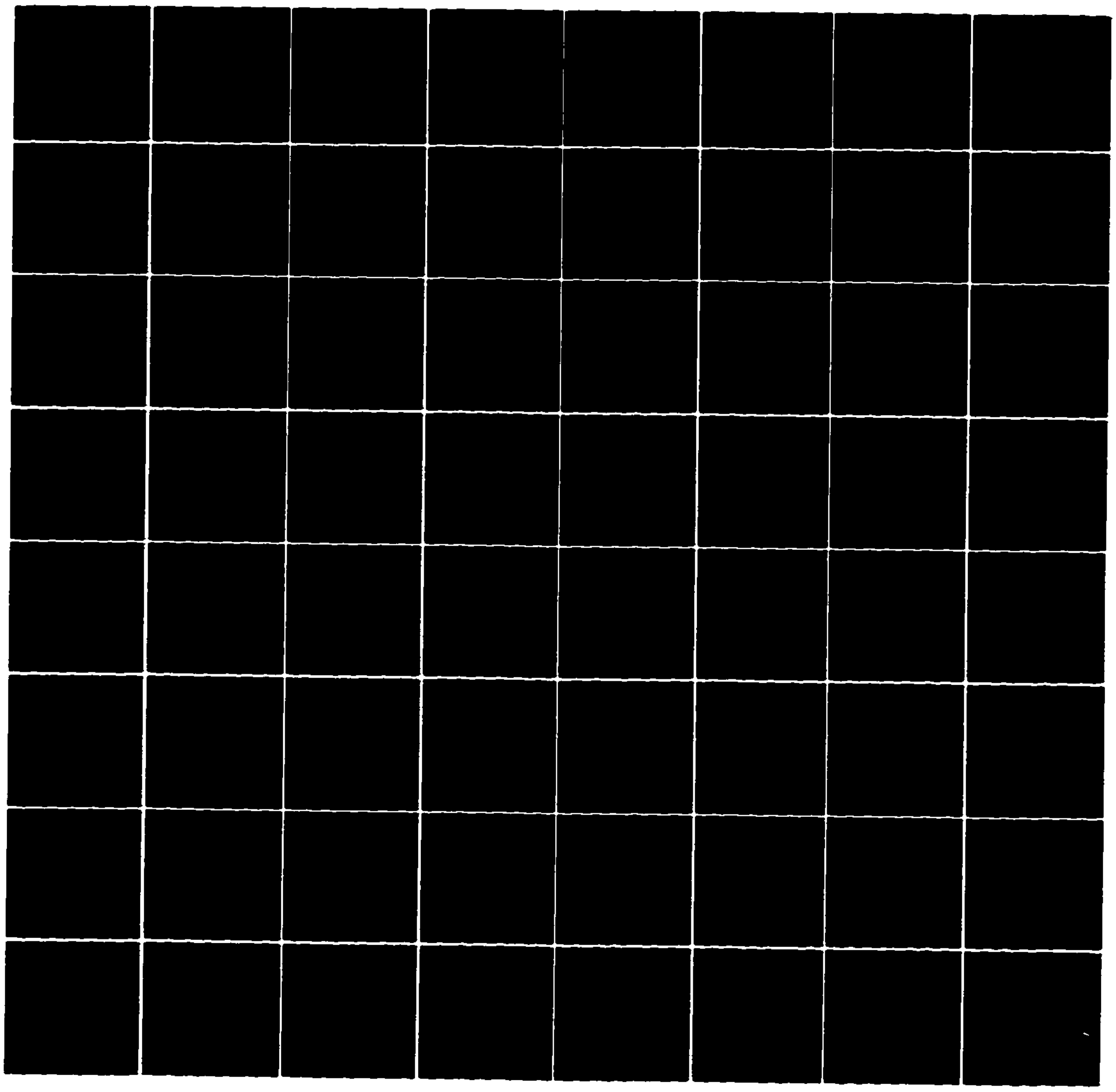

Figure 7.29: The linear line-pair pattern before speckle noise is injected.

Results of applying the Kalman filters designed in Chapters 4, 5, and 6 are given in the Figures 7.38, 7.39, 7.40 below.

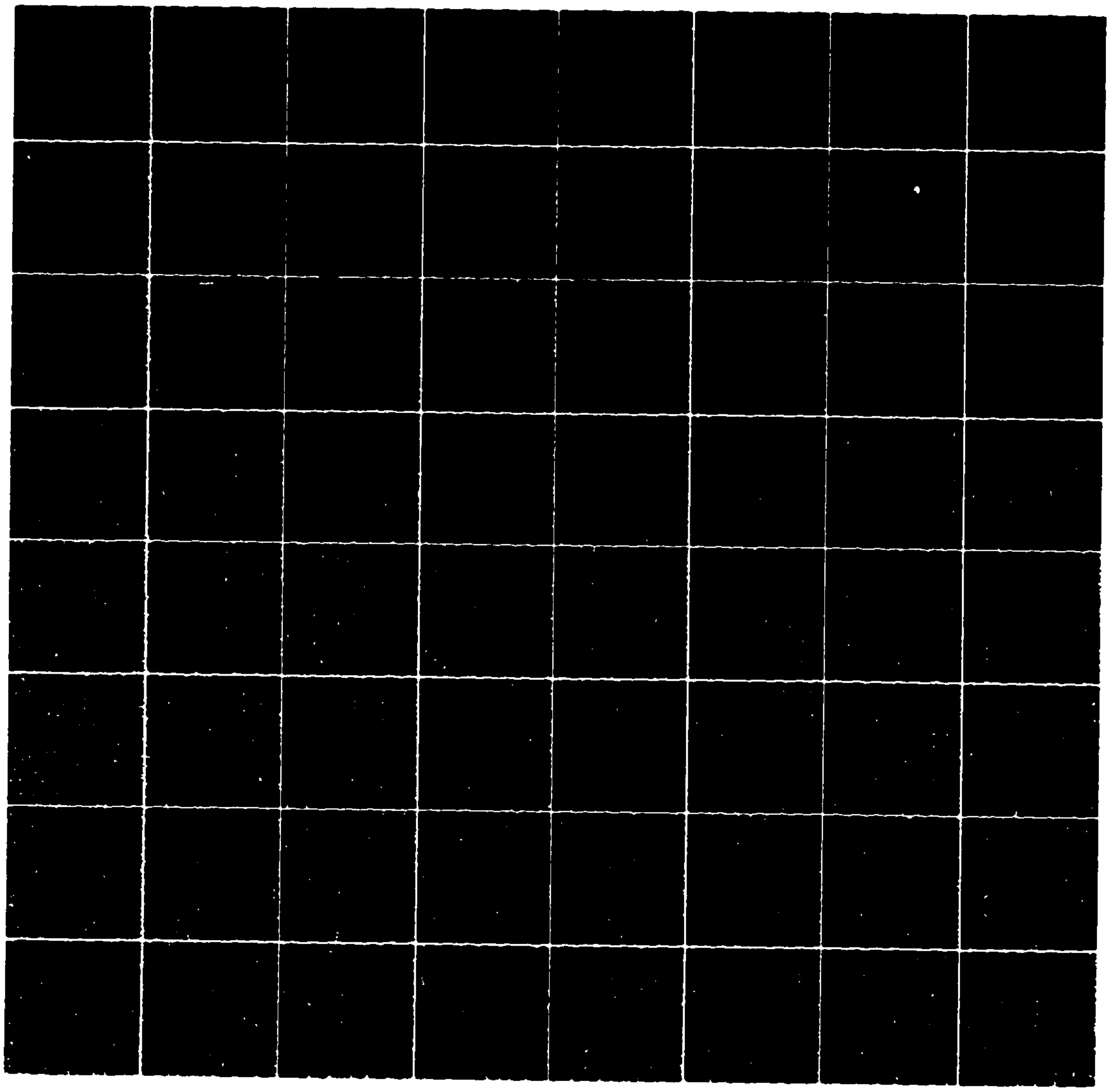

Figure 7.30: The appearance of the linear line-pairs after speckle noise is injected.

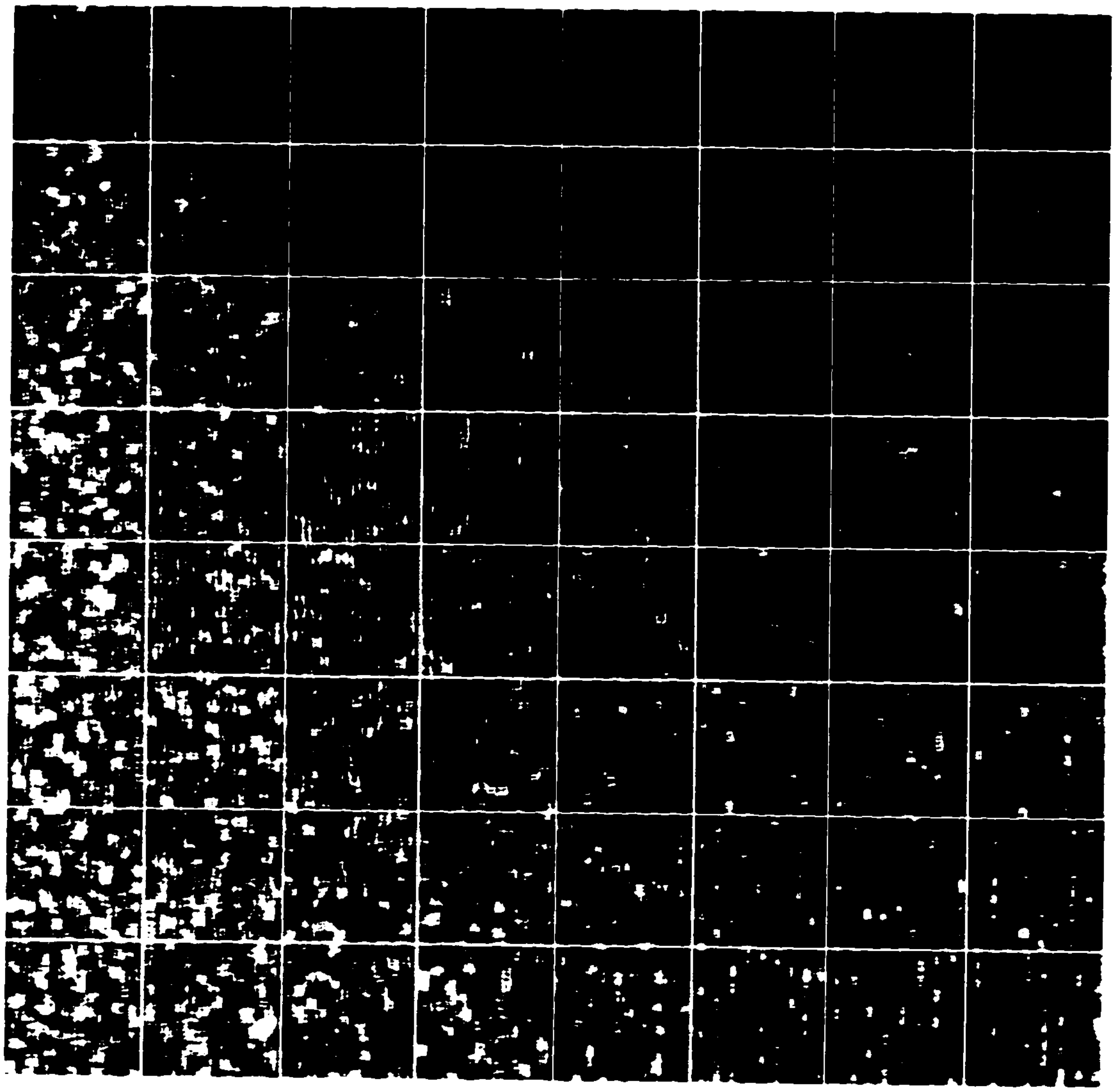

Figure 7.31: The appearance of the linear line-pairs after a box filter with a scanning window of 11 x 11 is applied.

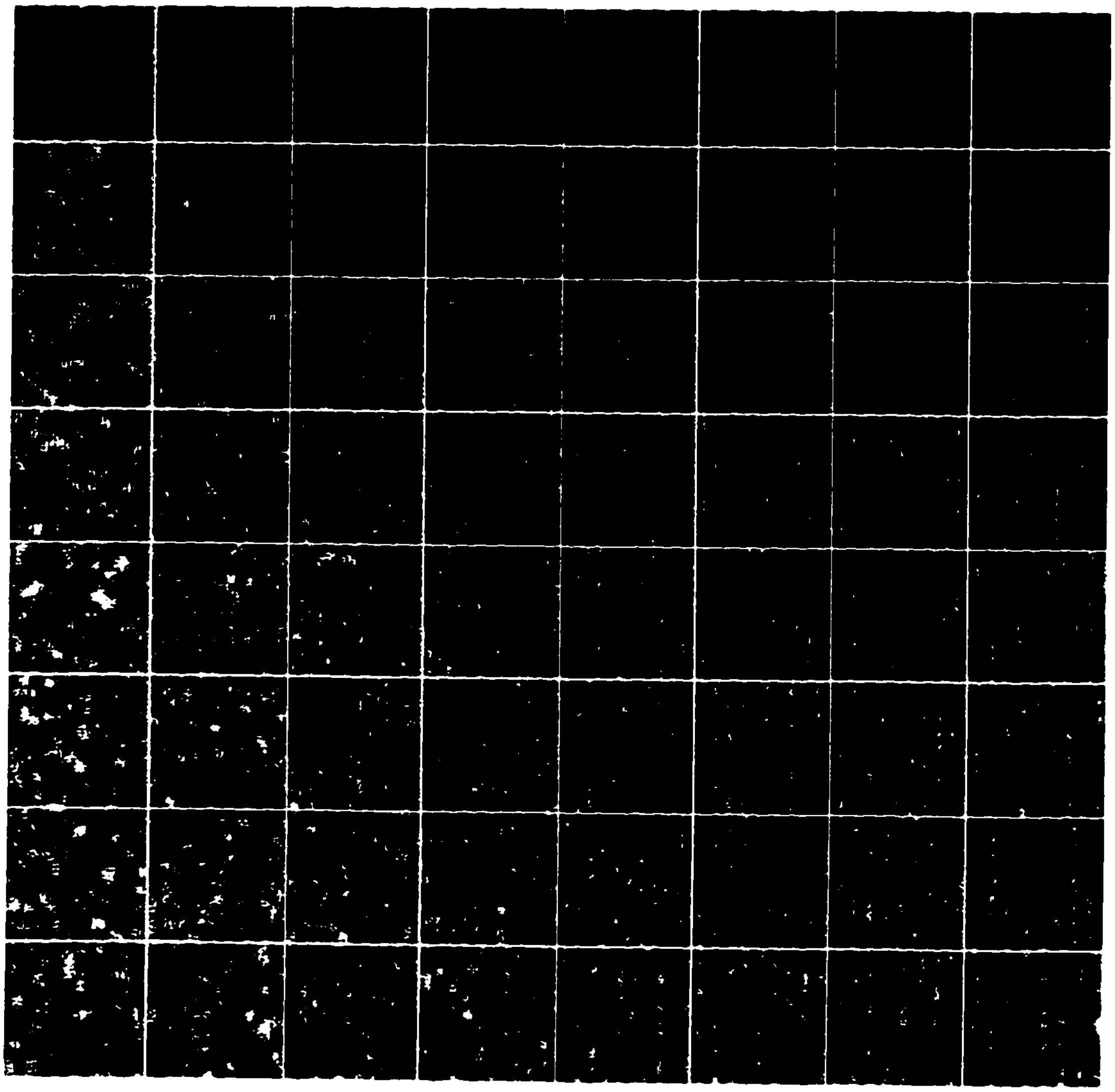

Figure 7.32: The appearance of the linear line-pairs after a Lee filter with a scanning window of 11 x 11 is applied.

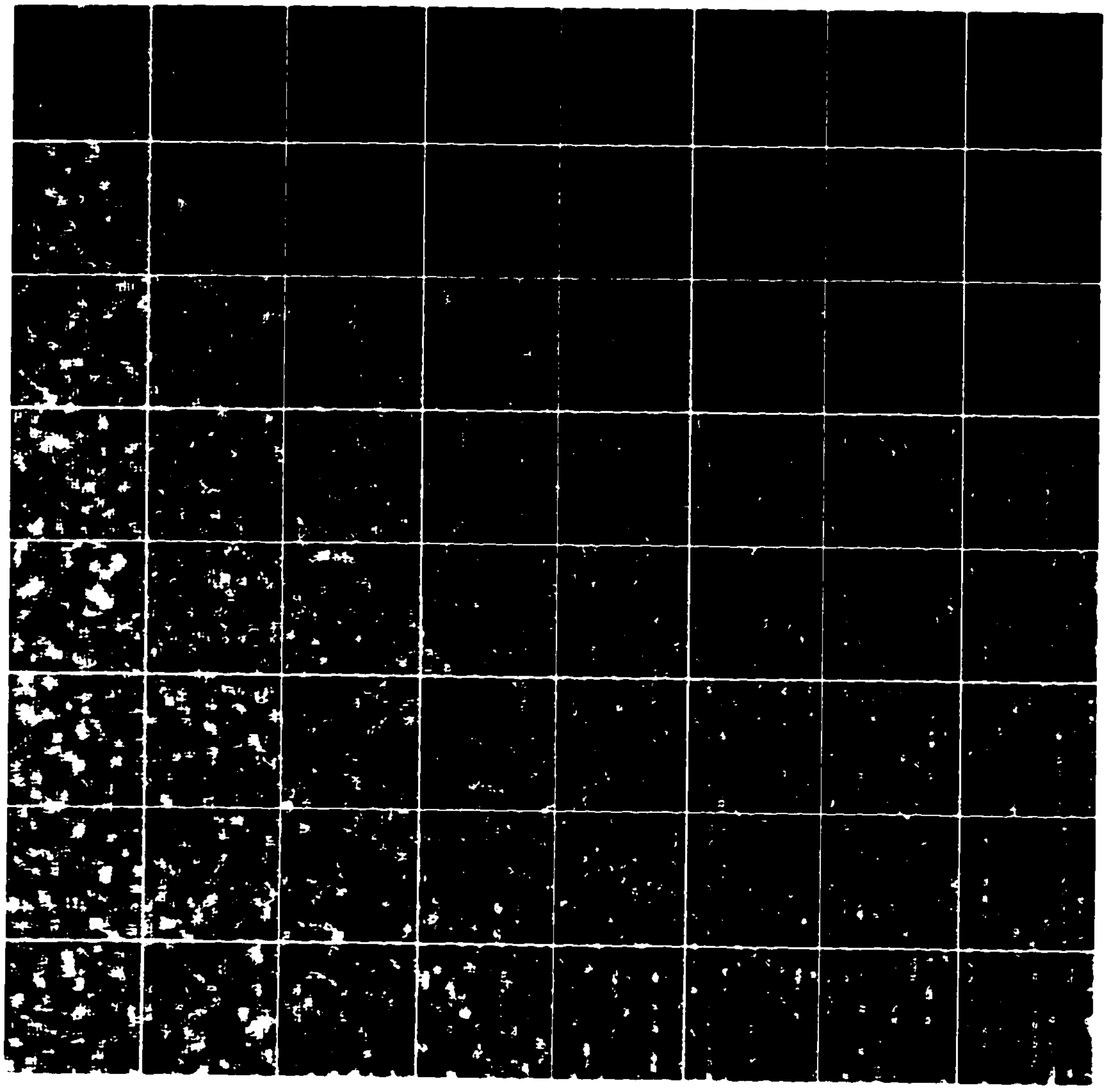

Figure 7.33: The appearance of the linear line-pairs after a Kuan filter with a scanning window of 11 x 11 is applied.

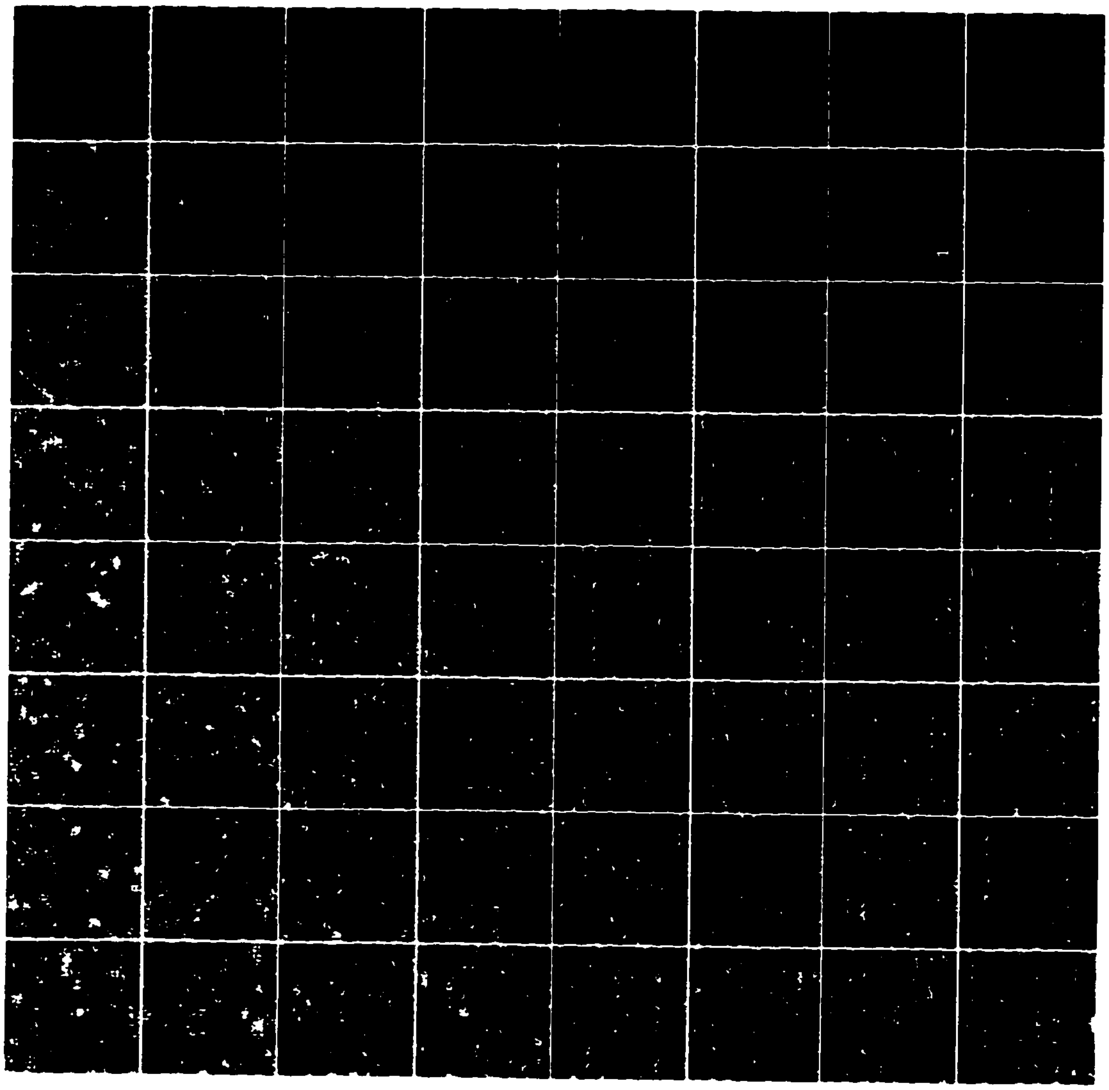

Figure 7.34: The appearance of the linear line-pairs after a Enhanced Lee filter (K=1) with a scanning window of 11 x 11 is applied.

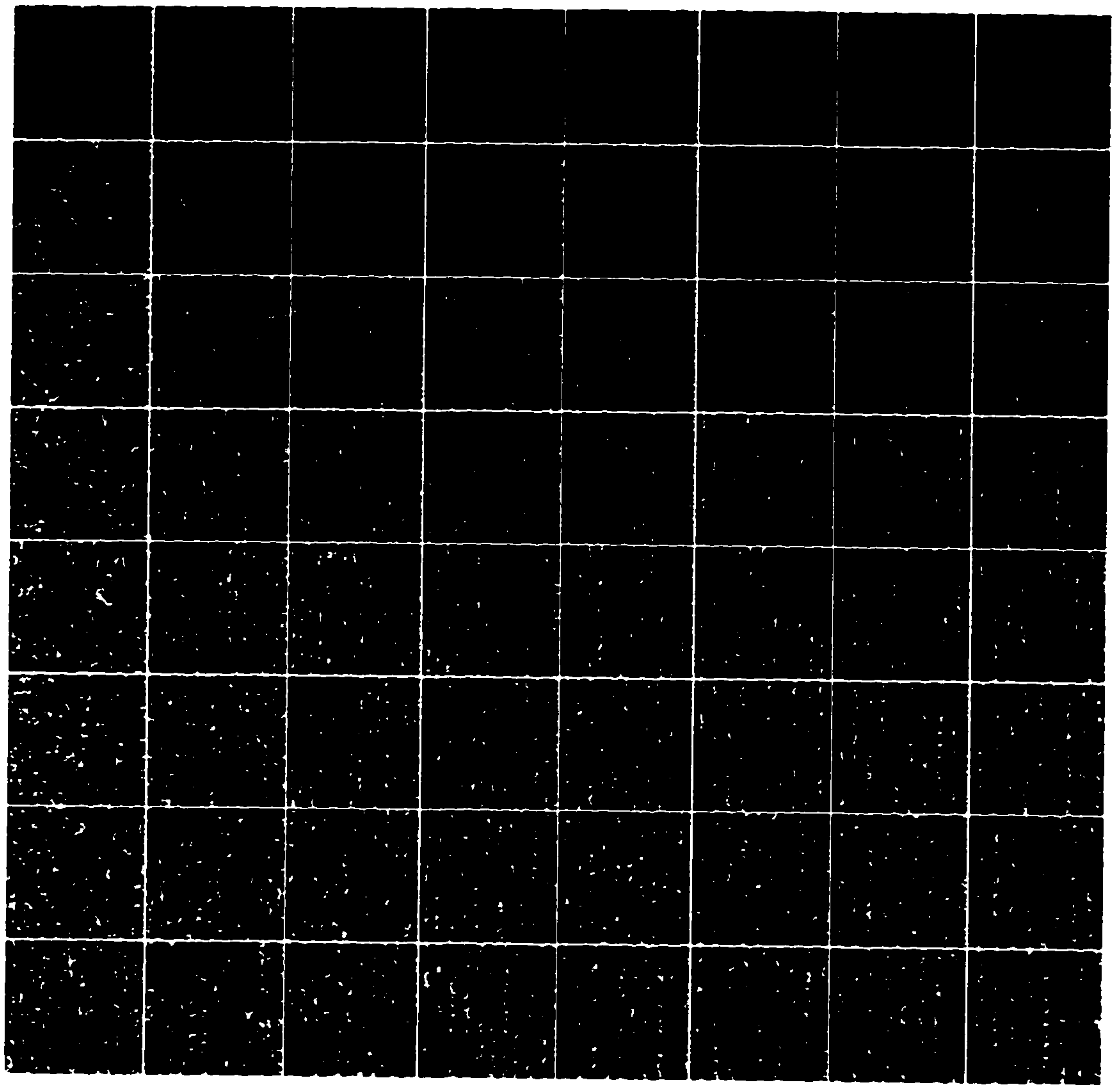

Figure 7.35: The appearance of the linear line-pairs after a Frost filter (K=1) with a scanning window of 11 x 11 is applied.

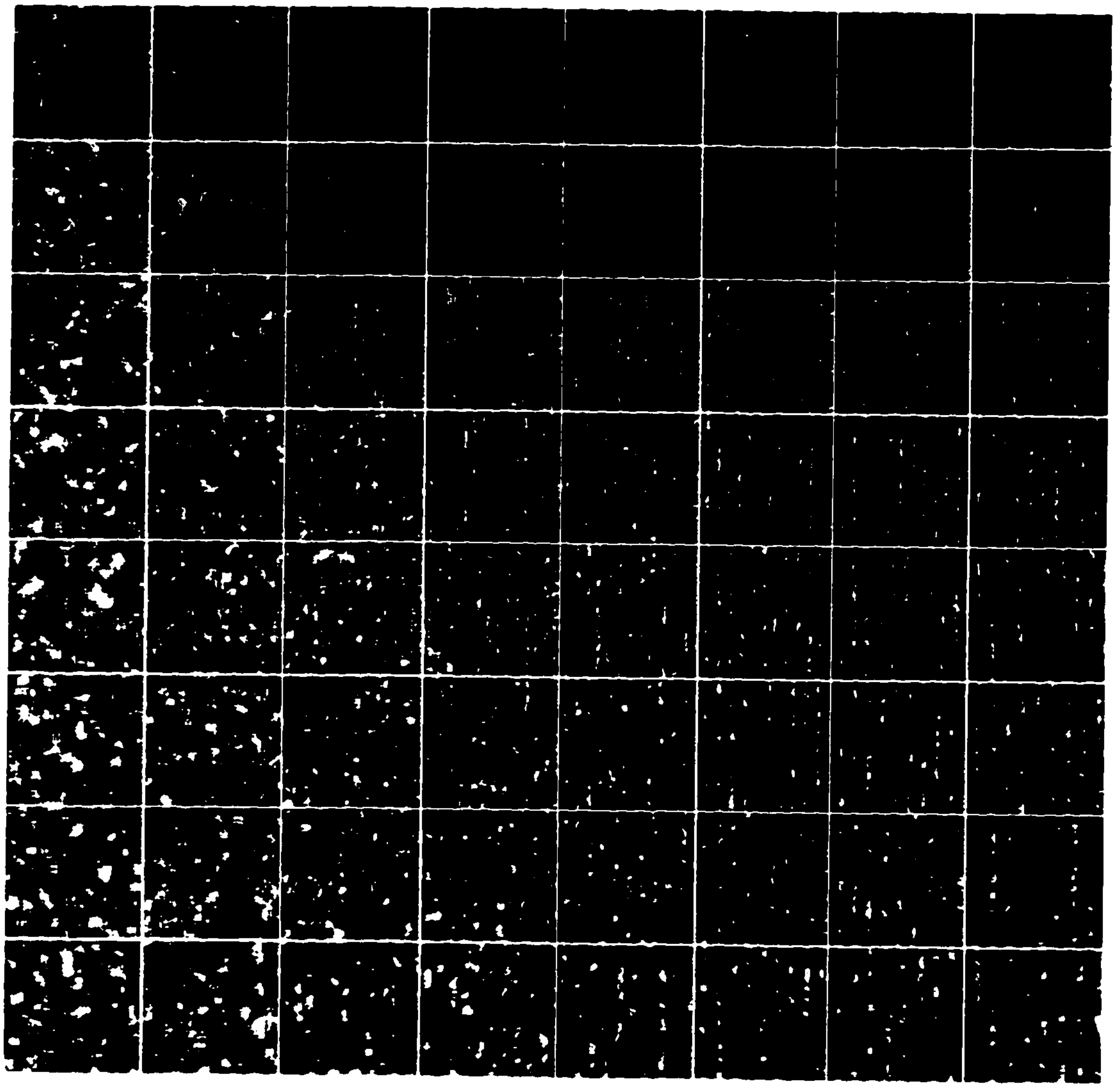

Figure 7.36: The appearance of the linear line-pairs after a Enhanced Frost filter (K=1) with a scanning window of 11 x 11 is applied.

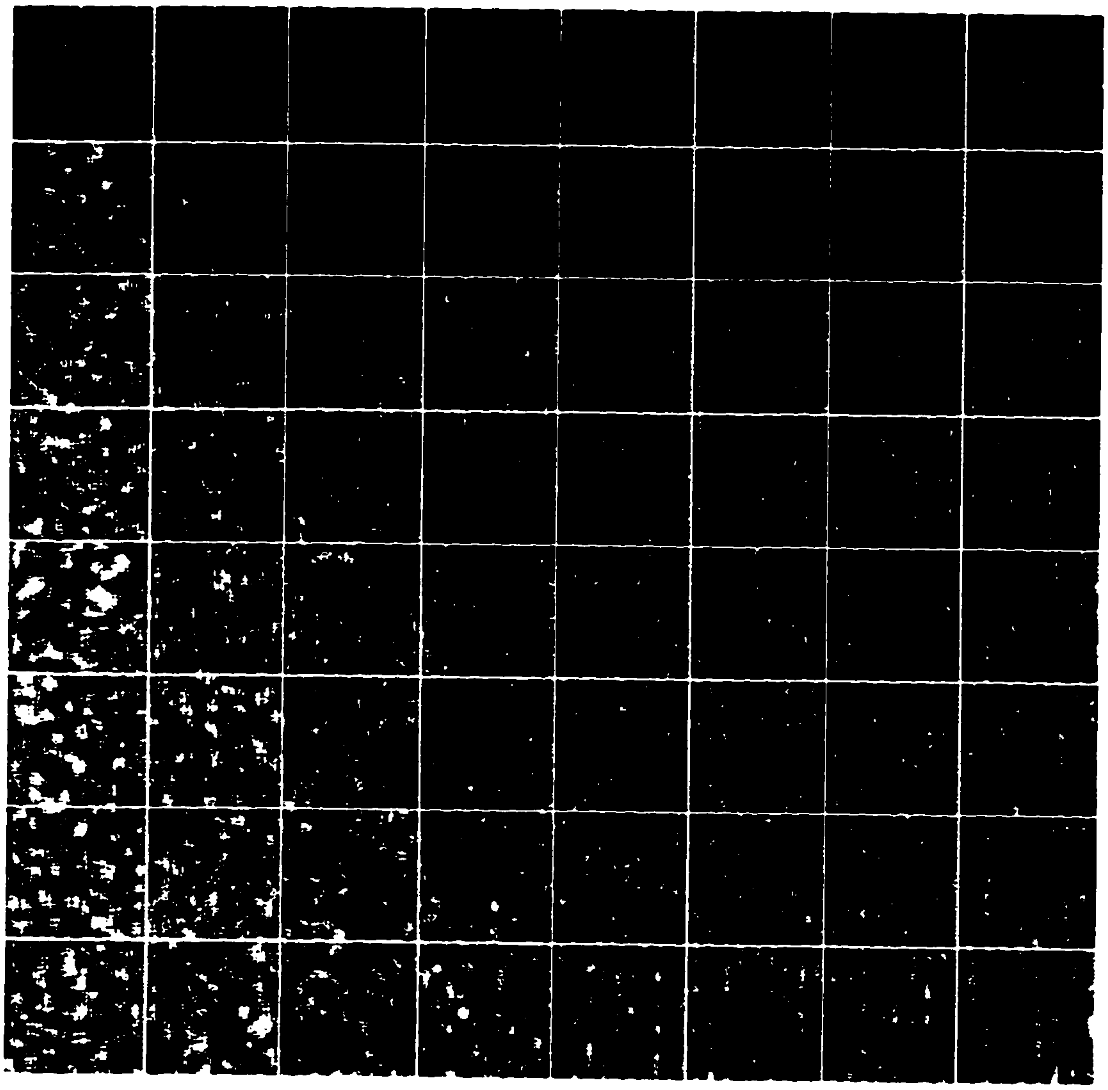

Figure 7.37: The appearance of the linear line-pairs after a Gamma filter with a scanning window of 11 x 11 is applied.

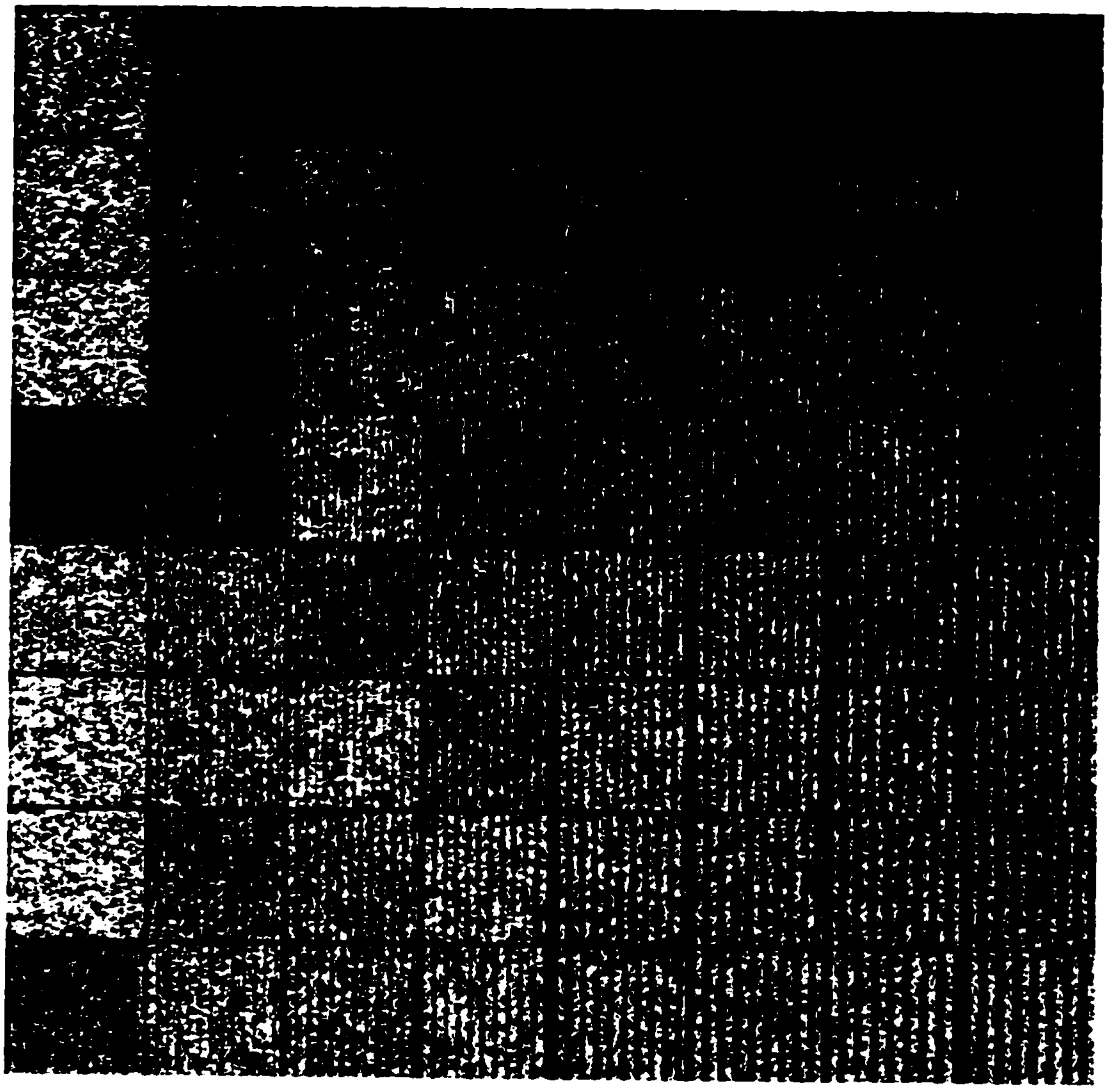

Figure 7.38: The appearance of the linear line-pairs after a Markov full plane Kalman filter with a $\sigma_u^2 = 3.e06$ is applied.

7.2.4 Angular Structure

Similar to edges, this test is designed to measure the ability of the filters to restore angular features. This time, we attempt to measure the ability of the filters to restore angular structure without speckle. Thus, the test image consists simply of an angular pulse shaped like a triangular tower (see Figure 7.41).

The results of passing this image through the series of filters examined above are shown in the next few images (starting with Figure 7.42). The image presented in Figure 7.42 shows the behavior of the Gamma MAP filter while filtering the triangular pattern. It can be seen that the triangular pattern is distorted; the filter cannot preserve the vertical slope of the triangular prism making it a pyramid. However, the shape of the plateau is preserved (triangular). The texture of the gray face is also distorted. The edges of the prism are also chopped. The filter cannot respond to high frequencies.

In view of the above analysis, one can see from Figure 7.43, that the results obtained by filtering the triangular prism using the Box filter have almost the same quality in its response.

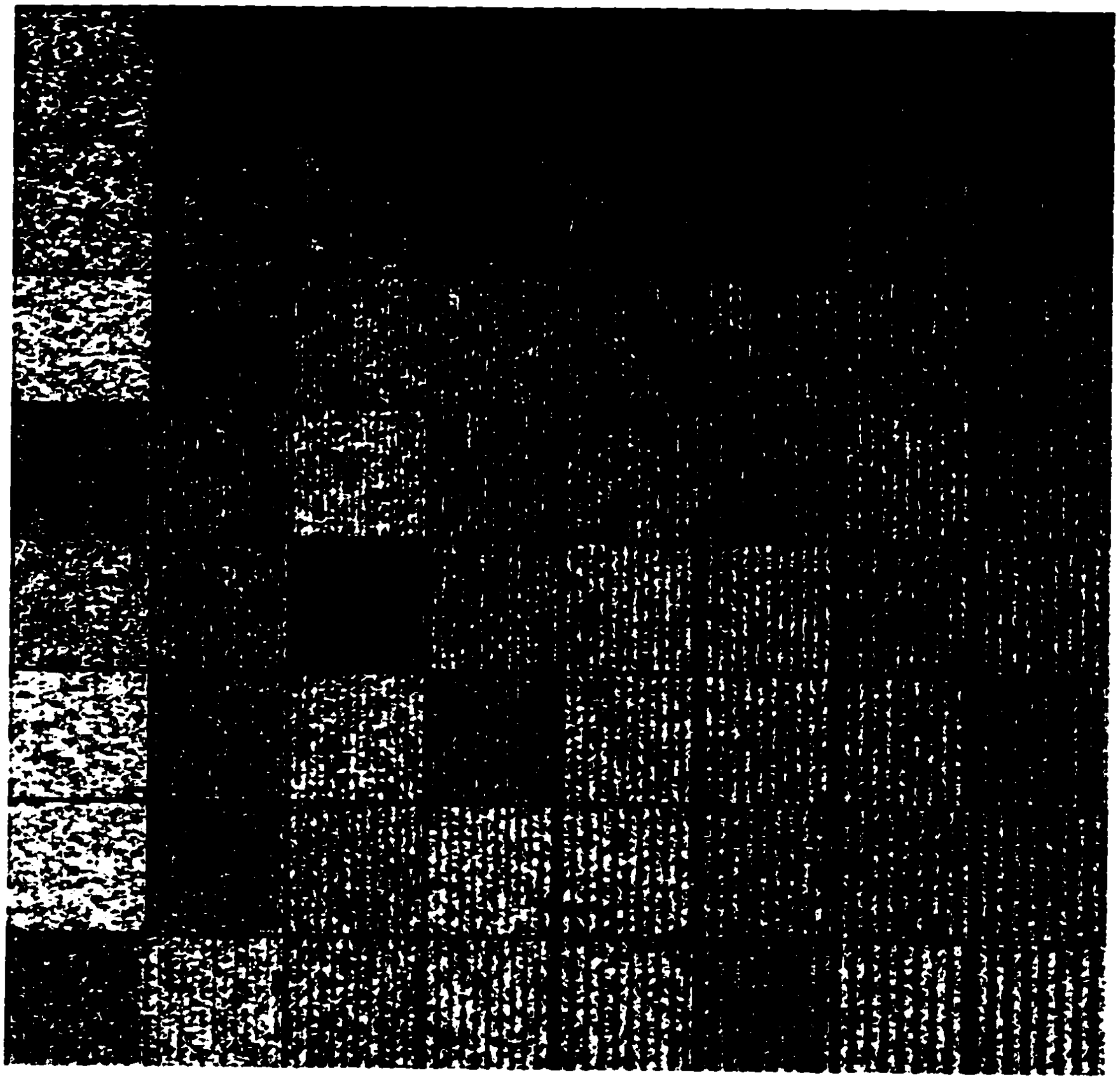

Figure 7.39: The appearance of the linear line-pairs after a full plane Kalman filter with a multiplicative noise and $\sigma_u^2 = 3.e07$ is applied.

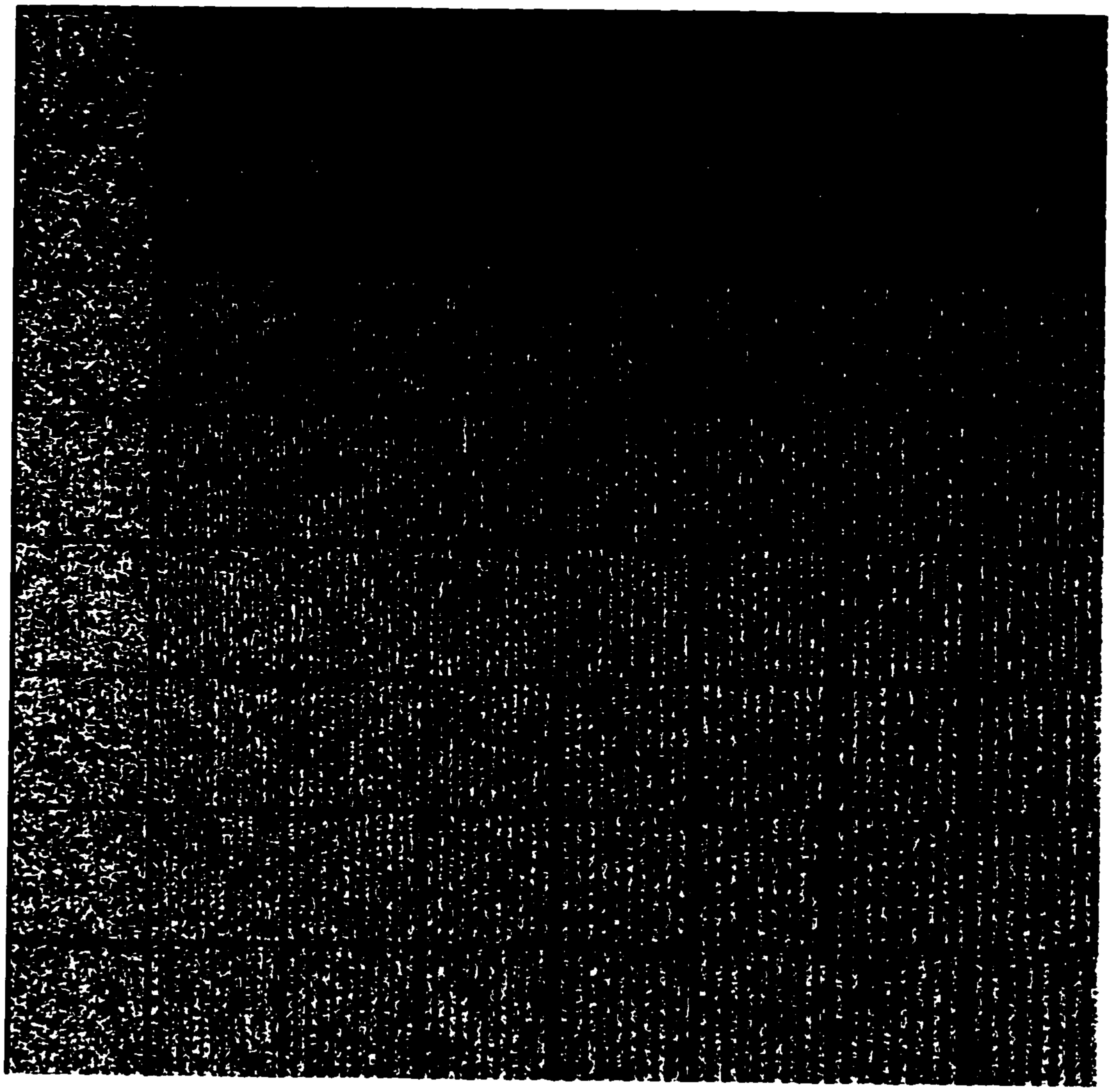

Figure 7.40: The appearance of the linear line-pairs after an optimal full plane Kalman filter with a $\sigma_u^2 = 3.e06$ is applied.

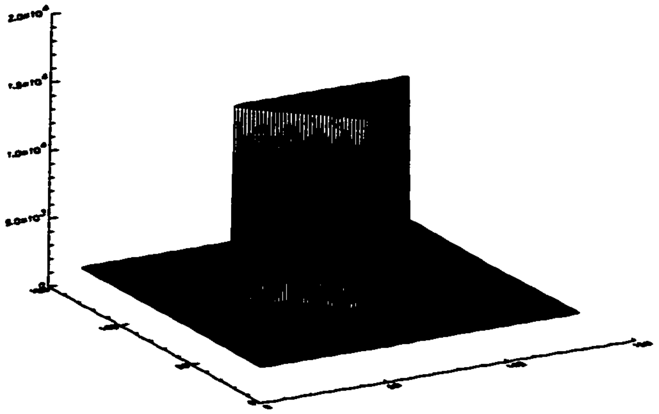

Figure 7.41: The pattern of the angular structure on the test image

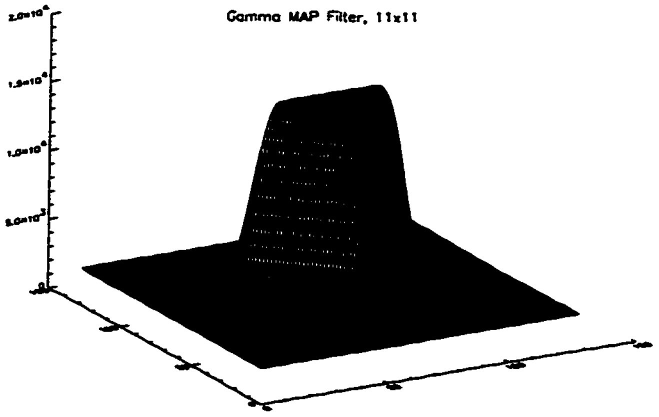

Figure 7.42: The result of the angular pattern after filtering by Gamma Map filter with a scanning window of 11 x 11

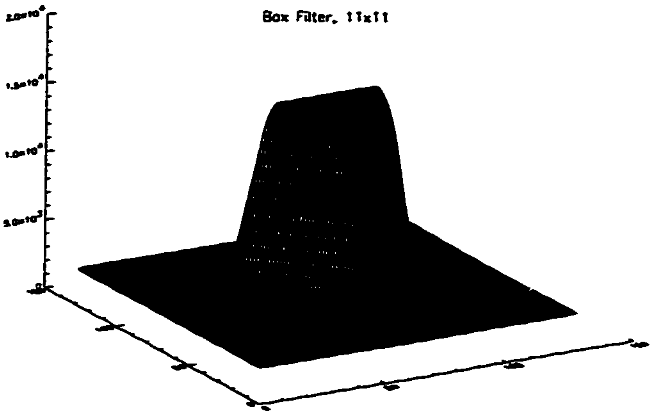

Figure 7.43: The result of the angular pattern after filtering by Box Filter with a scanning window of 11 x 11

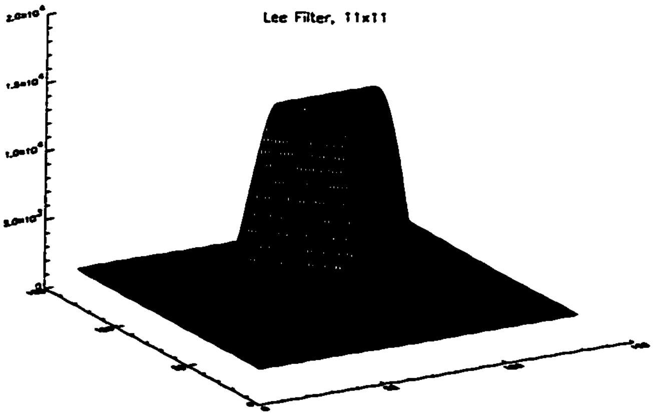

Figure 7.44: The result of the angular pattern after filtering by Lee Filter with a scanning window of 11 x 11

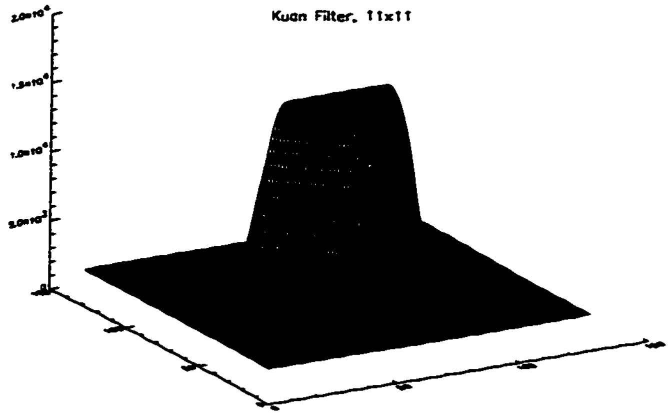

Figure 7.45: The result of the angular pattern after filtering by Kuan Filter with a scanning window of 11 x 11

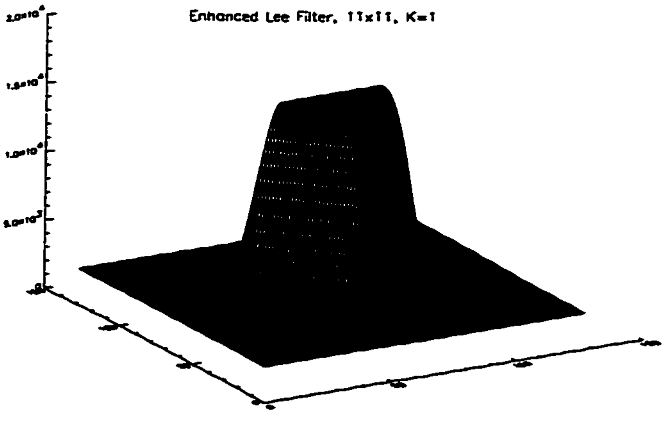

Figure 7.46: The result of the angular pattern after filtering by Enhanced Lee Filter (K=1) with a scanning window of 11 x 11

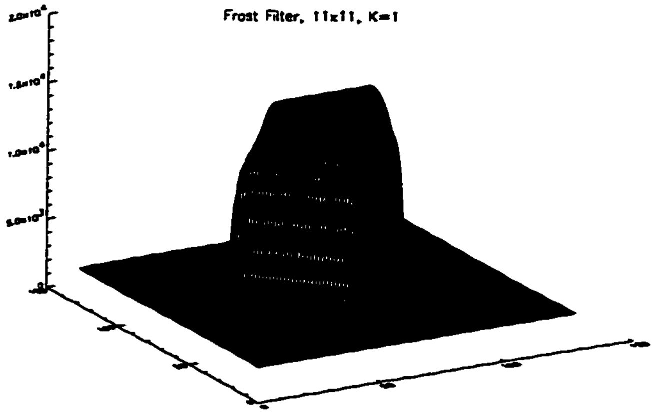

Figure 7.47: The result of the angular pattern after filtering by Frost Filter (K=1) with a scanning window of 11 x 11

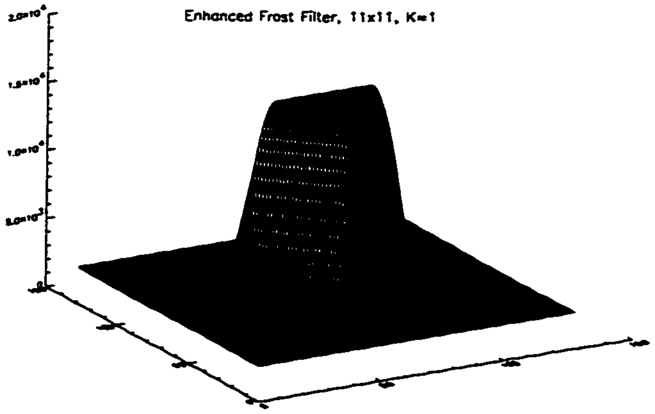

Figure 7.48: The result of the angular pattern after filtering by Enhanced Frost Filter (K=1) with a scanning window of 11 x 11

The Kalman filter results on filtering the noise on an angular pattern are given below.

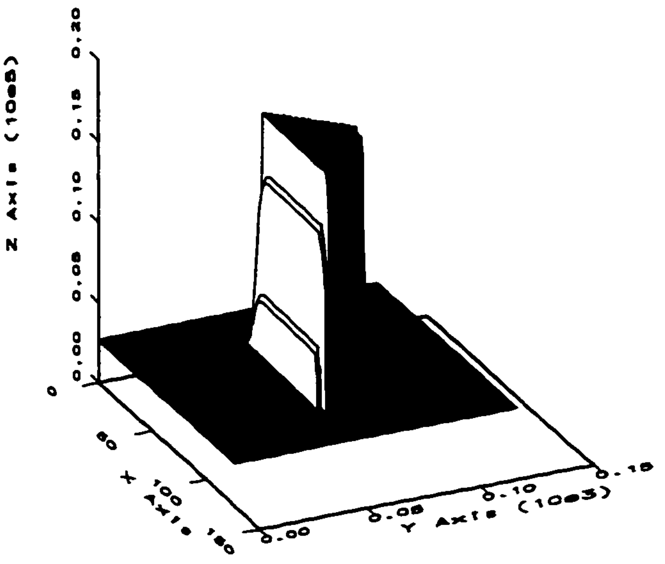

t

Figure 7.49: The result of the angular pattern after filtering by a full plane Kalman filter with $\sigma^2 = 3.0e5$

The full plane adaptive block Kalman filter, the FABKF, does some edge distortions due to the different arrangement of the block and the region over which the same parameters are applied. The effect of varying the state transition noise is analogous to a damping factor, where the smaller the value of σ_u^2, the slower the filter responds to the change. In processing the homogeneous region, a value of σ_u^2 set too low causes the filter to diverge from the actual image value creating invalid output. As the value is increased, the filter responds much quicker, but it becomes more susceptible to an increase in the noise. The inclusion of the multiplicative term in the state transition matrix in the MMFABKF seems not to have very much effect.

This image contains no noise, so that the error covariance matrix will be very small resulting in little difference achieved by changing the multiplicative state transition noise term. However, varying the maximum coefficient of variation, Cr_{max}, results in much improved response to sharp edges and points.

Continuing the analysis of the images obtained by filtering the triangular prism, one can state that almost all the filters presented above are low pass filters dealing badly with high frequencies, thus distorting objects that have sharp vertical edges. The filter which behaves the worst, in this test, is the Frost filter. A nonlinear effect is added by distorting a straight line into a nonlinear curve. This can be seen in Figure 7.47. This effect is corrected, but not completely, in the Enhanced Frost version (Figure 7.48 of the above filter). The Kalman filter does not suffer from distortion if it is tuned correctly to the image situation. The absence of noise will not affect the filter behaviour. For some values of Cr_{max} there are present some edge effects due to the dynamics of the filter. However, these effects can be corrected accordingly by choosing an appropriate edge dynamics.

7.3 Results on Applying Various Filters on a Real SAR Image

In this section we will compare the speckle reduction effect of various filters introduced above on real SAR image taken over Victoria on the Vancouver Island. The image was previously shown in Chapter 3.

The test image was taken from the ERS-1 satellite data of Victoria, BC taken in August, 1993. The test data is a single look intensity image and is shown in

Figure 2.5 corresponding to the highlighted region in Figure 2.6. The test data is given again in Figure 7.50 displaying the pixels with equal dimensions in both the cross-track and along-track directions. This image was chosen because of the different classes of data that are present. It includes very low intensity regions that correspond to the harbour region juxtaposed with the high intensity dock and city regions. The image also contains large regions that fall between these two extremes.

Due to the use of the quadratic noise reduction criterion (4.52), the Kalman filters will be sensitive to large changes in the image process. This is very common in SAR imagery, and these statistical outliers must be removed. The tests were run using an image with the upper 2% of the image compressed to 5 values at the peak of the image intensity level. This reduces the mean value of the image to some degree, but does not greatly affect the distribution of the image intensity data.

It was found during testing that attempting to run the full plane Kalman filter on images with less than the upper 2% of the image compressed, the filter would often become numerically unstable. The modified filters, the SMABKF, the MMABKF, and the FABKF all maintained stability operating on images with only 1% of the image compressed.

In analyzing the results of the various filters on the image of Victoria, we will consider in turn the filter output, and the behaviour of the Kalman gains.

The output of the test runs of various filters are given in the following figures 7.51,7.52,7.53,7.54,7.55.

The output of the test runs of Kalman filter are given in Figures 7.56 - 7.58. Figure 7.56 shows the results of all four Kalman filters with $\sigma_u^2 = 3.0e5$ and $Cr_{max} = 2.5$. This value of the state transition noise parameter, σ_u^2, was found to give satisfactory

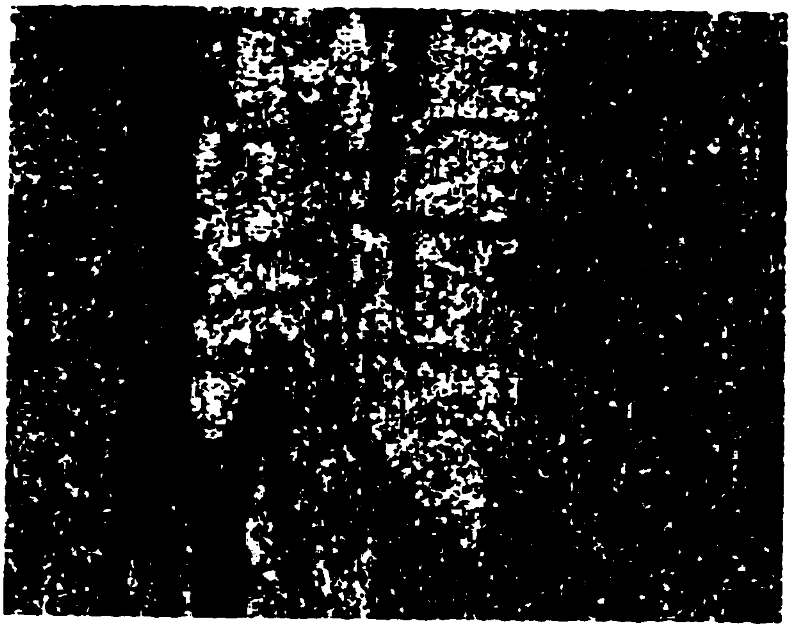

Figure 7.50: Single-Look Intensity Image of Victoria, B.C. from ERS-1.

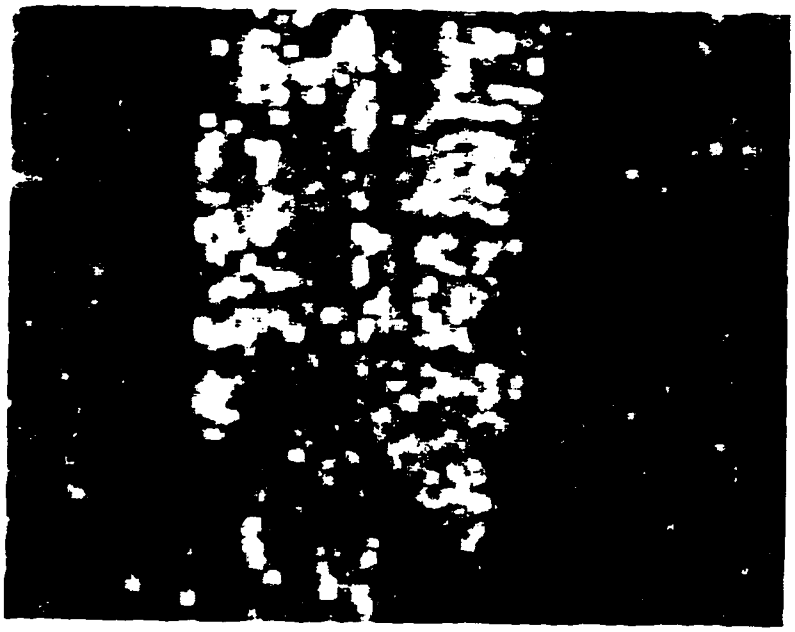

Figure 7.51: Single-Look Intensity Image of Victoria, B.C. from ERS-1 filtered by a Lee 5x5 window filter.

Figure 7.52: Single-Look Intensity Image of Victoria, B.C. from ERS-1 filtered by a Lee 7x7 window filter.

Figure 7.53: Single-Look Intensity Image of Victoria, B.C. from ERS-1 filtered by a Frost 5x5 window filter.

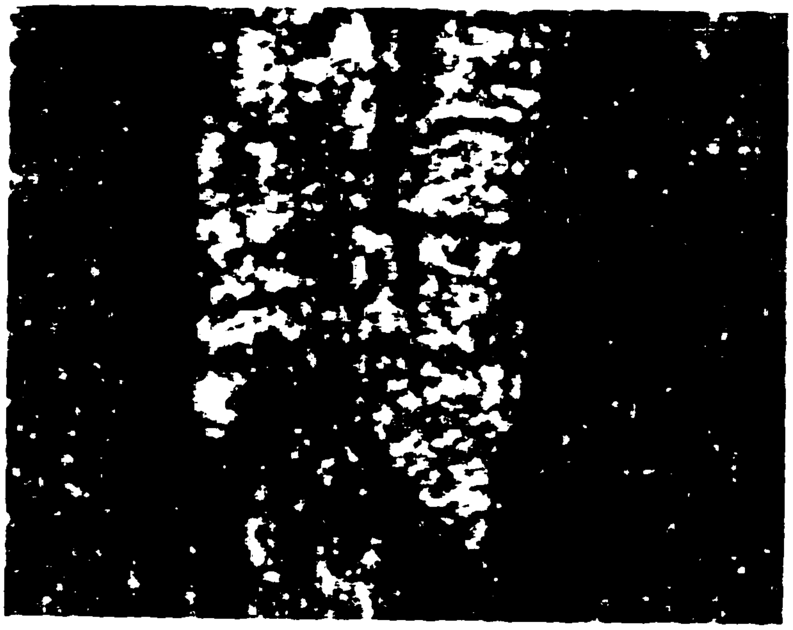

Figure 7.54: Single-Look Intensity Image of Victoria, B.C. from ERS-1 filtered by a modified Frost 5x5 window filter.

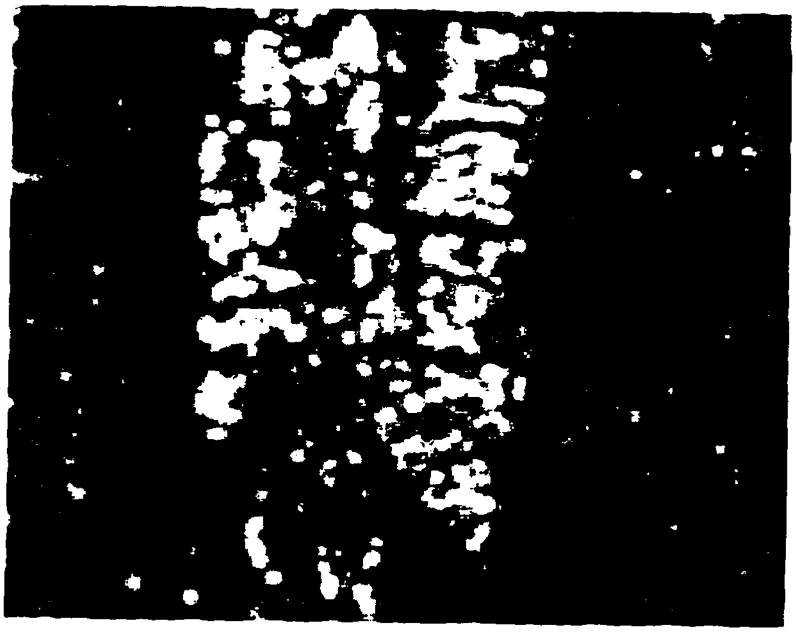

Figure 7.55: Single-Look Intensity Image of Victoria, B.C. from ERS-1 filtered by a Kuan 5x5 window filter.

results over both the high intensity urban area in the centre of the image and the regions at the left and right of the image. The maximum coefficient of variation value, Cr_{max}, was chosen so as to affect regions where the multiplicative noise assumption is no longer true, ie. $C_o > 2.0$. The SMABKF result in Figure 7.56d uses a value of the state transition multiplicative noise parameter, $\sigma_\psi = 0.25$. Obviously some results are indistinguishable over the homogeneous regions at the left and right of the image. This is due to the lack of objectivity of the bare eye observations. However, the major improvement in the MMABKF is identifiable in the high intensity urban region. Here the filter distorts the dark lines and edges of the intense region much less. The SMABKF was run with a value of $\sigma_\psi = 0.1$ and the results show a slight improvement in the edge regions as well as some improvement in image contrast. Currently there is no theoretical means of determining the ideal value of σ_ψ for such complex images. Experimentation suggests that 0.25 is acceptable but that a value too large, ie. > 0.5 results in very little improvement in the image over the input image. The FABKF results given in Figure 7.56b indicate a slight reduction in the smoothing of homogeneous regions for the same value of σ_u^2 but lack the asymmetric distortion that is prevalent in the non-symmetric region of support based filters.

The effect of varying the additive state transition noise parameter, σ_u^2, is shown in Figure 7.57. Figure 7.57a was processed with $\sigma_u^2 = 3.0e4$. This image is highly over-smoothed in the urban region, while the smoothing may be acceptable in the lower intensity regions. Processing the image with $\sigma_u^2 = 3.0e6$ resulted in very little reduction in the speckle noise over the lower intensity images, but an acceptable level of smoothing with less distortion over the high intensity region in the centre of the image.

The maximum coefficient of variation parameter, Cr_{max}, is designed to affect the filter most in the high intensity urban regions where the multiplicative noise

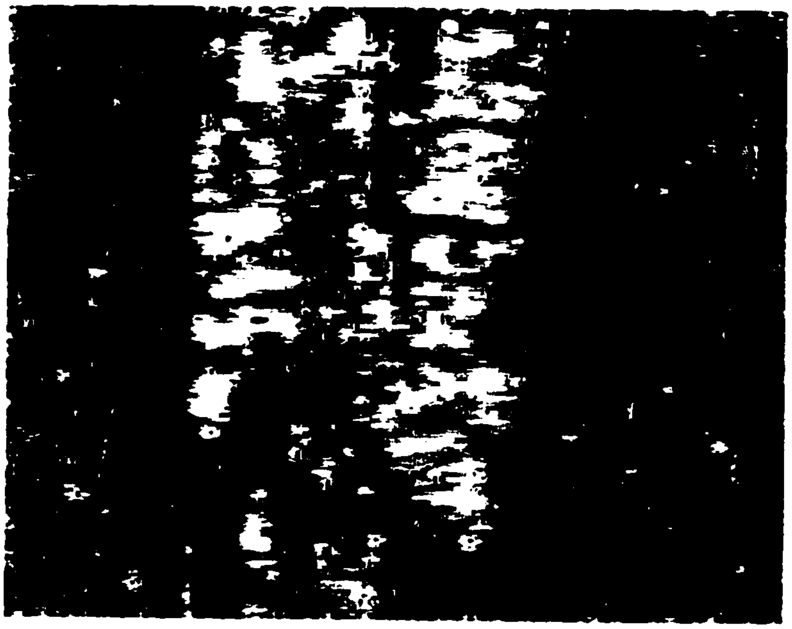

(a)

(b)

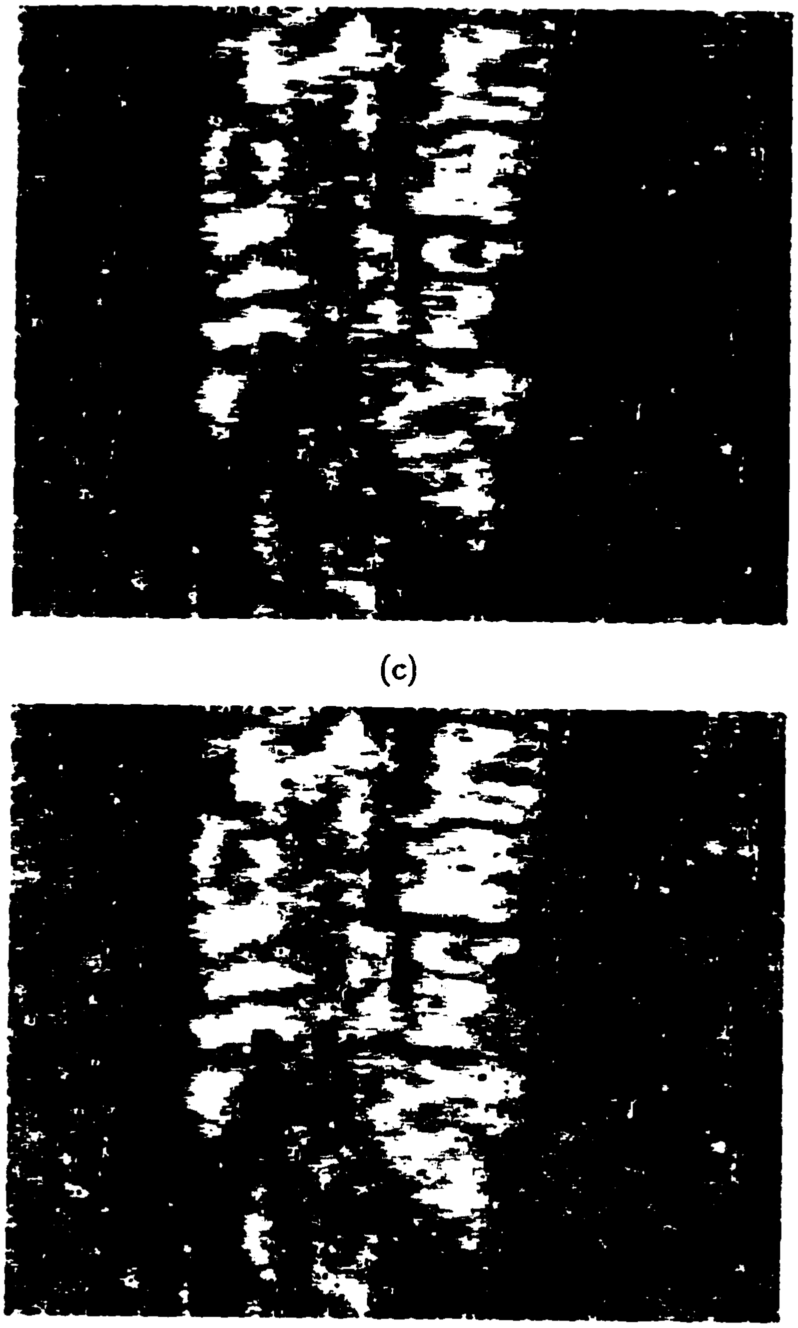

(c)

(d)

Figure 7.56: Results of Kalman Filters Applied to SAR Image a) modified full plane (MFABKF), b) full plane (FABKF), c)Markov modified full plane Kalman filter (MMFABKF), d) state multiplicative noise full plane Kalman filter (SMABKF) , $\sigma_\psi^2 = 0.25$. The state transition covariance, σ_u^2, is set to 3.0e5 for all images.

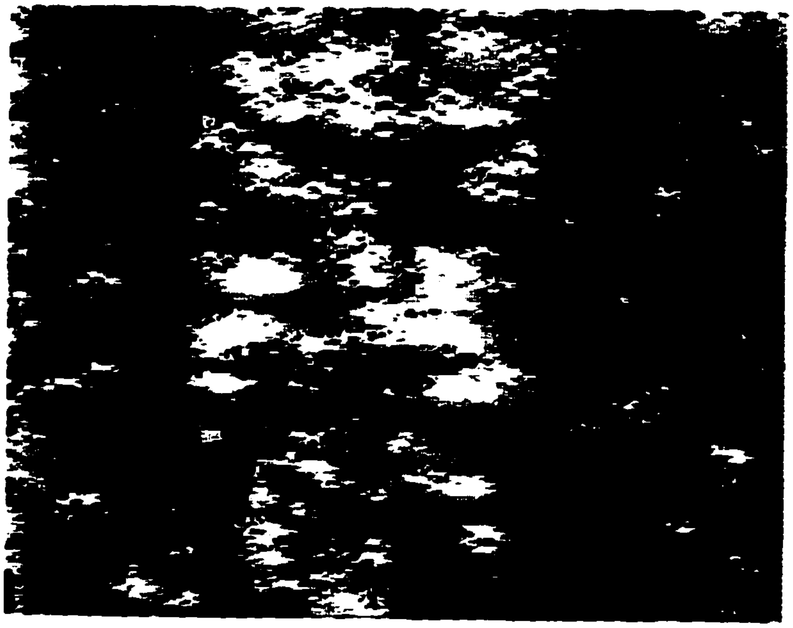

(a)

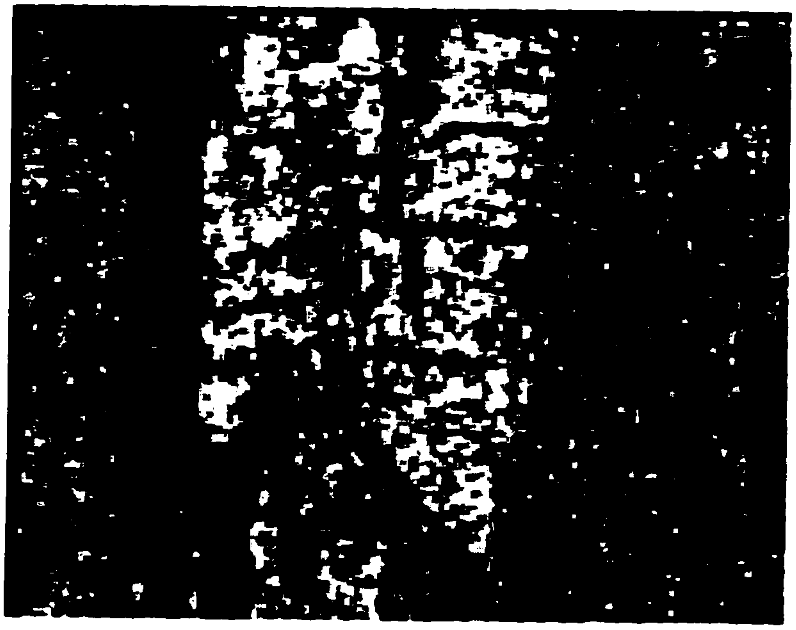

(b)

(c)

Figure 7.57: Comparison of FABKF with varying State Transition Variance on a SAR image a) $\sigma_u^2 = 3.0e4$, b) $\sigma_u^2 = 3.0e5$, c) $\sigma_u^2 = 3.0e6$,

assumption does not hold due to large numbers of strong reflectors. The effect of processing the image with a lower maximum threshold is seen in Figure 7.58. As in Section 4.5 the suggested C_{omax} is approximately 1.73. A Cr_{max} value of 2.0 begins the detuning of the Kalman filter at a local coefficient of variation of 1.5, just below the value suggested by Lopes et al. [55]. The results indicate that this factor is very important in the use of the Kalman filter as the high intensity region suffers from much less distortion using the lower value of Cr_{max}.

A typical variation of a full plane Kalman filter when filtering the above SAR image of Victoria is given in figure 7.59 where the norm of the Kalman filter gain matrix is calculated for the first ten rows of the test image as shown in figure 7.50.

From the tests shown above, an obvious conclusion is to be drawn: the Kalman

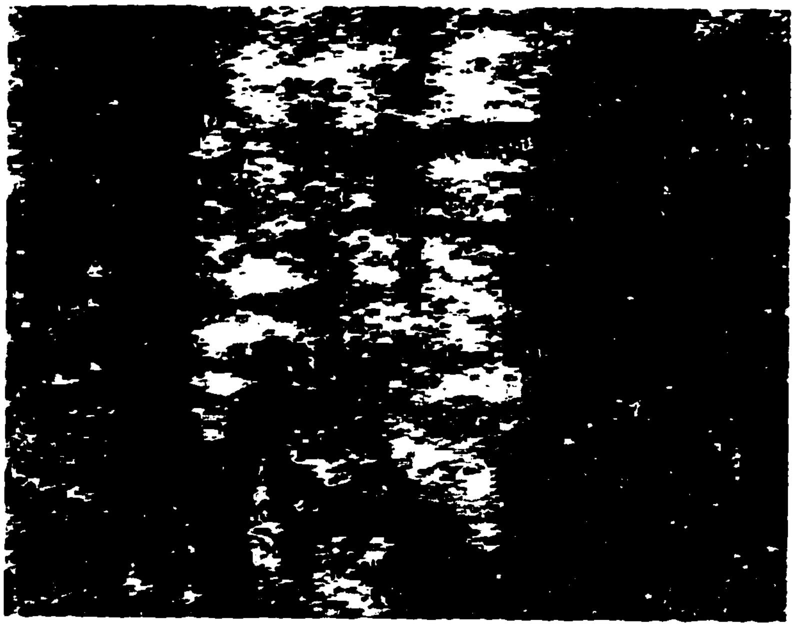

Figure 7.58: Effect of Changing Threshold Coefficient of Variation on a SAR image, $Cr_{max} = 2.0$, using FABKF.

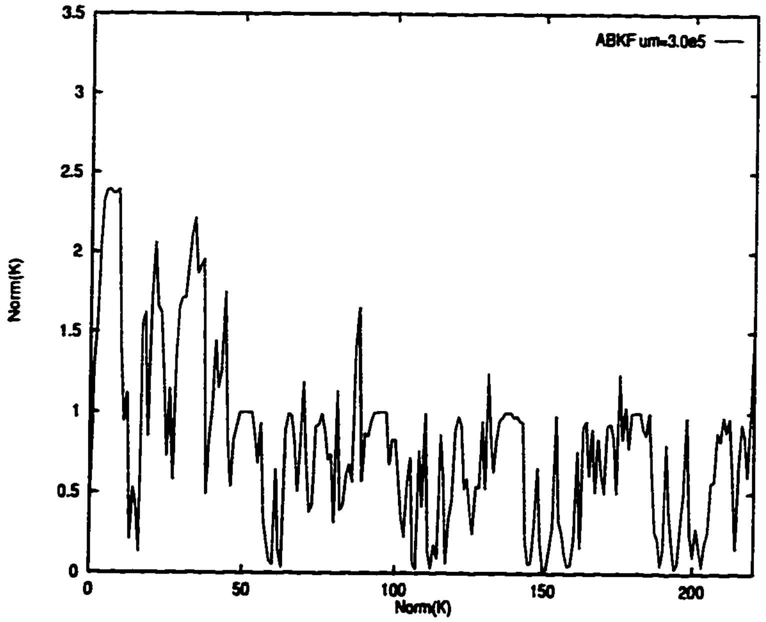

Figure 7.59: The norm of the Kalman filter gain matrix for the first 10 rows of the SAR image of Victoria.

filter proved itself more flexible and more powerful in filtering the speckle noise than all other filters. The adaptation criteria and capacity of the Kalman filter to various types of noises and regions of the image makes it more attractive for getting higher quality filtering results. However, the price to pay is in the computational complexity and time.

7.4 Conclusions

This chapter introduced a few tests which measure the performance of filters for speckle noise reduction. The principle of creating the test images was to combine a type of image such as a step, a point target, an angular structure, and a texture of linear patterns with a speckle noise collected from a homogeneous area of real SAR image. The results of filters discussed in this thesis were collected and displayed. A final test on a real SAR image from Victoria BC was also run and results presented.4. The superiority of various Kalman filters was also illustrated.

Chapter 8

Conclusions

In this thesis, new Kalman filtering methods have been developed and applied to SAR images in order to reduce the speckle noise. Kalman filtering techniques have been applied to SAR imagery before [8], etc. However, these filters were developed for largely homogeneous images and on images which were artifacts and not real SAR images. After the launch of the European ERS-1, the Japanese JERS-1 and the Canadian RADARSAT, Synthetic Aperture Radar (SAR) images of urban areas have become common place. These images are much more complex than those tested by the earlier Kalman filters. These urban scenes contain image textures beyond the assumptions used by these earlier Kalman filters. Thus, the overall reduction in speckle is not acceptable.

Because the speckle effect in single look image is by far the most pronounced, but statistically tractable; and also the fact that single look SAR images generated by advanced SAR processors, which preserve the phase information, is the key to sub-wavelength accuracy in elevation model derivation and more advanced applications, this thesis concentrated on dealing with the reduction of speckle in single look SAR images.

To correct the above deficiencies in existing Kalman filters and to extend the use of Kalman filtering technique to urban SAR scenes, the derivation of filters was re-examined and those areas involving incorrect assumptions were addressed. This involved the evaluation of the multiplicative noise assumption during the processing of the image and the tuning of the filter in those regions where the effect of scene texture surpasses that caused by speckle. The modeling of the speckle noise in the state and in the observation with the Markovian assumption was introduced. As well, the derivation of the parameter estimation technique used was also re-evaluated and modified so that the parameters continue to be adaptive over the entire image. This process led to the development of full plane Kalman filters for multiplicative state noise components, for Markov noises in the observation, and for dynamic state multiplicative noise components in this thesis. Because the tuning process of Kalman filters is a very time consuming operation, a new method for determining the optimal noise parameters has been developed as well.

In all the new developments listed above, the image model was built assuming a full plane region of support. The justification is based on the previous work done by Geling [24] in which results from using models designed for half and full plane regions of support were compared. It was found in [24] that the latter is superior in terms of resultant image quality and processing requirements.

A series of tests which address the performance of the Kalman and other filters for speckle noise reduction was designed, developed, implemented and applied to the mostly known and used filters. A comparison of results showing the outputs by different filters is presented in Chapter 7. From these results it can be seen that the Kalman filter is superior to all other filters due mainly to its capacity to be tuned to the noise factor present in the image and adapted to the goal pursued by the user. Much of the improved response of the Kalman filter can be attributed to the inclusion of the coefficient of variation test to detune the filter when the filter assumptions were invalid. There is, however, a price to be paid: the complexity of the model and filter requires increased computational power and time. The tuning of the method also requires special skills and understanding of the method.

To address the requirement for greater filter flexibility over complex urban regions, the image formation model used for the image formation process was improved by introducing a multiplicative noise in the state transition equations. The filter resulted in greater parameter variation over the image and improvement in response, thus allowing greater filter flexibility. Overall, the performance of the MMABKF was slightly better in complex urban regions offering some improvement in contrast. However, the new noise parameter introduces a new difficulty in designing and tuning the Kalman filter, which is the difficulty of determining an acceptable value for σ_{ψ}. The Markov noise in the output adds other tuning parameters which are the Markov model matrix and the intensity of the noise parameter η.

Running the optimization process first on the models above, the tuning problem can be solved. However, the correct choice of the initial point and the delicate stability of the nonlinear programming algorithm, which in this case runs on linear operators (matrices), make this last method also available to knowledgeable users only.

In comparing the results of these filters with other known filters for speckle noise reduction such as the Lee, Frost, Kuan etc. statistical filters, it is seen that improvements are substantial (especially for linear patterns and point target preservation). The edges and strong reflectors, such as the two point targets that are located in the harbour that are blurred by the Lee filter as shown in Figure 3.2, are well preserved by the Kalman filters. Due to the greater simplicity of some filters they might be better suited for routine use. However, as SAR images become more in demand at higher resolutions, methods such as those defined here will be the only way to improve the quality of a SAR image and, furthermore, to make it more suitable for further image processing operations.

8.1 Summary of Contributions

As a summary of the above conclusions, the contributions of this thesis are:

- The development of a Kalman filter with a Markovian noise in the observation. This enhanced the capacity of the Kalman filter to be applied to an exponential noise.
- The derivation of the Kalman filter and parameter estimation equations for a state transition equation including multiplicative state transition noise for the full plane model of support. This enhanced the ability of the Kalman filter to follow the variations common in SAR images containing complex features in urban environmental settings, while having a reduced effect on homogeneous regions.
- The derivation of the Kalman filter and parameter estimation equations for a state transition equation including multiplicative state transition noise for a Markovian noise in the state. This new model made the Kalman filter more appropriate to exponential noise in urban areas.

- The development of an optimal method for the determination of all noise factors without any prior knowledge about the real noise present in the image. This resulted in shorter experimental time when tuning the Kalman filter.

8.2 Further Work

In the present thesis a few extensions and improvements of Kalman filters for speckle noise reduction in SAR images were examined and introduced. However, many options were left untouched. Both sides of the Kalman filtering process can be explored in future works; in other words, the parameter estimation scheme and the filtering method can be approached in different ways.

The parameter estimation scheme used in the development of the Kalman filters in this thesis is taken over from Geling's works [24] - and the motivation was given many times in the thesis. His work was based on the recursive parameter estimation(RPE) technique by Ljung and Söderström [51]. Before starting to use it we have explored some other methods for parameter estimation. One of them looked appealing; it was the estimation method proposed by [76]. Because of the full plane model, which we have preferred due to its increased performance over SAR image, we have abandoned the development of the previous parameter estimation method, our goal being the improvement of the second element of the scheme; in other words, the Kalman filtering technique per se. However, we still consider that a good subject to be investigated might be the development of a new full plane Kalman filter with a new set of state equations obtained by applying the parameter identification method as developed by Sugimoto and Jain or a combination of RPE with the model introduced in [37].

From experiments conducted on all Kalman filters developed in this thesis it can be observed that the quality of the filter depends on the direction of the image artifacts. The horizontal move of the blocks along the image makes the filter more suitable for filtering horizontal patterns. This suggests that the filter's region of support has to consider patterns which should not have a preferred direction.

There are many suggestions for the Kalman filter itself. Besides the suggestion made by Geling in his future work description, we claim that the SAR image model should be nonlinear and, therefore, the Kalman filter should be extended to such a case. This implies the use of Zakai's equations and filter. This suggestion applies also to the parameter identification process as well.

Another suggestion is to consider a Kalman filter designed for sliding mode processes as introduced in Aitken's thesis [2]. This type of a Kalman filter might be much faster than the usual Kalman filter, implying less calculations to be performed.

Definitely, the list of future work might continue with more suggestions as there are, as yet, many unsolved problems.

Appendix A

Gâteaux Derivative and Gradient

A.1 Definition of Gâteaux Derivative

Let

X and **Y** be the Banach spaces [69],

U $\subseteq$ **X** is open,

T be the non-linear transform defined on domain **U** and having range Y.

Then **T** has a Gâteaux derivative at $\phi \in \mathbf{U}$ if, $\forall \alpha \in \mathbf{U}$, the following limit exits:

$$\begin{aligned} \nabla \mathbf{T}(\phi, \alpha) &= \lim_{t \to 0} \frac{\mathbf{T}(\phi + t\alpha) - \mathbf{T}(\phi)}{t} \\ &= \frac{d}{dt} \mathbf{T}(\phi + t\alpha)|_{t \to 0} \end{aligned} \tag{A.1}$$

The Gâteaux derivative, if it exists, is unique. The Gâteaux derivative of $\mathbf{T}$ at ϕ in the direction α is written as $\nabla\mathbf{T}(\phi, \alpha)$.

A.2 Definition of Gradient

The gradient of a field transformation $\mathbf{T} : \Phi(\Omega_1) \longrightarrow \Phi(\Omega_2)$ is defined to be the field $\mathbf{K} \in \Phi(\Omega_2 \times \Omega_1)$ with the following property:

$$\mathbf{T}'(\phi)(\alpha) = \mathbf{K}\alpha, \quad \forall\alpha \in \Phi(\Omega_1) \tag{A.2}$$

The derivative $\mathbf{T}'$ is an integral operation with the kernel $\mathbf{K}$. We denote $\nabla\mathbf{T}(\phi)$ the gradient of $\mathbf{T}$ at ϕ, giving:

$$\mathbf{T}'(\phi)(\alpha) = [\nabla\mathbf{T}(\phi)]\alpha \tag{A.3}$$

By using the notation $\nabla_\alpha\mathbf{T}(\phi)$ for the directional derivative of $\mathbf{T}$ in the direction of α, we have:

$$\begin{aligned} \nabla_\alpha\mathbf{T}(\phi) &= \nabla\mathbf{T}(\phi)\alpha \\ &= \mathbf{T}'(\phi)(\alpha) \end{aligned} \tag{A.4}$$

Furthermore, for higher order directional derivatives, we have:

$$\begin{aligned} &\mathbf{T}^k(\phi)(\alpha_1)(\alpha_2)...(\alpha_k) \\ &\qquad = \nabla^k\mathbf{T}(\phi)\alpha_1\alpha_2...\alpha_k \\ &\qquad = \nabla^k\mathbf{T}(\phi)\alpha_k \wedge \alpha_{k-1} \wedge ... \wedge \alpha_1 \\ &\qquad = \nabla_{\alpha k}...\nabla_{\alpha 1}\mathbf{T}(\phi) \end{aligned} \tag{A.5}$$

Bibliography

[1] R.C. Agarwal and J.W. Cooley. New algorithms for digital convolution. *IEEE Transactions on Acoustics, Speech, and Signal Processing*, ASSP-25(5):392–410, October 1977.

[2] Victor C. Aitken. *Sliding Mode State Estimation for Nonlinear Discrete-time Systems: Applications in Image Sequence Analysis.* PhD thesis, Carleton University, Ottawa, Ontario, Canada, 1994.

[3] B.D.O. Anderson and J.B. Moore. *Optimal Filtering.* Information and Systems Science Series. Prentice-Hall, Inc., Englewood Cliffs, N.J., 1979.

[4] H.C. Andrews and B.R. Hunt. *Digital Image Restoration.* Number ISBN 0-13-214213-9 in Signal Processing Series. Prentice-Hall, Inc., Englewood Cliffs, N.J., 1977.

[5] H.H. Arsenault and M. Levesque. Combined homomorphic and local-statistics processing for restoration of images degraded by signal-dependent noise. *Applied Optics*, 23(6):845–850, March 1984.

[6] M.R. Azimi-Sadjadi. *Block Implementation of Two-Dimensional Digital Filters.* PhD thesis, Imperial Colege Sci. Technol., Univ. London, London, England, 1981.

[7] M.R. Azimi-Sadjadi. Speckled image restoration by adaptive block Kalman filtering. In *Proceedings of IGARSS 87 Symposium*, pages 1449–1455, Ann Arbor, Michigan, May 18-21 1987.

[8] M.R. Azimi-Sadjadi and S. Bannour. Two dimensional adaptive block Kalman filtering of SAR imagery. *IEEE Transactions on Geoscience and Remote Sensing*, 29(5):742–753, September 1991.

[9] M.R. Azimi-Sadjadi and S. Bannour. Two-dimensional recursive parameter identification for adaptive Kalman filtering. *IEEE Transactions on Circuits and Systems*, 38(9):1077–1081, September 1991.

[10] M.R. Azimi-Sadjadi and R.A. King. Two-dimensional block processors: Structures and implementations. *IEEE Transactions on Circuits and Systems*, CAS-33(1):42–50, January 1986.

[11] Mokhtar S. Bazaraa, John J. Jarvis, and Hanif D. Sherali. *Linear Programming and Network Flows.* Number ISBN 0-471-63681-9. John Wiley and Sons, New York, 1990.

[12] W.M. Brown and L.J. Porcello. An introduction to synthetic aperture radar. *IEEE Spectrum*, pages 52–62, September 1969.

[13] R.G. Caves, P.J. Harley, and S. Quegan. Edge structure in ERS-1 and airborne SAR data. In *Proceedings of IGARSS 92 Symposium*, pages 1117–1119, Houston, Texas, May 26-29 1992.

[14] L.J. Chastant, L. Porcello, and J. Stevenson. Imaging radar systems. In *Manual of Remote Sensing*, volume I and II, pages 429–474. American Society of Photogrammetry, 1983.

[15] S. Citrin and M.R. Azimi-Sadjadi. A full plane block Kalman filter for image restoration. *IEEE Transactions on Image Processing*, 1(4):488–495, October 1992.

[16] T.R. Crimmins. Geometric filter for speckle reduction. *Applied Optics*, 24(10):1438–1443, May 1985.

[17] John C. Curlander and Robert N. McDonough. *Synthetic Aperture Radar: Systems and Signal Processing.* John Wiley & Sons, Inc, 1991.

[18] F. Dewaele, P. Wambacq, and A. Oosterlinck. Comparison of some speckle reduction techniques for SAR images. In *Proceedings of IGARSS 90 Symposium*, pages 2417–2422, College Park, Maryland, May 20-24 1990.

[19] J.M. Durand, B.J. Gimonet, and J.R. Perbos. SAR data filtering for classification. *IEEE Transactions on Geoscience and Remote Sensing*, GE-25(5):629–637, September 1987.

[20] K. Eldhuset. Principles and performance of an automated ship detection system for SAR images. In *Proceedings of IGARSS'89 Symposium*, pages 358–361, Vancouver, Canada, July 10 1989.

[21] V.S. Frost, J.A. Stiles, K.S. Shanmugan, and J.C. Holtzman. A model for radar images and its application to adaptive digital filtering of multiplicative noise. *IEEE Transactions on Pattern Analysis and Machine Intelligence*, PAMI-4(2):157–165, March 1982.

[22] K. B. Fung, G. W. Geling, and D. Ionescu. Test and evaluation criteria for SAR speckle reduction filters. *IEEE Trans. on Geoscience and Remote Sensing, submitted April*, 1996.

[23] K.B. Fung, C. Andronic, T. Damerji, and D. Ionescu. An interactive system for matching optical images. In *Proceedings of IGARSS'93 Symposium*, pages 1342–1344, Tokyo, Japan, August 18-21 1993.

[24] G. Geling. Speckle noise reduction of Synthetic Aperture Radar imagery using Kalman filter. Master's thesis, University of Ottawa, 1995.

[25] G. Geling and D. Ionescu. An edge detection operator for SAR images. In *Proceedings of CCECE 93*, pages 707–709, Vancouver, Canada, September 14-17 1993.

[26] G. Geling and D. Ionescu. A Kalman filter for speckle reduction in SAR data. In *Proceedings of CCECE 94*, pages 405–408, Halifax, Canada, September 24-27 1994.

[27] G. Geling and D. Ionescu. A Kalman filter with state multiplicative noise for SAR data. In *Proceedings of IGARSS'95*, pages 405–408, Florence, Italy, July 9-14 1995.

[28] J.W. Goodman. Some fundamental properties of speckle. *Journal of the Optical Society of America*, 66(11):1145–1149, Nov. 1976.

[29] C. Gosselin and R.J. Brown. Multiple-look effects on SAR classification accuracies. In *Proceedings of 10th Canadian Symposium on Remote Sensing*, pages 861–865, Edmonton, Alberta, May 5-8 1986.

[30] M.S. Grewal and A.P. Andrews. *Kalman Filtering: Theory and Practice*. Prentice Hall, Englewood Cliffs, New Jersey, 1993.

[31] A. Habibi. Two-dimensional Bayesian estimate of images. *Proceedings of the IEEE*, 60(7):878–883, July 1972.

[32] A. Hendry, S. Quegan, and J. Wood. The visibility of linear features in SAR images. In *Proceedings of IGARSS 88*, pages 1517–1520, Edinburgh, U.K., Sept 12-16 1988.

[33] S.A. Hovanessian. *Introduction to Synthetic Array and Imaging Radars.* Number ISBN 0-89006-082-7. Artech House, Inc., 1980.

[34] D. Ionescu and G. Geling. Automatic detection of large object features from SAR data. In *Proceedings of IGARSS 93 Symposium*, pages 1225–1227, Tokyo, Japan, August 18-21 1993.

[35] D. Ionescu and J.Y. Lin. The optimal robust stabilization compensator design; a deterministic approach. *International Journal on Control*, AC-28(7):745–756, July 1991.

[36] A.K. Jain. *Fundamentals of Digital Image Processing.* Prentice-Hall, Englewood Cliffs, New Jersey, 1989.

[37] Tohru Katayama and Sueo Sugimoto. *Parameter Identification for Two-Dimensional Image Enhancement*, chapter 10.

[38] H. Kaufman, J.W. Woods, S. Dravida, and A. M. Tekalp. Estimation and identification of two-dimensional images. *IEEE Transactions on Automatic Control*, AC-28(7):745–756, July 1983.

[39] J.L. Kovaly, editor. *Synthetic Aperture Radar.* Artech House, Dedham, Massachusetts, third edition, 1981.

[40] D.T. Kuan, A.A. Sawchuk, T.C. Strand, and P. Chavel. Adaptive noise smoothing filter for images with signal dependent noise. *IEEE Transactions on Pattern Analysis and Machine Intelligence*, PAMI-7(2):165–177, March 1985.

[41] D.T. Kuan, A.A. Sawchuk, T.C. Strand, and P. Chavel. Adaptive restoration of images with speckle. *IEEE Transactions on Acoustics, Speech, and Signal Processing*, ASSP-35(3):373–383, March 1987.

[42] F.W. Leberl. *Radargrammetric Image Processing.* Artech House, Inc., 1990.

[43] J. S. Lee. Refined filtering of image noise using local statistics. *Computer Graphics and Image Processing*, 15:380–389, 1981.

[44] J.S. Lee. Digital image enhancement and noise filtering by use of local statistics. *IEEE Transactions on Pattern Analysis and Machine Intelligence*, PAMI 2(2):165–168, March 1980.

[45] J.S. Lee. Digital image smoothing and the sigma filter. *Computer Vision, Graphics, and Image Processing*, 24(2):255–269, November 1983.

[46] J.S. Lee. A simple speckle smoothing algorithm for synthetic aperture radar images. *IEEE Transactions on Systems, Man, and Cybernetics*, SMC-13(1):85–89, Jan/Feb 1983.

[47] J.S. Lee. Speckle suppression and analysis for synthetic aperture radar images. *Optical Engineering*, 25(5):636–643, May 1986.

[48] J.S. Lee and I. Jurkevich. Segmentation of SAR images. *IEEE Transactions on Geoscience and Remote Sensing*, 27(6):674–680, November 1989.

[49] J.S. Lee, I. Jurkevich, P. Dewaele, P. Wambacq, and A. Oosterlinck. Speckle filtering of synthetic aperture radar images: A review. *Remote Sensing Reviews*, 8:313–340, 1994.

[50] F.K. Li and M. Leonard Bryan. Tradeoffs among several synthetic aperture radar image quality parameters: Results of a user survey study. *Photogrammetric Engineering and Remote Sensing*, 49(6):791–803, June 1983.

[51] L. Ljung and T. Söderström. *Theory and Practice of Recursive Identification.* MIT Press, Cambridge, Massachussetts, 1983.

[52] A. Lopes, E. Nezry, R. Touzi, and H. Laur. Maximum a posteriori filtering and first order texture models in SAR images. In *Proceedings of IGARSS 90 Symposium*, pages 2409–2412, College Park, Maryland, May 20-24 1990.

[53] A. Lopes, E. Nezry, R. Touzi, and H. Laur. Structure detection and statistical adaptive speckle filtering in SAR images. *Internation Journal of Remote Sensing*, 14(9):1735–1758, June 1993.

[54] A. Lopes and R. Touzi. Adaptive speckle filtering for SAR imagery. In *Proceedings of IGARSS 88 Symposium*, volume 3, pages 1263–1266, Edinburgh Scotland, September 13-16 1988.

[55] A. Lopes, R. Touzi, and E. Nezry. Adaptive speckle filters and scene heterogeneity. *IEEE Transactions on Geoscience and Remote Sensing*, 28(6):992–1000, November 1990.

[56] F.J. Martin and R.W. Turner. SAR speckle reduction by weighted filtering. *Int. Journal of Remote Sensing*, 14(9):1759–1774, 1993.

[57] E. Nezry, A. Lopes, and D. Ducros-Gambart. Supervised radiometric and textural segmentation of SAR images. In *Proceedings of IGARSS 93 Symposium*, pages 1426–1428, Tokyo, Japan, August 18-21 1993.

[58] E. Nezry, A. Lopes, and R. Touzi. Detection of structural and textural features for SAR images filtering. In *Proceedings of IGARSS'91 Symposium*, pages 2169–2172, Espoo, Finland, June 3-6 1991.

[59] A. Papoulis. *Probability, Random Variables, and Stochastic Processes.* McGraw-Hill Inc, New York, third edition, 1991.

[60] Y.A. Phillis. A smoothing algorithm for systems with multiplicative noise. *IEEE Transactions on Automatic Control*, 33(4):401–403, April 1988.

[61] Y.A. Phillis. Estimation and control of systems with unknown covariance and mulitplicative noise. *IEEE Transactions on Automatic Control*, 34(10):1075–1078, October 1989.

[62] C. Prati, F. Rocca, and A. Monti Guarnieri. Effects of speckle and additive noise on the altimetric resolution of interferometeric SAR surveys. In *Proceedings of IGARSS'89 Symposium*, pages 2469–2472, Vancouver, Canada, July 13 1989.

[63] H.Ch. Quelle and J.M. Boucher. Combined use of parametric spectrum estimation and frost algorithm for radar speckle filtering. In *Proceedings of IGARSS 90 Symposium*, pages 295–297, College Park, Maryland, May 20-24 1990.

[64] R. Keith Raney. Towards quantitative observation from synthetic aperture radar. In *Proceedings of IGARSS'89 Symposium*, pages 12–15, Vancouver, Canada, July 10-14 1989.

[65] R. Keith Raney and Paris W. Vachon. A phase preserving SAR processor. In *Proceedings of IGARSS'89 Symposium*, pages 2588–2591, Vancouver, Canada, July 10-14 1989.

[66] R.K. Raney. Radar fundamentals: Technical perspective. *Manual of Remote Sensing*, 1993.

[67] R.K. Raney and G.J. Wessels. Spatial considerations in SAR speckle simulation. *IEEE Transactions on Geoscience and Remote Sensing*, GE-26(5):666–672, September 1988.

[68] R. P. Roesser. A discrete state-space model for linear image processing. *IEEE Transactions on Automatic Control*, AT-20(1):1–10, February 1975.

[69] H.L. Royden. *Real Analysis.* Number Library of Congress catalog card number: 68-10518. The Macmillan Company, London, 1968.

[70] R. Samadani and J.F. Vesecky. Finding curvilinear features in speckled images. In *Proceedings of IGARSS 89 Symposium*, pages 1198–1202, Vancouver, Canada, July 10-14 1989.

[71] E. Shaw and E.J. Langham. Radarsat: Canada's microwave satellite. In *Proceedings of IGARSS'89 Symposium*, pages 197–199, Vancouver, Canada, July 10-14 1989.

[72] Zhenghao Shi and K.B. Fung. A comparison of digital speckle filters. In *Proceedings of IGARSS 94 Symposium*, pages 2129–2133, Pasadena, California, August 8-12 1994.

[73] M. St-Pierre. Radarsat: Review of pertinent economic and commercial issues. In *Proceedings of IGARSS'89 Symposium*, pages 200–203, Vancouver, Canada, July 10-14 1989.

[74] G. Stein and M. Athans. The lqg/ltr procedure for multivariable feedback control design. *IEEE Transactions on Automatic Control*, AC-32(6):105–114, September 1987.

[75] E.R. Sudibjo, G.D. Lodwick, and S.H. Paine. Digital enhancement of STAR-1 SAR imagery for linear feature extraction. In *Proceedings of IGARSS 89*, pages 2242–2245, Vancouver, Canada, July 10-14 1989.

[76] S. Sugimoto and A.K. Jain. Identification of a large vector ar model and its applications to image processing. In *Proceedings of 6th IFAC Symposium - Identification Syst. Parameter Estimation*, pages 1421–1426, Arlington, Virginia, June 1982.

[77] A.M. Tekalp, H. Kaufman, and J.W. Woods. Edge-adaptive Kalman filtering for image restoration with ringing suppression. *IEEE Transactions on Acoustics, Speech, and Signal Processing*, ASSP-37(6):892–899, June 1989.

[78] R. Touzi, A. Lopes, and P. Bousquet. A statistical and geometrical edge detector for SAR images. *IEEE Transactions on Geoscience and Remote Sensing*, 26(6):764–773, Nov 1988.

[79] Spyros G. Tzafestas. *Multi-dimensional Systems - Techniques and Applications*. Electrical Engineering and Electronics/29. Marcel Dekker, Inc., New York, New York 10016, 1986.

[80] F.T. Ulaby, T.F. Haddock, and R.T. Austin. Fluctuation statistics of millimeter-wave scattering from distributed targets. *IEEE Transactions on Geoscience and Remote Sensing*, 26(3):268–281, May 1988.

[81] F.T. Ulaby, F. Kouyate, B. Brisco, and T.H. Lee Williams. Textural information in SAR images. *IEEE Transactions on Geoscience and Remote Sensing*, GE-24(2):235–245, March 1986.

[82] T. Wahl and A. Skoelv. SAR imaging of ships and ship wakes during norcsex'88. In *Proceedings of IGARSS'89*, pages 366–368, Vancouver, Canada, July 1989.

[83] F. Wong, I. Cumming, and R. Keith Raney. Processing simulated radarsat SAR data with a high precision algorithm. In *Proceedings of IGARSS'93*, pages 1176–1178, Tokyo, Japan, August 18-21 1993.

[84] J.W. Woods. Correction to "Kalman filtering in two dimensions". *IEEE Transactions on Information Theory*, IT-25(5):628, September 1979.

[85] J.W. Woods and J. Biemond. Comments on "A model for radar images and its application to adaptive digital filtering of multiplicative noise". *IEEE Trans-*

actions on Pattern Analysis and Machine Intelligence, PAMI-6(5):658–659, September 1984.

[86] J.W. Woods and V.K. Ingle. Kalman filtering in two dimensions: Further results. *IEEE Transactions on Acoustics, Speech, and Signal Processing*, ASSP-29(2):188–197, April 1981.

[87] J.W. Woods and C.H. Radewan. Kalman filtering in two dimensions. *IEEE Transactions on Information Theory*, IT-23(4):473–482, July 1977.

[88] Jin Yun Zhang and William Steenaart. High speed Kalman filtering for image restoration. *SPIE Visual Communications and Image Processing IV*, 1199:125–135, 1989.